6/2/92 (1612)	17.13 6/7
6/2/92 2130	4.12.95. (7.45)
10/2/92 (1717)	11.4.97 – 4.34
11/5/92 1746	
8.10.92 2.47	
15. 11.93 2.01	
19/11/93 (1301)	
2/3/94 13:57	
21/3/94 1724	
27.4.94 1339	
17/6/94 15.45	

DEVELOPMENT OF INSTRUMENTATION INCORPORATING SOLID STATE GAS SENSORS FOR MEASUREMENT OF OXYGEN PARTIAL PRESSURE

Mohieddine BENAMMAR

A thesis submitted in partial fulfilment of the requirements of the Council for National Academic Awards for the degree of Doctor of Philosophy.

April 1991

The work was carried out in the Energy Technology Centre at Middlesex Polytechnic, Bounds Green Road, London N11 2NQ

ABSTRACT

Electronic instrumentation was developed for the measurement of the oxygen partial pressure, P_1, in a sample gas using fully-sealed zirconia pump-gauge oxygen sensors operated in an AC mode. These sensors, operated typically at 700°C, consisted of two discs of zirconia with porous platinum electrodes on each face separated by a gold seal and enclosing a small internal volume. One disc was operated as a pump enabling oxygen to be electrochemically transferred into and out of the enclosed volume; the other disc operated as a gauge, the Nernst EMF across the electrodes providing a measure of the ratio of the internal to the external oxygen partial pressure. By careful design of the circuitry it was possible to measure the oxygen partial pressure, P_1, without the need for a separate reference gas supply. Subsequently, a novel "tracking" mode of operation was proposed and implemented in which leakage effects generally associated with sealed pump-gauge devices were minimised: the sensor was operated in a feedback control-loop in order to adjust automatically the mean internal reference oxygen partial pressure, P_0, so as to maintain the ratio (P_1/P_0) close to unity. The signal-to-noise ratio was markedly improved by using gauge EMFs with high amplitudes which inevitably display a distorted sinusoid due to the logarithmic term in the Nernst equation. Surprisingly, mathematical analysis predicted that the linearity of the output of the instrument using phase-sensitive detection should not be affected by the deviation from a sinusoid and this was confirmed experimentally: signal processing was practically implemented using simple analogue electronics. As anticipated there was a strong influence of sensor temperature on the output of the instrument: consequently, methods for temperature compensation were proposed and shown to be feasible with minimum hardware.

The theory of operation of leaky pump-gauge was also developed which indicated that a physical leak in the sensor should cause a phase shift and amplitude change in the sensor output. Experimental results were, in general, in agreement with the theory demonstrating the influences of the geometry and dimensions of the leak and of the operating frequency. Importantly, the theory predicted that, when operated in the AC mode, devices with major leakage may still be used for oxygen partial pressure measurement: again this was confirmed by experiment and the additional benefit of a concomitant substantial simplification of the electronic circuitry also realised. Interestingly an unexpected but small influence of oxygen concentration on the phase shift was observed: this requires additional study.

ACKNOWLEDGEMENTS

I wish to express my sincere gratitude to my supervisor Dr. W.C. Maskell for his constant guidance and interest and for the many valuable discussions throughout this work which I thoroughly enjoyed.

I wish to acknowledge the British Council and Middlesex Polytechnic for the financial support of this work. My appreciation and thanks are due to Dr. W.C. Maskell for organising my funding. My thanks also to Prof. M. Annabi and Prof. M. Ksouri for their assistance in getting my scholarship.

I would like to thank all my colleagues at the Energy Centre for their help and support; in particular Mr. A. Ioannou, Mr. J. Larcin, Mr. D. Malpas and Mr. R. Copcutt.

Finally, my sincere thanks to Rohani for all the support and encouragement.

CONTENTS

CHAPTER 2 (Contd)

CHAPTER 3 (Contd)

CHAPTER 4 (Contd)

LIST OF THE MAJOR SYMBOLS USED

A	amplitude of the AC current
C_{O2}	oxygen concentration
D	oxygen diffusion coefficient
E	gauge EMF
E_A	activation energy of diffusion coefficient
E_{pp}	amplitude peak-to-peak of the gauge EMF
E_{-p}	amplitude of the negative peak of the gauge EMF
f	frequency of the pumping current
F	Faraday constant ($9.64846\ 10^4$ C mol^{-1})
G	thickness of the gold seal
$I=A\sin(\omega t)$: pumping current	
I_{lim}	limiting current
I_0	DC offset in the pumping current
J	oxygen flux
L	length of the pore
MSR	mark-to-apace ratio
n	number of moles of oxygen
P_{O2}	oxygen partial pressure
P_1	oxygen partial pressure in the sample gas
P_2	oxygen partial pressure in the internal volume
P_0	mean value of P_2
Q	electric charge
R	gas constant (8.31441 J K^{-1} mol^{-1})
S	total cross-sectional area of the diffusion pore(s)
t	time
T	operating temperature
T_D	time constant of oxygen diffusion
v	internal volume of the sensor
V_r	DC reference voltage
$x=\omega t$	
Ψ	phase shift caused by the leak
ω	angular frequency
λ	time delay caused by the slow response of the electrode
ϕ	effective diameter of the diffusion pore
σ	leak conductance of diffusion barrier

CHAPTER 1

INTRODUCTION TO OXYGEN GAS SENSING

"I durst not laugh, for fear of opening my lips and receiving bad air" SHAKESPEARE, Julius Caesar (1599-1600) 1.2.250.

1.1 BACKGROUND

By the end of the 19th century, science and technology had begun to transform the traditional agriculture-based way of life into a fast growing industry-based system. As a consequence, the standard of living has risen steadily and the luxuries of yesterday have become today's necessities. This has caused the energy consumption to rise dramatically and also the level of pollution as a consequence. Until recently, scientists argued that nature can cope with emissions of pollutant gases. However with the continuous and steady destruction of rain forests, evidence of pollution started to emerge.

The last ten years have seen a growing public awareness and concern for this problem. As a consequence, environmental pollution has become a political issue. This is reflected by the growth of "green" political parties throughout the induatrialised world. New unilateral legislations are being introduced in order to tackle this problem. Pollution has no borders, and it is now widely believed that this problem can only be solved through proper coordination and joint efforts between all countries.

These new regulations will create the need to develop sensors to monitor and control emissions of pollutant gases and minimise energy consumption. The potential U.K. market (figure 1.1) for these devices is estimated to be £170 million over the next five years; overseas markets could multiply this figure by a factor of five (Bogue 1990).

In general sensors are devices which convert physical quantities into electrical signals. The sensor is an interface between the physical quantity and the electronic instrument used to measure and/or control this quantity. Dietz et al (1977) defined a gas sensor as "a device with which the concentration of certain gaseous components can be measured. In the broad sense of the term, it includes the electronic transducer, to which usually an electronic evaluating device is connected".

Sensors are generally associated with electronic control systems. However the advance made in electronics and computing was not matched by the development of accurate, reliable and cheap sensors. When associated with transducers, electronics and computer techniques can play an important role in correcting for the technological defects of the transducer. Thus sensor design and construction may be made easier. However, despite the enormous amount of literature published on gas sensors in the last 5-10 years, there is little evidence of wide cooperation between electronics specialists and physicists.

1.2 NEED FOR GAS SENSORS

The scope of applications of gas sensors is wide. They include the following.

Hazard monitoring

The early sensors were intended for use in the mining industry where the hazard of flammable gases is prevalent and potentially catastrophic. Sensors play an important role in detecting toxic gases in the working environment.

These include CO, H_2S, NO_x which can be fatal. Gas sensors may also be used to detect fires: when materials are heated or burn a wide range of gaseous products is evolved. The main toxic gas generated is generally CO. Jones (1989) also suggested the possible use of gas sensors in the detection of some explosives.

Pollution monitoring and control

Heavy industry, power generation and internal combustion engines have been identified as the main source of atmospheric pollution. The main pollutant gases include NO_x and SO_x which are responsible for acid rain. Other industrial pollutants are CO_2, CO, HCl, NH_3 and various hydrocarbons, while in vehicle emission the interest is in CO, CO_2 hydrocarbons and NO_x. In many applications, such as internal combustion engines, the control of gaseous emissions is not only a benefit for the environment but can also improve energy efficiency.

Process monitoring and control

From laboratory to industrial applications, sensors can be widely used to monitor and control various gases. The scope for sensors in this area is great.

Medical applications

Besides detection of harmful gases, sensors may be used in controlled environment areas. Gas sensors may also provide on-line analysis of exhaled breath to monitor the patient's condition or to aid diagnosis.

1.3 OXYGEN SENSORS

The high chemical reactivity of oxygen and its role in supporting the dominant forms of life on this planet makes its monitoring, measurement and control highly desirable.

1.3.1 Applications

The main applications of oxygen sensors include the following.

(i) Energy management: Control of combustion in boilers burning fossil fuel to maximise fuel efficiency and minimise the generation of CO (Fouletier 1982/3, Williams and McGeehin 1984, Vitter et al 1983, Franx 1982, Bergman and Franx 1984). Use in 'lean-burn' car engine systems which offer the advantage of fuel economy combined with low emissions of CO, NO_x and hydrocarbons (Kobayachi et al 1984). Control of car exhaust gases for protection of three-way catalyst systems (Young and Bode, 1979).

(ii) Industrial processes: Gas purity monitoring and control. Monitoring and control of atmospheres in metallurgical heat treatment furnaces (Fairbank, 1977). Area monitoring and control (oil tankers, food storage, food packaging, fermentation, etc...).

(iii) Laboratory studies: The control of oxygen partial pressure in laboratory applications (Agrawal et al 1974, Fouletier et al 1975). Use in glove boxes, sputtering machines (William and Paul 1989) etc...

(iv) Physiological applications: The control of aircraft atmosphere. Use in life support breathing systems (Calvert 1968, Joyce 1968, Joyce and Woods 1975, Stein 1976). Use in medical applications.

1.3.2 Principles of oxygen sensing

A wide range of oxygen sensors based on the physical, chemical and electrochemical properties of oxygen have been developed. The review by Kocache (1986) is particularly relevant.

1.3.2.1 Methods based on chemical properties of oxygen

The early methods for oxygen measurement were based on its chemical activity. This measurement may be achieved by using the chemical volumetric technique (Haldane and Graham 1935): A known volume of sample gas is taken and the oxygen content is removed by absorbing it with a chemical reagent. The change in volume of the sample is equal to its oxygen content.

1.3.2.2 Methods based on the physical properties of oxygen

Various methods based on the physical properties of oxygen have also been used. Most of these are based on magnetic principles. Other techniques include a method based on UV absorption of oxygen: oxygen has a much higher absorption coefficient than most of the other gases. This principle was utilised in a practical device by Kaplan et al (1971). The thermal conductivity of gases may also be used for the measurement of partial pressure of any gas provided the gaseous species are known (Wang et al 1989).

1.3.2.3 Methods based on the electrochemical properties of oxygen

Sensors with aqueous electrolytes

These sensors generally include an aqueous solution with mobile ion and two electrodes. Various techniques may be used for the measurement of O_2 concentration/ partial pressure using such sensors. One such technique is called the polarographic method: when an EMF is applied between the two electrodes which are in contact with the solution, redox reactions are induced. If a thin solid membrane (generally PTFE) is placed between the cathode and the sample gas, the rate of diffusion of oxygen (required in the redox reaction) may be limited by the barrier. If the applied voltage is sufficiently high, a limiting current is reached where the rate of O_2 diffusion is limited only by the barrier (Bergman 1970, 1974). The limiting current is then proportional to the oxygen concentration in the sample gas.

Sensors with solid electrolytes

ZrO_2 forms solid solutions with aliovalent oxides including CaO, MgO, Y_2O_3. This may be achieved by mixing ZrO_2 and oxide powders, pressing and sintering at sufficiently high temperature to promote inter-diffusion of the cations. The added oxides are referred to as stabilisers and the solid solution as zirconia. In zirconia, a fraction of Zr^{4+} ions are replaced by lower valency ions such as Ca^{2+}, Mg^{2+} or Y^{3+}. As a result oxygen vacancies are created in the solid solution and oxygen ions can move through the crystal. This mobility is a thermally activated process becoming significant for temperatures above 300°C. Stabilised zirconia therefore behaves as an electrolyte with oxygen ions able to drift in an imposed electric field and may be used in oxygen generation/removal and oxygen sensing.

A solid electrolyte cell may be represented as follows (Maskell and Steele 1986):

$$O_2(P_2),M_2/SE/M_1,O_2(P_1) \tag{1.1}$$

where M_1 and M_2 are porous electronic conductors (e.g. Pt or Ag) in contact with the solid electrolyte SE. The latter must be physically impermeable to the gas (O_2) which is at partial pressures P_1 and P_2. Provided that the electronic conductivity of the ceramic is low, the cell (1.1) develops an EMF given by the Nernst equation:

$$E = \frac{RT}{4F}\ln\left(\frac{P_1}{P_2}\right) \tag{1.2}$$

where R,F and T are respectively the gas constant, the faraday and the operating temperature (in kelvin). The EMF in equation (1.2) is generated by the tendency of oxygen ions to diffuse from the high to low pressure side, which is counterbalanced by the resulting electrical field. If P_2 is known (reference gas) then P_1 may be determined from a measurement of E (at a given T). Thus the cell may be used as a <u>gauge</u> for the measurement of unknown oxygen partial pressures.

By applying a current (I) to the cell (1.1), oxygen may be electro-chemically transferred from the cathode side to the anode side of the cell. The electrode reaction is

$$O_2 + 4e \underset{anode}{\overset{cathode}{\rightleftharpoons}} 2O^{2-} \tag{1.3}$$

Through the oxidation-reduction of oxygen, the electronic current applied to the cell is transformed into ionic current through the electrolyte. The number (n) of moles of O_2 electrochemically "transferred" through the solid electrolyte is given by Faraday's law:

$$dn = -\frac{dQ}{4F} \tag{1.4}$$

where Q is the charge passed. The negative sign in eqn.(1.4) is due to the oxygen flux being in the opposite direction to the pumping current (see eqn.1.3). The amount of oxygen transferred is proportional to the charge passed through the electrolyte. The cell (1.1) can therefore act as an <u>oxygen pump</u> (Yuan and Kroger 1969). This technique has been used for the production of pure oxygen, or removal of oxygen from gases (Alcock and Zador, 1972).

1.3.2.4 Comparison of the various methods

The methods based on chemical properties of oxygen do not provide an output which can be automatically converted into an electrical quantity and therefore such sensors can not be interfaced with electronic instruments. The methods based on the physical properties of O_2 generally require complicated hardware and therefore are not suited for small size applications. The methods based on the electrochemical properties of oxygen combine the advantage of electrical output signals and the simplicity of construction. In general, solid-state devices operating on electrochemical principles have many advantages over aqueous electrochemical sensors:

i- Solid state electrolytes are non-volatile enabling operation in high temperature environments.

ii- The elevated temperature required for the operation of solid-state sensors can facilitate the catalysis of reactive gases so that equilibrium gas concentrations may be measured where required. However the operation at high temperature can be a disadvantage if the device is used in potentially exploaive mixtures of gases where a flame trap must be used to prevent ignition.

iii- Solid state devices are highly selective where only one ion type is mobile; furthermore side reactions at the electrodes are normally unimportant.

iv- Solid state devicea have a faster response to changes in gas concentration.

v- In solid atate devices, complete separation of anode and cathode compartment is automatically achieved by the non-porous solid electrolyte itself.

vi- When used for oxygen generation, solid state pumps produce highly pure and dry gas.

1.3.3 EXISTING ZIRCONIA-BASED OXYGEN SENSORS

Potentiometric sensors

These consist of a zirconia wall separating the reference and sample atmospheres (cell 1.1). The output of such a sensor is given by eqn.(1.2). Various designs have been used in practical devices (Hickam 1967; Sayles 1975; Cleary and Elikan 1975; Kocache and Holman 1978, 1979; Maskell and

Steele 1986). The reference pressure in these devices is obtained from a supply of a stable reference gas (generally air). In order to avoid the problems associated with the piping of a reference gas, some authors (Deportes et al 1977) have described sensors with the internal reference oxygen partial pressure obtained from a redox couple such as Pd/PdO.

Amperometric sensors

A schematic diagram of the limiting-current device (Dietz 1982) is shown in figure (1.2). If a sufficient voltage is applied to the pump of the device then oxygen is electrochemically pumped from the cathode to the anode reducing the oxygen partial pressure at the cathode to a value close to zero because the porous barrier fixed in front of the cathode restricts the transport of oxygen to the electrode. A limiting condition I_{lim} is then achieved and the pumping current is controlled by the rate of oxygen diffusion through the porous barrier according to Fick's first law. For a diffusion barrier consisting of a hole of cross-section S and length L, the limiting current is given by:

$$I_{\lim} = 4FD\left(\frac{S}{L}\right)C_{O2} \tag{1.5}$$

where D is the diffusion coefficient of O_2 and C_{O2} is the concentration of O_2 in the sample gas. Equation (1.5) shows that the limiting current is proportional to the gas concentration.

The applications of these sensors require very simple electronics. However there are some problems associated with these devices: the magnitude of the pumping current is restricted by the ionic conductivity of the ceramic; this means that the ratio (S/L) must be small enough in order to reach the limiting condition even at high oxygen concentrations. Dietz (1982) described various forms of diffusion barriers to achieve this requirement. The second disadvantage of this type of sensors is that the device can not distinguish the rich and lean regions as there is no change in sign of the current on traversing stoichiometry (Maskell 1991a).

Coulometric sensors

The device used in this mode is similar in construction to the limiting-current type device. The principle of operation (Heyne 1976) of this mode can be explained as follows. Initially a constant current is applied to the pump to remove oxygen rapidly from the cavity much faster than its rate of leakage through the diffusion barrier. When almost all oxygen is removed from the internal volume the voltage on the pump rises sharply at which point the current is automatically discontinued. Oxygen is then allowed to leak into the cavity until the inner oxygen partial pressure approaches the external pressure. The pumping current is then re-applied and the cycle repeated. The oxygen partial pressure P_1 in the sample gas can then be calculated by invoking Faraday's law,

$$P_1 = \frac{RT}{4Fv} Q \tag{1.6}$$

where Q is the charge passed, v is the internal volume and T is the operating temperature. If the current applied is constant (I) then P_1 is given by

$$P_1 = \frac{RTI}{4Fv}t \qquad (1.7)$$

Equation (1.7) shows that P_1 is directly proportional to the pumping time (t).

Pump-gauge devices

By combining oxygen pump and gauge cells, the effect of oxygen generation or extraction by the pump can be monitored by the gauge (Beekmans and Heyne 1970, Agrawal et al 1974). By using appropriate electronics the signal from the gauge may be used to control the pumping effect in order to produce gases with controllable percentage of oxygen (Philips 1971). The combination of oxygen pump and gauge can be used for oxygen sensing without the need for reference gas. The device with an enclosed volume (v) consists of an oxygen pump and a gauge. The device can be hermetically sealed or may have a pore or porous material connecting the inner and outer regions. The external and internal oxygen partial pressures are represented as P_1 and P_2 respectively. A number of different modes of operation of such devices have been proposed. In all these modes one half of the device is used to pump electrochemically oxygen into or out of the internal volume, and the other half is used to measure the Nernst EMF between P_1 and P_2.

Coulometric

This mode of operation was first reported by Haaland (1977). A number of related methods were then reported by Hetrick et al (1982) and by DeJong (1983). The pump-gauge device was placed in the sample gas of unknown oxygen partial pressure P_1. Oxygen was electrochemically pumped out of the internal volume (v) until the gauge EMF, E, reached a predetermined value E_y corresponding to an internal oxygen partial pressure equal to P_y. The current was then reversed and oxygen pumped into the device until E reached a predetermined value E_z corresponding to an internal oxygen partial pressure P_z. The current was then reversed and the cycle repeated. Thus the internal oxygen partial pressure was pumped between P_y and P_z respectively. Under simplifying conditions (Maskell 1991a), the external oxygen partial pressure may be determined according to the following equation

$$P_1 = \left(\frac{RT}{4F}\right)^2 \frac{I\gamma}{2v\,(E_y - E_z)} \tag{1.8}$$

where I is the amplitude of the pumping current, γ is the cycle time and v is the internal volume.

Amperometric without fixed reference

In this mode of operation (Hetrick et al 1981) a device with diffusion hole was used. The pumping current was automatically adjusted to hold the gauge EMF at some predetermined value E_s. At the steady state $E=E_s$ where E is given by eqn.(1.2). The pumping current I_p, is given by

$$I_p = F\sigma(P_1 - P_2) \tag{1.9}$$

where σ is the leak conductance of the diffusion barrier.

Thus

$$I_p = F\sigma P_1\left[1 - \exp\left(\frac{-4F}{RT}E_s\right)\right] \tag{1.10}$$

For a given E_s, the current was proportional to the oxygen partial pressure in the sample gas.

Amperometric with fixed reference

This mode of operation was suggested by Dietz (1982). By providing a gas of fixed composition adjacent to the anode on a single two-electrode amperometric sensor, the two sides of stoichiometry may be distinguished. Soejima and Mase (1985) translated this idea into practical device using air as reference gas.

Potentiometric with monitored internal reference

Maskell et al (1987) have described a novel mode of operation of a fully-sealed pump-gauge device. This mode of operation is explained in details in the next section. The present work was based on this mode of operation.

1.4 OXYGEN PUMP-GAUGE OPERATING IN THE AC MODE

Maskell et al (1987) suggested that by applying a sinusoidal current to the pump of the device, the internal oxygen partial pressure may be caused to oscillate at the same frequency. This should result in a pseudo-sinusoidal EMF on the gauge. By appropriate signal processing of the gauge EMF, the mean internal oxygen partial pressure may be determined and adjusted if required. Potentiometric measurement of the oxygen partial pressure in the sample gas can then be made relative to the known mean internal reference pressure. The main advantage of this mode is the continuous rather than intermittent measurement of oxygen partial pressure.

1.4.1 Theory of operation

The theory of operation of the fully sealed device operated in the AC mode has been developed by Maskell et al (1987). A schematic cross section of the pump-gauge used is shown in figure (1.3). The external and internal oxygen partial pressures are designated as P_1 and P_2 respectively. The ideal gas equation may be written for the internal volume.

$$\frac{dP_2}{dt} = \frac{RT}{v}\frac{dn}{dt} \tag{1.11}$$

v is the internal volume and n the number of moles of O_2 contained. By applying a current to the pump the number of moles of oxygen transferred through the solid electrolyte is given by Faraday's law (eqn. 1.4). Assuming ideality, i.e. no sorption on internal surfaces, no oxidation-reduction of the inner electrodes and negligible changes in stoichiometry of the ceramic, then the following equation may be written

$$\frac{dP_2}{dt} = -\frac{RT}{4Fv}I \tag{1.12}$$

and

$$P_2 = -\frac{RT}{4Fv}\int I dt \tag{1.13}$$

If, in this mode of operation, the applied current is sinusoidal, then

$$I = A \sin\omega t \tag{1.14}$$

A is the amplitude and ω the angular frequency. From eqns. (1.13) and (1.14),

$$P_2 = \frac{RTA}{4F\nu\omega}\cos\omega t + P_0 \tag{1.15}$$

P_0 is a constant equal to the mean oxygen pressure inside the device, i.e. the average value of P_2.

It is shown in Appendix (D) that the internal volume of the device, being "charged" and "discharged" with an oxygen flux resulting from the pumping current, is equivalent to an ideal capacitor being charged and discharged using a pumping current. The oxygen partial pressure difference across the gauge is equivalent to the voltage across the capacitor. The phase difference between the pumping current and internal O_2 partial pressure is equal to 90°. The same phase shift is found between the "charging" current and voltage across the capacitor.

Equation (1.15) may be written

$$P_2 = \frac{RTA}{4F\nu\omega}\cos x + P_0 \tag{1.16}$$

where $x=\omega t$. (1.16a)

The internal oxygen partial pressure eqn.(1.16) cannot be negative. Physically, the limit is reached when all oxygen contained in the enclosed volume is pumped out of the device. Therefore the following relation must not be violated in order to ensure proper functioning of the device:

$$\frac{RTA}{4F\nu\omega P_0} < 1 \tag{1.17}$$

The gauge EMF, E, is given by eqn.(1.2)

$$E = \frac{RT}{4F}\ln\left(\frac{P_1}{P_2}\right) \tag{1.2}$$

Uniformity of O_2 concentration within the internal volume may be estimated as follows. The time constant of the gas diffusion from the internal pump-electrode to the gauge electrode is given by (Crank 1956)

$$T_D = \frac{G^2}{D} \tag{1.18}$$

where G is the distance between the internal electrodes (i.e. thickness of the gold seal) and D is the gas diffusion coefficient. In the present work, a mixture of oxygen and nitrogen was used to test the devices for which a value for D of $164mm^2\ s^{-1}$ at 700°C was calculated (Chapter 6): this together with G=0.05mm led to a T_D value of 15μs. On the other hand, the maximum operating frequency of the device employed in this work was 4Hz (refer to Chapter 3). Thus the time constant of oxygen diffusion inside the device was very small when compared to the minimum signal period (250ms) of the pumping current. Therefore under the operating conditions, the oxygen concentration may reasonably be assumed to be uniform throughout the internal volume.

Under the operating conditions, the internal gauge-electrode is assumed to respond rapidly to changes in P_2. In general, the response of the electrodes depends (refer to section 6.3.5 in Chapter 6) on the partial pressure, operating temperature and electrode composition (Fouletier et al 1974, Winnubst et al 1985, Maskell and Steele 1986). Substituting for P_2 from eqn.(1.16) into eqn.(1.2) gives:

$$E = \frac{RT}{4F}\left[\ln\left(\frac{P_1}{P_0}\right) - \ln\left(1+\frac{RTA}{4Fv\omega P_0}\cos x\right)\right] \tag{1.19}$$

This is the general theoretical equation for the variation of the gauge EMF resulting from the application of a sinusoidal current.

If

$$\frac{RTA}{4Fv\omega P_0}<0.1 \tag{1.20}$$

then equation (1.19) may be simplified to

$$E = \frac{RT}{4F}\left[\ln\left(\frac{P_1}{P_0}\right) - \frac{RTA}{4Fv\omega P_0}\cos x\right] \tag{1.21}$$

Equation (1.21) shows that the EMF in its simplified form is the sum of DC and AC components.

$$E = E_o - B\cos x \tag{1.22}$$

where

$$E_0 = \frac{RT}{4F}\ln\left(\frac{P_1}{P_0}\right) \tag{1.22a}$$

and

$$B = \frac{R^2T^2A}{16F^2v\omega P_0} \tag{1.22b}$$

Clearly eqn.(1.21) predicts a phase shift of $\pi/2$ between the EMF and the pumping current.

The amplitude peak to peak (E_{pp}) of the AC component of the gauge EMF (eqn.1.19) depends on the magnitude of the term ($RTA/4Fv\omega P_0$).

$$E_{pp} = \frac{RT}{4F}\left[\ln\left(1+\frac{RTA}{4Fv\omega P_0}\right)-\ln\left(1-\frac{RTA}{4Fv\omega P_0}\right)\right] \tag{1.23}$$

An increase in the term ($RTA/4Fv\omega P_0$) is accompanied by an increase in E_{pp} and a progressive deviation of the EMF from a sinusoidal shape. This deviation is caused by the logarithmic effect on the second term of eqn.(1.19). Figure (1.4) shows the calculated E_{pp} at 700°C versus ($RTA/4Fv\omega P_0$). For low values of the latter theory predicts linearity becoming increasingly non-linear at high values. Note that the relation of eqn.(1.20) corresponds to an amplitude of the AC component less than 4.2mV peak-to-peak at 700°C.

1.4.2 Results

The above theory has been verified by Maskell et al (1987). Excellent agreement was found between theory and experiment. Figure (1.5) shows experimental results using a device with an internal volume $v=1mm^3$ operated at 700°C in air. The two plots of the gauge EMF were obtained with two different amplitudes of the pumping current (A_1=20 and A_2=400μA): these correspond to the two values 0.045 and 0.86 of the term ($RTA/4Fv\omega P_0$) respectively. Distortion of the gauge EMF from a pure sinusoid is clearly evident in figure (1.5b).

In the present work, this theory of operation constitutes the basis of the development and testing of the electronics associated with pump-gauge devices operated in the AC mode.

1.4.3 Proposed signal processing

The theory of operation of sealed pump-gauge devices operated in the AC mode confirmed by existing experimental data indicates that with an applied sinusoidal pumping current, the device producea a gauge EMF which is a function of both the external partial pressure (quantity to be measured) and the mean internal oxygen partial pressure. This gauge EMF is composed of two components: an AC component dependent upon the mean internal oxygen partial pressure and a DC component dependent upon both the mean internal and external partial pressures.

The idea of aeparating the two terms (AC and DC) of the gauge EMF waa first suggested by Maskell et al (1986). The mean internal oxygen partial preasure may be determined from a meaaurement of the amplitude (B) of the AC component. From eqn.(1.22b),

$$P_0 = \frac{R^2T^2A}{16F^2\nu\omega B} \tag{1.24}$$

Then the oxygen partial pressure in the sample gas (P_1) may be computed from the DC component and the calculated P_0 using eqn.(1.22a). Thus the mean internal oxygen partial pressure acts as reference for the measurement of P_1.

$$P_1 = \frac{R^2T^2A}{16F^2\nu\omega B}\exp\left(\frac{4F}{RT}E_0\right) \tag{1.25}$$

The possible signal processing options were further developed by Maskell (1986). The operation of the device in a controlled loop system (figure 1.6) was suggested, where an appropriate bias signal may be used to adjust the frequency (ω), the amplitude of the current (A) or the mean internal oxygen partial pressure (P_0) in order to keep the gauge EMF within the low signal condition [i.e. AC component purely sinusoidal; see eqn.(1.17) and eqn.(1.22b)]. In addition, the feedback should ensure that the system does not saturate for instance through an offset in the sinusoidal pumping current.

1.5 AIMS AND OBJECTIVES OF THE WORK

In the present work the objective was to develop instrumentation for the measurement of oxygen partial pressure based upon pump-gauge sensors operated in the AC mode. This included the following investigations.

(i) Implementation of the signal processing options suggested by Maskell et al (1986) to fully sealed devices with additional refinements where appropriate.

(ii) Implementation of an important modification with a fully sealed device in which the mean internal and external gas pressures are maintained equal.

(iii) Development of the theory for leaky devices together with implementation and verification.

(iv) Consideration and implementation of methods for temperature compensation with particular emphasis on minimisation of hardware.

(v) Development of circuitry for maintaining the sensor at a predetermined temperature.

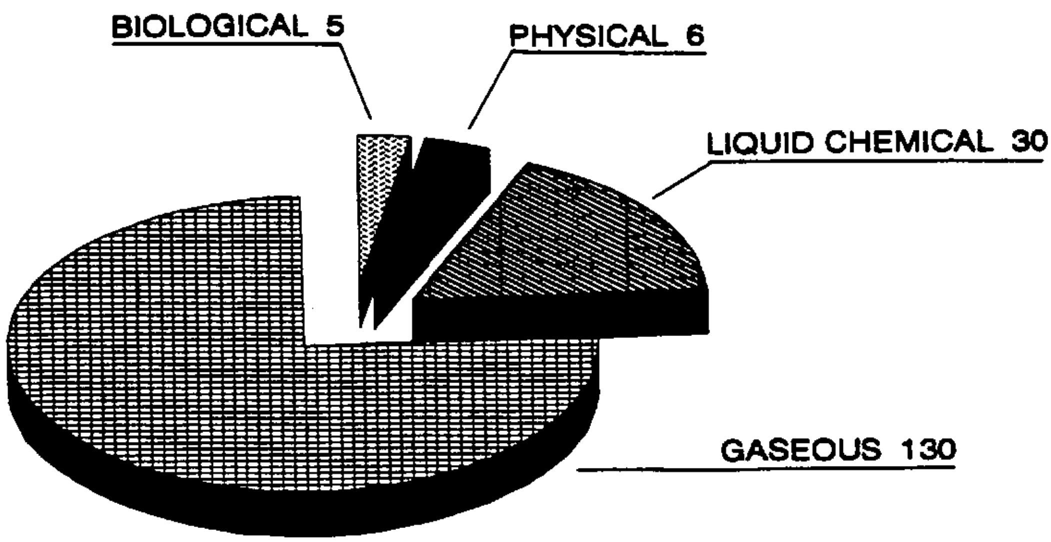

Figure (1.1): *Potential U.K. market for sensors over the next five years; values in £M. (Source: Bogue 1990)*

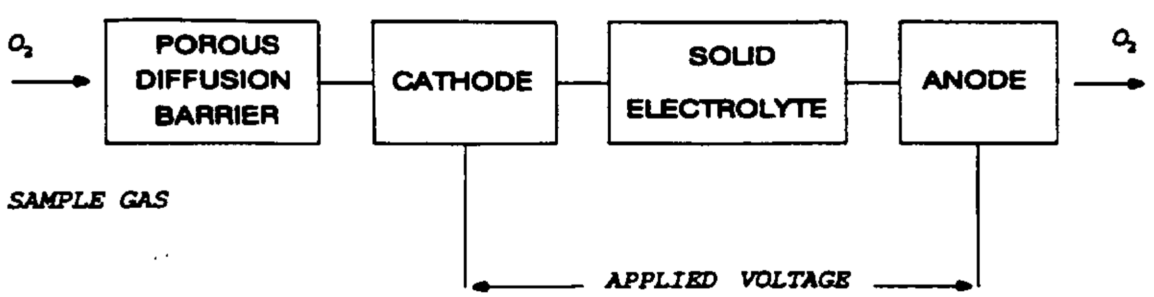

Figure (1.2): *Schematic diagram of a limiting-current sensor. (Source: Dietz 1982)*

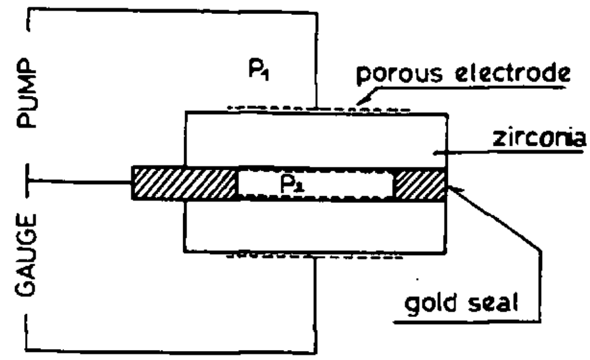

Figure (1.3): Sealed pump-gauge device without heater.

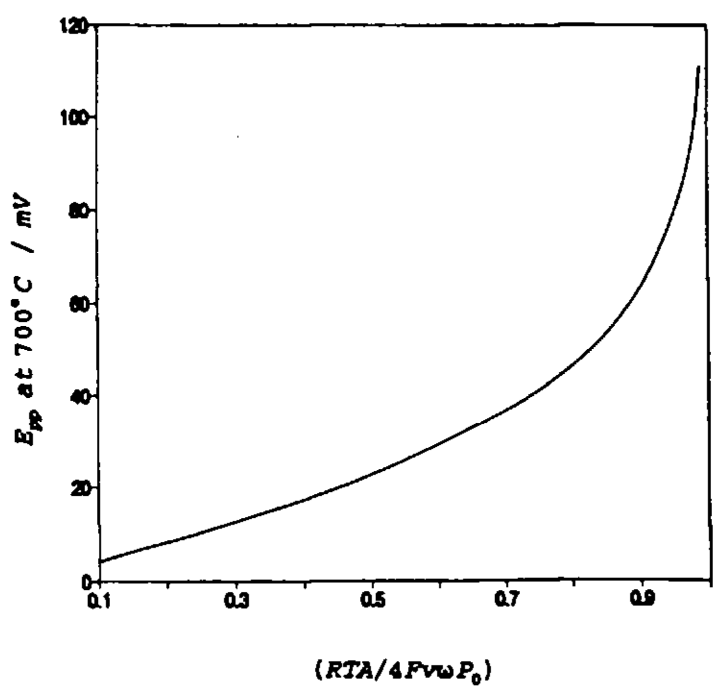

Figure (1.4): Calculated amplitude of the gauge EMF as a function of its level of distortion (i.e. deviation from a sinusoid).

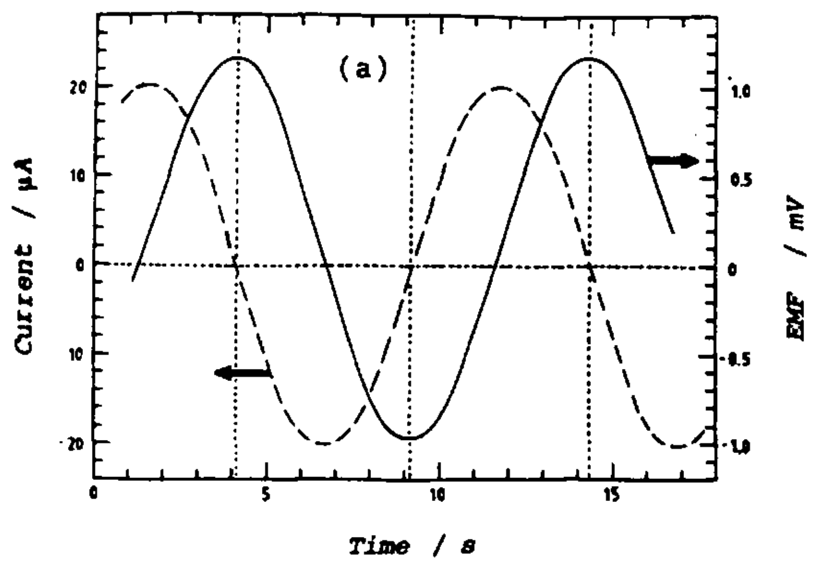

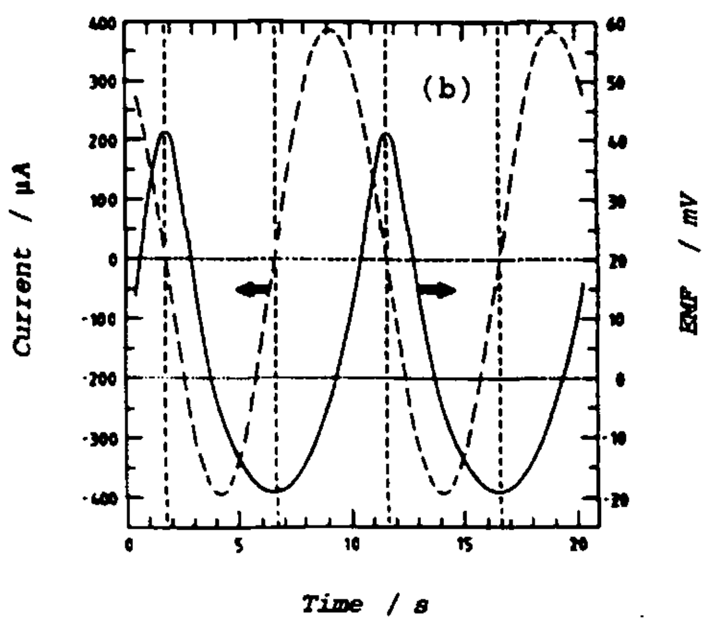

Figure (1.5): *Gauge EMF versus time at 800°C in air, at two different pumping currents. (a): A=20µA, (b): A=400µA. (source: Maskell et al 1987)*

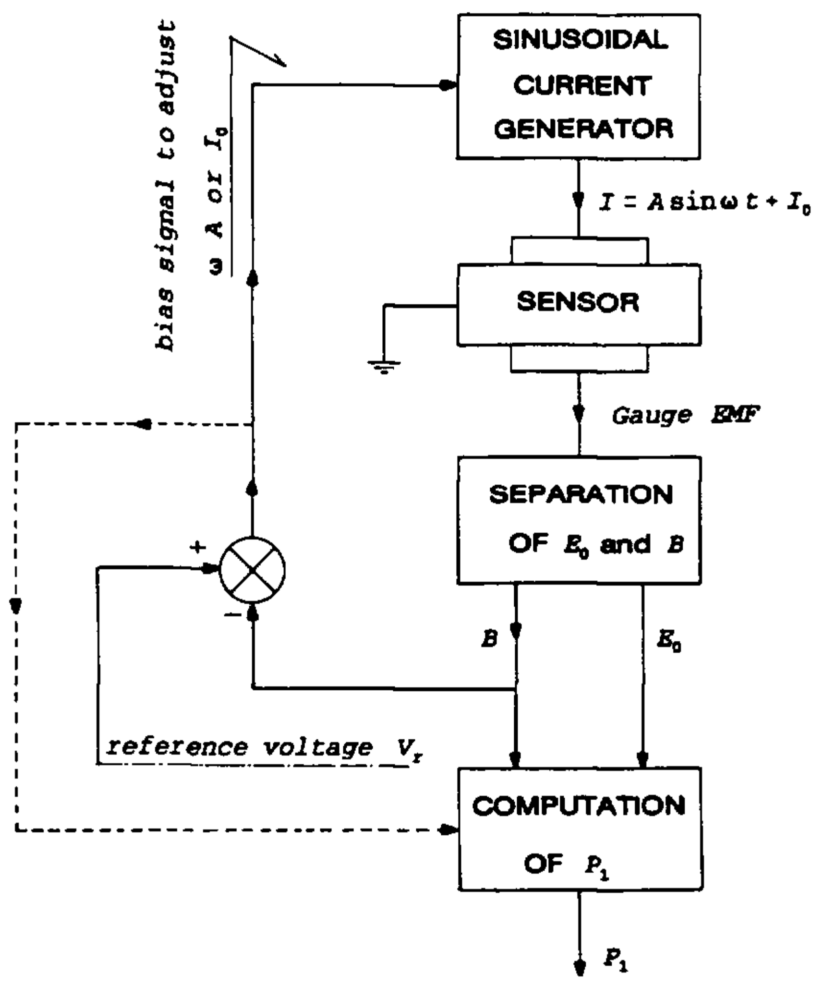

Figure (1.6): Measurement of oxygen partial pressure using pump-gauge device operated in the AC mode: Simplified schematic diagram of the system.

CHAPTER 2

EXPERIMENTAL

"The great tragedy of science - the slaying of a beautiful hypothesis by an ugly fact." Thomas Henry Huxley. Biogenesis and Abiogenesis (1870).

2.1 INTRODUCTION

In this section, the construction of the pump-gauge devices, used in the present work, is described. The various pieces of equipment used in testing the sensors are also described.

2.2 CONSTRUCTION OF FULLY SEALED DEVICES

The zirconia ceramic used for making the device contained 6 mole % Y_2O_3 in ZrO_2 and was so-called partially-stabilised zirconia (PSZ). Other types of zirconia solid solutions include fully-stabilised zirconia (FSZ), typically containing 9 mole % Y_2O_3 in ZrO_2. For a given application, the choice of ceramic type depends upon the ionic conductivity, electronic conductivity, toughness and strength of the material required. The ionic conductivity of PSZ is lower than that of FSZ (Butler et al 1984, Bonanos et al 1984), but the toughness/strength of PSZ is double that of FSZ (Subbarao 1981). The electronic conductivity of both PSZ and FSZ are generally acceptable (Maskell 1991a) over the range of normal operation (P_{O2} values 10^{-18} - 10^{6} Pa).

2.2.1 Preparation of the components

2.2.1.1 Zirconia preparation

The zirconia powder (6Y) was manufactured by TOYO SODA MANUFACTURING CO. Ltd. This powder was pressed in a punch and die followed by isostatic pressing (at 200MPa) into pellets. The pellets were then fired at 1550°C for 2 hours; the temperature was taken up and down at a rate of 5°C/minute. This resulted in pellets 28mm in diameter and 10mm thick with a density of 97% of theoretical.

2.2.1.2 Ceramic drilling and slicing

Cylinders of zirconia were drilled from the pellets using a diamond-tipped hollow drill (from D.K. Holdings, G.B.) fitted into a water chuck. The cylinders were then glued into alumina tubes with Lakeside cement and sliced on a Capco diamond saw to produce discs 7.8mm in diameter and 900μm thick. After cutting, the discs were cleaned with methanol.

2.2.1.3 Grinding

In order to achieve an hermetic seal between the zirconia discs and gold seal, the ceramic is normally ground flat and then polished to a smooth finish. However, this process is lengthy and expensive. The method (Maskell 1991b) employed in the present work did not require the polishing treatment while still resulting in an hermetic seal. Using the normal grinding treatment usually results in a surface with scratches (grooves) traversing the seal; this results in pores connecting the internal volume of the device and external atmosphere with the result that oxygen may leak into or out of the internal volume. The method (Maskell 1991b) obviated this problem by ensuring that grooves did not traverse the seal. This was achieved by rotating the zirconia disc about an axis perpendicular to the fixed grinding surface (carborundum paper, grade 1000) and to the surface being prepared. By ensuring that the axis of rotation was close to the centre of the disc, grooves following segments of concentric circles were obtained. This is illustrated in figure (2.1). This treatment enabled an hermetic seal to be achieved with the gold foil upon sensor assembly.

2.2.1.4 Sputtering and screen printing of the electrodes

Both sides of each disc were masked and then sputtered with platinum using a Nordiko Sputtering Machine (model number NSM2000). The mask allowed a 5mm diameter electrode on each side of the disc. The sputtering time and the R.F. power used were 45min and 100W respectively.

Platinum films were then screen printed over the sputtered electrodes using a non-fritted platinum ink (ESL 5542) from Electro-Science Laboratories. The printing was achieved using a thick film printing machine (type DEK 1202). After printing, the discs were dried and then fired at 1000°C for 15min. The thickness of the electrode, measured using an Alphastep, was 6-8μm.

2.2.1.5 Preparation of the spacers

Rings were cut from alumina tube using the Capco machine. The thickness was 0.8mm and inner and outer diameters were 5 and 7.8mm respectively.

2.2.1.6 Preparation of the gold seal and connections

The gold seals were cut from strips of 50μm thick gold foil (Engelhard) with prepunched 5mm diameter holes. The gold seal consisted of a ring (7.8mm o.d. and 5mm i.d.) with a protruding tab. The latter was used for electrical connections to the electrodes of the device.

2.2.1.7 Preparation of the heaters

Thick film printed heaters have been developed by other workers in the Energy Technology Centre for operation at temperatures in excess of 600°C. The design of the heaters (Maskell 1988) allowed uniform temperature distribution on the substrate. Nine heaters were screen printed on a $650mm^2$, 0.7mm thick alumina substrate. Individual heaters were then laser-cut by Laser Mitronic Ltd. The cut heaters (figure 2.2) were 8mm in diameter with a hole, 1mm in diameter in the middle of the disc. This hole ensured that after assembly, the outer electrodes were exposed to the ambient gas.

Electrical connections to the heaters were made with platinum wire, 0.1mm in diameter using platinum ink (ESL 5544). This resulted in good electrical and mechanical connection after firing at 1000°C for 15min.

2.2.2 Assembly of the sensor

The pump-gauges were assembled as shown in figure (2.3). Each device consisted of 2 zirconia discs, 2 alumina spacers (i.e. rings) 2 gold connections and 1 gold seal. The components were then pressed together with a force of 50N in a jig (figure 2.4) designed for the purpose by other workers in the Energy Technology Centre. The sensor was then fired in the jig in air for 16h at 1025°C (i.e. temperature a little below the gold melting point of 1062°C) resulting in a good seal. The temperature was "ramped" up and down at a rate of 30°C/min.

The connections to the gold tabs were made using platinum wire, 0.15mm in diameter. Silver-loaded glass of melting point 950°C was used to ensure strong connection between the wire and the gold tab.

Each sensor consisted of a pump-gauge device and two heaters attached to the alumina spacers using paste containing powdered glass in an organic medium. The pump-gauge was sandwiched between the two heaters (figure 2.5). The thick films were on the two exposed faces of the assembled device, this configuration improved the temperature distribution, thus minimising the errors introduced by temperature difference between the electrodes (Fouletier et al 1974) and reducing the risk of cracking.

A type R thermocouple (Pt-Pt13Rh) made with wires, 40µm in diameter was attached to one of the heaters using glass allowing the temperature of the sensor to be monitored. The complete sensor was then fired at 1000°C for 15min to allow the glass to melt and secure all connections.

2.2.3 Mounting of the sensor

An 8 way transistor header was used to hold the sensor as shown in figure (2.6). The thermocouple was on the top side of the sensor. The upper half of the sensor was used as the gauge while the lower half was used as pump. A small wad of ceramic fibre (TRITON Kaowool ceramic fibre) was used to create a support for the sensor. The platinum wires used for the electrical connections were wound around the header wires, the joints were then coated with flux and permanent connections made by melting silver solder with a flame from a small hand-held gas torch. The sensor was finally mounted in a holder fitted with an 8-way socket compatible with the transistor header.

2.3 CONSTRUCTION OF LEAKY DEVICES

These devices were constructed in a similar way to the fully sealed sensors. After the grinding treatment of the zirconia discs, holes were laser-drilled by Micrometric Techniques Ltd in the centre of some of these discs. An additional mask was used for the sputtering and screen printing of the electrodes of the laser-drilled discs so that the holes were not covered with platinum. For each leaky device, a laser-drilled disc and a normal disc were used. Once the device had been assembled, the disc with hole(s) was used as the gauge.

2.4 LABORATORY EQUIPMENT USED

2.4.1 Gas mixing equipment

A small brass chamber was made to fit the sensor holder so that the environment around a device could be controlled. Gas mixtures of air and oxygen-free nitrogen were used to test the devices. Mass flow valves of the type 5850TR and 5850E from Brooks Instrument were used to mix these gases (figure 2.7). Each valve allowed a maximum flow rate of 100ml/min. A controller/meter (from Brooks Instrument) was used in conjunction with these valves to provide accurate setting and digital reading (over 3½ digits) of the flow. This controller (model 5878) enabled simultaneous control of four mass-flow valves. Regular checking of the calibration of this equipment was achieved using the burette-bubble technique.

For the measurement of the response time of the devices a fast solenoid valve, with two inlets and one outlet, was used to switch from one premixed gas to another. As shown in figure (2.8), two bubblers were used at the inlets of the valve. This arrangement was adopted to avoid pressure build-up at the non-selected channel (i.e. inlet). The solenoid valve used was of the type G3312-24VDC from BP Pneumatics. This miniature valve (with a nominal power of 0.65 watts) was operated from a 24V DC supply and had a response time of 5ms.

2.4.2 Barometer

The ambient pressure was measured using a barometer from GRIFFIN & TATLOCK Ltd, serial number M766.

2.4.3 Oscilloscope

The digital Tektronix 2211 storage oscilloscope used incorporated important features including a CRT readout and cursor measurement display. It could be used for the measurement of voltage amplitude and phase shift. Associated software (Grabber) enabled the transfer (through a serial port) of captured screen traces from the scope to a microcomputer. These traces, stored in an HPGL-format file could be plotted or printed as required.

2.4.4 Function generator

A Feedback-type function generator (type SFG606, serial number 606/7/CX) was used for the generation of the pumping sinewave and TTL clock. The frequency range of this generator was 0.1mHz--1kHz.

2.4.5 Timer/Counter

A type PACAL-DANA 9900 (serial number: 9531), with a digital display over 6 digits Timer/Counter was used for accurate measurement of the time lapse between two consecutive edges of one or two square waves. The signs of the edges required for starting and stopping count were selected externally. Combination of positive and negative edges enabled measurement of signal periods, phase shifts, mark-to-space ratio (MSR), etc....

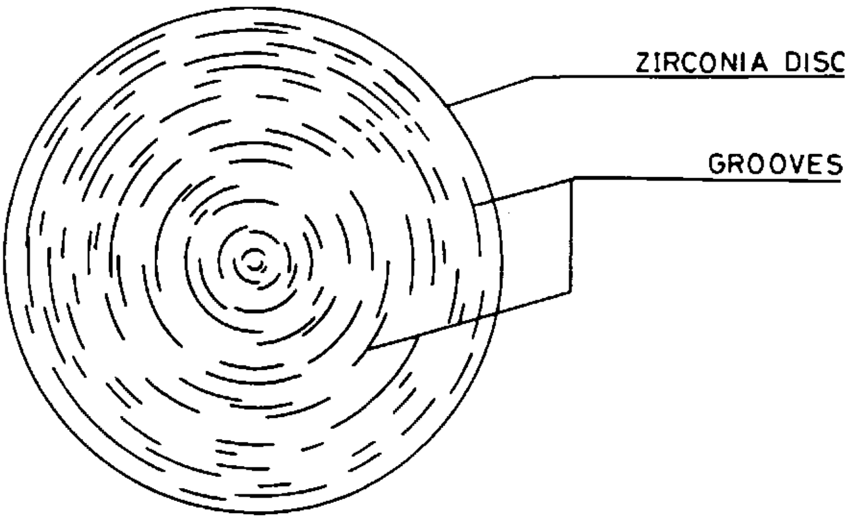

Figure (2.1): Typical pattern of grooves resulting from the grinding method used. (source: Maskell 1991b)

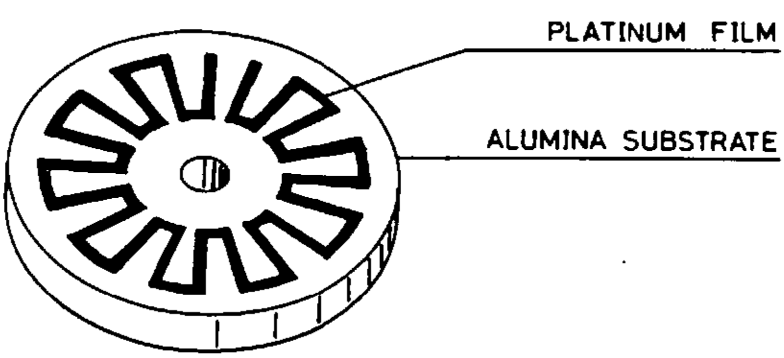

Figure (2.2): Thick film platinum heater on an alumina substrate.

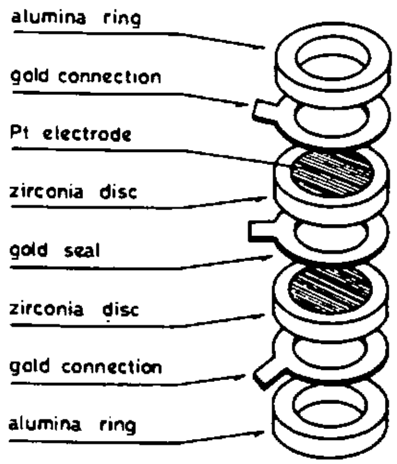

Figure (2.3): Assembly of the pump-gauge device.

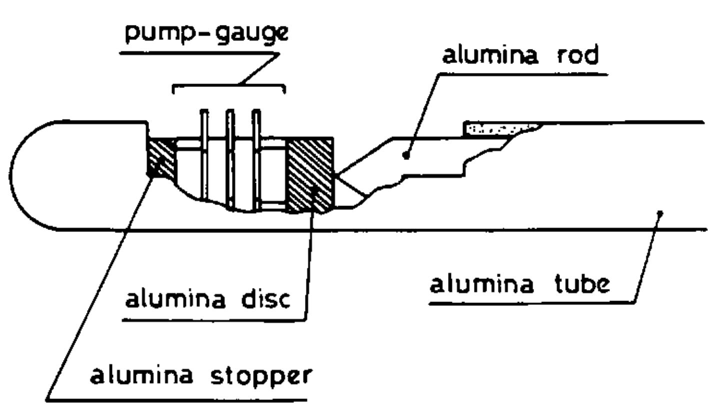

Figure (2.4): Jig used for assembling the device: The alumina rod was spring-loaded with a force of 50N; the device in the jig was then fired in air at 1025°C for 16h.

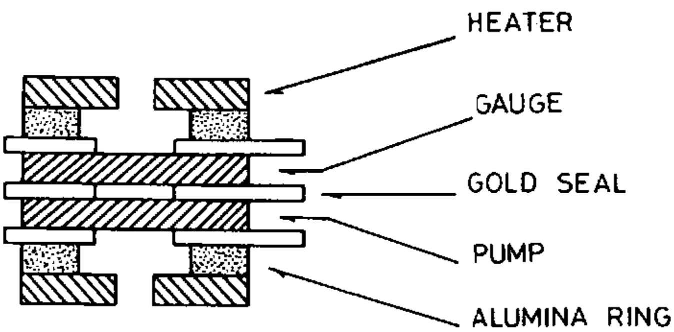

Figure (2.5): Cross-section of the complete sensor.

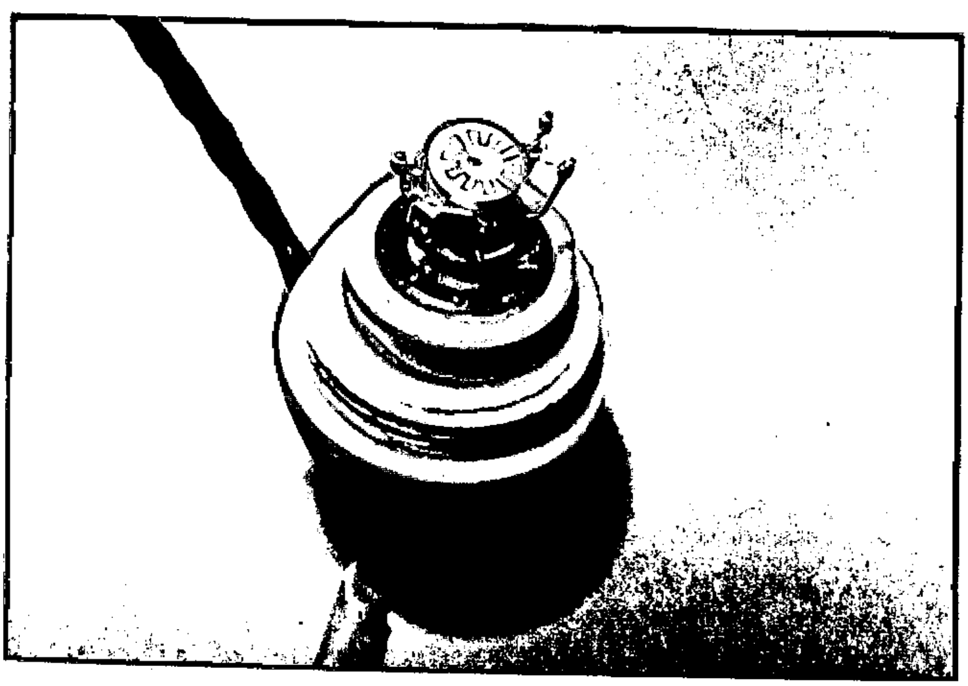

Figure (2.6): Photograph of the complete sensor mounted on a transistor header.

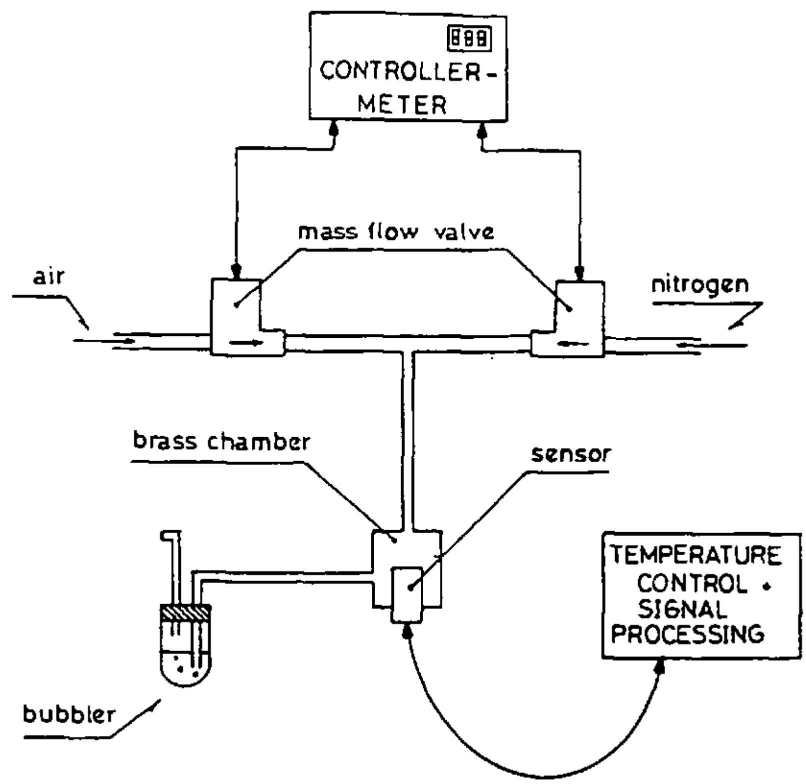

Figure (2.7): Arrangement used for testing the sensor.

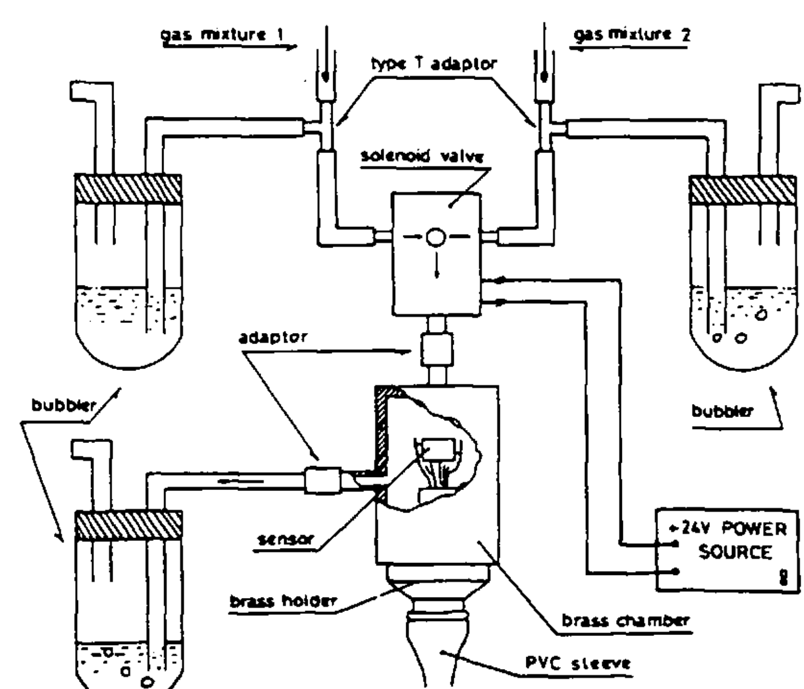

Figure (2.8): System used for evaluating the response time of the sensor.

CHAPTER 3

OPERATION OF SEALED PUMP-GAUGES IN THE POTENTIOMETRIC MODE

"All things are possible until they are proved impossible -

and even the impossible may only be so, as of now."

Pearl S. Buck, A Bridge for Passing (1962),3.

3.1 INTRODUCTION

The theory of operation in the AC mode of sealed pump-gauge devices has been developed by Maskell et al (1987). This theory, given in Chapter 1, predicted that under a sinusoidal pumping current, the device should produce a pseudo-sinusoidal EMF. Under simplifying condition, the AC component of the gauge EMF may be assumed sinusoidal. This AC component was dependent on P_0. The DC component of the gauge EMF on the other hand was dependent on both P_1 and P_0.

Maskell et al (1986) suggested that by appropriate signal processing the AC and DC components of the gauge EMF may be separated. From the AC component, the mean internal oxygen partial pressure P_0 may be determined, then from the DC component potentiometric measurement of P_1 may be made relative to the known P_0 and hence in the present work this mode of operation has been termed the "Potentiometric Mode".

In this chapter various methods suggested by Maskell (1986) for the practical implementation of this mode of operation are discussed. A number of practical refinements have been added to ensure high performance.

3.2 SEPARATION OF THE AC AND DC COMPONENTS

Phase Sensitive Detection (PSD) is a powerful technique which may be used for the measurement of the mean amplitude of AC signals, often obscured by noise.

PSD is normally used in applications where the signal results from the application of an AC stimulus to a system under test (Blair and Sydenham, 1975). In order for PSD to operate it requires a reference signal coherent with the signal of interest. This reference is in general obtained from the AC stimulus. The PSD can be viewed as a synchronously driven full-wave rectifier. The coherent input signal gives a DC output after filtering, the value of which depends on both amplitude and phase of the input signal. The non-coherent signal accompanying the signal of interest is filtered out because of the zero average value of the rectified output. The PSD can be highly selective making it widely used in instrumentation including the use as a power factor meter (Babu and Wong, 1989), in modulated Wheatstone bridge circuits (Jones and Richards 1973, Stacey et al 1969, Bach et al 1970, Pardy 1969, Williams 1965, Mukhopadhyay and Raychaudhuri 1986), in various auto-ranging component meters (Evans and Skyes 1989, Riggs and Evans 1981, Oliver and Cage 1971) and many more applications in instrumentation (Huang et al 1988, Tay and Murti 1984, Miramontes and Castro 1990).

In the present application PSD may be used for the measurement of the amplitude of the AC component of the gauge EMF. The DC component of the EMF may be easily measured using a sample and hold circuit as described below.

3.3 THEORY OF OPERATION

Under the low amplitude condition (eqn.1.20),

$$\frac{RTA}{4Fv\omega P_0}<0.1 \tag{1.20}$$

the AC component of the EMF (E) may be assumed sinusoidal. From eqn.(1.22)

$$E = \frac{RT}{4F}\ln\left(\frac{P_1}{P_0}\right) - \frac{R^2T^2A}{16F^2v\omega P_0}\cos x \tag{1.22c}$$

The amplitude (B) of the AC component (eqn.1.22b) is inversely proportional to P_0. From a measurement of B, P_0 may be calculated:

$$P_0 = \frac{R^2T^2A}{16F^2v\omega}\frac{1}{B} \tag{1.24}$$

The DC component (E_0) of the EMF is given by eqn.(1.22a). The external oxygen partial pressure may then be determined from the known P_0 and a measurement of E_0.

$$P_1 = P_0\exp\left(\frac{4F}{RT}E_0\right) \tag{3.1}$$

3.3.1 Measurement of P_0

The measurement of B may be achieved using PSD with a square wave as reference signal as shown in figure (3.1). The PSD is then a synchronised rectifier followed by an averaging low pass filter. The output of the PSD, V_p, is given by

$$V_p = \frac{1}{2\pi}\int_{\pi/2}^{3\pi/2} E dx - \frac{1}{2\pi}\int_{3\pi/2}^{5\pi/2} E dx \tag{3.2}$$

Under the simplifying condition (eqn.1.20), the gauge EMF (E) is given by eqn.(1.22c) and it can readily be shown that

$$V_p = \frac{R^2T^2A}{8\pi F^2 v\omega P_0} = \frac{2}{\pi}B \tag{3.3}$$

This result is valid only under the low gauge-amplitude condition (eqn.1.20) equivalent to an AC component less than 4.2mV peak-to-peak at 700°C.

The disadvantage of the application of this theory is the restriction imposed on the amplitude of the AC component of the gauge EMF and consequent low signal-to-noise ratio as well as offset problems. It is shown below, however, that the method is applicable using AC signals with much larger amplitude without introducing significant errors in the computation of P_1 and P_0; thus the signal-to-noise ratio may be improved without penalty. The general expression of the EMF is given by eqn.(1.19)

$$E = \frac{RT}{4F}\left[\ln\left(\frac{P_1}{P_0}\right) - \ln\left(1 + \frac{RTA}{4Fv\omega P_0}\cos x\right)\right] \tag{1.19}$$

Using eqn.(3.2) the output of the PSD, V_p, was numerically calculated for an EMF, E, given by eqn.(1.19). As shown in figure (3.2), numerical integration indicated that

for

$$\frac{RTA}{4Fv\omega P_0} \leq 0.35 \tag{3.4}$$

the following relation may be written with a maximum error of only 2%

$$V_p = \frac{R^2T^2A}{8\pi F^2 \nu\omega P_0} \tag{3.5}$$

The linearity between V_p and $(1/P_0)$ suggests that the method for measurement of P_0 may be used with signals with large distortion (≡large amplitude). The condition of eqn.(3.4) is equivalent to an AC component less than 15.3mV peak-to-peak at 700°C.

Maskell et al (1986) suggested the operation of the sensor in a closed loop system in which the condition represented by eqn.(1.20) may be satisfied by applying a bias signal in order to adjust A,ω or P_0. The same principle may be applied for signals with high distortion in order to satisfy eqn.(3.4).

3.3.2 Computation of P_1

The component E_0 of the gauge EMF (eqn. 1.22a) may be determined by measuring the value of the gauge EMF (eqn.1.19) at x=(π/2)+nπ, (n=1,2,3.....). P_1 may then be determined using eqn.(3.1). From eqn.(3.1) and eqn.(3.5) the following equation may be written

$$E_0 = \frac{RT}{4F}\left[\ln(P_1 V_p) + \ln\left(\frac{8\pi F^2\nu\omega}{R^2T^2A}\right)\right] \tag{3.6}$$

This equation is used later to compare theory with observation.

3.4 CONTROL OF THE AMPLITUDE OF THE AC COMPONENT

The methods suggested by Maskell (1986) were based on adjusting one of the variables (ω, A, P_0) in order to keep the amplitude of the AC component within a certain range.

3.4.1 Control of ω

This method (figure 3.3) was based on the use of a voltage controlled oscillator. The bias signal necessary for controlling the frequency of the pumping current was obtained from a measurement of the amplitude of the AC component.

In practice, there are serious complications for the practical implementation of this method. In addition to the fact that the range of operating frequency is limited by the sensor response, the practical implementation would require the use of filters with variable characteristics in order to match the variable operating frequency. This is extremely difficult to achieve especially at the operating frequency range of the sensor (up to 5Hz). The computation of P_1 would require the use of three variables (V_p, E_0 and ω).

3.4.2 Control of A

This solution was based on adjusting the amplitude of the current using a four quadrant multiplier (figure 3.4). This method should not require complicated hardware. However, care must be taken to ensure that the maximum pumping current does not require high voltage across the pump which may induce electronic conductivity. The computation of P_1 would require the use of three parameters (V_p, E_0 and A).

3.4.3 Control of P_0

This solution (figure 3.5) was based upon adjusting the mean internal oxygen partial pressure. This pressure may be easily controlled by applying a bias current to the pump of the device. Similar systems were used by Meas (1978), Alesksakov and Godin (1982) and Agrawal et al (1974) to control oxygen partial pressure inside the sealed chamber using air as reference gas. In other modes of operation Dietz (1982) and Hetrick (1981) have used bias signals to control the ratio between the external and internal pressures in pump-gauge devices. The computation of P_1 would require the measurement of two parameters only (V_p and E_0). Ideally, P_0 could be kept constant by keeping V_p constant and the computation of P_1 would become easier. This method does not require complicated hardware and therefore was adopted in the present work.

3.5 PRACTICAL IMPLEMENTATION

Figure (3.6) shows the schematic disgram of the circuit used for testing this mode of operation. The output V_p of the PSD was compared to a reference voltage V_r to produce the bias signal required for the control of P_0. The circuit was constructed using analogue electronics, although a combination of analogue and digital electronics could be used but would not offer any significant advantage at this stage. If, however, the sensor were part of a complete system used to measure and control oxygen partial pressure, then a microprocessor could be used to process the gauge EMF, convert it into measurement of P_1 and simultaneously to take appropriate action in order, for instance, to maintain the oxygen partial pressure equal to a preset value.

The detailed circuit diagram of the electronics is given in figure (G.10) in Appendix (G). In the following the various blocks of the diagram of figure (3.6) are discussed separately.

3.5.1 Sinewave generator

Earlier work (Maskell et al 1987) indicated that the upper limiting operating frequency of the sensor was in the region of 1Hz. However in the present work it was found that the sensor worked satisfactorily at frequencies up to 5-6Hz. The operating frequency is limited by a number of factors (Fouletier et al 1974) including the operating temperature, the internal partial pressure, the ceramic type, and the electrode composition and preparation procedure. Unless otherwise specified the operating frequency used was 4Hz. The choice of this frequency was a compromise taking into account the easy practical implementation of the electronics and lower sensor sensitivity to leakage (see Chapter 6) at higher frequencies and the ideal behaviour of the perfectly sealed sensor at lower frequencies. In the present work, the sinewave generator used was adopted from Jung (1974).

3.5.2 Voltage to current converter

Bipolar voltage controlled current sources have large scale application in instrumentation. A number of authors (Hart and Barker 1975, Haslett and Rao 1980) have described a variety of schemes; most of these rely on accurate transistor-based current mirrors for the purpose of transfer of current to the output. To avoid the problems associated with the requirement for precision mirrors, some authors (Graeme et al 1971, Huijsing 1990, Patranabis et al 1986, Patranabis et al 1988, Kahler 1979, Morgan et al 1986) have described circuits using a combination of monolithic and discrete components. However the number of constraints put on the passive components in most of these schemes makes the implementation very difficult. The converter used was adopted from Froelicher et al (1980). It was easy to implement and required one operational amplifier only. This was capable of delivering the maximum pumping current (1mA) used in the present work.

3.5.3 Amplifier and voltage limiter

To have fast response of the control loop and to minimise errors at steady state, a simple proportional type controller was found to give satisfactory results. In most feedback controlled systems, voltage limiters are used for the bias signal (Meas 1978, Agrawal et al 1974) to avoid high distortion of the stimulus, i.e. sinewave in the present work. The voltage limiter should not affect the performance of the system at steady state where the bias signal should be very low.

3.5.4 Instrumentation amplifier

Any device connected to the gauge must have high input impedance to avoid stray current that may electrochemically transfer oxygen into or out of the internal volume (Heyne 1974). To minimise such currents a high input impedance, low drift instrumentation amplifier was used.

3.5.5 Measurement of the amplitude of the AC component

Many authors have described practical realisations for the PSD, namely Clayton (1973), Jones and Richards (1973), Marzetta (1971), and Williams (1965). In the present work, the PSD was built around an FET transistor and two operational amplifiers.

3.5.6 Computation of the external oxygen partial pressure

The measurement of E_0 was obtained using a sample and hold circuit which was synchronised with the pumping sinewave. The sample and hold circuit used was the LF398. The trigger input of this circuit was obtained from the pumping sinewave using a combination of comparator and differentiator circuits.

3.5.7 Circuit modification

As shown in figure (3.7) additional elements had to be added to the circuit to ensure proper functioning of the system.

When switching on the electronics the output of the PSD was initially low because of the time constant of its internal low pass filter. This was interpreted by the control loop as a very high mean internal oxygen partial pressure P_0. The amplified bias signal, obtained from the difference between the reference voltage V_r and the output of the PSD, was high and produced a positive current which pumped oxygen out of the device. This led to a fast rise of the DC component causing saturation of the instrumentation amplifier. The PSD then did not detect any AC component and the bias signal remained high: the system never recovered. To solve this problem, the reference voltage was increased slowly from zero when switching on, thus allowing a soft start of the loop. This was achieved by the inclusion of a low pass filter in the circuit generating the reference voltage (see figure G.10 in Appendix G).

To achieve good accuracy, high amplification of the EMF was required. This arose because of the restriction imposed on the amplitude of the AC component. If P_1 changed to a value out-of-range, the DC component of the EMF became very high and caused saturation of the instrumentation amplifier. The system saturated for the same reasons explained above. The loop could not recover even if P_1 went back to within the working range. To solve this problem, a second loop was added in the circuit (Fig.3.7). A window comparator (Graeme 1973) produced a signal to keep the DC component within a certain range far from saturation levels of the instrumentation amplifier. A similar system has been used by Filanovsky and Stromsmoe (1986) to control the amplitude of an RC oscillator. When used in the present application an auto-ranging system may be achieved by using the signal from the window comparator. The latter may be used to indicate whether to switch to a higher or lower range to bring the system to steady state. The various ranges may be obtained by using a variable amplitude for the pumping current.

3.6 EXPERIMENTAL

The device (with approximately $0.98mm^3$ internal volume) was tested in the excess-air region by mixing air and nitrogen at the atmospheric pressure using mass flow controllers as described in Chapter (2). The system was primarily destined for use in domestic boilers (Patterson and Dann 1985, Franx 1982, Bergman and Franx 1984) working nominally at 20% excess air (i.e. 5% oxygen in the exhaust). Therefore, tests were made at the ambient barometric pressure (0.1MPa) in the oxygen partial pressure range 1-10kPa. However the system may be operated in any range by appropriate choice of the reference voltage V_r and/or the amplitude of the pumping current (i.e. for a constant temperature and frequency). The device was operated at 700°C and temperature was controlled to ±5°C (Benammar and Maskell 1989). The amplitude of the pumping current was 1mA and the reference voltage V_r was chosen to keep the amplitude of the AC component less than 12mV peak-to-peak.

3.7 RESULTS AND DISCUSSION

The separation of the AC and DC components is shown in figure (3.8). The AC component was obtained from the output E_0 of the sample and hold circuit and the gauge EMF, E, using an adder.

Figure (3.9a) shows the amplitude of the AC and DC components for the oxygen partial pressure range 1-10kPa. The variation of the amplitude of the AC component indicates that the control loop was unable to hold P_0 constant within the whole range of P_1. This can be explained by the presence of physical and electrochemical leakage (refer to Chapter 6) of oxygen into and out of the internal volume. Within the range 1-10kPa, E_0 was negative (Figure 3.9a). This indicates that the mean internal oxygen partial pressure (P_0) was higher than P_1 (see eqn. 3.1); for P_1 varying between 1 and 10kPa, calculation (using eqn. 3.1) suggested that P_0 varied between 5.3 and 12.7kPa. Therefore under the operating conditions, oxygen was effectively leaking out of the device.

The results shown in figure (3.9b) were obtained using data from figure (3.9a). The straight line obtained indicates good agreement with the theory (eqn.3.6). The slope of the straight line was equal to 0.98 which was in good agreement with the theoretical slope (i.e. equal to 1.00). From the intercept of the straight line in figure (3.9b), the internal volume may be determined. This intercept was equal to -2.47 and led to v=0.94mm^3 which was in good agreement with the value determined from the dimensions of the seal (0.98mm^3).

3.8 CONCLUSION

By using appropriate signal processing, oxygen partial pressure measurement over a wide range was achieved using pump-gauge devices operating in the

AC mode. Good agreement between the theory and experimental results was demonstrated. However, because it was not possible to maintain the mean internal oxygen partial pressure constant, the computation of the oxygen partial pressure of the sample gas required the measurement of two signals. This is a disadvantage which could be ameliorated if the device used were replaced by one with substantially lower leakage, in which case one of the two measured signals (V_p) could readily be maintained constant. Future work will be aimed at improving the quality of the seal which should make the practical implementation of the electronics for this mode simpler.

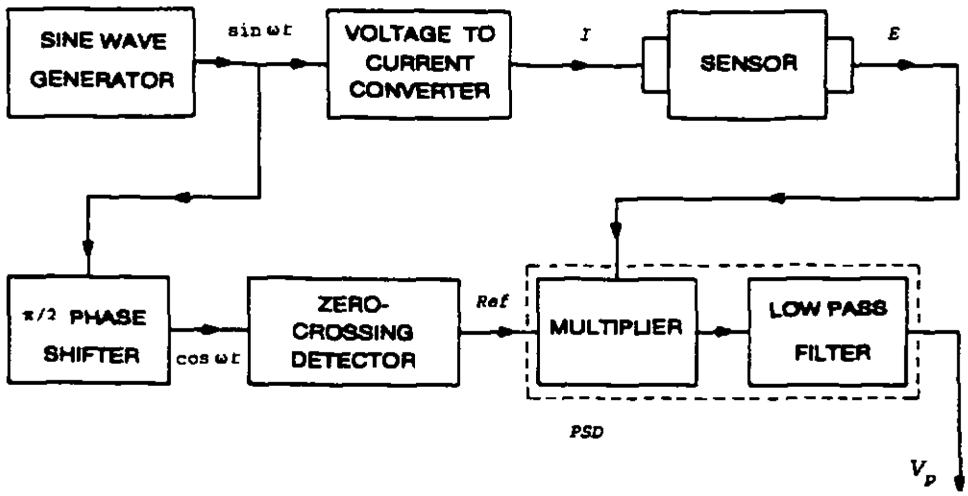

Figure (3.1): Measurement of the amplitude of the AC component using PSD technique.

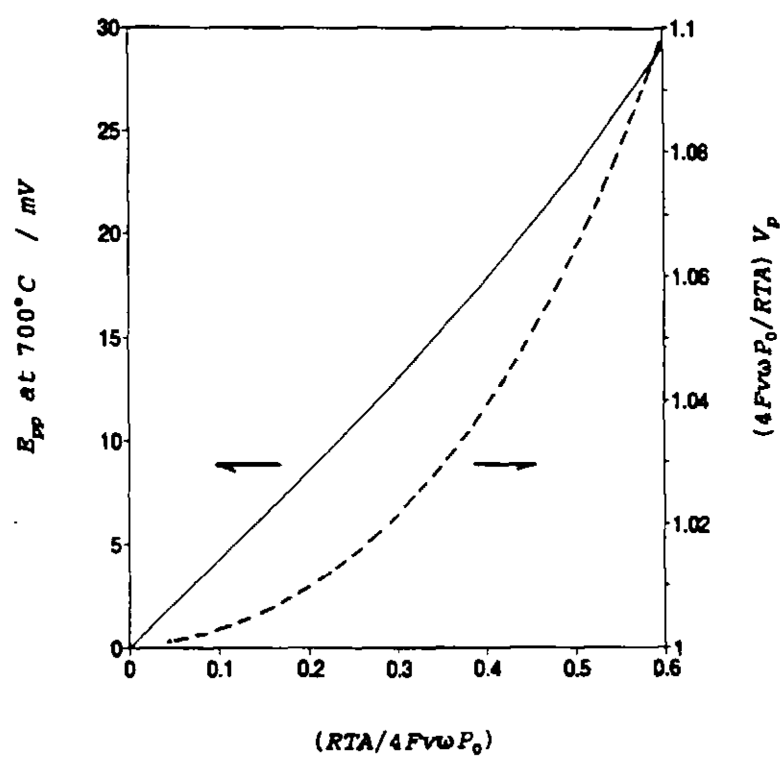

Figure (3.2): Calculation of the output (V_p) of the PSD using eqn.(3.2).

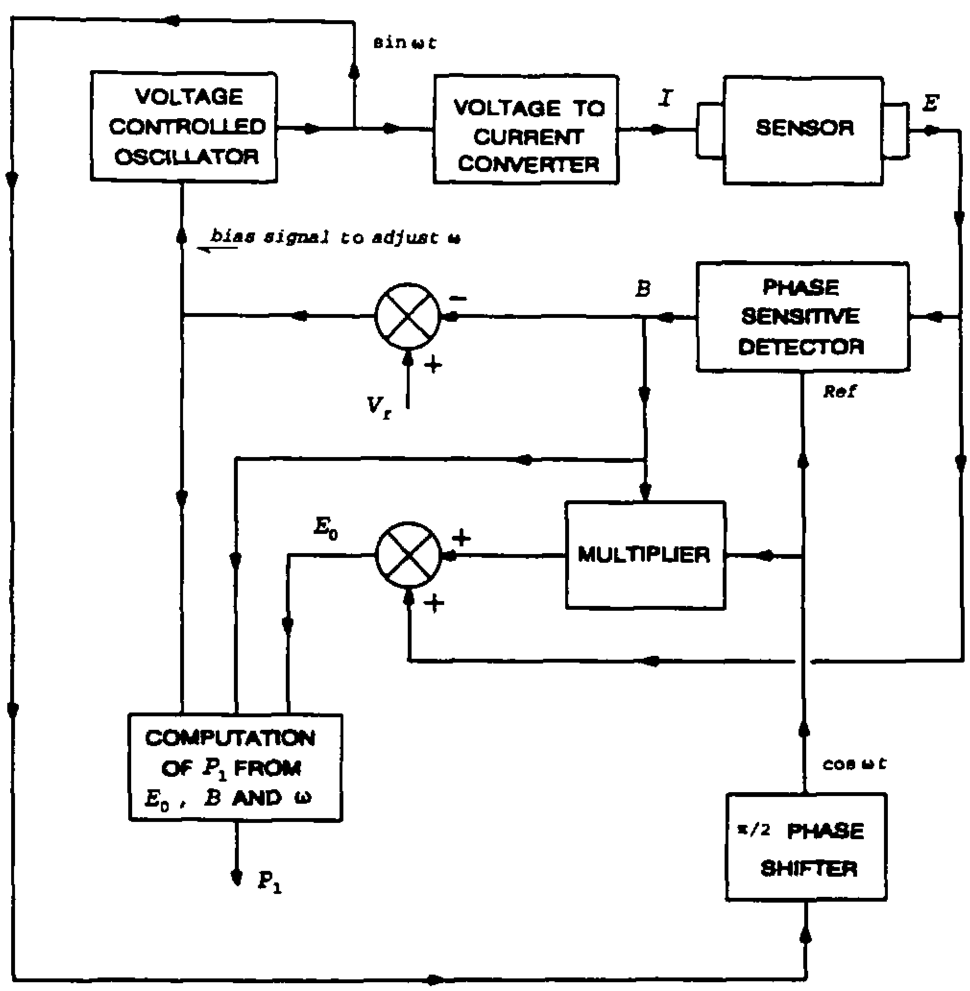

Figure (3.3): Control of the amplitude (B) of the AC component by adjusting the frequency of the pumping current.

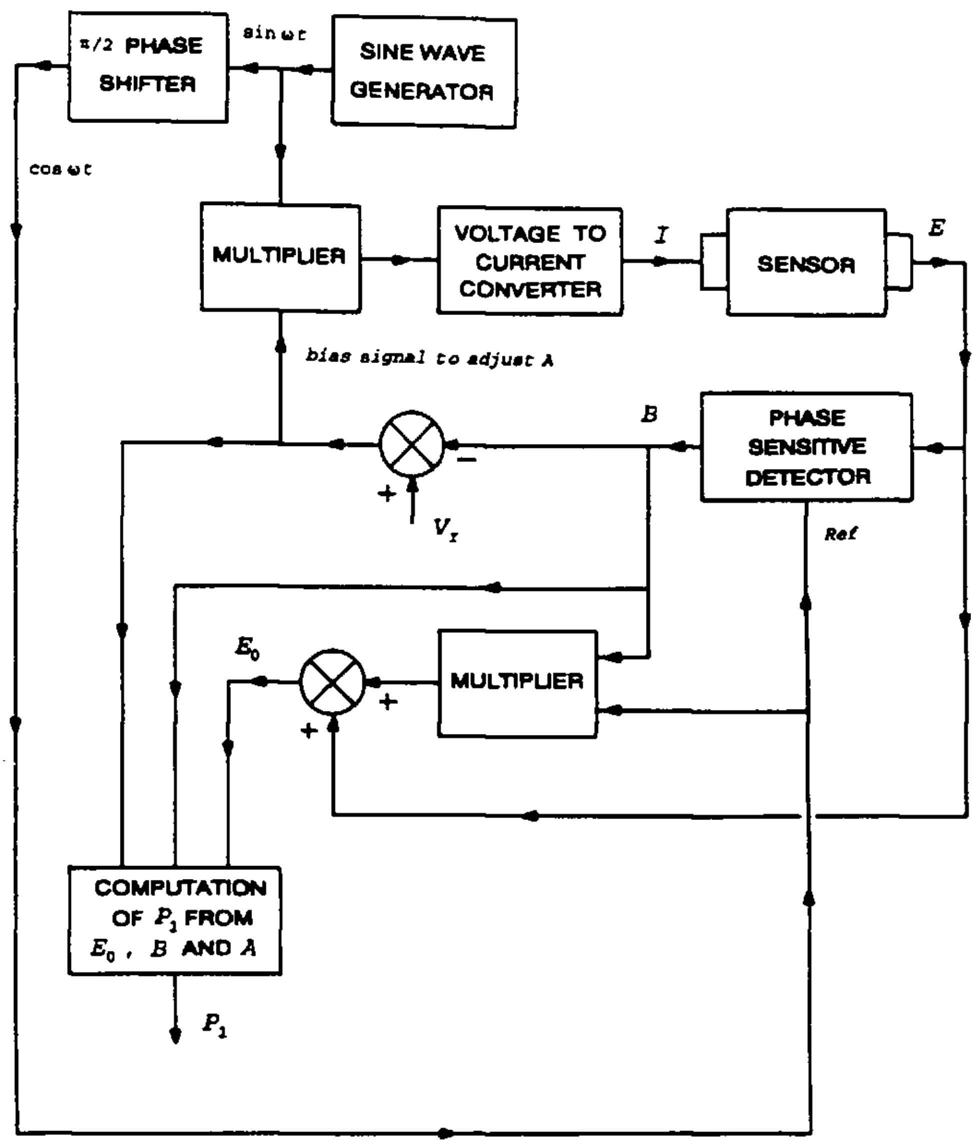

Figure (3.4): Control of the amplitude (B) of the AC component by adjusting the amplitude of the pumping current.

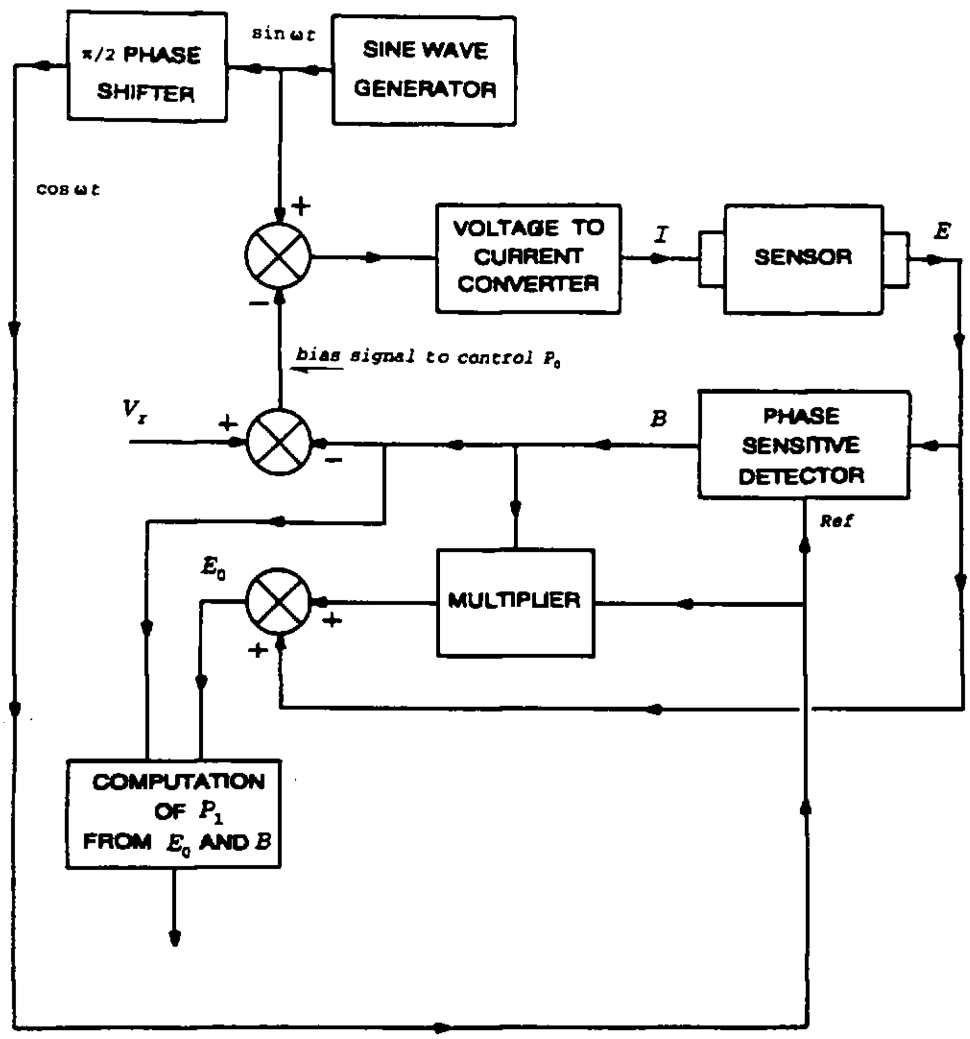

Figure (3.5): Control of the amplitude (B) of the AC component by adjusting the mean internal oxygen partial pressure.

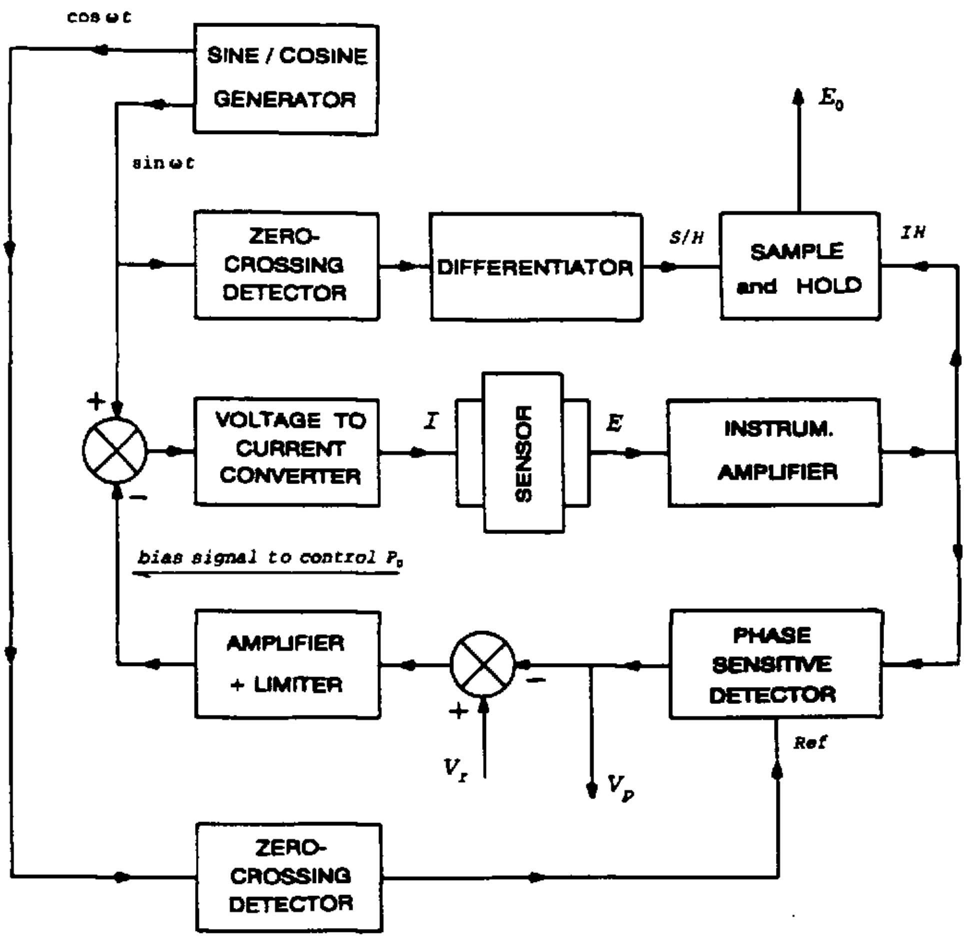

Figure (3.6): Schematic diagram of the circuit adopted for implementing the Potentiometric Mode of operation of sealed pump-gauge devices.

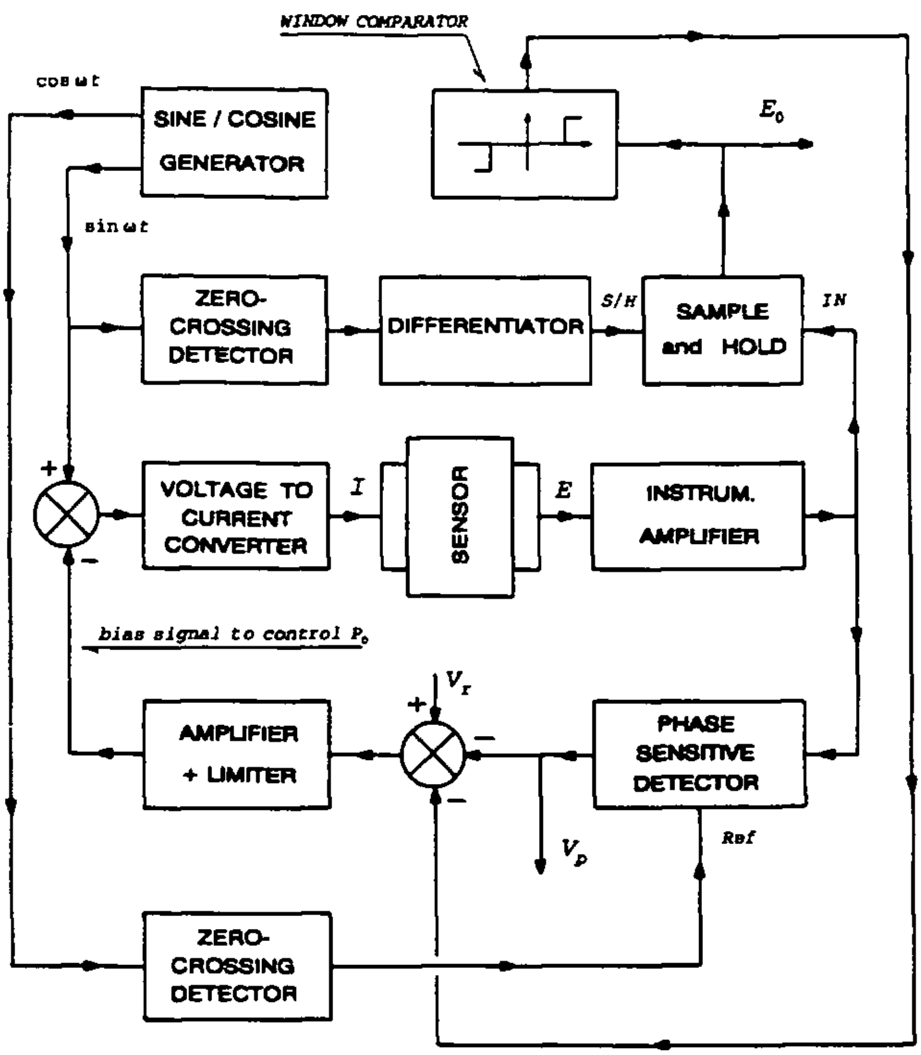

Figure (3.7): Modified version of the circuit of figure (3.6) to solve the problem of saturation of the instrumentation amplifier.

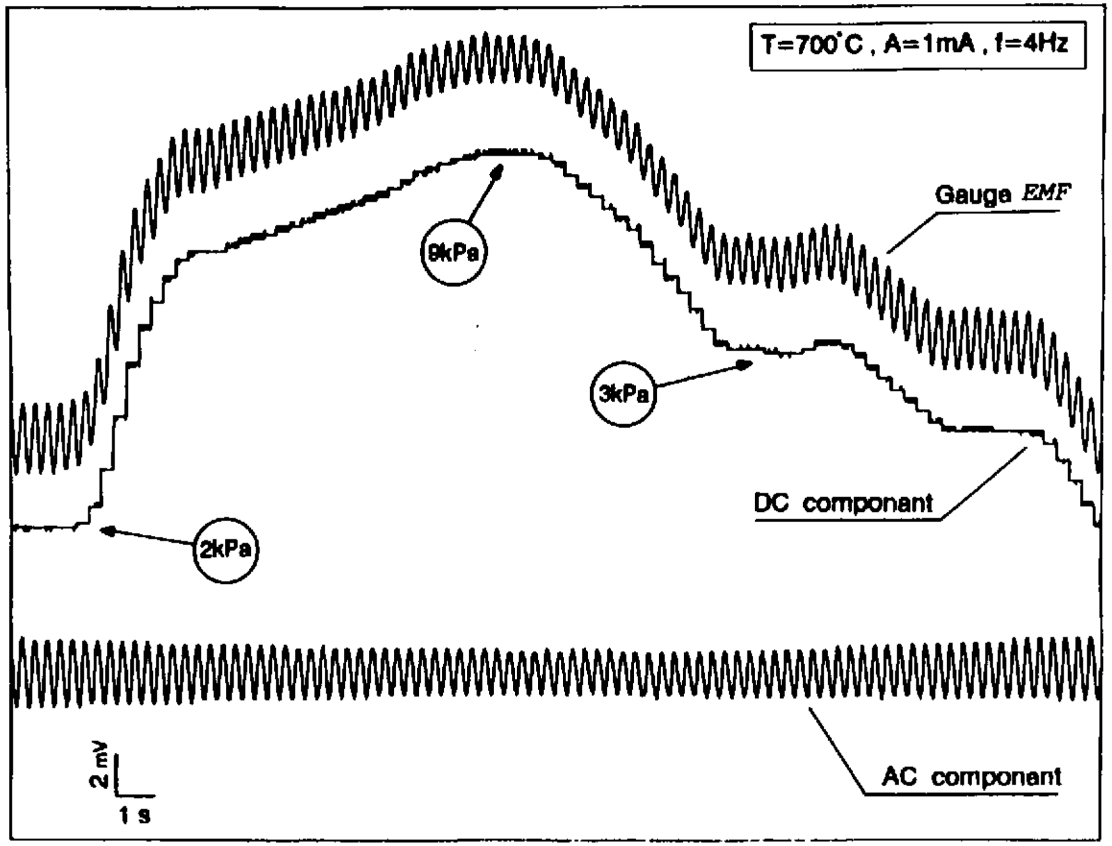

Figure (3.8): Results obtained by operating a sealed device in the Potentiometric Mode: separation of the AC and DC components of the EMF. The AC component was reconstructed from the DC component and the gauge EMF using an adder.

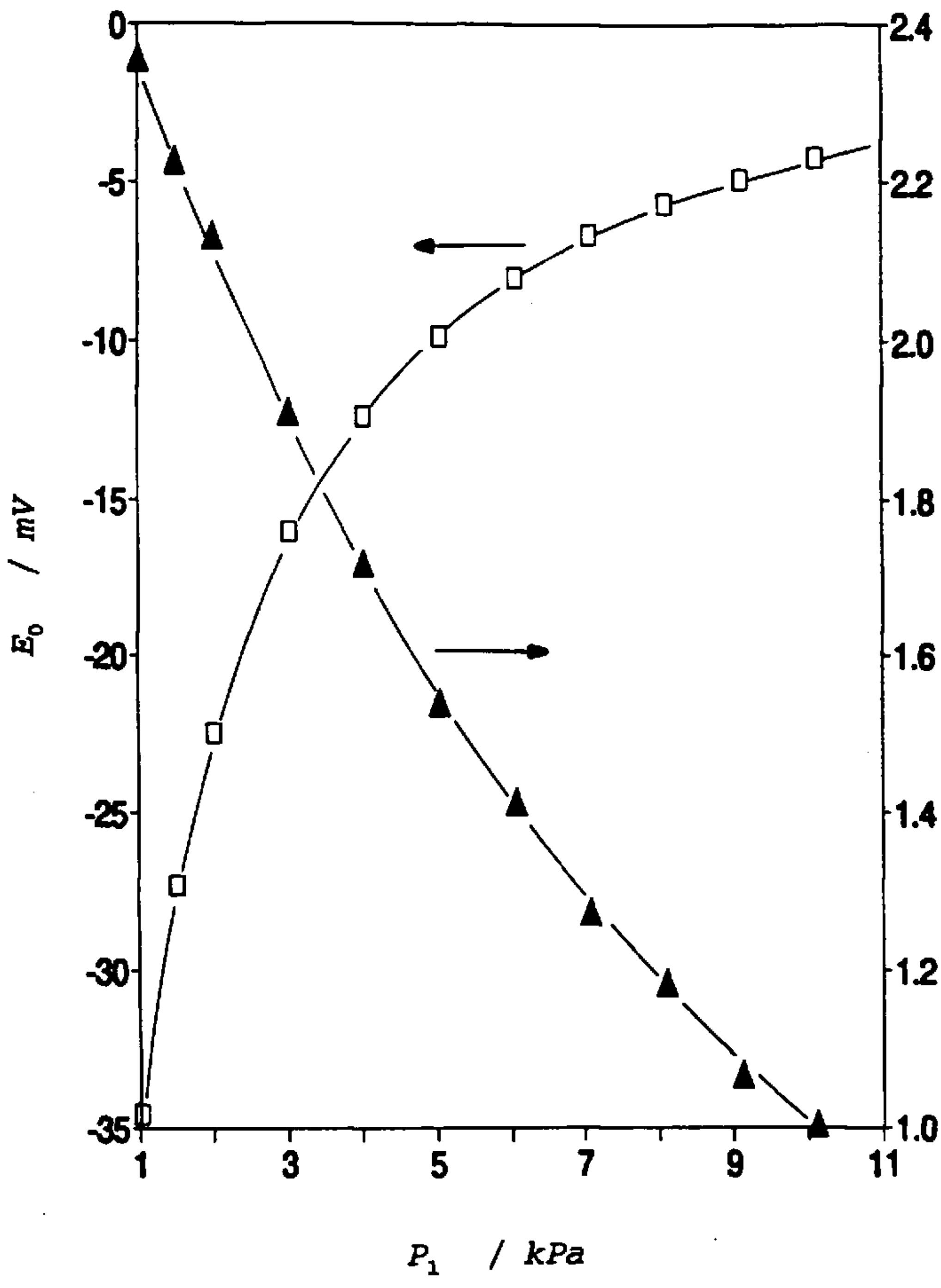

Figure (3.9a): *Typical results obtained by operating a device with an internal volume of 0.98mm^3 in the Potentiometric Mode. The plotted data does not include an amplification factor. T=700°C, A=1mA, f=4Hz.*

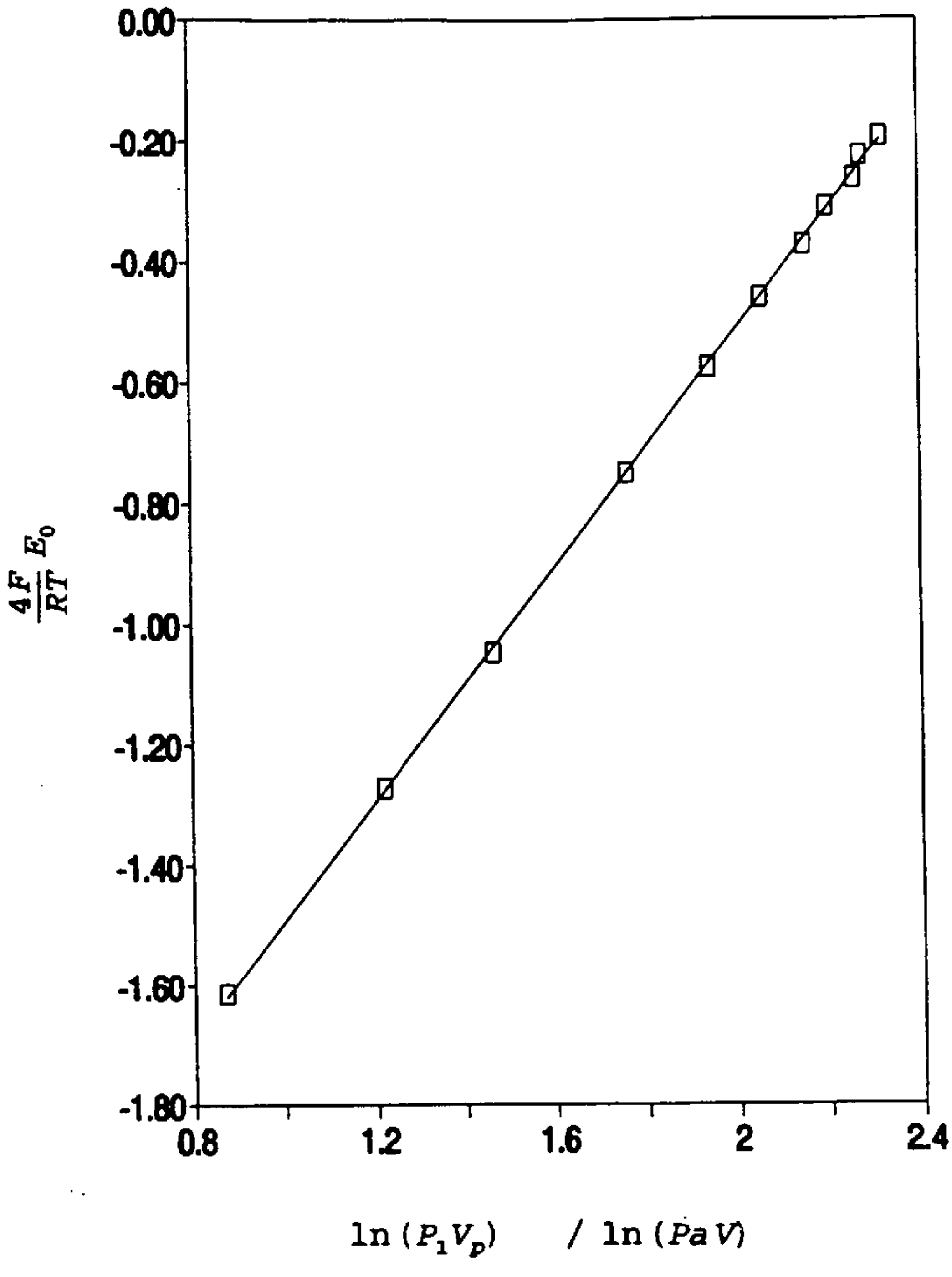

Figure (3.9b): Plot of the component E_0 of the gauge EMF versus $ln(P_1V_p)$ using the data of figure (3.9a).

CHAPTER 4

OPERATION OF FULLY SEALED PUMP-GAUGES IN THE TRACKING MODE

"The whole science is nothing more than a refinement of everyday thinking" EINSTEIN, Out of my later years (1950), 13.1.

4.1 INTRODUCTION

The Potentiometric Mode of operation of the pump-gauge described in the last chapter was successfully implemented and tested. It was found however that the practical analogue implementation required relatively complicated hardware to overcome various problems.

In this chapter a novel and simple mode of operation of the pump-gauge device is described. This method was based on the theory of operation of fully sealed devices in the AC mode.

4.2 PRINCIPLE

The device was operated in a closed loop system. A bias current obtained from a measurement of the DC component of the EMF, was used to control the mean internal oxygen partial pressure P_0. By adjusting the P_0, the control loop ensured that, at steady state, a well defined relation between P_0 and P_1 waa maintained. Thus P_0 followed (or tracked) the variations of the external O_2 pressure and hence the designation Tracking Mode.

It is shown that in the Tracking Mode the amplitude of the AC oscillation of the EMF was directly related to the external oxygen partial pressure. On the other hand the amplitude of the EMF was shown to be related to its level of distortion caused by the logarithmic effect on the cosine (Chapter 1, figure 1.4). The analysis of this mode was therefore done using the original equation for the EMF (eqn.1.19). This study enabled the device to be used with large

AC signals making it possible to cover a wide range of oxygen partial pressures. It also improved the signal-to-noise ratio and minimised the effects of offsets.

Note that when compared to the case of the Potentiometric Mode, the roles of the AC and DC components of the EMF were reversed. In the Potentiometric Mode the amplitude of the AC component was used in the control loop and the DC component was used in the output reading of the oxygen pressure. In the Tracking Mode, the AC and DC components exchanged roles.

4.3 THEORY

With an applied sinusoidal pumping current

$$I = A \sin x \tag{1.14}$$

where x=ωt, the gauge EMF is given by

$$E = \frac{RT}{4F}\left[\ln\left(\frac{P_1}{P_0}\right) - \ln\left(1 + \frac{RTA}{4Fv\omega P_0}\cos(x)\right)\right] \tag{1.19}$$

In the Tracking Mode the mean internal oxygen partial pressure P_0 is continuously adjusted to follow P_1. In the following, two methods are described for implementing this idea.

4.3.1 Method 1: Constant mean value of the gauge EMF

4.3.1.1 Control of the mean internal oxygen pressure

In this mode of operation, the DC component (i.e. mean value) of the gauge EMF is minimised via a feedback loop aiming to maintain the DC component constant and equal to zero. The following equation may be written:

$$\frac{1}{\pi}\int_0^{\pi} E\,dx = 0 \tag{4.1}$$

where E is the gauge EMF given by eqn.(1.19). Note that E is symmetrical with respect to $x=\pi$, therefore analysis was done for the interval $[0,\pi]$ only. By solving (Appendix A) the integral in eqn.(4.1), a well defined relation between the mean internal and external oxygen partial pressures was found.

$$P_0 = P_1 + \frac{1}{4P_1}\left[\frac{RTA}{4Fv\omega}\right]^2 \tag{A.23}$$

In the present implementation of the Tracking Mode of operation, the control loop continuously adjusted the mean internal oxygen partial pressure in order to satisfy equation (A.23). It is shown (Appendix A) that the general expression for the EMF, obtained by substituting for P_0 in eqn.(1.19), is then given by

$$E = -\frac{RT}{4F}\ln(1+u^2+2u\cos x) \tag{A.21}$$

where

$$u = \frac{RTA}{8Fv\omega P_1} \tag{A.22}$$

Equation (A.21) and (A.22) show that in the Tracking Mode the gauge EMF is a function of the external oxygen partial pressure P_1 only. It is shown in Appendix (A) that eqn.(A.21) is valid for u<1. This condition is equivalent to the necessary condition (eqn.1.17) for proper operation of pump-gauge devices in the AC mode.

$$\frac{RTA}{4Fv\omega P_0}<1 \qquad (1.17)$$

In practice the situation u=1 corresponds to the pumping out of all the oxygen present from the internal volume at a point during the cycle. The condition u>1 causes distortion of the EMF and the sensor deviates from ideal behaviour. In theory, the amplitude of the positive peak of the gauge EMF tends to infinity when u≥1. This situation may be detected by measuring the amplitude E_{-p} of the negative peak of the gauge EMF.

$$E_{-p} = -\frac{RT}{4F}\ln(1+u^2+2u) = -\frac{RT}{2F}\ln(1+u) \qquad (4.2)$$

For u≥1 , $E_{-p}\leq-(RT/2F)\ln 2$. Therefore knowing the operating temperature and by measuring E_{-p}, the situation where u≥1 may be avoided by automatically switching to a lower pumping current for example (i.e. switching to a lower scale of oxygen partial pressure). As an example if the device used had an internal volume of $1mm^3$, an operating temperature of 800°C and frequency of operation of 4Hz, then the minimum oxygen partial pressure that the device could measure may be calculated for a given amplitude of the pumping current using eqn.(1.17). For A=1mA, the minimum measurable P_1 is 456Pa. This limit corresponds to E_{-p}=-32.05mV.

Note that the mean value of the gauge EMF is maintained constant and equal to zero. It is shown however in Chapter (5) that by expressing this mean value as a function of the temperature (measured with a thermocouple) it is possible to achieve analogue temperature compensation with minimum hardware.

4.3.1.2 Computation of the external oxygen partial pressure

In the following several methods are described for the conversion of the gauge EMF (eqn.A.21) into a measure of P_1.

4.3.1.2.1 RMS converter

The DC output of this converter is given by

$$V_{01} = \frac{1}{\pi} \int_0^{\pi} |E|\, dx \tag{4.3}$$

where E is given in eqn.(A.21). An analytical solution of the integral of eqn.(4.3) has not been found. However numerical analysis (Appendix B) indicated that to a close approximation

$$V_{01} = \left(\frac{R^2 T^2 A}{8\pi F^2 v\omega} \right) \frac{1}{P_1} \tag{4.4}$$

regardless of the level of distortion of the gauge EMF. Thus, high signal-to-noise ratio may be achieved by using a gauge EMF highly distorted from a sinusoid (i.e. high amplitude). Equation (4.4) suggests that the system may require one or two measurements only to calibrate it for a wide range of oxygen partial pressure. It is particularly an advantage if the system is used as an oxygen pressure meter where the computation of the pressure P_1 can easily be done even with an analogue implementation. Of course if a microprocessor is used with the sensor, the signal processing and computation of the external oxygen partial pressure may also be readily performed. Even a very non-linear output may be linearised easily by using the look-up technique (Brignell and Dorey 1983, Regtien and Trimp 1990).

Equation (4.4) suggests that the DC voltage V_{01} is directly proportional to the square of temperature. It is shown in Chapter (5) that analogue temperature compensation may then be readily achieved with minimum hardware.

4.3.1.2.2 Phase Sensitive Detector

By using a PSD with a cosine as multiplier, the gauge EMF (eqn.A.21) may be converted into a DC voltage given by:

$$V_{02} = \frac{1}{\pi}\int_0^{\pi} E \,.\, \cos x \, dx \tag{4.5}$$

where E is given in eqn.(A.21). The analytical solution of the integral of eqn.(4.5) has been given by Gradshteyn and Ryzhic (1980) as

$$V_{02} = \frac{RT}{4F} u \tag{4.6}$$

Substituting for u, from eqn.(A.22), in eqn.(4.6) it follows that

$$V_{02} = \left(\frac{R^2 T^2 A}{32 F^2 v \omega} \right) \frac{1}{P_1} \tag{4.7}$$

Using this AC-DC converter, the output voltage V_{02} should be, in theory, perfectly linear with the inverse of the oxygen partial pressure in the sample gas. This should be true regardless of the level of distortion from a pure sinusoid of the gauge EMF making it possible to cover wide range of O_2 pressures and to work at high signal-to-noise ratios.

4.3.1.2.3 Sample and Hold

The two converters described above for the AC-DC conversion have the disadvantage of slow response to changes in oxygen concentration because they incorporate averaging low pass filters with relatively large time constant (i.e. at least five times the period of the pumping current).

In many applications these sensors are used in controlled loop feedback systems. In these systems the sensor monitors oxygen activity downstream and its output signal is fed back to the controller to adjust the appropriate parameters in order to optimise the combustion conditions. As an example the reading of the sensor may be used to control the amount of air required for optimum combustion in domestic boilers (Patterson and Dann 1985, Bergman and Franx 1984) which may be achieved by adjusting the speed of the air fan (Vitter et al 1983, Franx 1982). In such applications the inherent speed of response of the sensor and associated circuitry to variations in oxygen concentration may therefore be extremely important if the controlled loop feedback system is to work effectively. While some allowance for delayed sensor response can be built into the controller, major problems arise if the response rate of the sensor is slower than that required by the process controller (Badwal et al 1988).

Fast AC-DC transformation has been of special interest in fast amplitude control of sinusoidal oscillators, automatic line voltage regulation (Jou et al 1988), and uninterruptible power supplies (Chauprade 1977). Many authors (Mikhael and Tu 1984, Meyer-Ebrecht 1972, Vannerson and Smith 1974, Wojtysna 1989, Jou et al 1991, Richman and Walker 1971, Karybakas and Micholitis 1980, Mahmood et al 1985) have described practical designs for such converters. However these systems were designed for purely sinusoidal signals. In the present application, using these techniques would restrict the amplitude of the EMF to low values in order to approximate it to a sinusoid.

Fast AC-DC conversion may also be carried out by employing a sample and hold technique (Mikhael and Tu 1984, Filanovsky and Fortier 1985). This technique does not depend on the shape of the signal of interest and may be used to produce DC outputs with fast response time. The sample and hold circuit may be used to measure the positive peak of the gauge EMF (i.e. maximum amplitude). If the sample and hold circuit is triggered at $x=(2n+1)\pi$ [n=0,1,2...] then from eqn.(A.21), the output (V_{03}) of the sample and hold circuit should be:

$$V_{03} = -\frac{RT}{4F}\ln\left(1+u^2-2u\right) \tag{4.8}$$

i.e.

$$V_{03} = -\frac{RT}{2F}\ln(1-u) \tag{4.9}$$

Substituting for u in eqn.(4.9) reveals

$$V_{03} = -\frac{RT}{2F}\ln\left(1-\frac{RTA}{8F\nu\omega P_1}\right) \tag{4.10}$$

Rearranging eqn.(4.10) enables the following expression to be written for P_1.

$$P_1 = \frac{RTA}{8F\nu\omega\left[1+\exp\left(\frac{-2F}{RT}V_{03}\right)\right]} \tag{4.11}$$

4.3.2 Method 2: Constant mark-to-space ratio

In the previous implementation (4.3.1), a relation between P_1 and P_0 was established (eqn. A.23). The ratio (P_1/P_0) varies with the amplitude of the gauge EMF. It is shown in Appendix (B) that this ratio (figure B.2) varies between 1 and ½. An alternative mode may be proposed where this ratio is kept constant and equal to 1; then leakage effects resulting from the difference between the internal and external oxygen partial pressures will be small (Kaneko et al 1987). It is shown in the following that the principle of tracking may be implemented in another way which should, in theory, guarantee a ratio (P_1/P_0) constant and equal to 1.

Using a zero-crossing detector, the gauge EMF (eqn.1.19) may be transformed into a square wave. It can be shown that by controlling the mark-to-space ratio (MSR) of the resulting square wave, the relation $(P_1=P_0)$

may be achieved. From eqn. (1.19), for E=0 the following relation may be written:

$$\frac{P_1}{P_0} = 1+\frac{RTA}{4Fv\omega P_0}\cos x \tag{4.12}$$

It follows that

$$\cos x = \frac{4Fv\omega}{RTA}(P_1-P_0) \tag{4.13}$$

The zero-crossing of the gauge EMF occurs at two angles x_1 and x_2 in every single period. From eqn.(4.13)

$$x_1 = \cos^{-1}\left[\frac{4Fv\omega}{RTA}(P_1-P_0)\right] \tag{4.14}$$

and

$$x_2 = 2\pi - x_1 \tag{4.15}$$

The mark-to-space ratio (MSR) is given by:

$$MSR = \frac{x_2-x_1}{2\pi-(x_2-x_1)} \tag{4.16}$$

It follows that

$$MSR = \frac{\pi}{\cos^{-1}\left[\frac{4Fv\omega}{RTA}(P_1-P_0)\right]}-1 \tag{4.17}$$

Equation (4.17) suggests that by keeping MSR=1, the relation (P_1=P_0) may be achieved.

If the relation P_1=P_0 is satisfied, from eqn.(1.19) the gauge EMF may be written

$$E = -\frac{RT}{4F}\ln\left[1+\frac{RTA}{4Fv\omega P_1}\cos x\right] \tag{4.18}$$

and the computation of P_1 may easily be achieved for instance by measuring the positive peak V_m of the gauge EMF.

$$V_m = -\frac{RT}{4F}\ln\left[1-\frac{RTA}{4Fv\omega P_1}\right] \tag{4.19}$$

P_1 is then given by

$$P_1 = \frac{RTA}{4Fv\omega}\frac{1}{1-\exp\left(\frac{-4F}{RT}V_m\right)} \tag{4.20}$$

Note that the necessary condition of eqn.(1.17) for proper operation may be constantly checked by measuring the negative peak of the gauge EMF as in (4.3.1).

4.4 PRACTICAL IMPLEMENTATION

4.4.1 Method 1: Constant mean value of the gauge EMF

The simplified schematic diagram of this method is shown in figure (4.1); the detailed electronic circuit is given in figure (G.11) in Appendix (G).

4.4.1.1 Control of the mean internal oxygen pressure

A sinusoidal oscillator adopted from Jung (1974) was used to produce two sinusoidal signals in quadrature. The voltage-current converter, the instrumentation amplifier and the voltage limiter have been discussed in

Chapter (3). The DC component of the EMF was obtained from a low pass filter and produced the bias signal at the input of the voltage limiter.

4.4.1.2 Computation of the external oxygen partial pressure

4.4.1.2.1 RMS converter

This converter was based on a rectifier followed by an averaging low pass filter. The time constant of the low pass filter was 2s.

4.4.1.2.2 Phase Sensitive Detector

A Phase Sensitive Detector (PSD) was used as AC-DC converter. In this implementation the PSD consisted of a multiplier followed by an averaging low pass filter with a time constant of 2s. The PSD had a multiplying signal (cos x) readily available from the sinusoidal oscillator.

4.1.2.3 Sample and Hold

The sample and hold chip used was the LF398. Its trigger input (i.e. positive pulse) was obtained from the pumping sinewave using a combination of comparator and differentiator.

4.4.2 Method 2: Constant mark-to-space ratio

The detailed electronic circuit used for testing this method is given in figure (G.12) in Appendix (G). Figure (4.2) shows the simplified schematic diagram of this circuit. The gauge EMF was transformed into a square wave. An average value of the square wave was obtained using a low-pass filter. The output of the filter was related to the MSR. For a MSR=1 the output of the filter was equal to zero. However if MSR deviated from 1, then the output of the filter swung to a positive or negative value depending on whether E_0 was positive (i.e. $P_0<P_1$) or negative (i.e. $P_0>P_1$) respectively. The output of the filter was used to produce a bias signal in order to maintain MSR=1 which corresponds to $E_0=0$ (i.e. $P_0=P_1$). A similar system was used by Cox (1973) in a phasemeter that may be used for the measurement of phase shift between sinusoidal signals containing DC offsets [refer to chapter (6) for more details].

The measurement of V_m was achieved using a sample and hold circuit as in (4.4.1.2.3).

4.5 EXPERIMENTAL

Unleas otherwise specified the sensor was operated under the following conditions

- Barometric pressure= 0.1MPa.
- Operating temperature T=700°C.
- Pumping current as indicated on the figures.
- Operating frequency f=4Hz.

Tests were made in gas mixtures of oxygen and nitrogen using the gas mixing equipment described in Chapter (2). The range of oxygen partial pressure considered was 1-10kPa. This choice was made because the device was primarily destined for use in domestic boilers where the range of oxygen partial pressure is typically 2-5kPa. For the response time measurement, a fast solenoid valve was used (refer to Chapter 2) to switch from one premixed gas to another. Note that the measurement of response time of the systems was intended for comparison purpose only. This is because a true measurement of the response time would require a zero dead volume around the sensor.

4.6 RESULTS AND DISCUSSION

4.6.1 Method 1: Constant mean value of the gauge EMF

4.6.1.1 Control of the mean internal oxygen pressure

The measured response time of the circuit depends on the gas flow rate and the speed of response of the control loop. The latter depends on the sensor response, the total gain of the bias signal and the time constant of the low pass filter used to separate the DC component. The lower trace in figure (4.3) shows a typical response of the system to a step change in oxygen partial pressure from 2.5kPa to 8kPa. The system reached a steady state in 3-4 periods of the pumping current. This is a relatively fast response (~1s) and the response of the complete system including the AC-DC converter should be determined by the response of the converter only.

4.6.1.2 Computation of the external oxygen pressure

4.6.1.2.1 RMS converter

Figure (4.4) shows the output V_{01} versus $1/P_1$ for the range 1-10kPa oxygen partial pressure. The amplification factor in V_{01} was unknown, but the linearity was excellent showing good agreement with the theory (eqn.4.4).

This linearity, as theoretically predicted, was not affected by the distortion of the gauge EMF. This is illustrated in figure (4.4) where the peak-to-peak amplitude of the EMF was as high as 21mV.

The time constant of the low pass filter of the RMS converter was chosen large enough (3s) in order to minimise the ripples in the output voltage V_{01} without restricting the speed of response to changes in O_2 partial pressures. The upper trace in figure (4.3) shows the transient response of V_{01} to a step change of oxygen concentration. The response time of the system to 90% of the steady state was 5s.

4.6.1.2.2 Phase Sensitive Detector

Figure (4.5) shows the output V_{02} versus $1/P_1$ for the range 1-10kPa oxygen partial pressure. The linearity was excellent demonstrating that large AC signals may be used without introducing errors in the computation of P_1 using eqn.(4.7). The response of the system to a step change of O_2 concentration was identical to that of RMS converter since both systems incorporated low pass filters with the same time constants.

The analogue implementation of this converter was more difficult and required more hardware than that of the RMS converter with no improvement in performance.

4.6.1.2.3 Sample and Hold

Figure (4.6) shows the results at steady state for the range 1-10kPa of oxygen partial pressure. The slope of the straight line in figure (4.6) provides the internal volume of the device (eqn.4.11). This value ($1.10mm^3$) of the internal volume was within 10% of the theoretical value calculated from the dimensions of the seal ($v=0.98mm^3$). As expected, the response of this converter to a step change in oxygen partial pressure (shown in figure 4.7) was rapid (1s).

4.6.2 Method 2: constant mark-to-space ratio

Figure (4.8) shows the steady state results obtained at 700°C. Again the straight line obtained in figure (4.8) suggests good agreement with the theory (eqn.4.20). The slope of the best fit line provides the internal volume of the device. The determined value ($1.00mm^3$) was in good agreement with the one determined from the dimensions of the seal ($0.98mm^3$).

The measured transient response of the system depends on the speed of response of the control loop and on the gas flow rate. The dependence on the flow rate is illustrated in figure (4.9a) [recorded at 100ml/min flow rate] and figure (4.9b) [at 40ml/min] where oxygen partial pressure was switched from 1 to 4kPa. The response time of the system was 1.5s at 40ml/min and 1s at 100ml/min. However the improvement of the time response at higher gas flow rate was accompanied by small oscillations in the output voltage.

4.7 CONCLUSION

A novel method for the signal processing of sealed pump-gauges operated in the AC mode was suggested. This method, implemented in two ways, had excellent performance at steady state and transient; it allowed the measurement of oxygen partial pressure over a wide range with high tolerance to leakage. An important advantage of this method is that highly distorted gauge EMFs (≡ with high amplitude) may be used, enabling operation with high signal-to-noise ratio. An interesting finding related to the linearity of the output of the system when using signals with high amplitude was theoretically predicted and experimentally tested. This linearity was almost independent of the level of distortion of the gauge EMF.

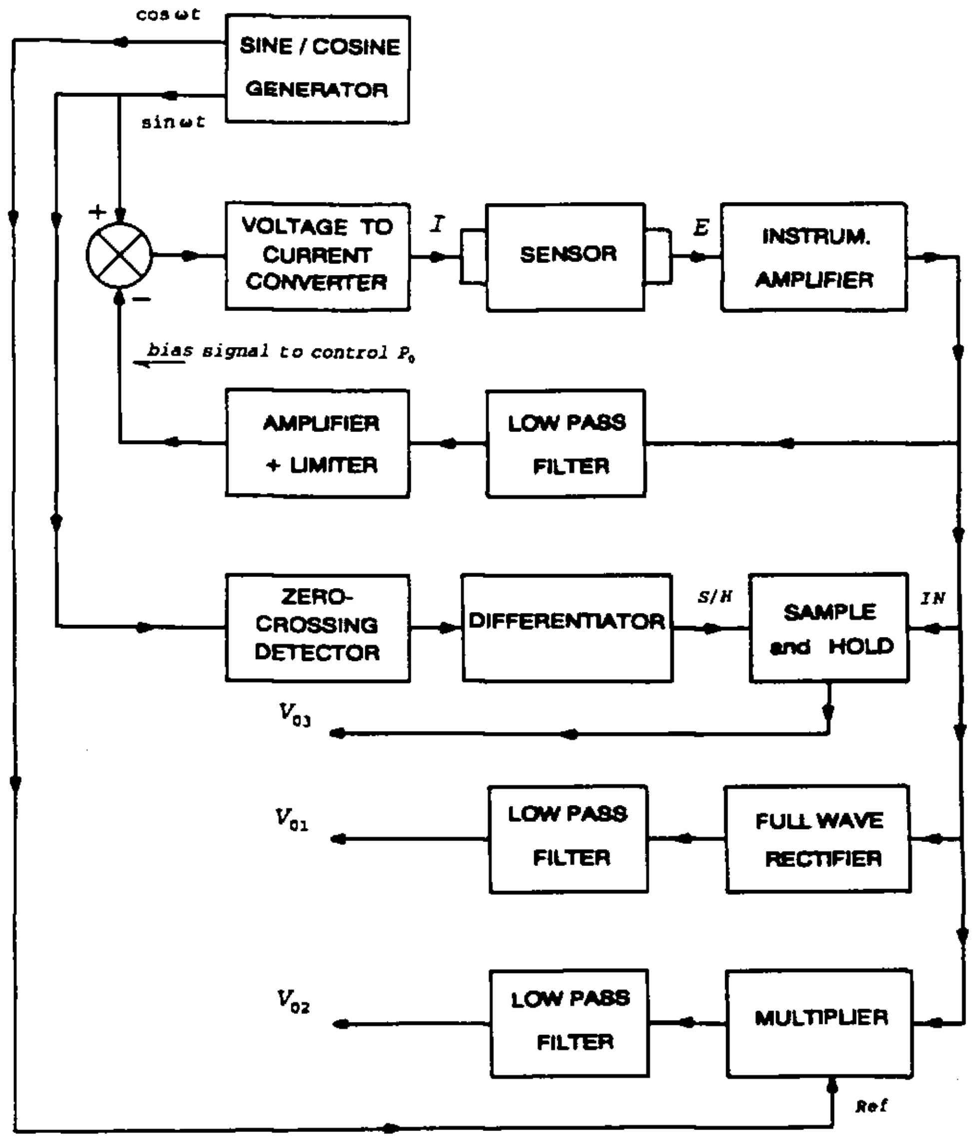

Figure (4.1): *Schematic diagram of the circuit used for operating sealed pump-gauges in the Tracking Mode, method 1: the circuit maintains the DC component of the EMF constant and equal to zero.*

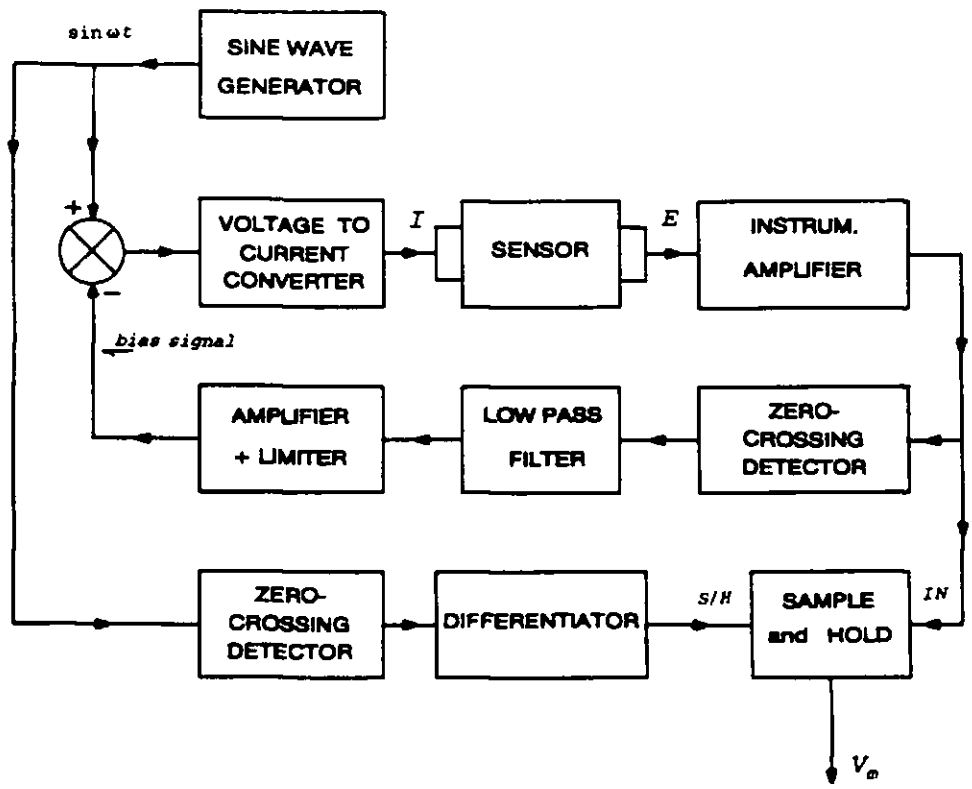

***Figure (4.2):** Schematic diagram of the circuit used for operating sealed pump-gauges in the Tracking Mode, method 2: the circuit maintains the ratio (P_1/P_0) equal to 1.*

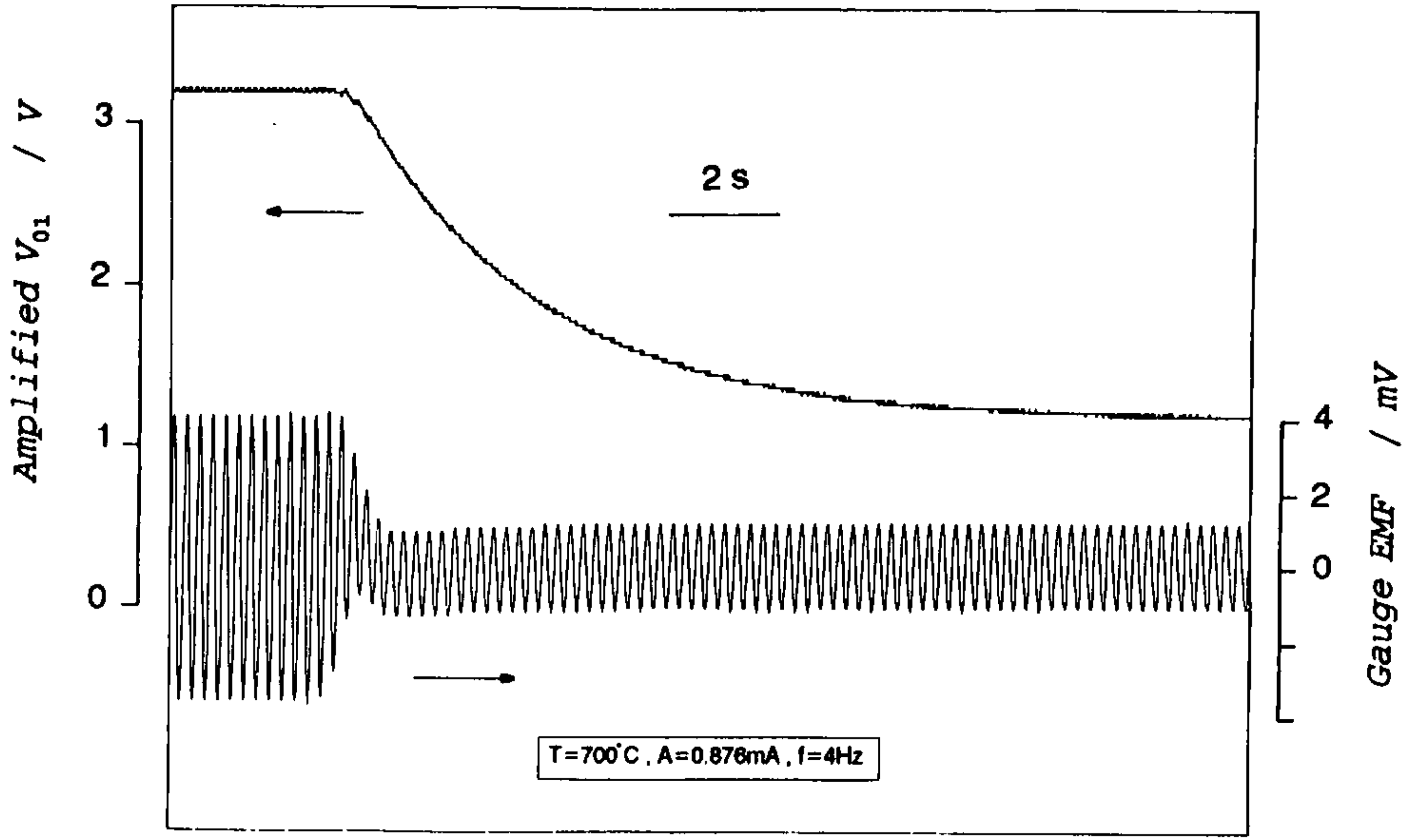

Figure (4.3): Transient response of the circuit of figure (4.1) to a "step" change in oxygen partial pressure from 2.5kPa to 8kPa.

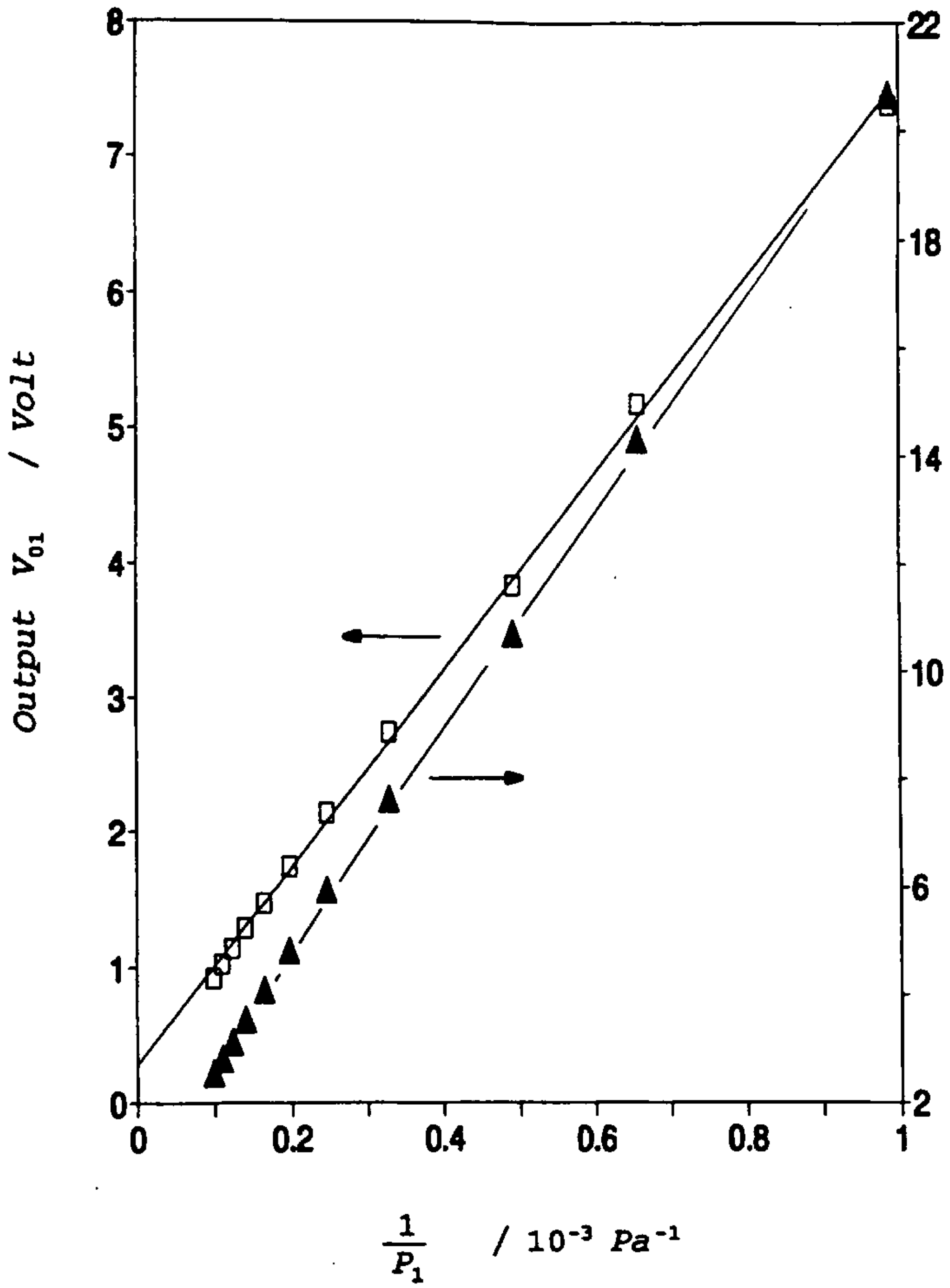

Figure (4.4): *Typical results obtained using a device with an internal volume of 0.98mm³ operated at 700°C, f=4Hz, A=0.87mA. Measurement of the output of the RMS converter (circuit of figure 4.1).*

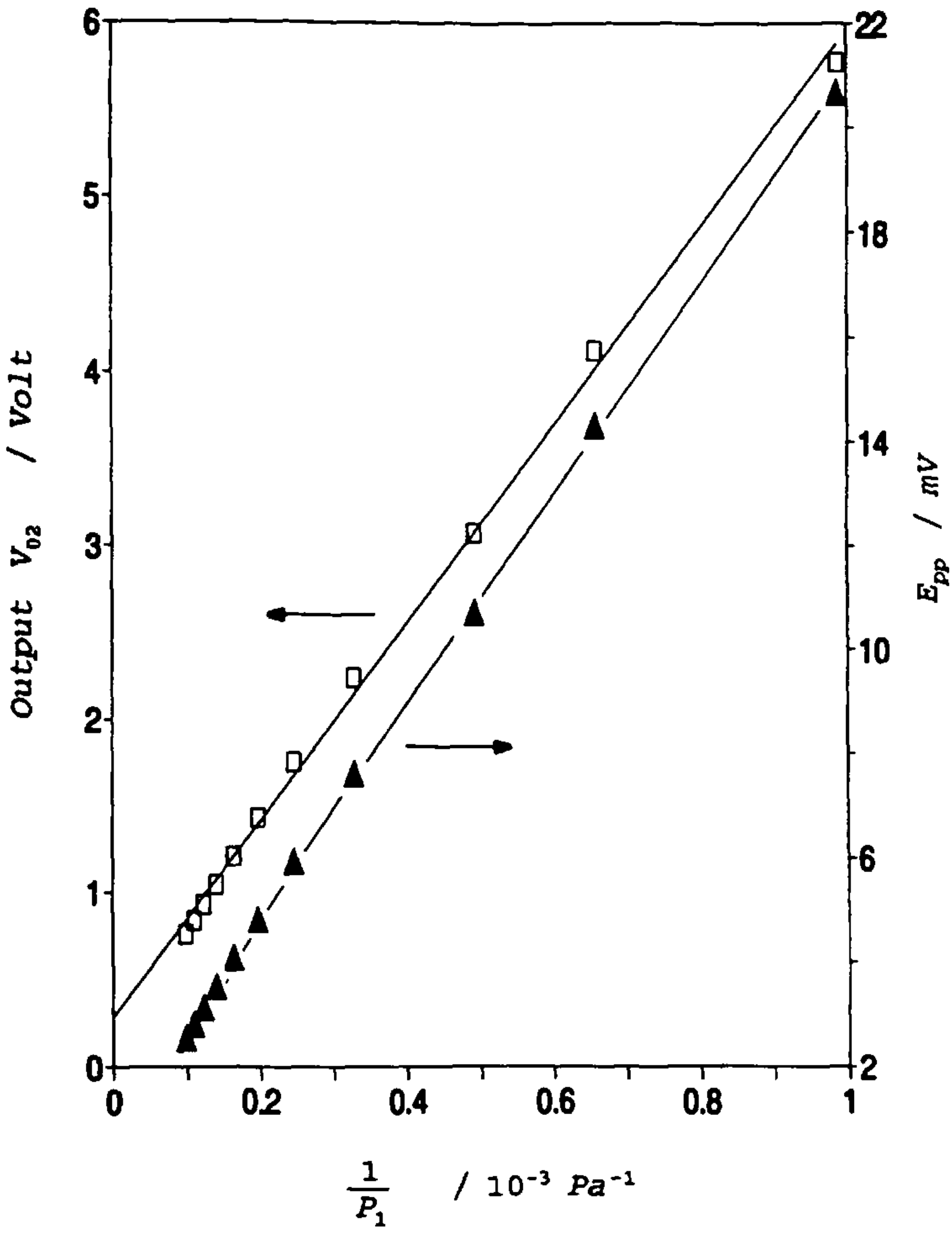

Figure (4.5): Results obtained using a device with an internal volume of 0.98mm^3 operated at 700°C, f=4Hz, A=0.87mA. Measurement of the output of the PSD (circuit of figure 4.1).

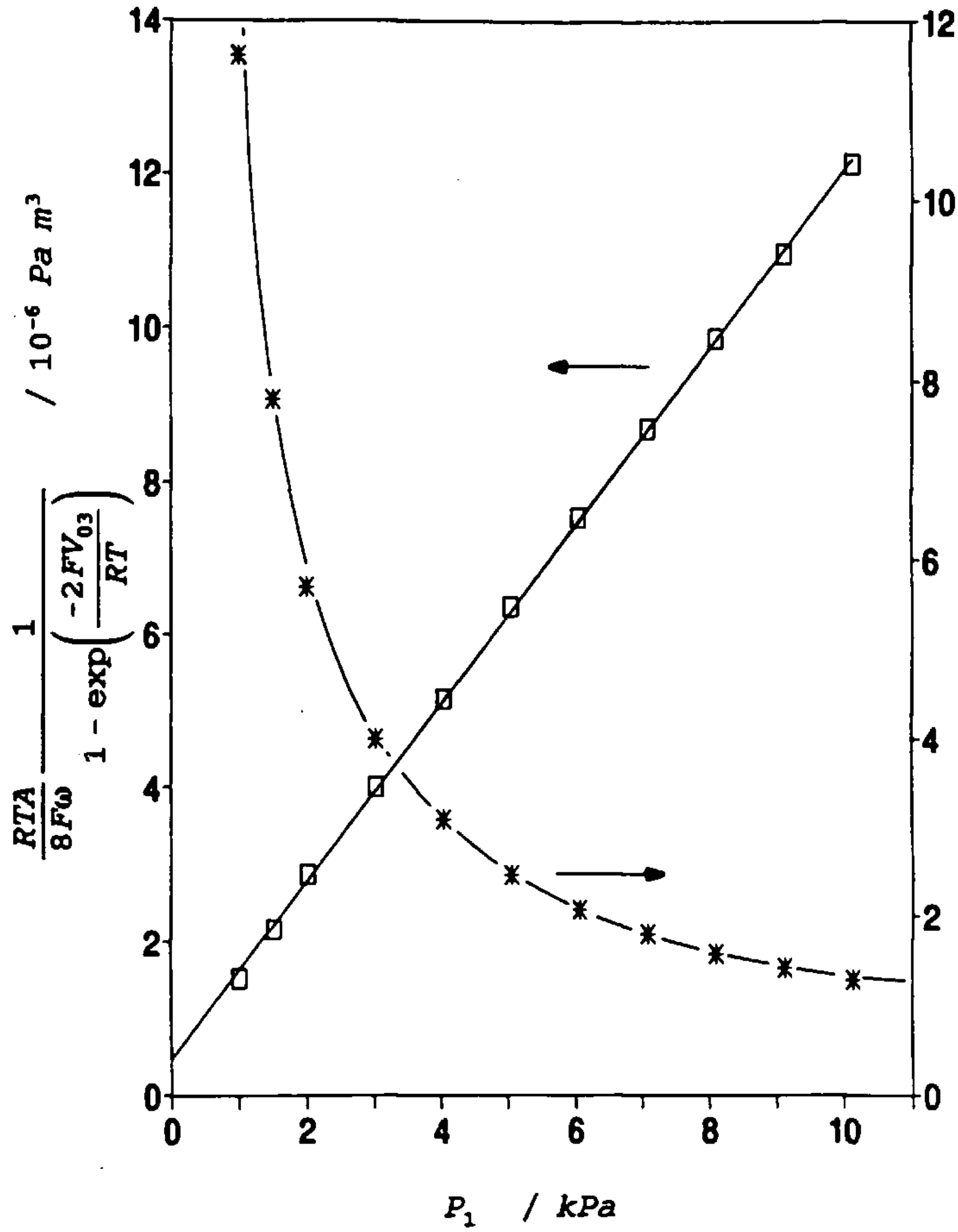

Figure (4.6): *Results obtained using a device with an internal volume of $0.98mm^3$ operated at 700°C, f=4Hz, A=0.87mA. Measurement of the output of the Sample and Hold. (circuit of figure 4.1).*

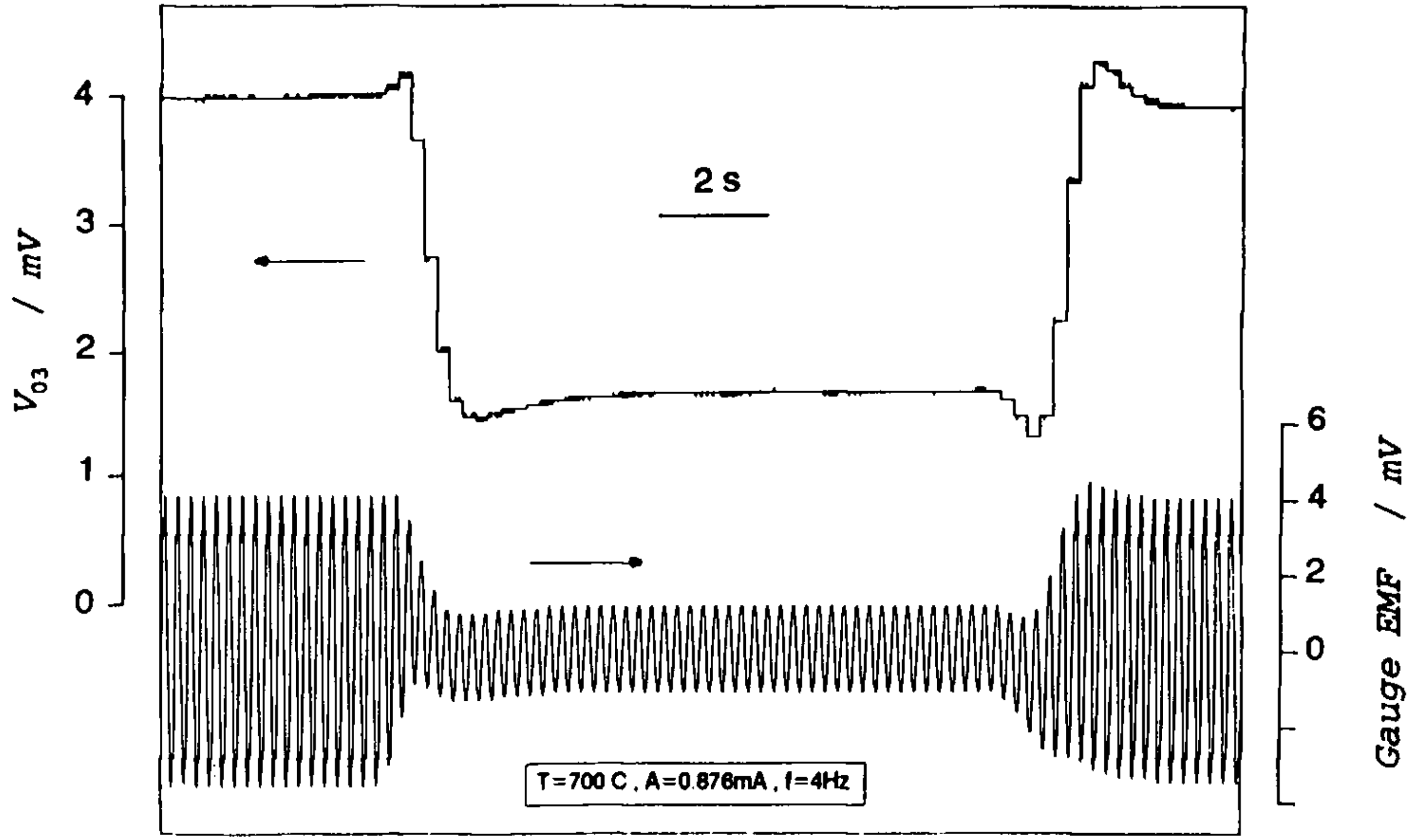

Figure (4.7): Transient response of the Sample and Hold circuit (figure 4.1) to a "step" change in oxygen partial pressure 2.5 - 8 - 2.5kPa.

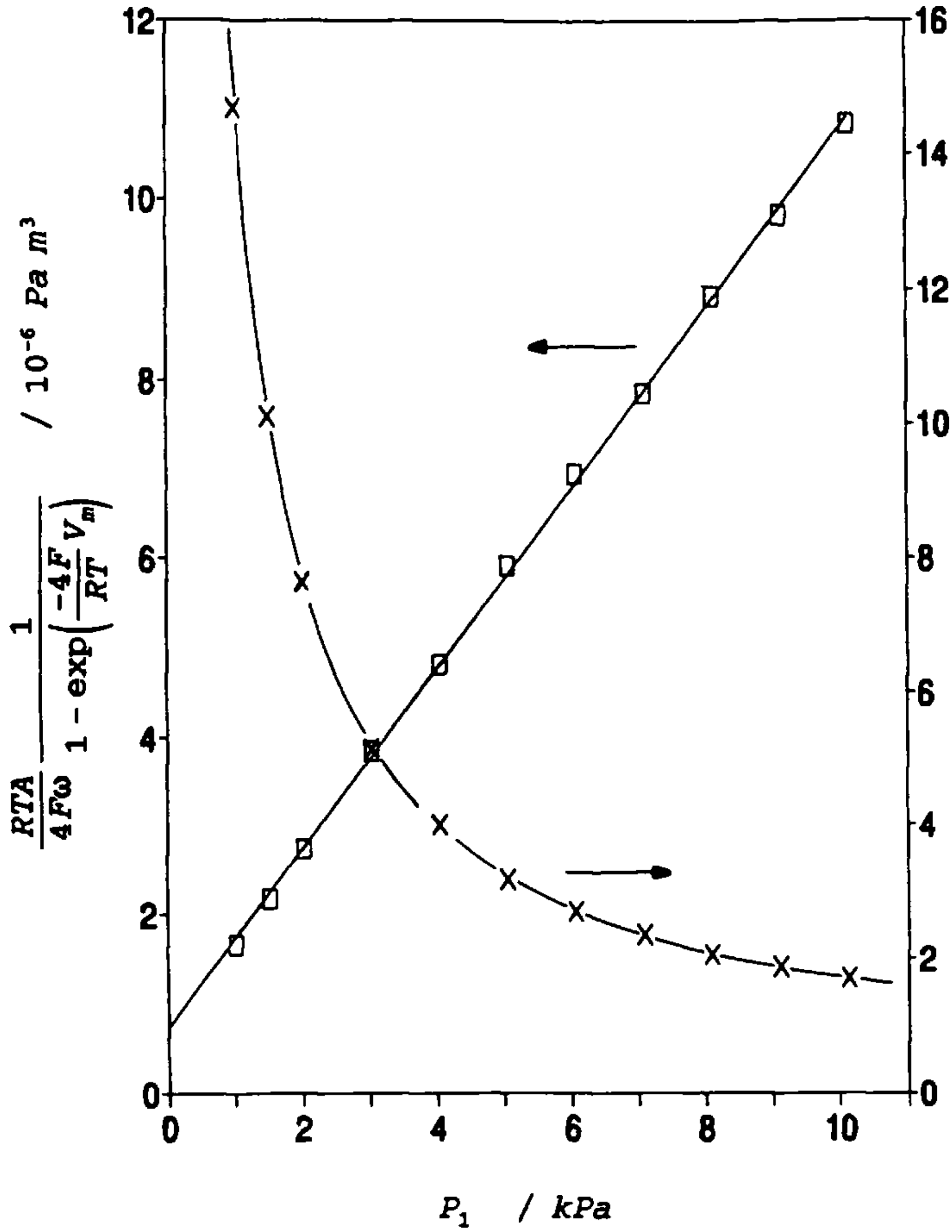

Figure (4.8): Steady state results obtained using the circuit of figure (4.2). The device with 0.98mm^3 internal volume was operated at 700°C, A=1mA, f=4Hz.

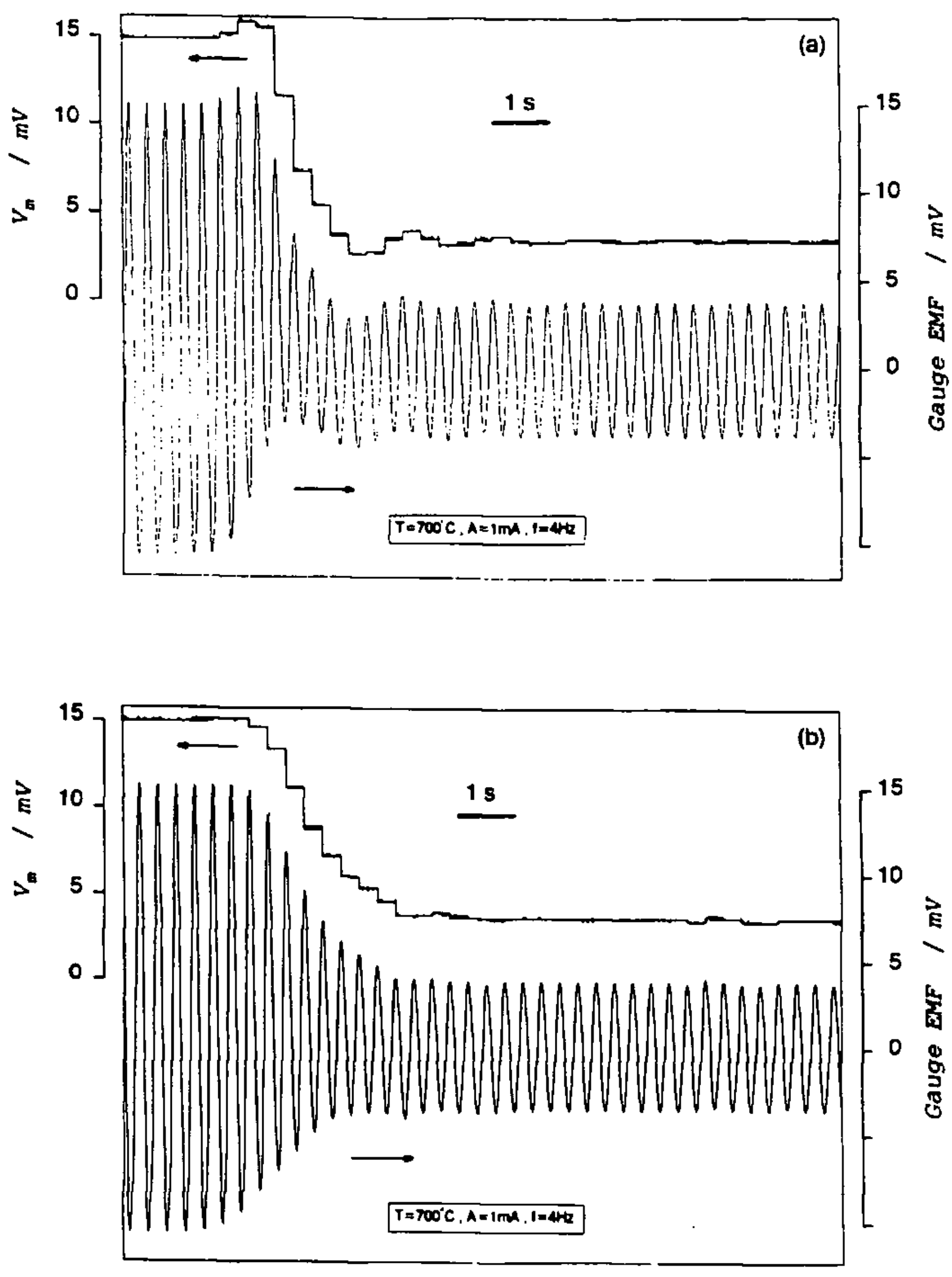

Figure (4.9): Transient response of the circuit of figure (4.2) to a "step" change in P_{O2} from 1 to 4kPa using two different gas flow rates. (a): 100ml/min, (b): 40ml/min.

CHAPTER 5

TEMPERATURE COMPENSATION OF THE SENSOR

"Science is the knowledge of consequences, and dependence of one fact upon another." THOMAS HOBBES, Leviathan (1651), 1.5.

5.1 INTRODUCTION

Different approaches may be adopted to minimise errors introduced by temperature variation. By imposing severe constraints on the temperature controller, the temperature of the sensor can be precisely controlled. T can then be taken as a constant. In the present work, the temperature control of the sensor was based on the control of the resistance of the platinum heaters using a Wheatstone bridge arrangement (Benammar and Maskell 1989). It was found, however, that the resistance of these heaters showed some long term drift (Ioannou and Maskell 1991). As a result the temperature of the sensor showed long term drift too, and consequently temperature compensation of the sensor output was investigated. Temperature compensation often offers more simplicity and requires less hardware than temperature control. Compensation may be achieved by measuring the temperature and including it in the signal processing (Agrawal et al 1974).

For solid state zirconia oxygen sensors, the operating temperature is generally above 600°C. Therefore accurate temperature measurement may best be done using a thermocouple. To avoid the problems associated with using a thermocouple (cold junction, complexity of design of miniature sensors) temperature compensation without a temperature sensing element would be preferred. Franx (1985) suggested a tailored solution for the temperature compensation of coulometric pump-gauge devices (Haaland 1977, Franx 1982 and 1984). This solution did not require the use of a thermocouple but did require the use of a microprocessor to handle the amount of processing required. On the other hand, Rohr (1983) developed a solution for the temperature compensation of conventional potentiometric cells using simple signal processing. However the compensated system required the use of a reference gas and two potentiometric cells.

Analogue-implemented temperature compensation (with thermocouple) of the device, operated in the Tracking Mode, is described in this chapter. Simplification of the hardware used is also discussed.

5.2 THEORY

In the previous Chapter (4), two methods were presented for the practical implementation of the Tracking Mode. The method of interest here is the one based on adjusting the mean internal oxygen partial pressure in order to keep the mean value of the EMF constant and equal to zero (i.e. Method 1 in chapter 4). It is shown in this chapter that by expressing this mean value as a function of temperature, temperature compensation of the DC output of the electronics may be achieved using minimum hardware.

Let the mean value of the gauge EMF be equal to a reference voltage V_r.

$$\frac{1}{\pi}\int_0^{\pi} E\,dx = V_r \qquad (5.1)$$

where E is given by eqn.(1.19). It is shown in Appendix (A) that the relation between the mean internal and external oxygen partial pressures is then given by:

$$P_0 = \frac{P_1}{\exp\left(\frac{4F}{RT}V_r\right)} + \frac{1}{4P_1}\left[\frac{RTA}{4F\nu\omega}\right]^2 \exp\left(\frac{4F}{RT}V_r\right) \tag{A.25}$$

Under these conditions, the expression of the AC component of the gauge EMF (i.e. difference between the EMF, E, and its mean value V_r) is given by:

$$E - V_r = -\frac{RT}{4F}\ln(1+u^2+2u\cos x) \tag{A.18}$$

where

$$u = \frac{RTA}{8F\nu\omega P_1}\exp\left(\frac{4F}{RT}V_r\right) \tag{A.24}$$

This AC component may be converted into a DC output from which the external oxygen partial pressure P_1 may be calculated. The converter of concern in this chapter is the RMS converter (refer to 4.3.1.2.1). It is shown in Appendix (B) that the output of this converter is given by:

$$V_{01} = \frac{R^2T^2A}{8F^2\nu\omega\pi}\exp\left(\frac{4F}{RT}V_r\right)\frac{1}{P_1} \tag{B.3}$$

The output of the RMS converter was dependent on T and T^2. In the following, two methods are presented for temperature compensation of the output V_{01}. These methods were based on the use of a type R thermocouple. Temperature compensation was investigated under two operating conditions: reference voltage equal to zero and variable reference voltage.

5.2.1 Reference voltage equal to zero

By using a zero reference voltage, the output becomes:

$$V_{01} = \frac{R^2 A}{8\pi F^2 \nu\omega}\frac{T^2}{P_1} \tag{4.4}$$

Temperature compensation can be achieved by dividing the output voltage by T^2 to produce an output independent of temperature within the operating range. The thermocouple EMF (e), measured with a 20°C cold junction, is to be converted into T^2. The straightforward solution is to use a thermocouple lineariser (Bentley 1984, Shubba and Ramesh 1986, Shepherd and Sandberg 1984) to convert the thermocouple EMF into temperature (T) and a squarer to obtain T^2. However, as figure (5.1) indicates, within the relatively small range (600-800°C) of operating temperature of the sensor , the linearity between (T) and (e) was excellent and the lineariser was not required. Furthermore, figure (5.1) suggests equally good linearity between T^2 and (e) making it possible to convert the thermocouple EMF into temperature square without the use of lineariser and squarer. This is an advantage in analogue implementation where non-linear circuits are often avoided for simplicity and cost reasons. The following equations may be written:

$$T=a_1e+b_1 \tag{5.2}$$

$$T^2=a_2e+b_2 \tag{5.3}$$

where a_1, b_1, a_2 and b_2 are constants. The values for the constants were calculated using linear regression :

$a_1=8.45\text{x}10^{-2}$ K μV^{-1} ; $b_1=412$ K

$a_2=164.5$ K^2 μV^{-1} ; $b_2=-141.5\text{x}10^3$ K^2

Theoretical calculation showed similarity between the theoretical errors introduced in the compensated output voltage by the approximations of eqn.(5.2) and eqn.(5.3). Maximum errors of 0.4% were calculated in the temperature range 600-800°C.

5.2.2 Variable reference voltage

The output of the electronics given in eqn.(B.3) may be written:

$$V_{04} = \frac{R^2 A}{8\pi F^2 \nu\omega}\frac{Y(T)}{P_1} \tag{5.4}$$

where

$$Y(T) = T^2 \exp\left(\frac{4FV_r}{RT}\right) \tag{5.5}$$

The idea of temperature compensation was based on automatically adjusting the reference voltage V_r in order to keep Y(T)=constant (Y(T)=C) within the operating temperature range. The output of the electronics (eqn.5.4) would then be independent of temperature.

$$V_{04} = \frac{R^2 A}{8\pi F^2 \nu\omega}\frac{C}{P_1} \tag{5.6}$$

In the case where the reference voltage is equal to zero the constant C is equal to T^2 [compare eqn.(4.4) and eqn.(5.6)]. A choice of $C=10^6$ is equivalent to a temperature T=1000K. From eqn.(5.5):

$$V_r = \frac{RT}{4F}\ln\left(\frac{C}{T^2}\right) \tag{5.7}$$

The expression of V_r as a function of temperature is complicated. However by plotting V_r versus the thermocouple EMF (e) for the range 600-800°C and

$C=10^6$, figure (5.2) shows that the required V_r for full temperature compensation may be expressed as a linear function of the thermocouple EMF.

$$V_r=a_3e+b_3 \tag{5.8}$$

where a_3 and b_3 are constants.

If e and V_r are in µV, the values for the constants were calculated using linear regression:

$a_3=-3.54$; $b_3=24.56\text{x}10^3$ µV

It can be shown that the maximum error introduced by the approximation of eqn.(5.8) is 0.52% (deviation of Y(T) from a constant). This is an important finding because temperature compensation is shown to be possible without using non-linear elements (analogue divider, squarer) making the electronics simple to implement.

The operation of the sensor in this mode caused a difference between the mean internal and external oxygen partial pressures. It has been shown in section (4.3.2) that the operation with a reference voltage equal to zero caused the ratio (P_1/P_0) to vary between 1 and ½. For a given reference voltage V_r, the analysis in Appendix (B) shows that the ratio (P_1/P_0) is given by:

$$\frac{P_1}{P_0} = \exp\left(\frac{4FV_r}{RT}\right)\frac{1+\sqrt{1-\left(\frac{RTA}{4Fv\omega P_0}\right)^2}}{2} \tag{B.6}$$

Figure (5.3) shows the calculated exponential term in eqn.(B.6) for the temperature range 600-800°C. This term varied between 0.85 and 1.3. On the other hand the second term of eqn.(B.6) was dependent on the degree of distortion from a sinusoid of the gauge EMF. This second term, shown in figure (B.2b) in Appendix (B), varied between ½ and 1. As a result the ratio in eqn.(B.6) should vary between 0.425 and 1.3. Thus the introduction of a DC component in the gauge EMF increased the ratio between the mean internal and external oxygen partial pressures; this was expected because a part of the DC component, given by eqn.(1.22a), is dependent on the ratio (P_1/P_0).

5.3 PRACTICAL IMPLEMENTATION

The thermocouple EMF was amplified (x1000) using an instrumentation amplifier. The errors introduced by the variation of the cold junction temperature are assumed to be small. Therefore automatic cold junction compensation was thought to be unnecessary.

5.3.1 Reference voltage equal to zero

The block diagram of the circuit used to test this mode of temperature compensation is shown in figure (5.4). The circuit producing the DC output (V_{01}) was identical to the one used for operation in the Tracking Mode (Chapter 4). The squarer was adopted from Shubba and Ramesh (1986) and the divider was built around an analog multiplier (Clayton 1971). The switch was used to select the parameter T^2 from the approximation of eqn.(5.2) or that of eqn.(5.3). The detailed circuit diagram is given in Fig.(G.13), Appendix(G).

5.3.2 Variable reference voltage

The block diagram of the circuit used to test this mode of temperature compensation is shown in figure (5.5). Using a simple adder, the amplified thermocouple EMF was converted to produce the reference voltage V_r required for the temperature compensation. The DC component of the gauge EMF, obtained from a low pass filter, was compared to the reference V_r and produced a bias signal in order to adjust P_0. At steady state the mean value of the gauge EMF should be equal to V_r. The detailed electronic circuit used for implementing this method is given in figure (G.14) in Appendix (G).

5.4 EXPERIMENTAL

The device used to test these methods for temperature compensation was constructed as described in Chapter (2). The temperature was measured with a type R thermocouple attached to the sensor close to the gauge as recommended by Fouletier (1976). The temperature range considered was 650-800°C. The oxygen partial pressure was set to 4kPa using a mixture of air and nitrogen as described in Chapter (2). The frequency and amplitude of the pumping current were 4Hz and 0.8mA respectively.

5.5 RESULTS AND DISCUSSION

5.5.1 Reference voltage equal to zero

Figure (5.6) shows the output of the electronics for the range 650-800°C. The temperature compensation with and without the squarer was excellent: while the non-compensated output varied by 31.5%, the compensated outputs varied by 1.2%. The agreement between the results obtained using the approximation of eqn.(5.2) and eqn.(5.3) confirms that compensation can be achieved without the need for a squarer.

5.5.2 Variable reference voltage

Figure (5.7) shows the results obtained with and without compensation: within the range 650-800°C, the compensated output varied by 4.2% while the non-compensated output varied by 31.5%. The deviation from an ideal compensation could be caused by the difference between the DC component and the reference voltage, i.e. the bias signal was low but was not equal to zero. The compensaation could be improved by some fine tuning of the conatants a_3 and b_3.

5.6 CONCLUSION

Pump-gauge devices operated in the AC mode have strong temperature dependence. Techniques for temperature compensation, requiring simple hardware, were suggested and successfully tested; full temperature compensation was achieved over the whole range of operating temperature (i.e. 650-800°C) of the device. The simplicity and good performance of these systems suggests that temperature compensation could be used as an alternative for the usually cumbersome temperature control.

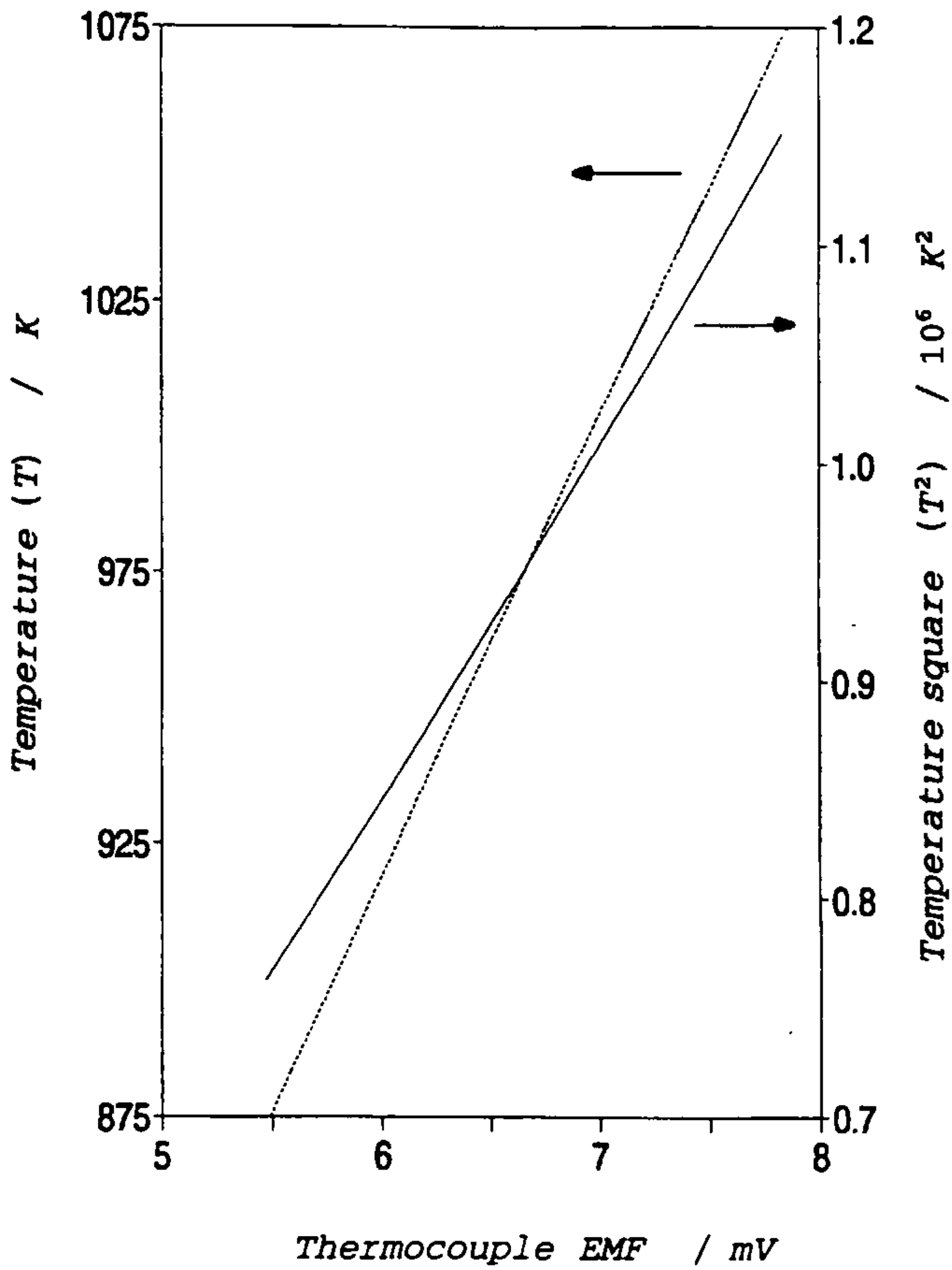

***Figure (5.1)**: Characteristics of a type R thermocouple at 20°C cold junction.*

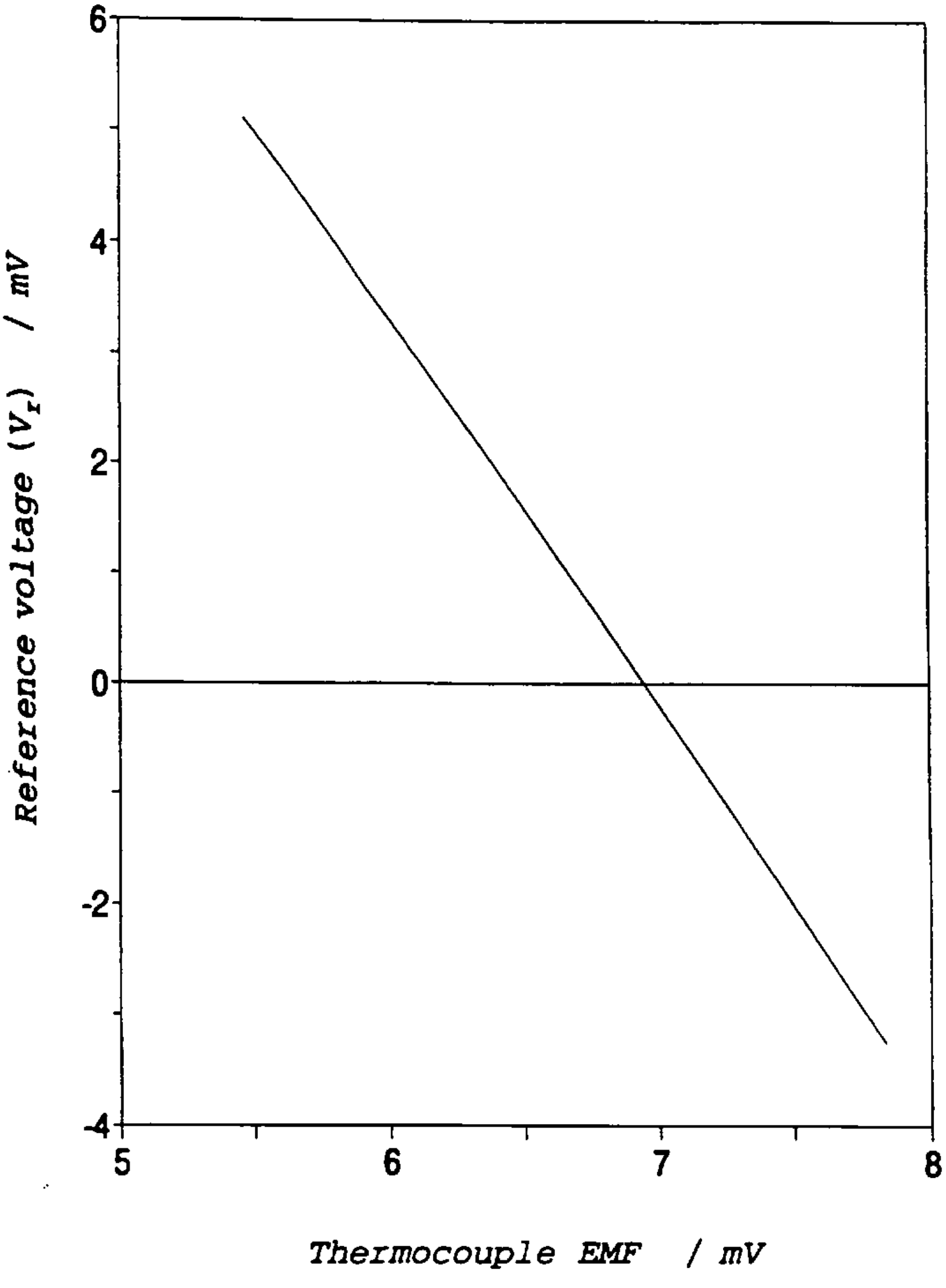

Figure (5.2): Temperature compensation with variable reference voltage V_r. Plot of the required V_r for full compensation.

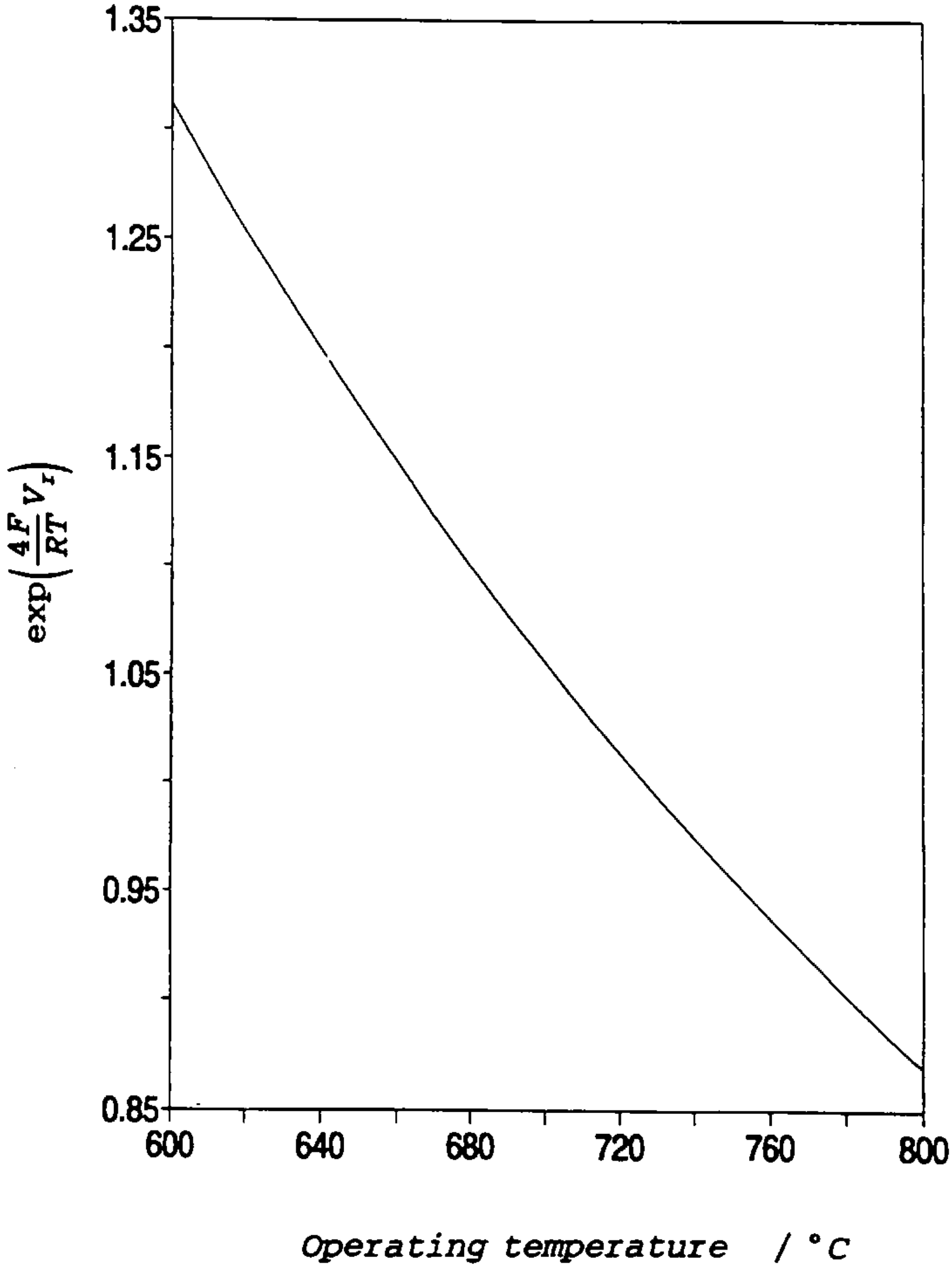

Figure (5.3): *Temperature compensation with variable V_r. Effects on the ratio (P_1/P_0).*

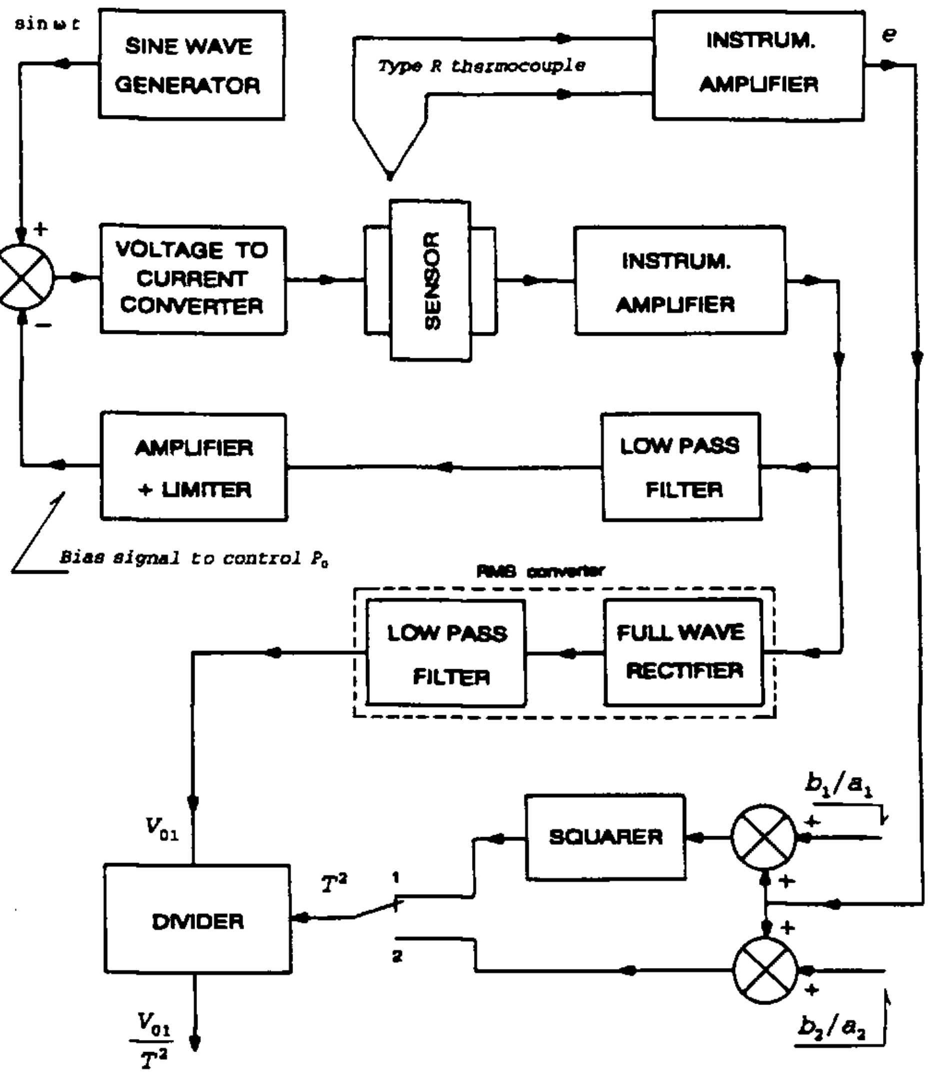

Figure (5.4): Schematic diagram of a temperature-compensated system for P_{O2} measurement.

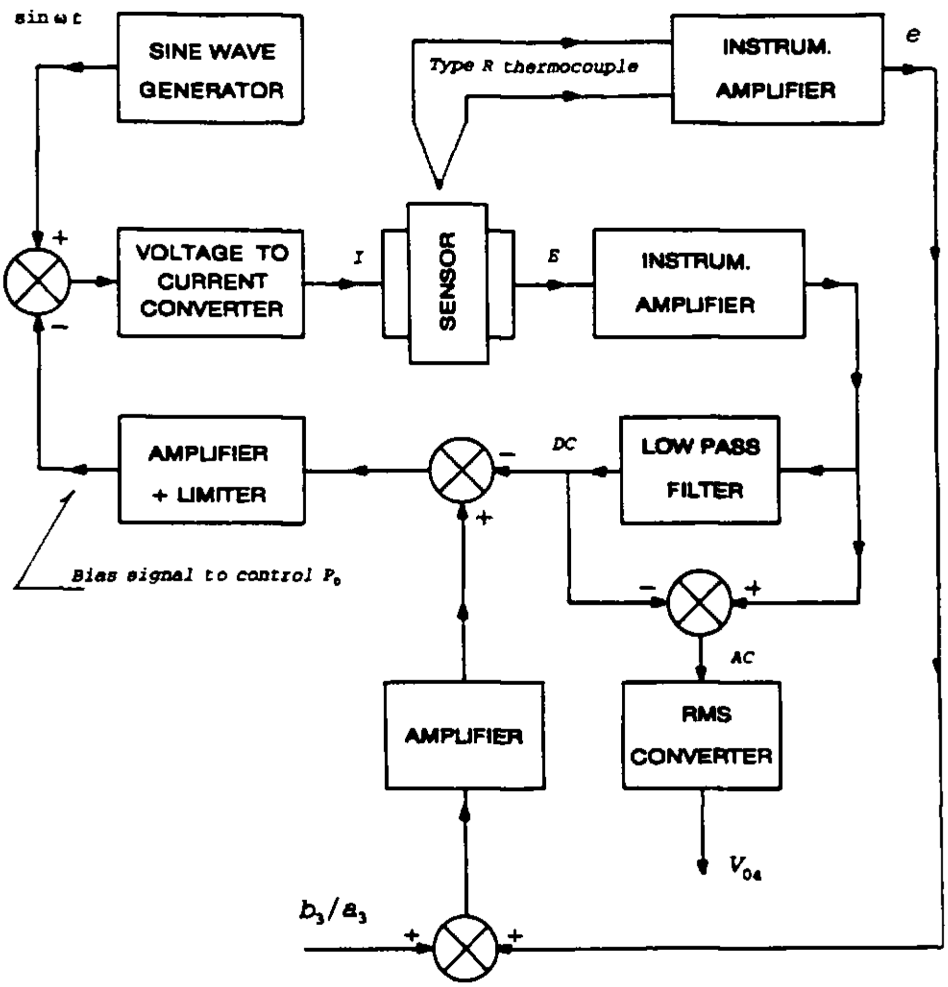

Figure (5.5): Temperature compensation by varying the DC component of the gauge EMF.

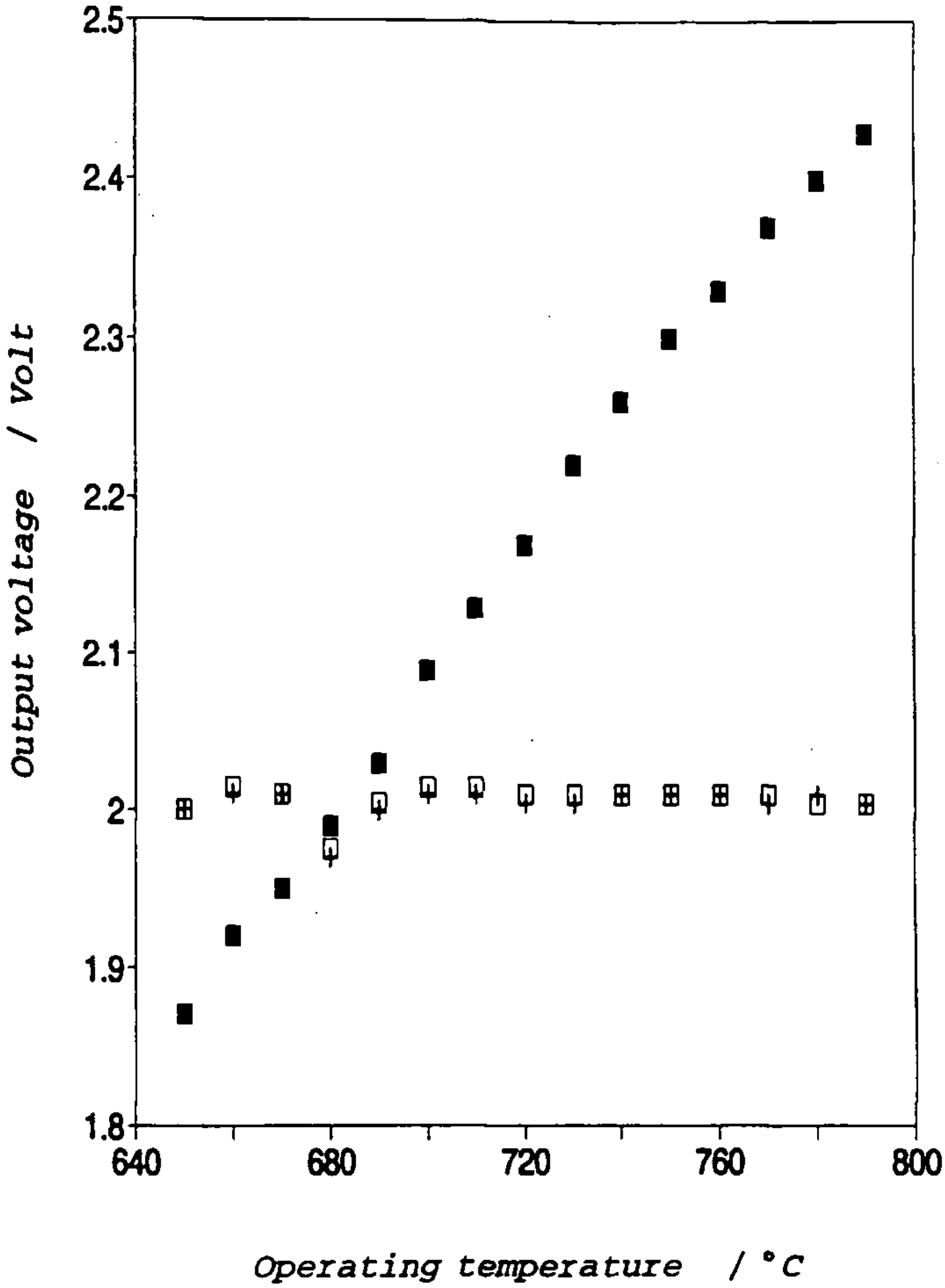

Figure (5.6): *Temperature compensation using the circuit of figure (5.4).*

P_1=4kPa, f=4Hz, A=0.8mA.

■ : *V_{01} without compensation,*

□ : *V_{01} compensated using the squarer,*

\+ : *V_{01} compensated without squarer.*

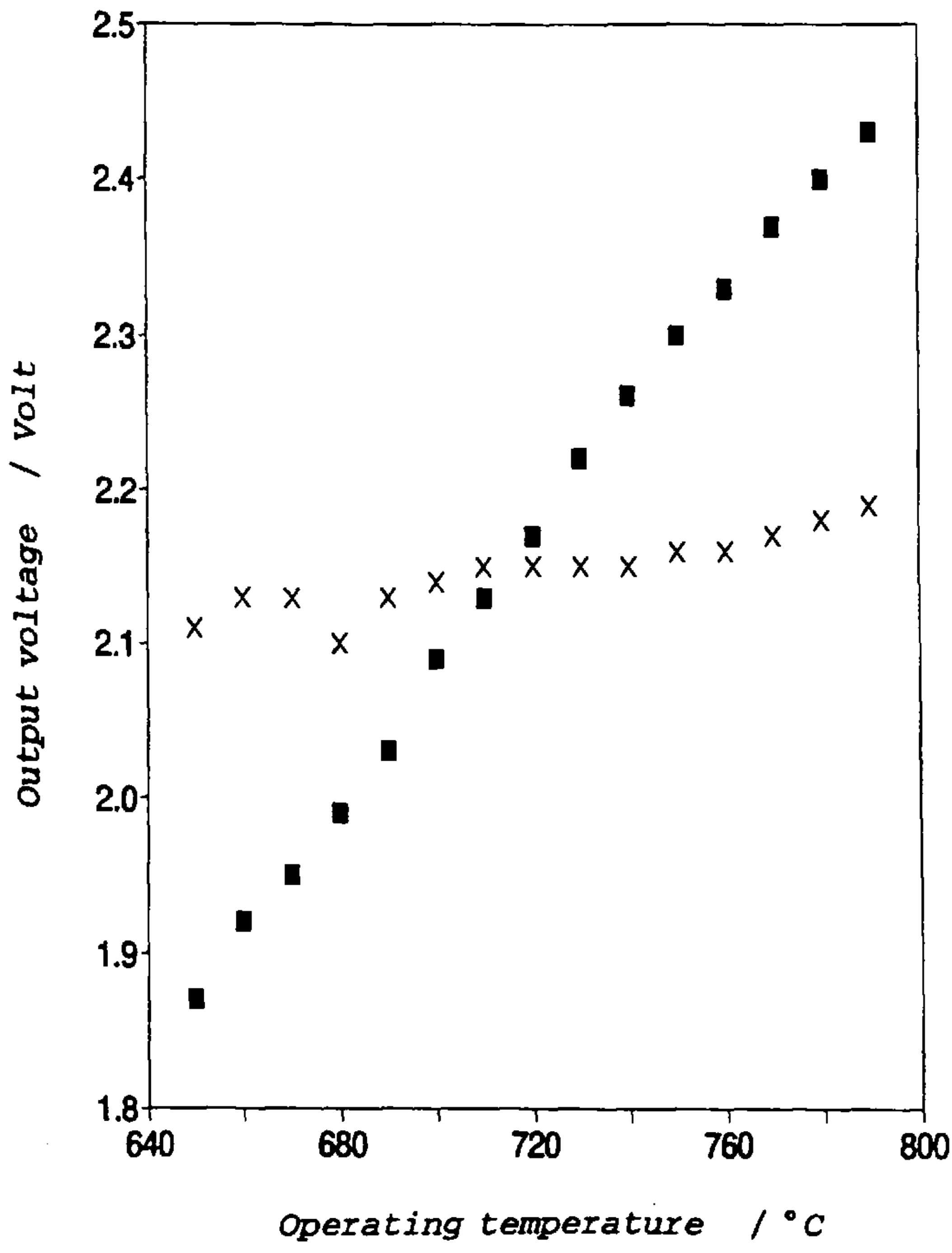

Figure (5.7): Temperature compensation by varying the DC component of the EMF. P_1=4kPa, f=4Hz, A=0.8mA. ■ : V_{01} without compensation, × : V_{04}

CHAPTER 6
OPERATION OF LEAKY DEVICES IN THE AC MODE

"In order to try whether a vessel be leaky, we first prove it with water before we trust it with wine" CHARLES CALEB COLTON, Lacon (1825), 1.46.

6.1 INTRODUCTION

Leakage can, in some instances, be a problem with fully sealed devices. This problem is compounded by the use of small pumping currents and small internal volumes which are usually associated with the miniaturisation trend in sensor making. Kaneko et al (1987) have studied the leakage mechanism in the type of fully sealed devices used in the present work. Indirect methods have been used to evaluate leakage current under various conditions. Three modes of leakage have been identified, physical leakage, semipermeability of the ceramic and electrochemical leakage via the gold seal. Under the operating conditions, the electrochemical leakage was found to be the dominant leakage mechanism.

In this chapter the effects of physical leakage on pump-gauge devices operating in the AC mode are discussed at length. Leakage of ostensibly fully-sealed sensors results from pores connecting the external atmosphere and internal volume which might result from flaws in the ceramic-metal seal or porosity in the ceramic. The leakage rate may increase with sensor aging.

6.2 AIMS AND OBJECTIVES

This study was done using a device caused to leak by the inclusion of one or more laser-drilled pores. The behaviour of such devices operated in the AC mode has been analyzed. This work has particular relevance to thick film sensors. Such devices can be mass produced at low cost making them important candidates for future gas sensors. However the production of low porosity ceramic film necessary for the operation of these devices in the limiting-current mode can be difficult to achieve. The construction of fully sealed devices using this technique is even more difficult.

6.3 THEORY

In the present analysis, the following assumptions are made.

- The oxygen partial pressure is uniform within the internal volume;
- The concentration profile is linear within the diffusion pore;
- The current applied to the pump is all translated into oxygen transfer; and
- The gauge electrodes respond to changes in oxygen partial pressure very rapidly compared with the period of one AC cycle.

These are reasonable assumptions if the frequency of operation is not greater than 10Hz. Let the cross-sectional area and the length of the pore be S and L respectively. The internal volume of the device retains its notation (v). Let the external, mean internal and internal oxygen partial pressures be P_1, P_0 and P_2 respectively. The convention adopted is that a positive current pumps oxygen out of the internal volume. Likewise, a positive oxygen diffusive flux represents oxygen transfer out of the internal volume.

When a current I is applied to the pump, oxygen may be electrochemically pumped into or out of the enclosed volume. Let n_t be the number of moles transferred by electrochemical pumping via the electrolyte. The resulting oxygen flux is then given by:

$$J_{curr} = -\left(\frac{dn_c}{dt}\right)_{curr} = \frac{I}{4F} \tag{6.1}$$

so that a positive current results in a positive flux. Simultaneously, there will be oxygen leaking through the diffusion hole given by:

$$J_{diff} = -\frac{DS}{RT}\frac{dP}{dx} \tag{6.2}$$

where dx is an elementary distance along the diffusion pore, P is the oxygen partial pressure inside the hole, D is the oxygen diffusion coefficient , and S is the cross-sectional area of the leak. R and T have their usual significance.

The concentration gradient within the pore of length L was assumed linear for the following reason. The time constant for oxygen diffusion (Crank 1956) through the hole is given by:

$$T_D = \frac{L^2}{D} \tag{6.3}$$

In the present work, the length of the pore was L=0.7mm and the oxygen gas diffusion coefficient, calculated in (6.5.2.1), $D=164mm^2/s$ at the operating temperature (700°C). This led to a time constant T_D=3ms. The maximum operating frequency of the device was f=4Hz. Therefore the time constant T_D was very small compared to the minimum signal period (250ms). As a result the electrochemical pumping of oxygen should not affect the linearity of the oxygen concentration within the pore. Eqn.(6.2) may then be written:

$$J_{diff} = \frac{DS}{RTL}(P_2-P_1) \tag{6.4}$$

where P_1 and P_2 are the external and internal oxygen partial pressures respectively. The sign in eqn.(6.4) can be verified as follows. Suppose $P_2>P_1$, then there will be diffusion of O_2 out of the internal volume which by convention must be a positive flux.

By combining eqn.(6.1) and eqn.(6.4), the total effective oxygen flux into or out of the internal volume of the device may be written:

$$J = J_{curr} + J_{diff} \tag{6.5}$$

$$= \frac{I}{4F} + \frac{DS}{RTL}(P_2-P_1) \tag{6.6}$$

$$= -\frac{dn}{dt} \tag{6.7}$$

where n is the effective total number of moles of oxygen transferred.

For the internal gas the ideal gas equation may be written:

$$\frac{dP_2}{dt} = \frac{RT}{v}\frac{dn}{dt} \tag{1.11}$$

Eliminating dn/dt between eqn.(1.11), (6.6) and (6.7) gives

$$\frac{dP_2}{dt} = -\frac{RT}{4Fv} I - \frac{DS}{vL}(P_2-P_1) \tag{6.8}$$

Equation (6.8) is the general differential equation relating the internal and external oxygen partial pressure of a leaky device under a pumping current I.

The AC mode of operation is based upon applying a sinusoidal current to the pump. An ideal sinusoidal signal is impossible to generate as there is normally a superimposed DC component. Let the general expression of the current applied to the pump be

$$I = A \sin\omega t + I_o \tag{6.9}$$

where A and ω are, respectively, the amplitude and the angular frequency of the sinusoidal component of the current. I_0 represents the DC offset in the pumping current. In the following expressions for the internal partial pressure P_2 and the gauge EMF are derived for a pumping current given by eqn.(6.9). Substituting for 1 in eqn.(6.8) gives:

$$\frac{dP_2}{dt} + \frac{DS}{vL}(P_2 - P_1) = -\frac{RT}{4Fv}(A \sin\omega t + I_o) \tag{6.10}$$

The solution of the differential equation (eqn. 6.10) is given by (Appendix C)

$$P_2 = \frac{RTA}{4Fv\omega}\cos\Psi \;\cos(\omega t + \Psi) + P_0 \tag{6.11}$$

where

$$\Psi = \tan^{-1}\left(\frac{DS}{\omega vL}\right) \tag{6.11a}$$

P_0, the mean value of P_2, is given by

$$P_0 = P_1 - \frac{RTLI_o}{4FDS} \tag{6.11b}$$

Equation (6.11) shows that applying a sinusoidal current to the pump of a "leaky" sensor results in a sinusoidal oscillation of its internal oxygen partial pressure P_2. When compared to a fully sealed device, "leaky" sensors are expected to exhibit a phase shift and amplitude change of the internal O_2 partial pressure [compare eqn.(6.11) and eqn.(1.16)].

An expression for the gauge EMF may now be derived. Assuming that the internal gauge electrode responds rapidly to the oscillations of P_2, then the sinusoidal variation in the pressure P_2 translates into a variation in the gauge EMF given by eqn.(1.2).

$$E = \frac{RT}{4F}\ln\left(\frac{P_1}{P_2}\right) \tag{1.2}$$

Note that the case where the electrode response is not sufficiently fast is treated in section (6.3.5). Substituting for P_2 from eqn.(6.11) in eqn.(1.2) gives

$$E = \frac{RT}{4F}\ln\left(\frac{P_1}{P_0}\right) - \frac{RT}{4F}\ln\left[1 + \frac{RTA}{4Fv\omega P_0}\cos(\Psi)\cos(x+\Psi)\right] \tag{6.12}$$

where $x=\omega t$. (1.16a)

When compared to the fully sealed device (compare eqn. 6.12 and eqn. 1.19), "leaky" devices produce an EMF with a phase shift Ψ and an amplitude decrease represented by the term $\cos(\Psi)$.

The theoretical equation predicts a phase shift dependent on the gas diffusion coefficient D (see equation 6.11a). On the other hand the molecular theory of gases indicates an inverse proportionality of D on the absolute pressure (see equation 6.22). Therefore if the dimensions of the device, the operating temperature, the operating frequency and the gas composition are known, then a measurement of the phase shift should provide a reading of the barometric pressure.

Equations (6.11) and (6.11a) indicate that the dimensionless quantity (DS/vLω) should determine how the device will behave. As expected, leakage effects should increase with an increase in diffusion hole size (S) and the oxygen diffusion constant (D). Larger internal volumes (v), higher frequencies (ω) and longer holes (L) should have the opposite effect. It has been explained in Chapter (1) that a perfectly sealed device behaves like an ideal capacitor. It is shown in Appendix (D) that a leaky device is then equivalent to an ideal capacitor with a leakage resistor in parallel.

In the following, expressions for the gauge EMF are derived for various modes of operation of the leaky device.

6.3.1 AC+DC mode

In this mode a sinusoidal current, given by eqn.(6.9), is applied to the pump. The term I_0 in the expression for the current represents the DC offset. The expression of P_2, the internal oxygen partial pressure, is given by eqn.(6.11). Substituting for P_2 in eqn.(1.2) gives:

$$E = \frac{RT}{4F}\ln\left[\frac{P_1}{\dfrac{RTA}{4Fv\omega}\cos(\Psi)\cos(x+\Psi)+P_0}\right] \tag{6.13}$$

Substituting for P_0 given by eqn.(6.11b) gives:

$$E = -\frac{RT}{4F}\ln\left[1-\frac{RTLI_0}{4FDSP_1}+\frac{RTA}{4Fv\omega P_1}\cos(\Psi)\cos(x+\Psi)\right] \tag{6.14}$$

Equation (6.14) indicates that the DC offset in the pumping current should result in an offset in the gauge EMF, the system reaching a steady state where the oxygen pumped electrochemically by the offset in the current is counterbalanced by oxygen leaking through the pore. From the practical point of view, this tolerance to small offsets is important because the associated electronics may be greatly simplified. The DC offset in simple sinusoidal current generators is generally inevitable. It may be caused by the non-symmetry in the two halves of the pumping sinewave (Paull and Evans 1974) or by offsets in the voltage to current converter. If an analogue sinewave generator is used, the distortion of the sinewave is generally caused by the shaping network used to convert the triangular wave into an approximate sinewave. This distortion can be minimised if an oscillator or digital generator (Huehne 1972) is used.

The amplitude of the gauge EMF [eqn.(6.14)] at x=π, 3π, 5π... is given by:

$$E_s = -\frac{RT}{4F}\ln\left[1-\frac{RTLI_0}{4FDSP_1}-\frac{RTA}{4Fv\omega P_1}\cos^2(\Psi)\right] \tag{6.15}$$

Equation (6.15) may be rearranged as follows:

$$\frac{4FP_1}{RT}\left[1-\exp\left(-\frac{4F}{RT}E_s\right)\right] = \left(\frac{L}{DS}\right)I_o-\frac{A}{v\omega} \tag{6.16}$$

This equation is used later to compare theory and experiment.

6.3.2 DC mode

In this mode of operation a purely DC current is applied to the pump of the device. The expression for the gauge EMF (E_s) may then be deduced from eqn.(6.14):

$$E_a = -\frac{RT}{4F}\ln\left[1-\frac{RTLI_0}{4FDSP_1}\right] \tag{6.17}$$

where I_0 is the amplitude of the applied DC current.

From eqn.(6.17) the following relation may be written:

$$\frac{I_0}{P_1} = \frac{DS}{L}\frac{4F}{RT}\left[1-\exp\left(-\frac{4F}{RT}E_a\right)\right] \tag{6.18}$$

Note that this mode of operation of the leaky device is similar to the one described by Hetrick et al (1981) [refer to section (1.3.3.1)].

6.3.3 AC mode

For a purely sinusoidal current (I_0=0), the expression of the gauge EMF may be deduced from eqn.(6.14).

$$E = -\frac{RT}{4F}\ln\left[1+\frac{RTA}{4Fv\omega P_1}\cos(\Psi)\cos(x+\Psi)\right] \tag{6.19}$$

The value for the gauge EMF at $x=\pi,3\pi,5\pi...$ is given by:

$$E_s = -\frac{RT}{4F}\ln\left[1-\frac{RTA}{4Fv\omega P_1}\cos^2(\Psi)\right] \tag{6.20}$$

Equation (6.20) may be rearranged as follows:

$$\frac{A\cos^2(\Psi)}{P_1} = \frac{4Fv\omega}{RT}\left[1-\exp\left(-\frac{4F}{RT}E_s\right)\right] \tag{6.21}$$

This equation is used later to compare theory and experiment.

This mode of operation of the leaky device is similar to the Tracking Mode of operation of fully sealed devices [section (4.3.2)]. In the second implementation (i.e. based on keeping the MSR constant and equal to 1) of the Tracking Mode the mean internal oxygen partial pressure P_0 is caused to follow the external O_2 pressure P_1 by applying an appropriate bias current through a feedback loop; at steady state $P_1=P_0$. The diffusion hole in leaky devices plays the role of the feedback loop since it should tend to maintain $P_1=P_0$.

6.3.4 Calculation of the O_2 gas diffusion coefficient

The diffusion coefficient for a species in a gas mixture is, in general, a function of temperature and pressure. Many simplified theoretical models have been given for the gas diffusion coefficient (Chapman and Cowling 1952; Fuller and Giddings 1965; Fuller et al 1966). In the present work this coefficient was calculated using the Fuller, Schettler, and Giddings (Perry's Chemical Engineer's Handbook) relation for a binary mixture of gases A and B.

$$D_{AB} = \frac{10^{-3}\, T^{1.75} \left[\dfrac{(M_A+M_B)}{M_A M_B}\right]^{1/2}}{P\left[(\Sigma v)_A^{1/3}+(\Sigma v)_B^{1/3}\right]^2} \tag{6.22}$$

where T is in kelvin, P in atmospheres, and D_{AB} is in cm^2/s. M_A and M_B are the molecular weights of gases A and B respectively. $(\Sigma v)_A$ and $(\Sigma v)_B$ are the atomic diffusion volumes for the gases A and B.

6.3.5 Effects of slow response of the gauge electrode

In a simple model where the internal gauge electrode does not respond rapidly to changes in P_2, the measured gauge EMF, E(t), at a given time t may be given by

$$E(t) = \frac{RT}{4F}\ln\left[\frac{P_1(t)}{P_2(t-\lambda)}\right] \tag{6.23}$$

where λ represents the time delay between the change in P_2 and its sensing by the internal gauge electrode, and should be dependent on the electrode composition, operating temperature and O_2 partial pressure (Fouletier et al 1974, Winnubst et al 1985). Assuming that $P_1(t)$ is constant and equal to P_1, then substituting for $P_2(t-\lambda)$ derived from eqn.(6.11) in eqn.(6.23) gives

$$E(t) = \frac{RT}{4F}\ln\left(\frac{P_1}{P_0}\right) - \frac{RT}{4F}\ln\left[1 + \frac{RTA}{4Fv\omega P_0}\cos\Psi\,\cos(\omega t + \Psi - \omega\lambda)\right] \tag{6.24}$$

Equation (6.24) predicts that a slow response of the electrode is translated into a phase shift ($\lambda\omega$) between the pumping current and gauge EMF. This phase shift is strongly dependent on the frequency of operation as anticipated; at high frequencies the phase shift is expected to become significant. It is important to note also that the phase shift ($-\lambda\omega$) caused by the slow response of the electrode should be of opposite sign to that caused by the leak (Ψ) because λ and Ψ are both positive; the phase shift (Ψ) should tend to bring the gauge EMF and pumping current into phase, while the phase shift ($\lambda\omega$) should tend to cause a phase shift towards 180°.

6.4 LEAKAGE TESTING OF FULLY-SEALED DEVICES

It has been shown that physical leakage would be expected to cause a phase shift in the output of a pump-gauge operated in the AC mode, this phase shift depending on the operating frequency. Equation (6.11a) suggests that when the device is operated at very low frequency this phase shift may be very large even for small leakage. The novel method of leakage testing presented is based on the measurement of the phase shift Ψ of the gauge EMF at low frequencies, the larger the phase shift the higher the leakage. Not that it should be possible to compensate for the effects of leakage by measuring the phase shift and introducing a correction factor (proportional to cos Ψ) in the amplitude of the EMF for full compensation. This compensation could be achieved using digital techniques.

6.5 EXPERIMENTAL

6.5.1 Details of the devices

6.5.1.1 Leaky devices

Five leaky devices with various leak rates were constructed to test the theory of operation developed in the previous section. The devices were constructed as explained in section (2.2). The five devices included 1,2,4,9, and 16 holes respectively. In the following these devices are referred to by the number of holes they include, for instance sensor 4 represents the device with 4 holes.

The holes (seen under the microscope) were of approximately conical shape and it was necessary to estimate therefore an average hole diameter from the maximum and minimum diameters of each hole. It is shown in Appendix (E) that if the holes were perfectly conical, the effective hole diameter (ϕ) would be given by the geometric mean of the minimum and maximum diameters.

$$\Phi = \sqrt{\Phi_{min}\,\Phi_{max}} \tag{E.10}$$

The measurement of the various hole sizes was carried out using a calibrated microscope. Details of the five devices are given in Table (6.1). The length L of the holes (i.e. thickness of the disc) was measured using an electronic micrometer as 0.70mm. The internal volume calculated from the dimensions of the gold seal was v=0.98mm^3.

SENSOR	16	9	4	2	1
Average ϕ_{min}/µm	63	100	63	63	100
Average ϕ_{max}/µm	100	150	100	100	150
Effective ϕ /µm	79	122	79	79	122
Total S / 10^3µm^2	78	105	19	10	12

***Table (6.1)**: Details of the five devices used. The first row gives the number of holes in a given device.*

6.5.1.2 "Fully-sealed" devices

In order to test the seal quality, two fully-sealed devices with different characteristics were constructed. The first device was fabricated using abraded zirconia discs as described in Chapter (2). The surface preparation was done using fine carborundum paper (Maskell 1991b). Experience indicated that good adhesion between the gold seal and the disc would be expected. The second device was fabricated using identical discs but without the grinding treatment; the roughness of the surface, caused by the diamond saw cutting, was expected to cause leakage at the gold seal-electrolyte interface.

6.5.2 Testing procedure

The theory of operation of leaky devices predicted a phase shift and amplitude decrease of the gauge EMF. This theory was investigated by operating the devices under a variety of conditions. The devices were tested in mixtures of nitrogen and air using the gas mixing equipment described in Chapter (2). All experiments were carried out at ambient atmospheric pressure; during the experiments this pressure was 0.1MPa. Unless otherwise specified the operating temperature was 700°C. This choice was made in order to minimise the phase shift that may be introduced by slow response of the electrodes at low temperatures.

6.5.2.1 Gas diffusion coefficient

The molecular weights (M_A and M_B) for oxygen and nitrogen are 32 and 28 respectively. The values for Σv the atomic diffusion volumes are 16.6 and 17.9 for oxygen and nitrogen respectively (Perry's Chemical Engineer's Handbook). Under the operating conditions, the oxygen gas diffusion coefficient was D=164mm²/s at 700°C. Fate et al (1981) reported a value of 192mm²/s at 800°C (corrected to 700°C, the latter is D=162mm²/s). Other workers (Tedmon et al 1969) have used a value of 250mm²/s at 900°C (corrected to 700°C, this is D=180mm²/s).

6.5.2.2 Schematic diagram of the electronics

The schematic diagram of the circuit used for testing the devices is given in Fig.(6.1). The detailed circuit diagram of the electronics is given in figure (G.15) in Appendix (G). The devices were operated in the three modes described above using the circuit of Fig.(6.1). A rotary switch was used to select the desired mode, the three positions were:

1: Operation in the AC mode.

2: Operation in the AC+DC mode.

3: Operation in the amperometric (DC) mode.

6.5.2.3 Measurement of the phase shift

Despite the existence of algorithms (Micheletti 1991) for the measurement of phase shift between periodic signals, the most common and practical methods used in instrumentation are still based upon combination of analogue and digital electronics. In general the measurement of phase shift between two periodic signals (I) and (E) of the same frequency is achieved by converting the two signals of interest into square waves $\bar{I}$ and $\bar{E}$ using zero crossing detectors. If (I) and (E) are free from offsets then the duty cycles of $\bar{I}$ and $\bar{E}$ would be 50%. A rectangular waveform may also be obtained from the two square waves as shown in figure (F.1) in Appendix (F). The duty cycle of the rectangular waveform is then proportional to the phase shift between the two signals of interest. However in the presence of offsets in the signals of interest (I) and (E), the duty cycles of $\bar{I}$ and $\bar{E}$ deviate from 50% and as a result large errors may be introduced in the measurement of the phase shift.

In the present application, the two signals of interest are the pumping sinewave and gauge EMF. Small offsets in the gauge EMF are inevitable. These may be caused by offsets in the electronics or by non-symmetry between the two halves of the pumping current. In order to minimise non-symmetry in the sinewave, a high quality digital function generator was built and this produced a sinewave with good symmetry. This generator, shown in figure (G.4) in Appendix (G), was of the ROM-read out type (Jeng 1988, Bervas 1985, Galbright 1982, Pichler and Bavuza 1988, Huehne 1972). The offsets in the various stages of the electronic circuit were minimised by careful adjustment of the offsets of the operational amplifiers.

Various techniques may be used for the measurement of the phase shift between signals containing DC offsets:

One solution for reducing the problem of offsets is to use a high-pass filter in order to block the DC components in the signals of interest. This solution has two major disadvantages: first the high-pass filters attenuate very low-frequency signals. Secondly, this method may be applied only for symmetrical signals (i.e. where the signals of interest have a mean value equal to zero).

In the present application the operating frequency is low (<10Hz) and the gauge EMF has a mean value different from zero. This solution was therefore not relevant in the present work.

The solution suggested by Cox (1973) was based on the use of a bias signal in order to guarantee a unity mark to space ratio of the square waves (figure 6.2). This was achieved by measuring the duty cycle of each signal and using a control loop, a bias DC current being added to the signal of interest in order to force a 50% duty cycle. This solution required complicated hardware. Moreover it was unsatisfactory at very low frequency because of the use of an averaging low-pass filter in the control loop.

However the solution suggested by Bames and Williams (1973) and refined by Wagdy and Lucas (1987) was very simple to implement and may be used even for ultra low frequency. This solution may be explained by referring to figure (F.1) in Appendix (F). By measuring the phase shift between the falling and rising edges (Ψ_F and Ψ_R) of the square waves $\bar{I}$ and $\bar{E}$, the phase shift (Ψ) may be measured independently of the offset. It is shown in Appendix (F) that

$$\Psi = \frac{\pi}{2} - \left(\frac{\Psi_F + \Psi_R}{2} \right) \tag{F.10}$$

This solution for the measurement of Ψ was adopted in the present work. The measurement of the duration of the two phase shift Ψ_F and Ψ_R was carried out using a Counter/Timer. Combination of the positive and negative edges of the two signals were used to start and stop the counter. The phase shift (Ψ) was computed according to equation (F.10).

6.5.2.4 Measurement of the amplitude of the gauge EMF

The values of the gauge EMF at $x=\pi, 3\pi, 5\pi...$ were measured using a sample and hold circuit as shown in figure (6.1).

6.6 RESULTS AND DISCUSSION

6.6.1 Testing of "leaky" devices

Figure (6.3) shows a plot of the pumping current and output gauge EMF of sensor 16 operated at 2Hz. The phase shift caused by the leak is indicated by the two lines parallel to the current axis.

6.6.1.1 Operation in the AC+DC mode

Phase shift measurement

Figure (6.4) shows that by applying a pumping current containing a DC offset, the computation of the phase shift Ψ from a measurement of Ψ_F and Ψ_R using eqn.(F.10) was possible as theoretically predicted. The phase shift Ψ was constant within 2% for a wide range of DC offset. Clearly in figure (6.4), for $I_0=0$, $\Psi_F \neq \Psi_R$ which indicates the presence of DC offset in the voltage to current converter and/or the instrumentation amplifier.

Amplitude measurement

The results of figure (6.5) were obtained using sensor 4. The amplitude of the AC component of the current and the operating temperature were maintained constant. The DC offset (I_0) was varied and the voltage E_s measured using a sample and hold circuit. The straight line obtained shows good agreement with the theory (eqn. 6.16). From the slope and intercept of the straight line the terms (DS/L) and (v) were determined. These results are shown in Table (6.2), in the AC+DC Mode column.

6.6.1.2 Operation in the DC mode

The devices were operated under various conditions.

6.6.1.2.1 Variable pumping current (I_0)

The oxygen partial pressure (P_1) and operating temperature (T) were maintained constant. Figure (6.6) shows the results obtained with the five leaky devices. The straight lines in figure (6.6) show excellent agreement with the theory (eqn.6.18). again from the slopes of the best fit lines in figure (6.6), the term (DS/L) was determined for each device. The results are shown in Table (6.2), column (DC Mode / variable:I_0).

The straight lines in figure (6.6) suggest that under the operating conditions, physical leakage through the pores was the dominant mode of leakage. However deviation from straight line may occur in the presence of strong electrochemical leakage via the seal (Kaneko et al 1987, Maskell and Steele 1988). This can be seen in figure (6.7), where a high pumping current was used. The deviation from a straight line for high pumping current suggests that the high ratio (P_1/P_2) between the external and internal oxygen partial pressures induced electrochemical leakage evidenced by the fact that the gauge EMF did not increase at the theoretical rate. From figure (6.7), it is deduced that the electrochemical leakage was induced for a ratio $(P_1/P_2) \geq 40$ (i.e. for $E \geq 80$mV).

6.6.1.2.2 Variable O_2 partial pressure (P_1)

In this mode the pumping current (I_0) and operating temperature were maintained constant. Figure (6.8) shows the results obtained by varying P_1 and measuring E. Again there was good agreement with the theory (eqn.6.18). From the slopes of the best-fit lines, the term (DS/L) was determined for each device. The results are shown in Table (6.2), column (DC Mode / variable: P_1).

6.6.1.2.3 Variable operating temperature (T)

From the slope of the Arrhenius plot of the gas diffusion coefficient (D), the activation energy for diffusion (E_A) may be determined. Tests were made using sensor 4. The amplitude (I_0) of the pumping current and oxygen partial pressure (P_1) were maintained constant. The values for (DS/L) were then determined from a measurement of the gauge EMF using eqn.(6.18). The results obtained are shown in figure (6.9a). The slope of the straight line should be equal to ($-E_A/R$) and this yielded the value $E_A = 13.7$ kJ mol^{-1}.

Figure (6.9b) shows the dependence of the diffusion coefficient on temperature; the observed $T^{1.67}$ dependence is comparable to the $T^{1.75}$ variation according to the theoretical equation (6.22). It is important to note here that the temperature range used in this test was small and consequently high accuracy was not possible.

6.6.1.3 Operation in the AC mode

6.6.1.3.1 *Variable frequency (ω)*

Phase shift measurement

Figure (6.10) shows the phase shift caused by the leak for the five devices for the frequency range 0.3-4Hz at a constant oxygen partial pressure (P_1=4kPa). Figure (6.11) shows the tangent of the phase angle for the same data: there is linearity between the tangent and the signal period which is in good agreement with the theory (see equation 6.11a). The slopes of figure (6.11) provide the term (DS/vL) for each device. The results obtained are shown in Table (6.2), column (AC Mode / variable: ω).

Amplitude measurement

The results obtained by measuring the amplitude of the gauge EMF are shown in figure (6.12). The linearity of these results was good, showing good agreement with the theory (eqn. 6.21). From the slopes of the best-fit lines, the internal volume may be calculated. The results obtained are presented in Table (6.2), column (AC Mode / variable: ω).

6.6.1.3.2 *Variable current amplitude (A)*

Phase shift measurement

Figure (6.13) shows the phase shift measured at various amplitude (A) of the pumping current. The trend, as theoretically expected, shows that the phase shift was not dependent on (A).

Amplitude measurement

The results obtained from a measurement of the amplitude of the gauge EMF are shown in figure (6.14). The linearity shows good agreement with the theory (eqn.6.21). From the slopes of the best-fit lines, the internal volume of each device may be calculated. The results obtained are given in Table (6.2), column (AC Mode / variable: A).

6.6.1.3.3 Variable O_2 partial pressure (P_1)

Phase shift measurement

The theory predicted that the phase shift should be independent of the oxygen concentration (C_{O2}). However as shown in figure (6.15), there was clear dependence of Ψ on C_{O2}. Possible explanations for this behaviour include errors in the measurement of Ψ, slow response of the electrodes, simplification in the theoretical model and dependence of the gas diffusion coefficient on the oxygen concentration: these are investigated in section (6.6.3).

Amplitude measurement

Figure (6.16) shows the results obtained by operating the devices at 700°C and varying P_1. The deviations from a straight line (refer to eqn.6.21) seem likely to be related to the variation of the phase shift with the oxygen concentration. From the slopes of best-fit lines, the internal volume of each device may be determined. The results are shown in Table (6.2), column (AC Mode / variable: P_1).

Despite the minor deviation from the predicted theory, the results in figure (6.17) show that, with appropriate calibration, devices with considerable leak (operated in the AC mode) may still be used for the measurement of oxygen partial pressure. Furthermore the electronic circuit could be made very simple as shown in figure (G.16) in Appendix (G).

6.6.1.4 Summary of Results

The values determined from the various experimental results are compared to those determined from the dimensions of the seal (v), length (L) and cross-sectional area (S) of the diffusion pore in Table 6.2.

For each device, the values for the term (DS/L) determined experimentally are similar in the AC, DC and AC+DC modes and comparable to the calculated ones. Interestingly, the values for the internal volume determined experimentally are 40 to 80% higher than the ones calculated from the dimensions of the seal. Two important points may be raised. Firstly, for each device, the experimental results are closely grouped. Secondly the determined values for all devices may be divided into two groups, one group of volumes 40% and the other 80% higher than calculated. These two groups do not depend on the number or size of the holes (refer to Table 6.1). Moreover the high 40-80% difference could not be accounted for even by adding the volume of the diffusion pore to that of the internal volume, in other words assuming that the hole forms part of the internal volume. From Table (6.1), the maximum volume of the diffusion pore is that of sensor 9; this volume is given by (LS) and calculation showed that this volume could only account for a difference of 7.4%. Since all the measurements of the internal volumes (v) were determined by operating the devices in the AC or AC+DC modes, the large values obtained for (v) may be linked to the deviation from theory described below in section (6.6.3).

		AC+DC MODE	AMPEROMETRIC MODE		AC MODE			CALCULATED VALUES
	VARIABLE	I_0	I_0	P_1	ω	A	P_1	
SENSOR 16	v	—	—	—	—	1.82	1.80	0.98
	(DS/L)	—	18.6	19.6	20.9 †	—	—	18.3 ▲
	(DS/vL)	—	—	—	11.56	—	—	—
SENSOR 9	v	—	—	—	—	1.78	1.84	0.98
	(DS/L)	—	20.0	20.1	21.3 †	—	—	24.6 ▲
	(DS/vL)	—	—	—	11.82	—	—	—
SENSOR 4	v	1.24	—	—	1.43	1.39	1.47	0.98
	(DS/L)	5.22	5.28	5.31	5.12 †	—	—	4.45 ▲
	(DS/vL)	—	—	—	3.56	—	—	—
SENSOR 2	v	—	—	—	1.53	1.48	1.53	0.98
	(DS/L)	—	2.19	2.16	2.31 †	—	—	2.34 ▲
	(DS/vL)	—	—	—	1.51	—	—	—
SENSOR 1	v	—	—	—	1.85	1.81	1.75	0.98
	(DS/L)	—	3.23	3.23	3.20 †	—	—	2.81 ▲
	(DS/vL)	—	—	—	1.73	—	—	—

Table (6.2): Summary of the results obtained. *v in mm^3, (DS/L) in $mm^3\ s^{-1}$, (DS/vL) in s^{-1}.*

† : *calculated from v and (DS/vL).*

▲ : *calculated from D,S and L from Table (6.1).*

6.6.2 Testing of "fully-sealed" devices

Figure (6.18) shows the phase shift of the two devices without drilled hole for the frequency range 0.03-0.4Hz. The trend of the phase shift versus signal period was identical to that of the leaky devices (compare to figure 6.10). At very low operating frequency the sealed devices showed substantial phase shifts indicating the presence of leakage. Figure (6.19) shows the tangent of the phase shift angle versus signal period.

The phase shift of the device with unground surfaces was higher than that with ground surfaces. At the normal operating frequency (4Hz) used in the present work (Chapter 3, 4 and 5) both devices showed very little dependence on leak. The effect of leak may be reduced further by operating the sealed devices in the Tracking Mode (chapter 4). Therefore the time consuming grinding treatment of the zirconia discs may be eliminated without causing the device to leak excessively and would have little effect on the operation of the sensor.

The effects of the slow response of the electrodes were investigated by operating the device with unground surface at various temperatures, frequencies and oxygen partial pressures. Figure (6.20) shows the results obtained by operating the device at a constant P_1 by varying the frequency of the pumping current. A positive phase shift indicates dominance of physical leakage and a negative one indicates dominance of slow response of the electrodes. For high frequencies (>1Hz), the phase shift caused by the leak was small (eqn. 6.11a), but the electrode was expected to introduce large phase shift ($\lambda\omega$). This is illustrated in figure (6.20) by a negative phase shift. However, for low frequencies, the phase shift introduced by the leak was high whereas the electrode response was fast by comparison with the operating frequency which resulted in a positive phase shift. The effect of varying the operating temperature may also be seen in figure (6.20). At low temperature, the response of the electrodes became very slow as expected. The dependence of the phase shift on the oxygen concentration is shown in figure (6.21) at four different temperatures. The results obtained show some evidence of phase shift dependence on oxygen concentration.

6.6.3 Investigation of the deviation from the predicted behaviour

The experimental results showed general agreement with the developed theory of operation of leaky devices in the AC and DC modes. In the amperometric mode of operation (i.e. DC mode), this agreement was excellent. However, in the AC mode experimental results showed minor deviation from the theory. This deviation concerned the dependence of the measured phase shift on the oxygen concentration (6.6.1.3.3) which was not predicted by the theory. Possible causes of this deviation are discussed below.

Errors in the measurement of Ψ

Variation of the oxygen concentration resulted in variation of the amplitude of the gauge EMF. Hence errors in the zero-crossing detectors (figure F.1) as a possible cause of some errors in the measurement of the phase shift need to be considered. Such errors seem unlikely because the deviations of Ψ, shown in figure (6.15), are not random. Moreover, the method used for the measurement of Ψ from an average of two phase shifts (eqn. F.10) should be fairly insensitive to uncertainty in the zero-crossing especially because the results were obtained by averaging multiple readings. This has been experimentally verified by operating the device with a constant amplitude of the sinusoidal current and by measuring Ψ for various values of P_1. Then a similar experiment was carried out but this time varying the amplitude of the pumping current in order to keep the amplitude peak-to-peak of the gauge EMF constant in the whole range of P_1. The results obtained are shown in figure (6.22) and indicate excellent agreement between the two sets of results. In fact, this test showed that the method of phase shift measurement employed was very precise.

Response time of the electrodes

The response of the internal electrodes to changes in oxygen partial pressure is dependent on the temperature and oxygen partial pressure as has been shown in section (6.6.2). However, in the developed theory, rapid response of the electrodes was assumed. The results of figure (6.15) were obtained by operating the devices at 700°C. This operating temperature was thought to be high enough to minimise errors introduced by slow response of the electrodes. In order to investigate the effect of operating temperature, tests were made using sensor 9 in the temperature range 700-850°C. The results obtained are shown in figure (6.23). The trend of each of these results is similar to that of the results in figure (6.15), i.e. there was not a trend towards independence of oxygen concentration with increasing temperature as might have been anticipated if slow response of the electrodes were responsible for the deviation from theory.

Further work should include testing devices with same leak rate (S/L) but with different electrode material which, because of the response time dependence on the electrode composition, may behave differently.

Over-Simplification of the theoretical model

In the theoretical analysis, oxygen concentration within the internal volume was assumed uniform, and the oxygen concentration gradient within the diffusion pore was assumed linear. While these assumptions may be true at very low frequencies (and of course the amperometric (DC) mode represents operation at zero frequency), errors may be introduced at higher frequencies. In the DC mode (6.6.1.2), measurements were made at steady state. This means that the slow response of the electrodes and simplification in the theoretical model should not affect the trend of the results. Indeed, the results obtained showed good agreement with the theory. However, when operated in the AC mode (i.e. with sinusoidal current), the system is a dynamic one: there are continuous oscillations of P_1 within the internal volume and diffusion pore. It is possible that, as a result, there may be significant radial concentration differences within the internal volume between the region in the vicinity of the diffusion hole and that towards the gold seal. In other words, the phase shift and amplitude change (caused by the leak) at various points of the electrode might be different. The gauge EMF measured somehow represents an "average" reading of all EMFs at different points radially along the gauge, with the possible result of some deviation from the predicted theory. This could not directly explain the dependence of Ψ on the oxygen concentration. However, this behaviour may be further investigated by making devices with various pore sizes (S) and lengths (L). Informative results may be found by operating devices with different combinations of (S) and (L) but with the same ratio (S/L). This may elucidate any effect of non-linearity of the oxygen concentration gradient within the pore, i.e. for high values of L, L^2/D may become comparable to the signal period. The effect on phase shift dependence of the position of the gauge electrode with respect to the diffusion pore may also be investigated by making and testing devices with different electrode position.

6.7 CONCLUSION

The theory of operation of leaky pump-gauge devices in the AC mode has been developed. This theory indicates that behaviour should be similar to that of fully-sealed devices: with application of a sinusoidal current to the pump, theoretical analysis indicates that a pseudo-sinusoidal EMF should appear at the gauge, with a phase shift and amplitude changes, compared with the fully-sealed sensor. Furthermore these phase shift and amplitude changes should be dependent on the leak size, internal volume, operating frequency, and oxygen diffusion coefficient. The theory predicts also that devices with considerable leak may still be used for oxygen partial pressure measurement. This theory was tested using devices designed for the purpose with well-defined leakage. Good agreement between theory and experiment was found in almost all respects. A minor deviation was found and concerned the dependence of phase shift with oxygen concentration which was not predicted by the theory. The reasons for this are not clear and suggestions are made for further investigations of this deviation.

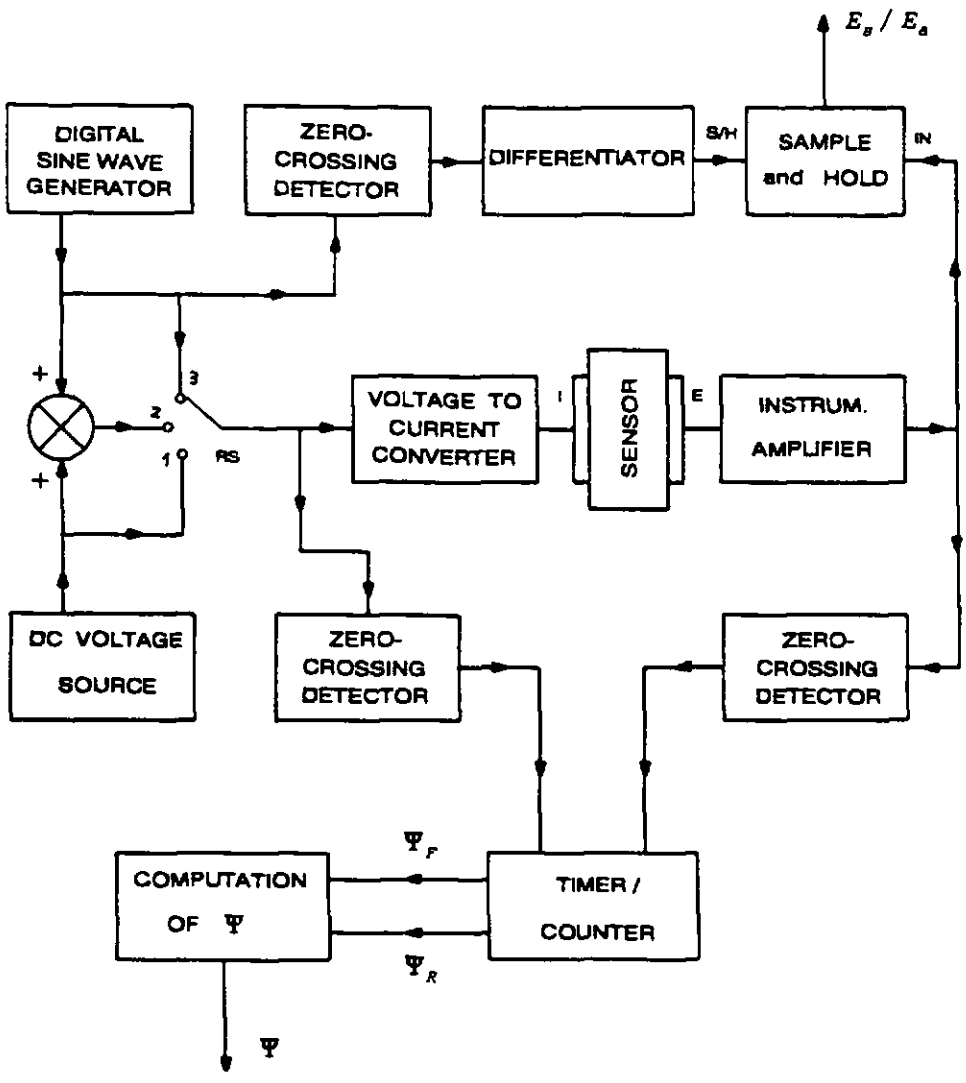

Figure (6.1): Schematic diagram of the electronics used for testing the theory of operation of leaky devices in the AC, AC+DC and DC modes.

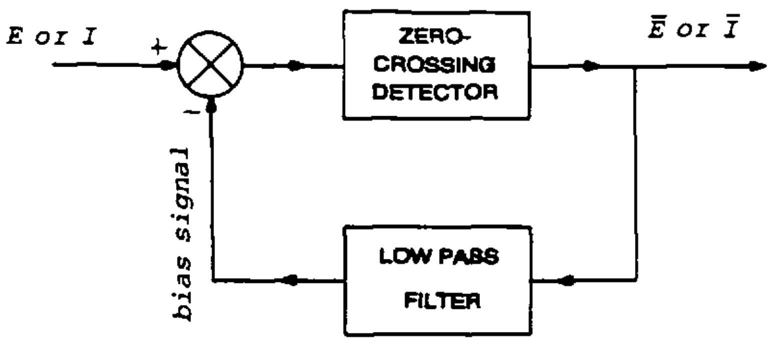

Figure (6.2): Schematic diagram of the circuit used by Cox (1973) for eliminating errors in the measurement of phase shift when employing the zero-crossing technique.

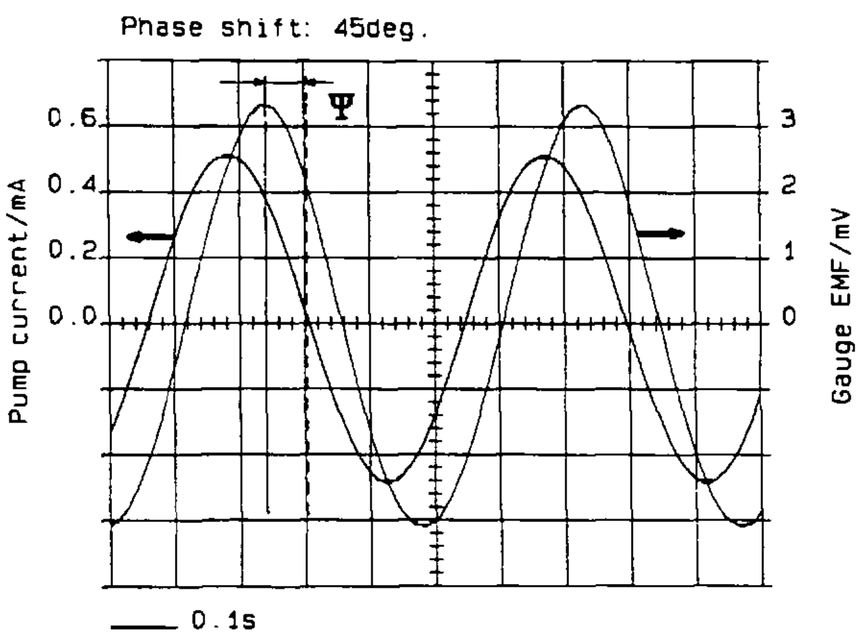

Figure (6.3): Sensor 9 operated in the AC mode at 700°C. Plot of the pumping current and gauge EMF showing the phase shift (Ψ) caused by the leak.

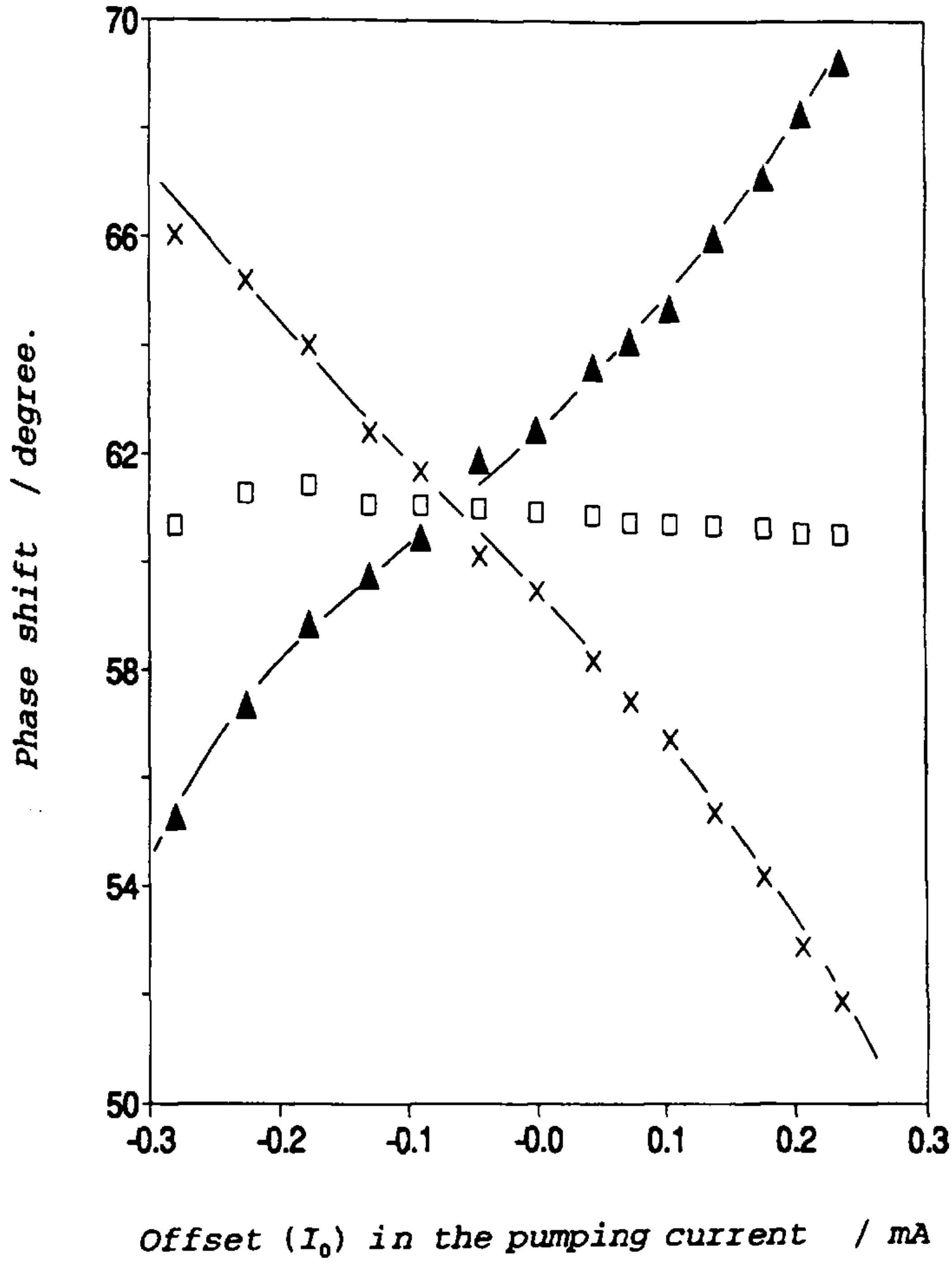

Figure (6.4): Sensor 4 operated in the AC+DC mode: measurement of the phase shift was not influenced by DC offsets. T=700°C, P_I=4kPa, A=0.43mA, f=0.38Hz. □ : Ψ, × : 90°-Ψ_P, ▲ : 90°-Ψ_R.

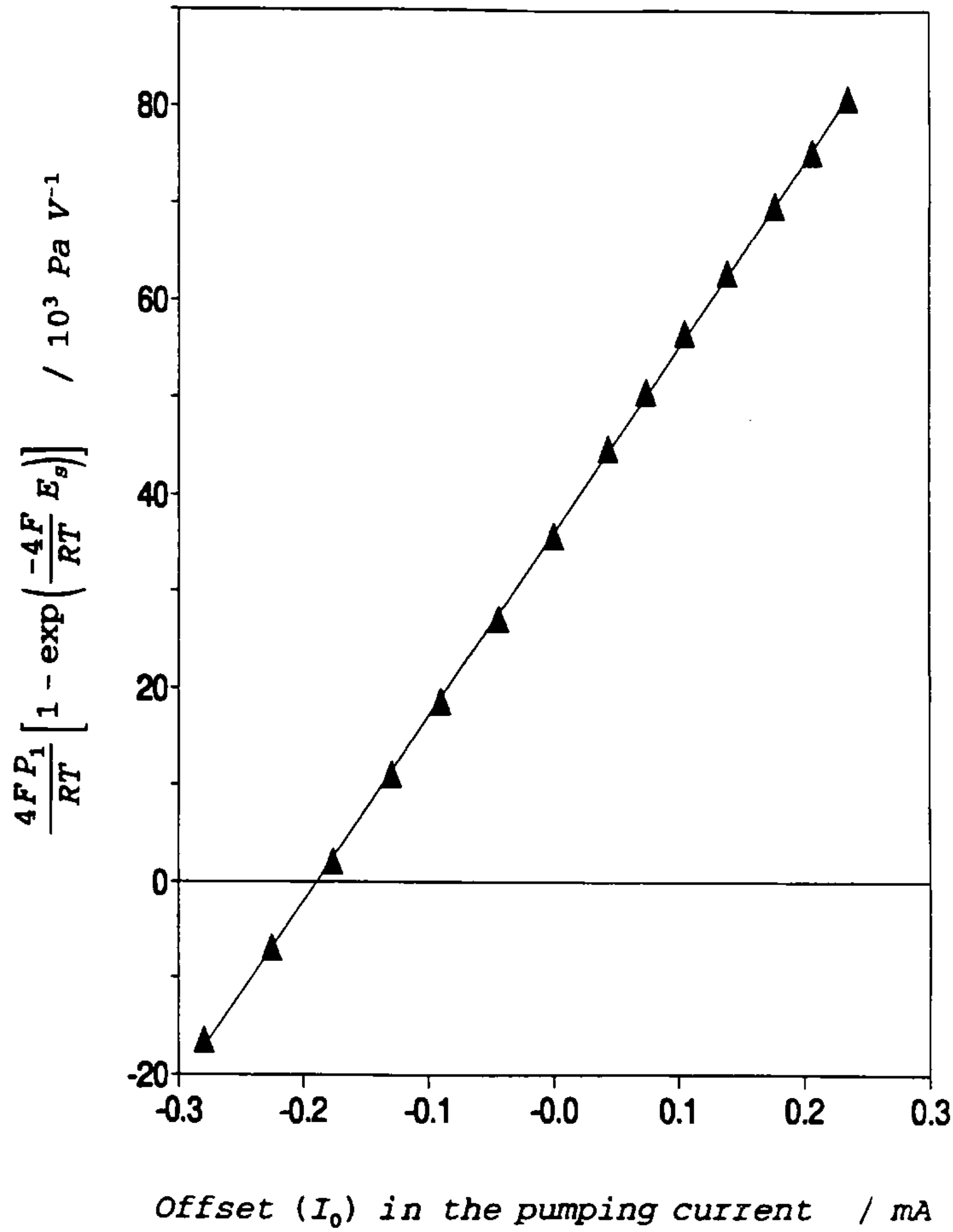

Figure (6.5): *Sensor 4 operated in the AC+DC mode: measurement of the amplitude of the gauge EMF. T=700°C, P_1=4kPa, A=0.43mA, f=0.38Hz.*

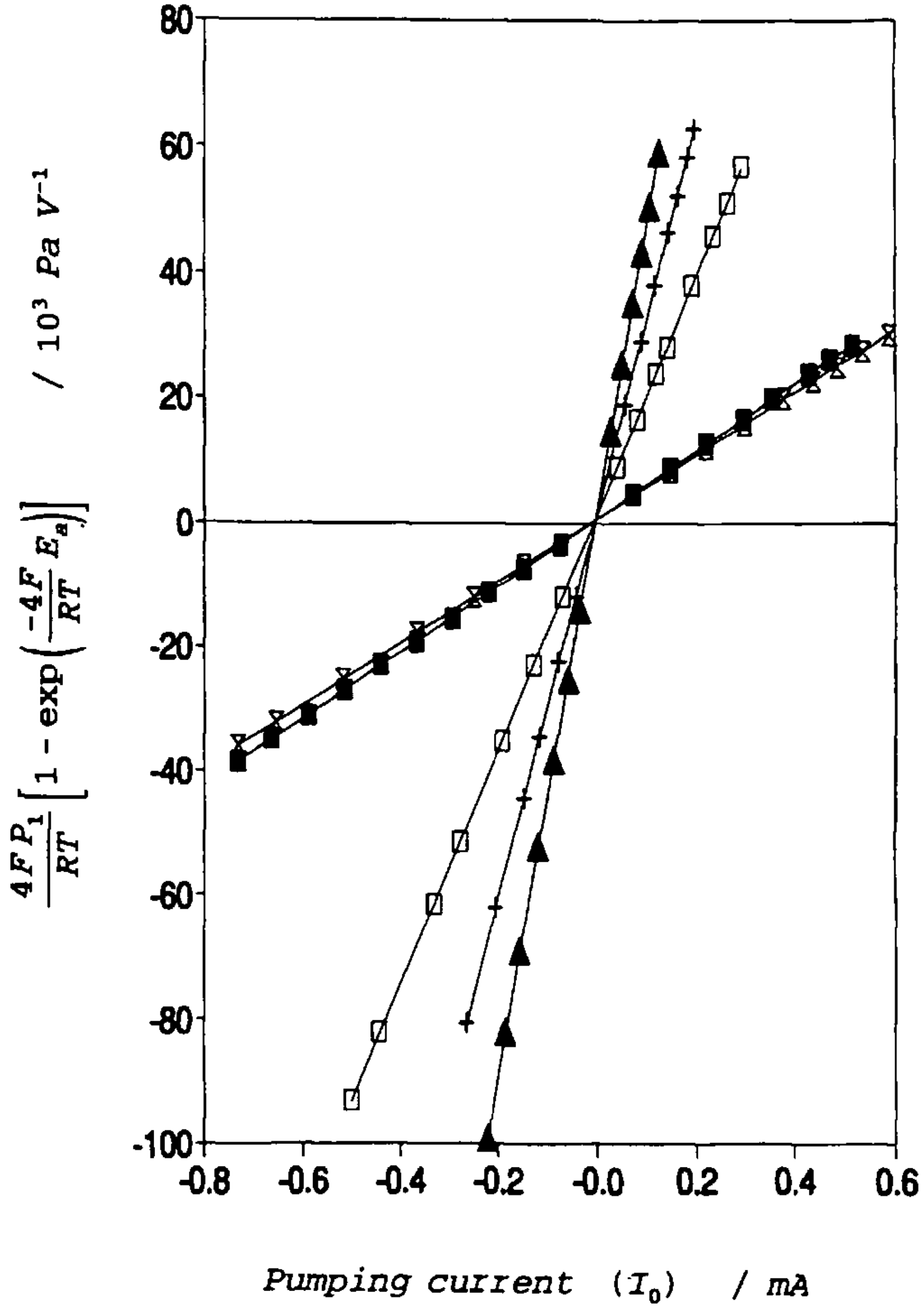

Figure (6.6): Operation in the DC mode: measurement of the amplitude of the gauge EMF at 700°C for a variable pumping current.

■ : sensor 16, P_I=1kPa.
⧗ : sensor 9, P_I=1kPa.
□ : sensor 4, P_I=2kPa.
▲ : sensor 2, P_I=2kPa.
+ : sensor 1, P_I=2kPa.

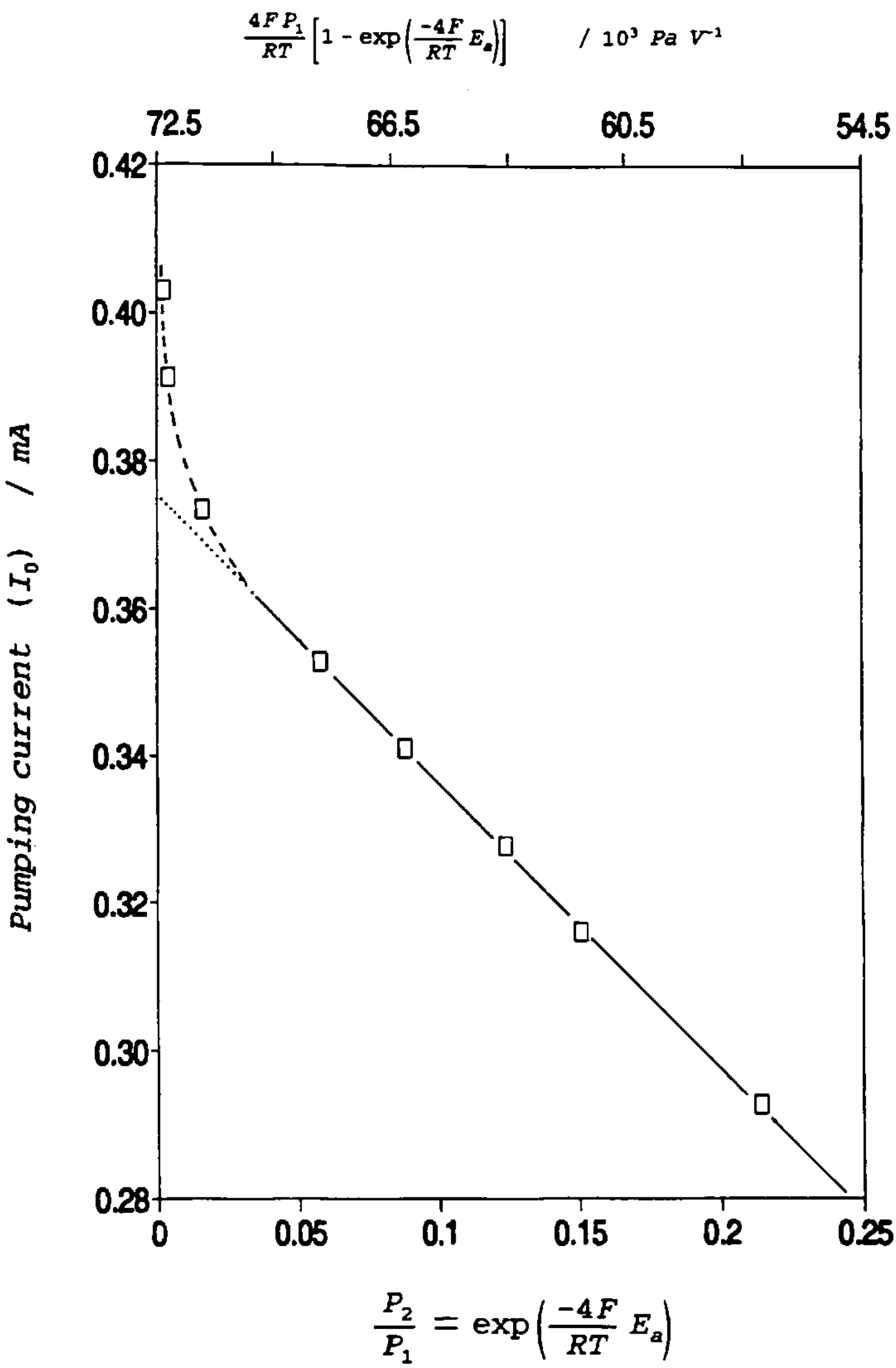

Figure (6.7): Sensor 4 operated in the DC mode: test showing electrochemical leakage effects occurring at high pumping current. (T=700°C, P_1=1.5kPa)

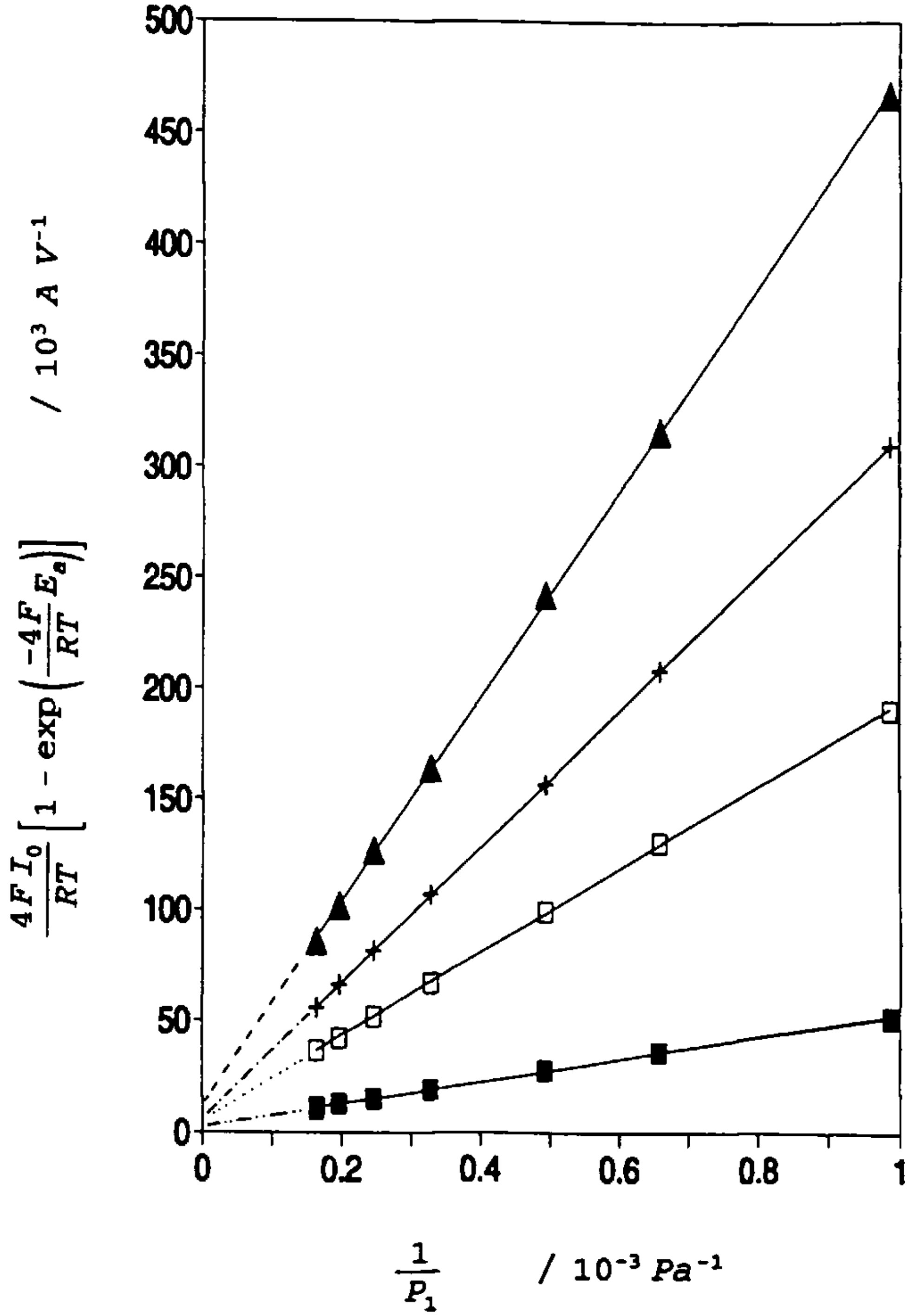

Figure (6.8)*: Operation in the DC mode: measurement of the amplitude of the gauge EMF at 700°C. (variable oxygen partial pressure)*

■ *: sensor 16, I_0=0.44mA.*

⧗ *: sensor 9, I_0=0.44mA.*

□ *: sensor 4, I_0=0.13mA.*

▲ *: sensor 2, I_0=0.06mA.*

\+ *: sensor 1, I_0=0.09mA.*

Note that on the graph, ⧗ *and* ■ *are superimposed.*

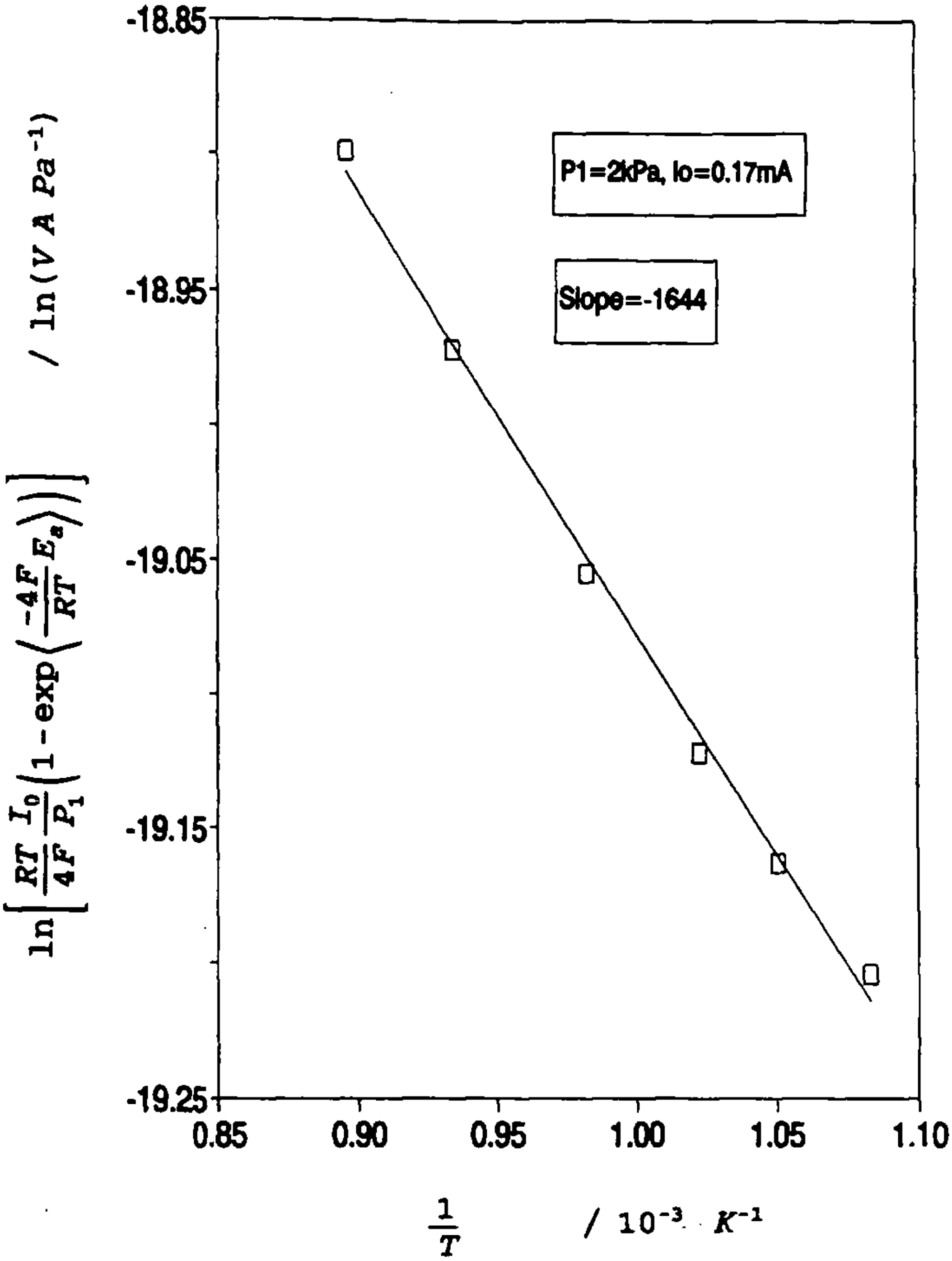

Figure (6.9a): Sensor 4 operated in the DC mode: Arrhenius plot of the oxygen diffusion coefficient. The computation of (DS / L) was achieved from a measurement of the amplitude of the gauge EMF.

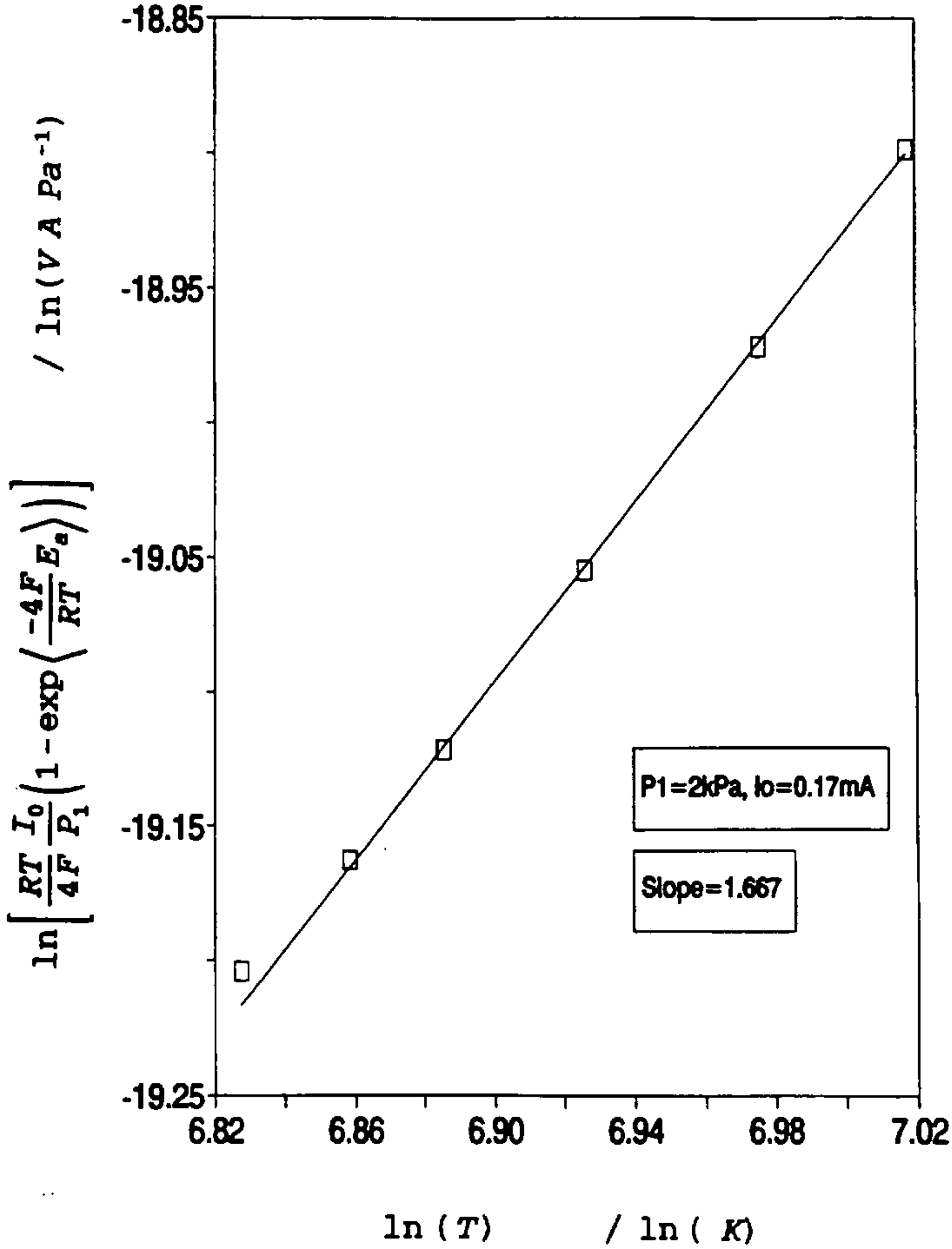

Figure (6.9b): Sensor 4 operated in the DC mode: dependence of D on temperature. The data of figure (6.9a) was used.

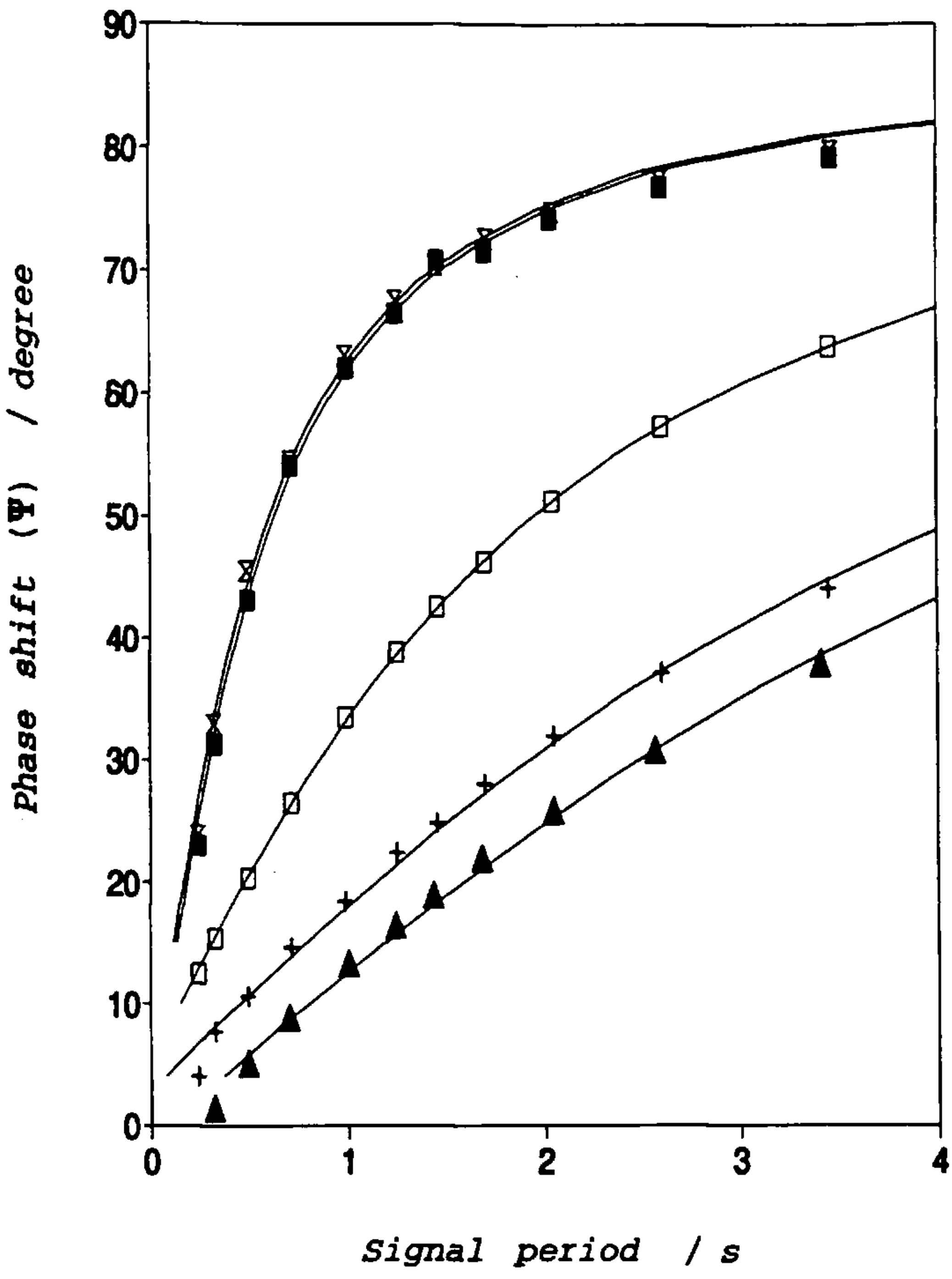

Figure (6.10): Operation in the AC mode: measurement of the phase shift for a variable frequency of the pumping current. T=700°C, A=0.77mA, P_I=4kPa.

■ : sensor 16, ⧖ : sensor 9, □: sensor 4,

▲ : sensor 2, + : sensor 1.

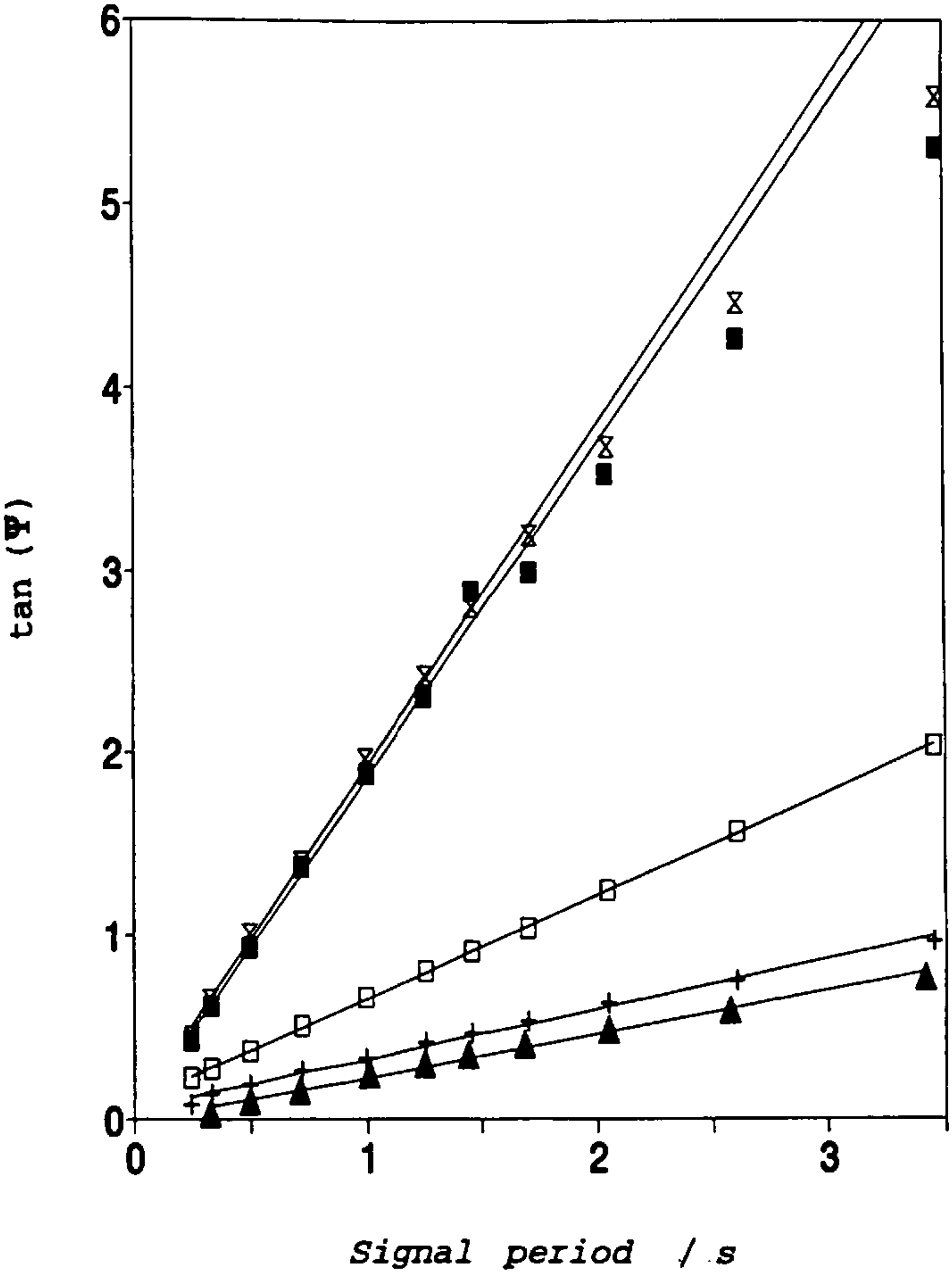

Figure (6.11): Plot of tan(Ψ) versus signal period using the data of figure (6.10).

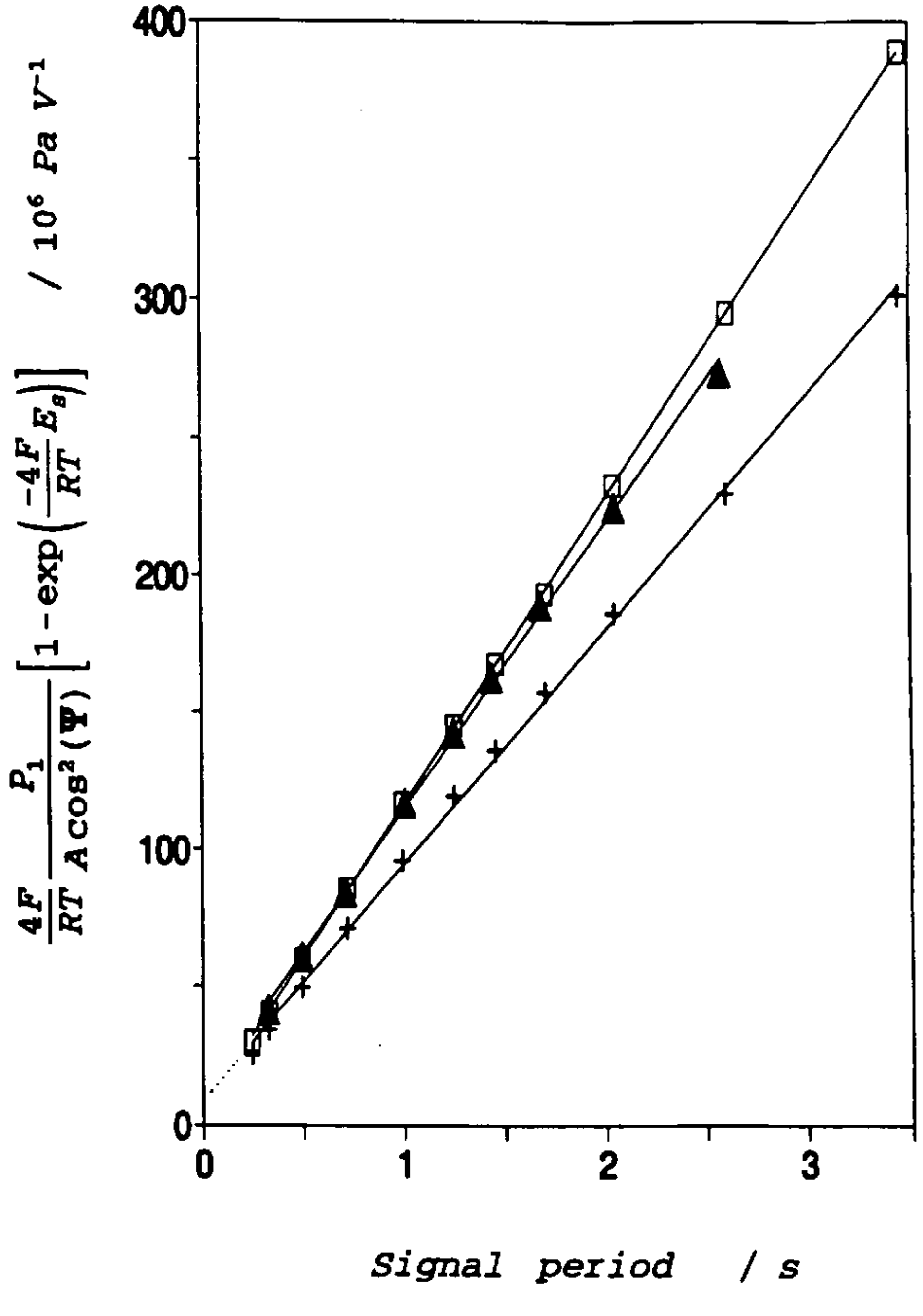

Figure (6.12): Operation in the AC mode: measurement of the amplitude of the gauge EMF. T=700°C, A=0.77mA, P_1=4kPa.

□ : sensor 4, ▲ : sensor 2, + : sensor 1.

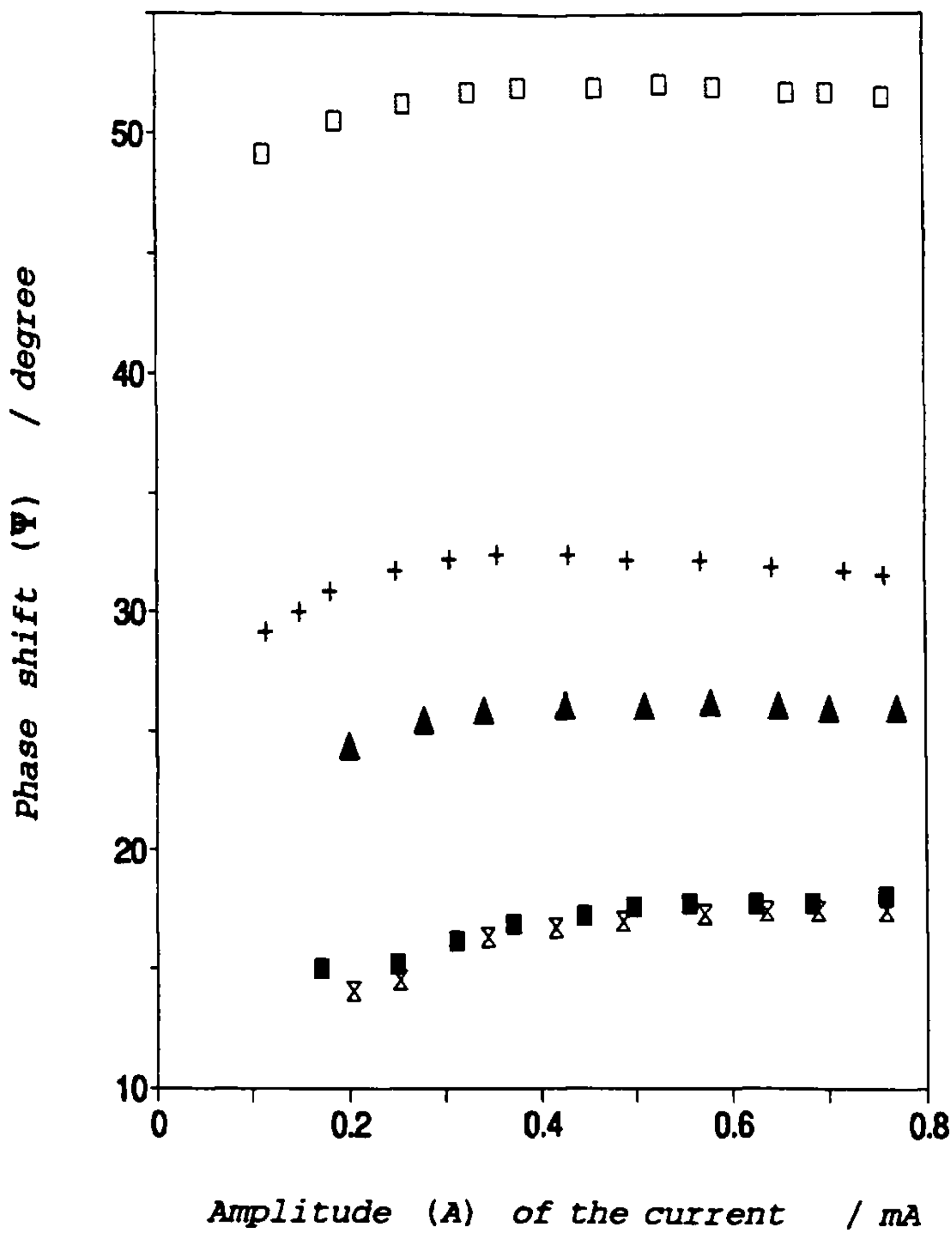

Figure (6.13): Operation in the AC mode: measurement of the phase shift for a variable pumping current. T=700°C.

■ : *sensor 16, f=4Hz, P_1=1kPa.*

⧗ : *sensor 9, f=4Hz, P_1=1kPa.*

□ : *sensor 4, f=0.5Hz, P_1=4kPa.*

▲ : *sensor 2, f=0.5Hz, P_1=5kPa.*

\+ : *sensor 1, f=0.5Hz, P_1=4kPa.*

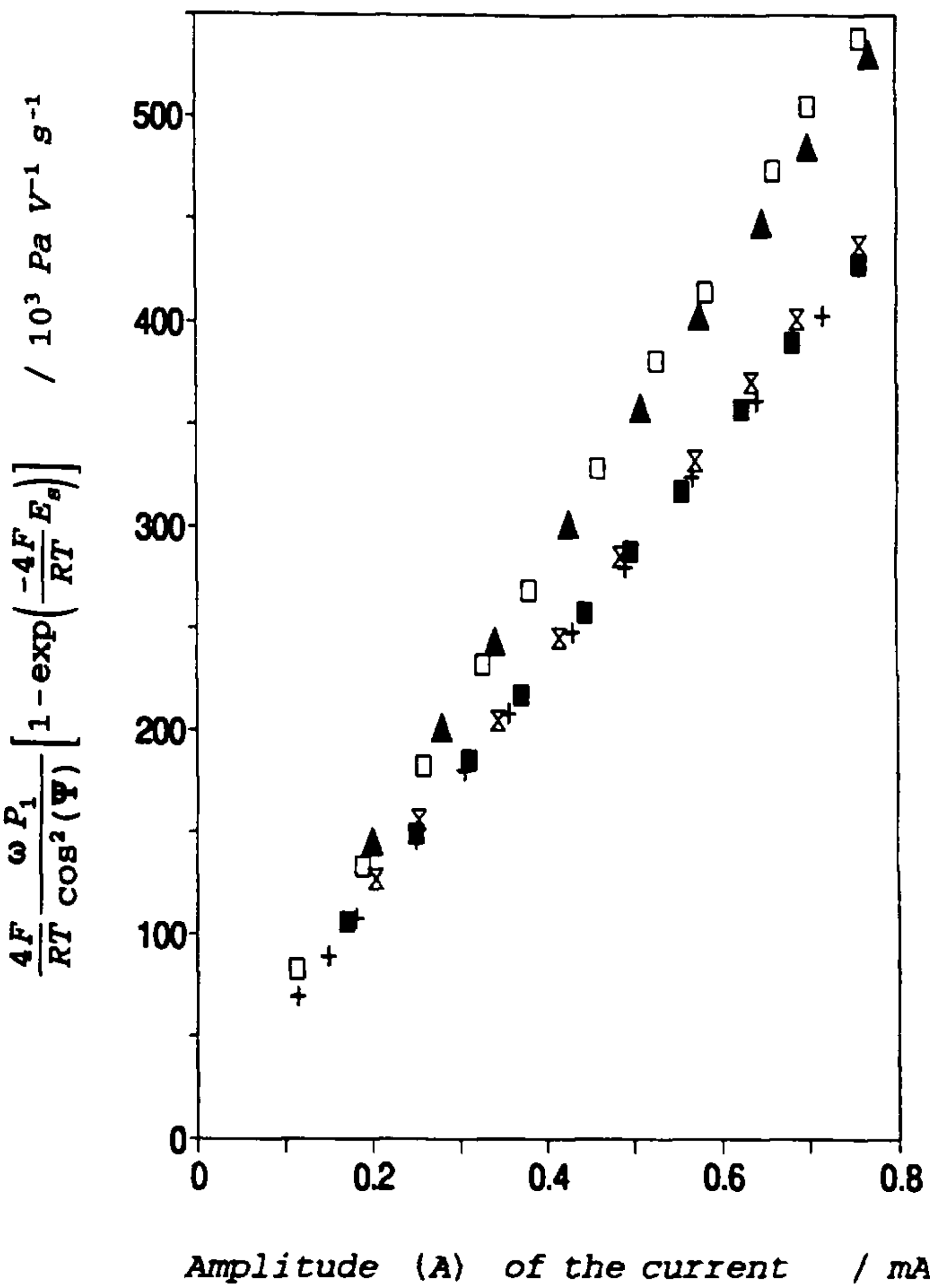

Figure (6.14): Operation in the AC mode: measurement of the amplitude of the gauge EMF. Markers and conditions as in Fig.(6.13).

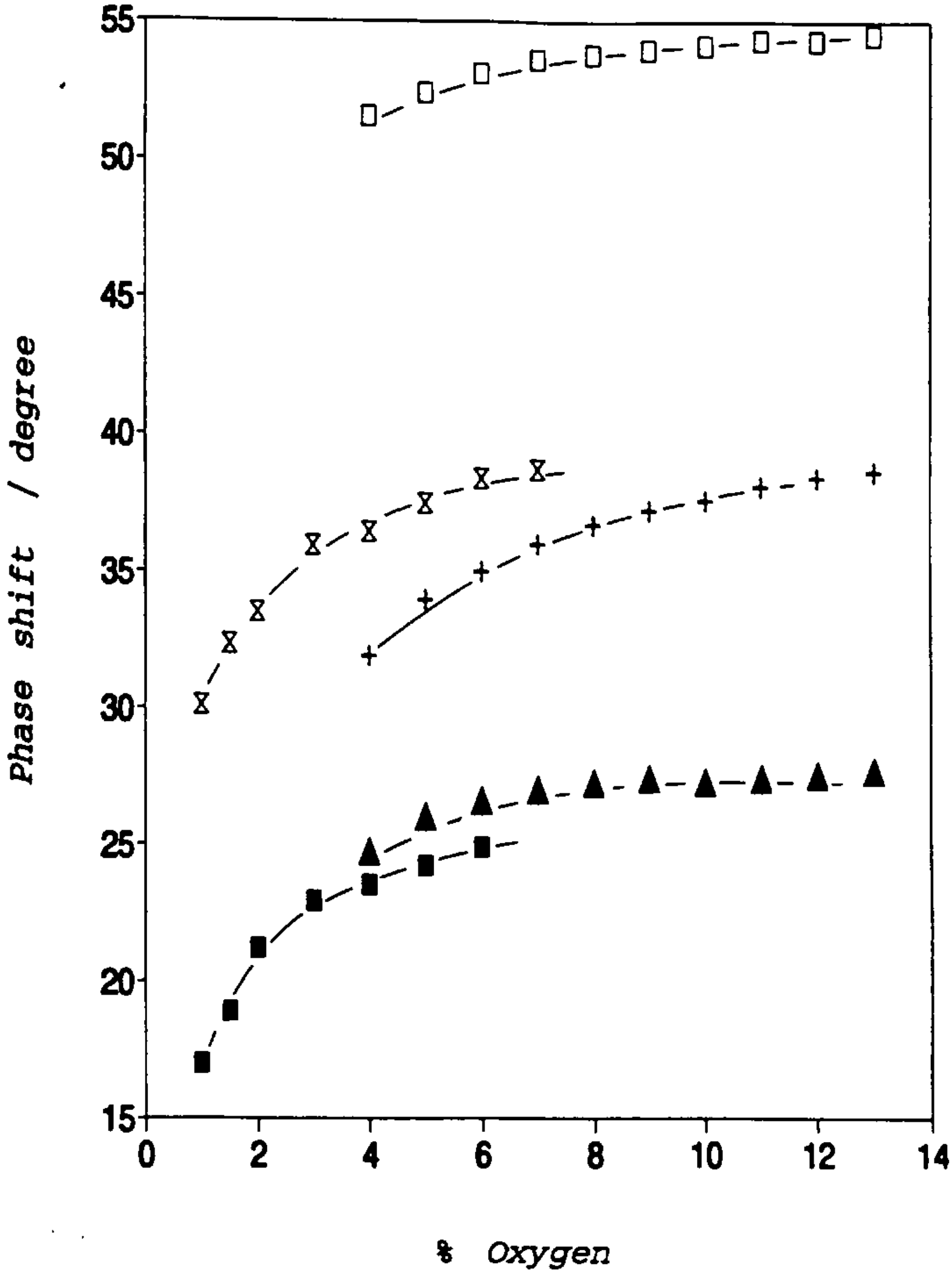

Figure (6.15): Operation in the AC mode: measurement of the phase shift for a variable oxygen concentration. T=700°C.

■ : *sensor 16, f=4Hz, A=0.76mA.*

⧗ : *sensor 9, f=2.9Hz, A=0.76mA.*

□ : *sensor 4, f=0.5Hz, A=0.76mA.*

▲ : *sensor 2, f=0.5Hz, A=0.62mA.*

\+ : *sensor 1, f=0.5Hz, A=0.76mA.*

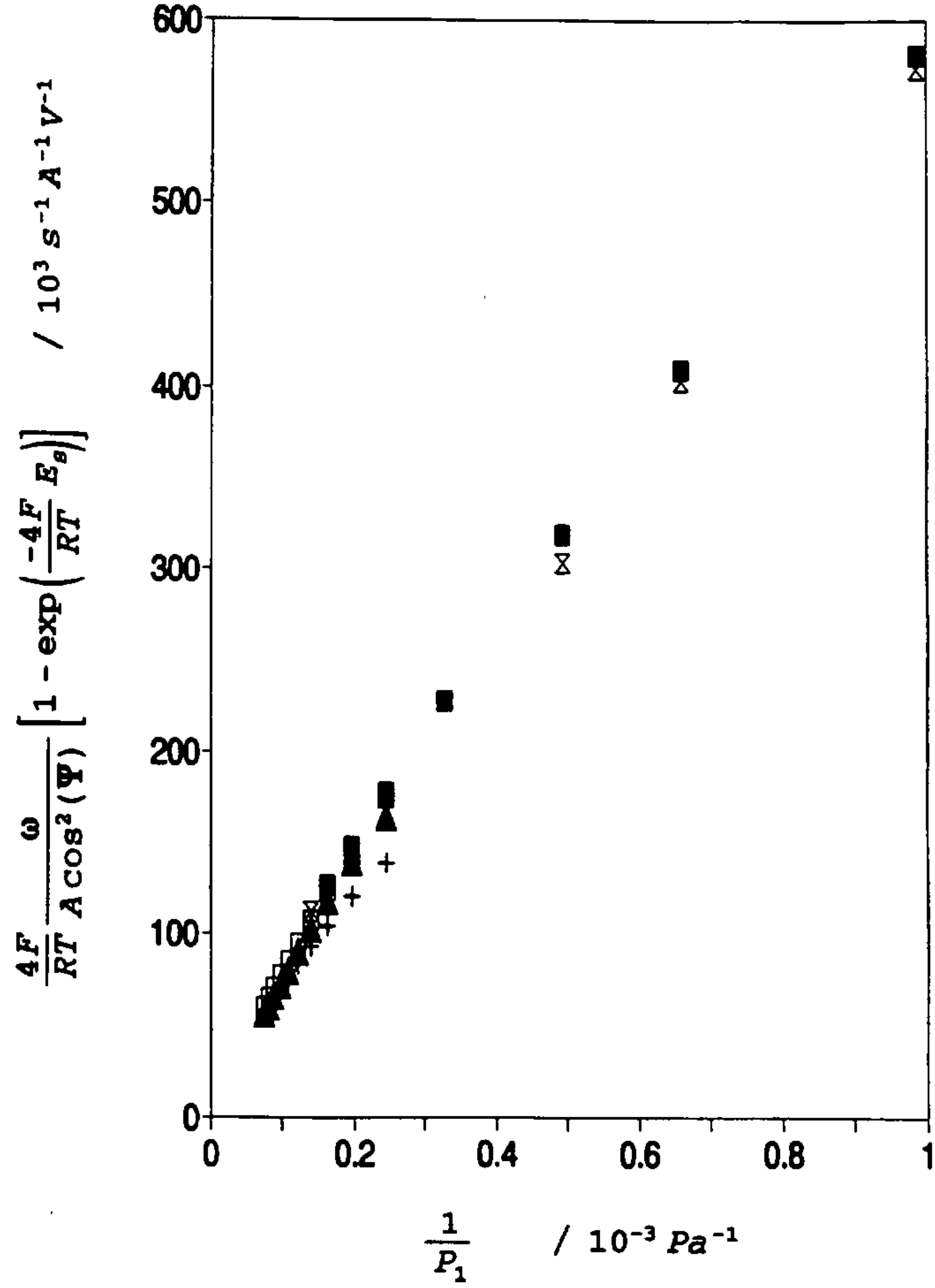

Figure (6.16): Operation in the AC mode: measurement of the amplitude of the gauge EMF. T=700°C.

■ : *sensor 16, f=4Hz, A=0.76mA.*

⧗ : *sensor 9, f=4Hz, A=0.76mA.*

□ : *sensor 4, f=0.5Hz, A=0.76mA.*

▲ : *sensor 2, f=0.5Hz, A=0.62mA.*

\+ : *sensor 1, f=0.5Hz, A=0.76mA.*

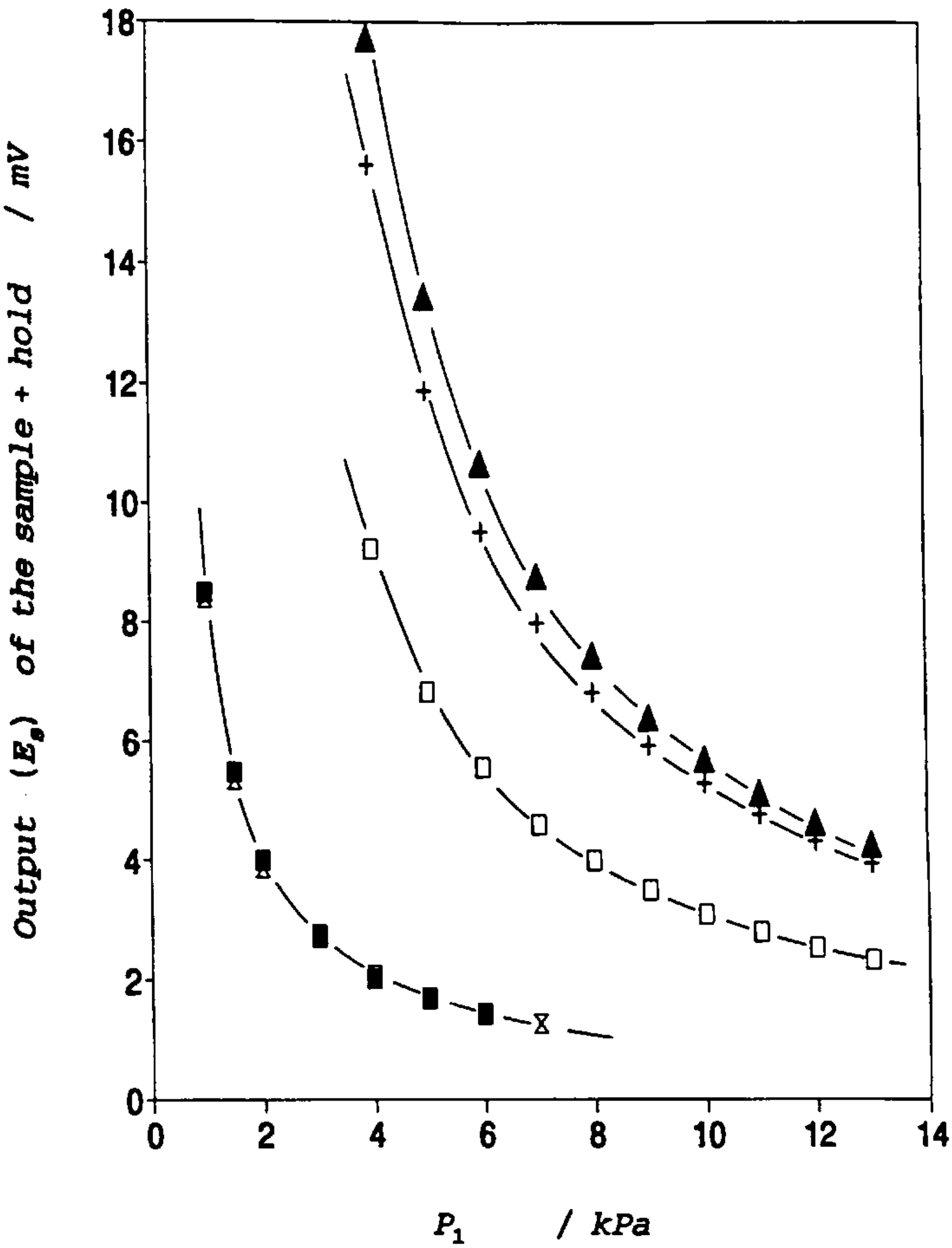

Figure (6.17): Operation in the AC mode: measured amplitude of the gauge EMF versus oxygen partial pressure. Markers and conditions as in figure (6.16).

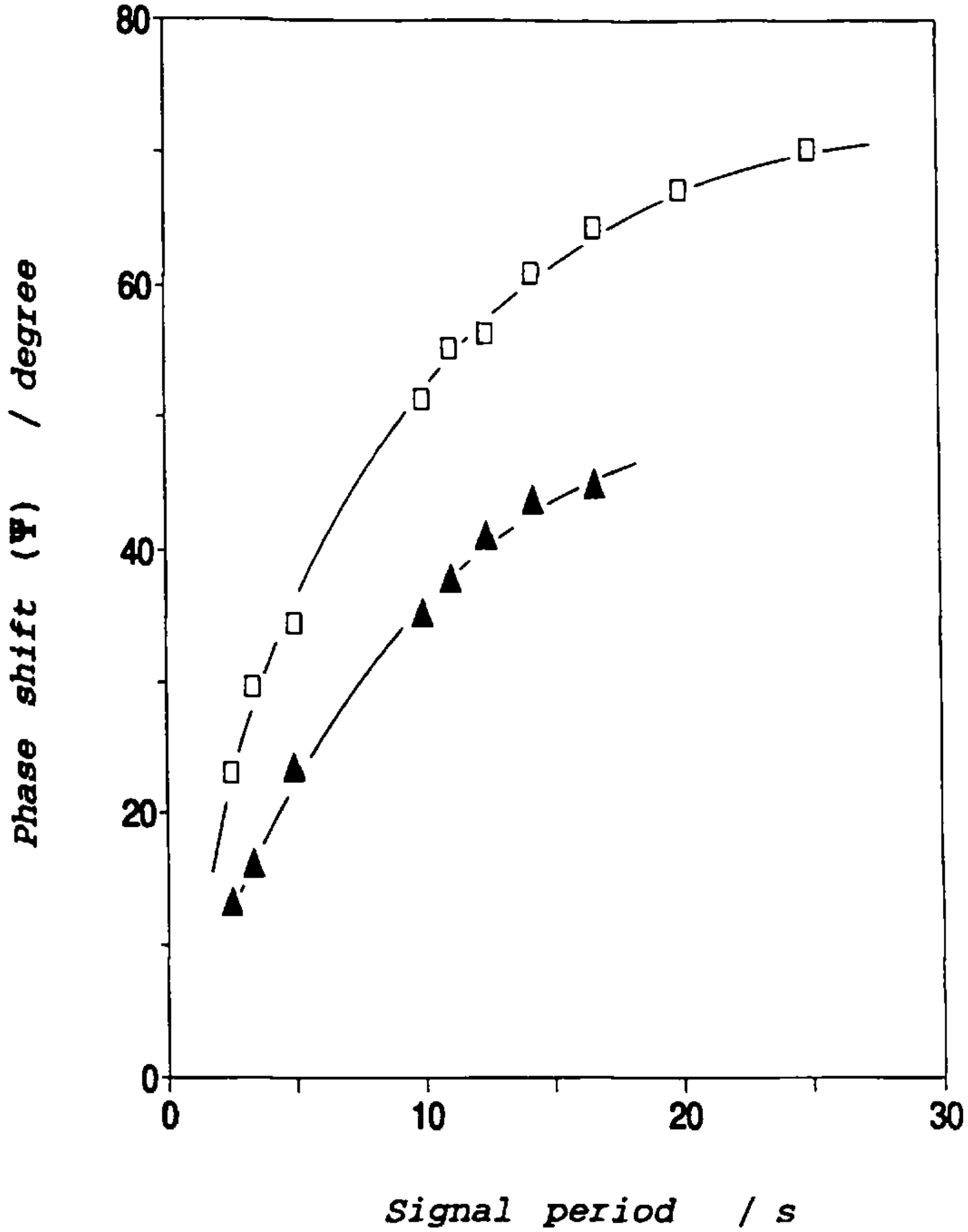

Figure (6.18): Measurement of phase shift in "fully" sealed devices. T=700°C, A=0.5mA, P_1=21kPa. ▲ : device with ground surface, □ : device with unground surface.

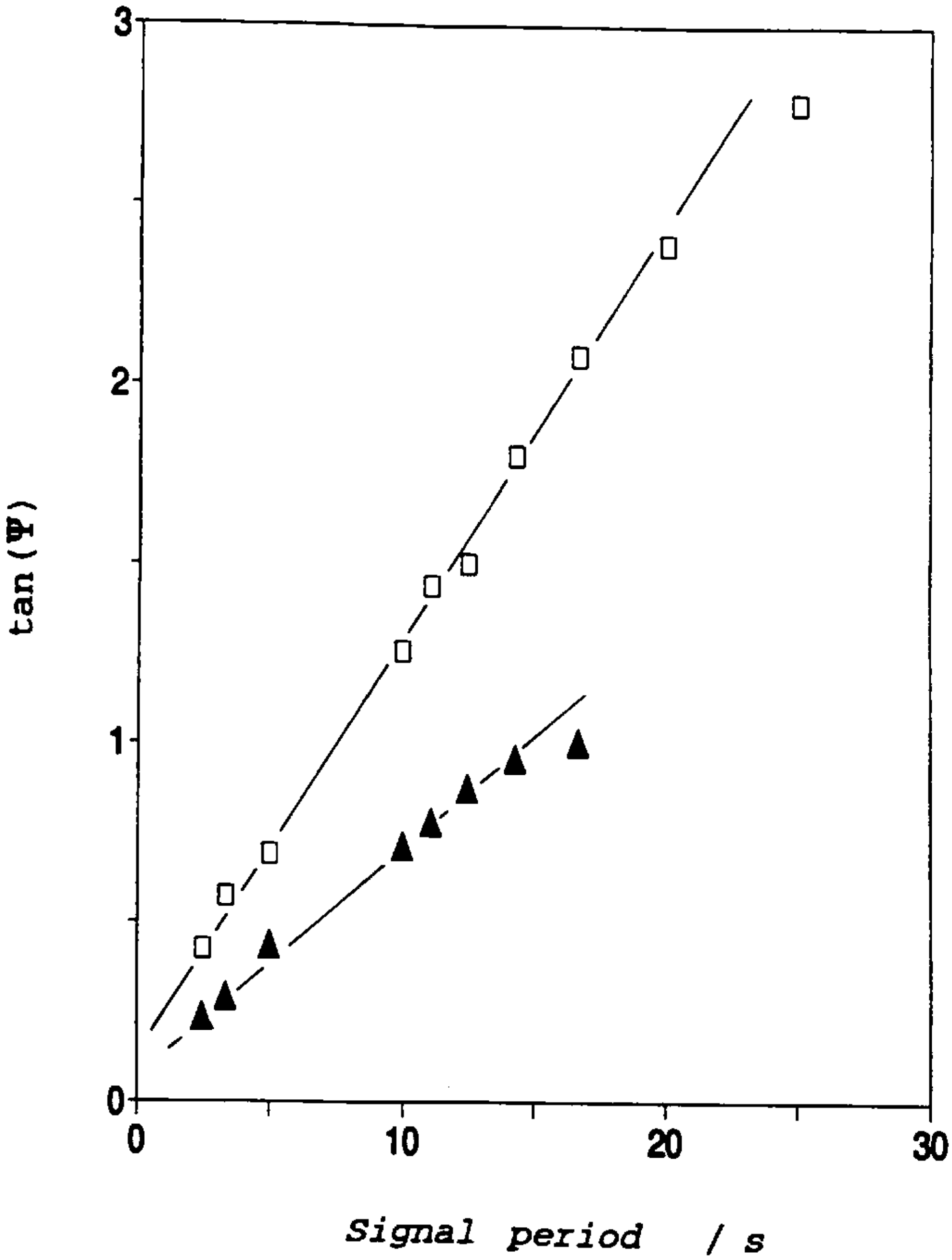

Figure (6.19): Tan(Ψ) versus signal period using the data of Fig.(6.18).

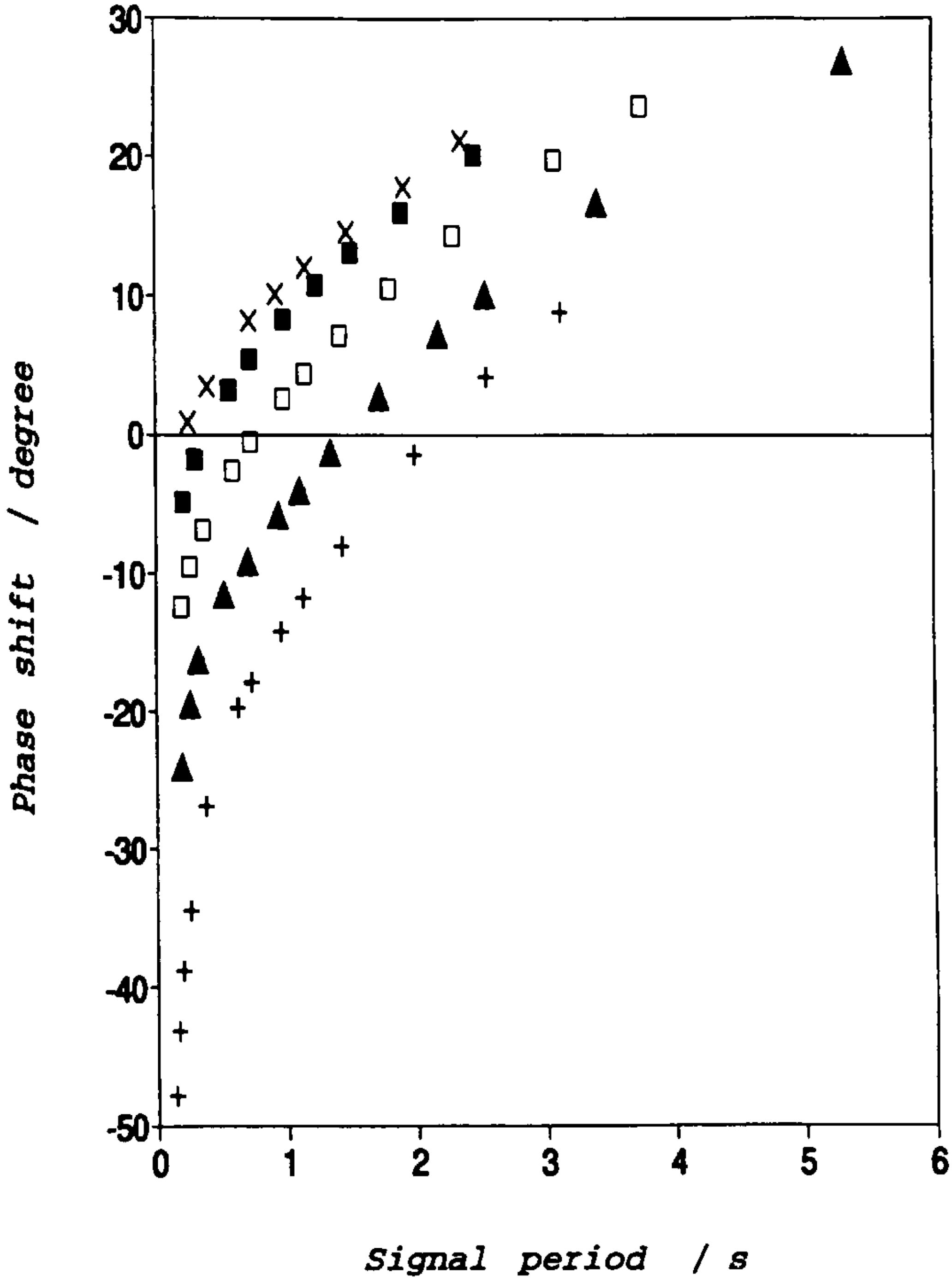

Figure (6.20): Measurement of phase shift using the device with unground surface operated at P_1=5kPa, A=0.63mA. Test at various temperatures showing the slow response of the electrodes manifested by the negative phase shift.
+ : 575°C, ▲ : 600°C, □ : 640°C, ■ : 680°C, × : 720°C.

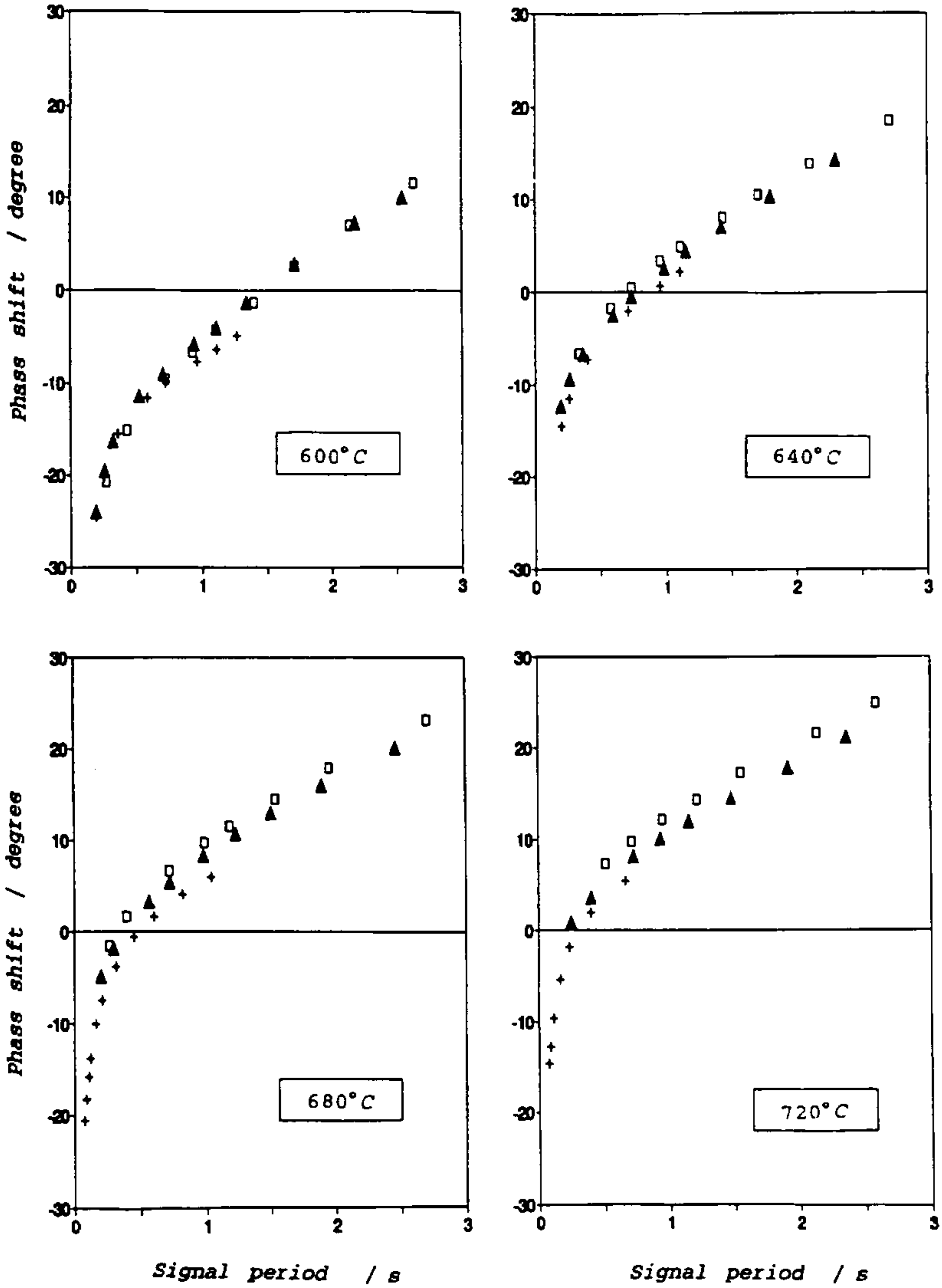

Figure (6.21): Phase shift measurement using the device with rough surface operated at various temperatures and oxygen partial pressures. A=0.63mA.
+ : 1kPa, ▲ : 5kPa, □ : 10kPa.

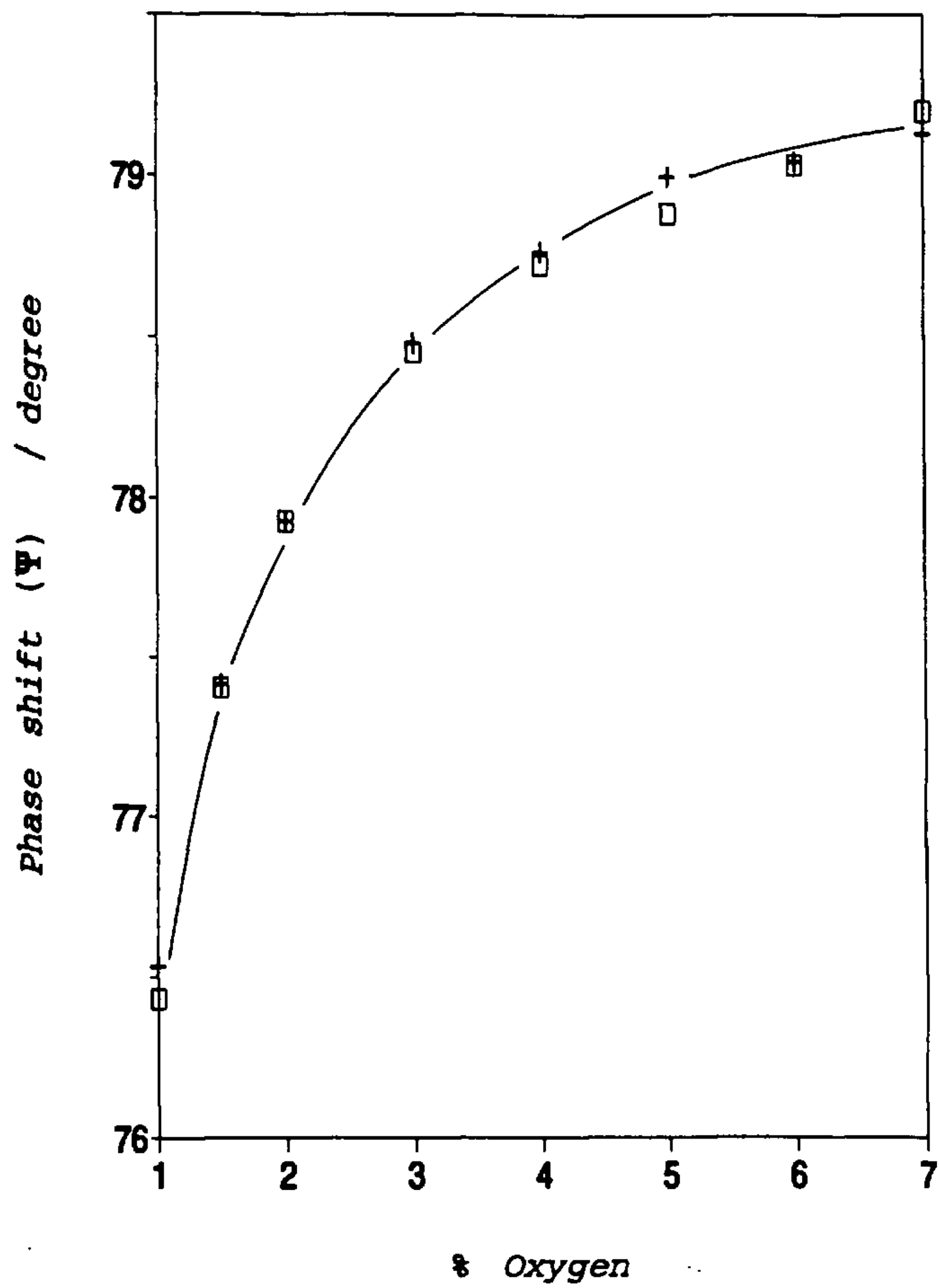

***Figure (6.22)**: Sensor 9 operated in the AC mode: measurement of the phase shift at T=850°C, f=0.6Hz under two conditions.*

□ : constant amplitude of the pumping current A=0.47mA,

+ : constant amplitude peak-to-peak of the gauge EMF (E_{pp}=18.6mV).

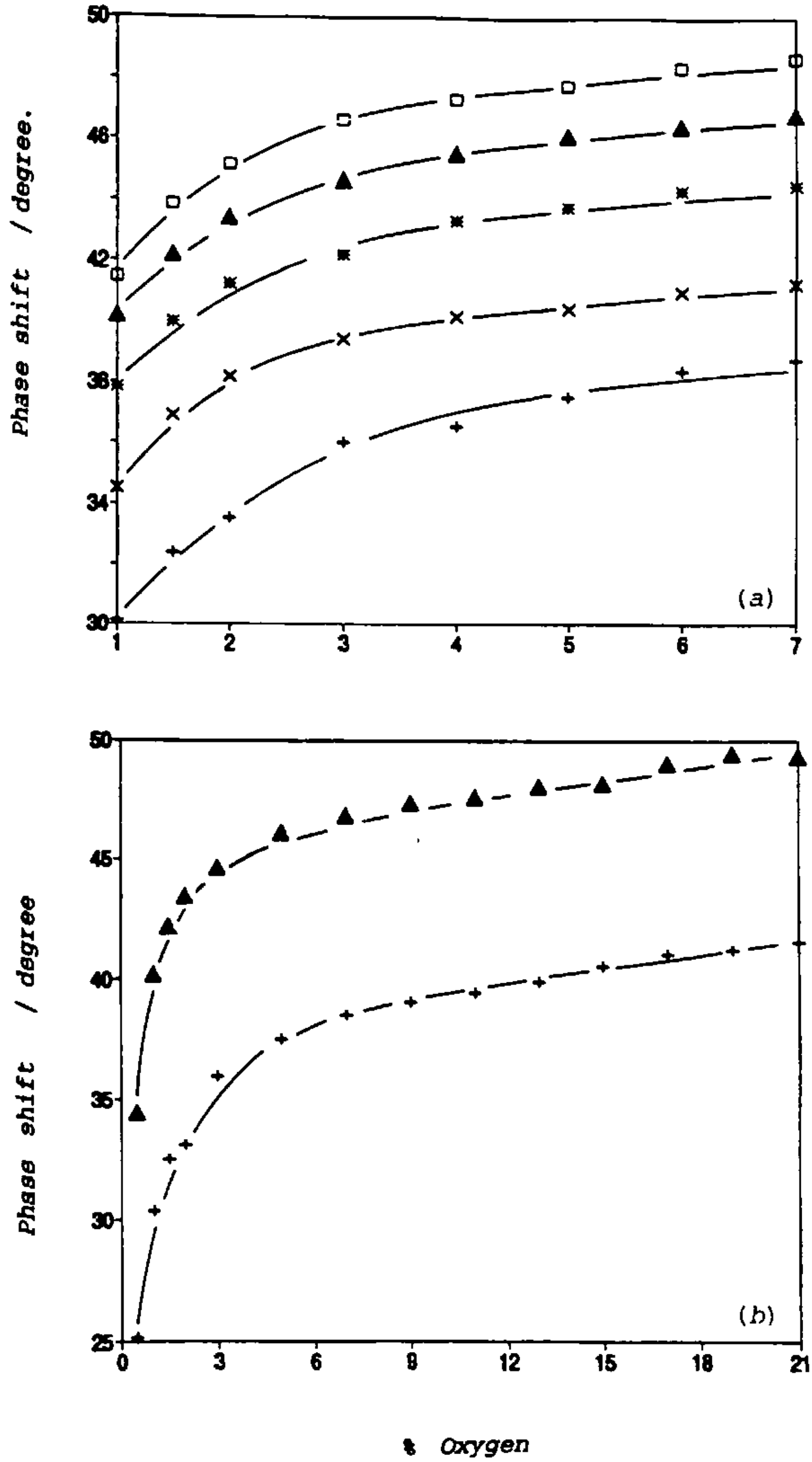

***Figure (6.23)**: Sensor 9 operated in the AC mode: phase shift measurement at various temperatures in the oxygen concentration range 1-7% (a) and 1-21% (b). f=2.9Hz, A=0.7mA. + : 700°C, × : 735°C, ✱: 775°C, ▲: 815°C, □ : 850°C.*

CHAPTER 7

CONCLUSIONS AND FURTHER WORK

"The world is round and the place which may seem like the end may also be only the beginning."

IVY BAKER PRIEST, Parade, Feb.16, 1958.

7.1 CONCLUSIONS

7.1.1 Fully-sealed devices

Zirconia-based fully sealed pump-gauge oxygen senaors and associated electronic circuitry were assembled for the measurement of oxygen partial pressure. Theory predicts that with a sinusoidal pumping current, the internal oxygen partial pressure may be caused to oscillate at the same frequency and should result in a pseudo-sinusoidal EMF to appear on the gauge,

$$E = \frac{RT}{4F}\left[\ln\left(\frac{P_1}{P_0}\right) - \ln\left(1 + \frac{RTA}{4F\nu\omega P_0}\cos x\right)\right] \tag{1.19}$$

Maskell et al (1986) suggested that by appropriate processing of the gauge EMF, the mean internal (P_0) and external (P_1) oxygen partial pressures may be measured simultaneously.

The device used normally operates in the temperature range 650-800°C. Previous work (Maskell et al 1987) indicated that maximum operating frequency of the pumping current to be around 0.1Hz, however experiments carried out in the present work showed that the device operated properly for frequencies up to 5-6Hz which made the practical implementation of the signal processing easier; the adopted frequency was 4Hz. Care was taken to ensure that the pumping current did not result in the imposition of a high voltage (~ above 2V) across the pump which might introduce electronic conductivity; in the present work a maximum current of 1mA was used.

Two techniques for the signal processing were developed: Potentiometric Mode and Tracking Mode. The Potentiometric Mode was originally suggested by Maskell et al (1986) and was based on the separation of the AC and DC components of the EMF: P_0, the mean internal (reference) oxygen partial pressure, was determined from a measurement of the amplitude of the AC component; for

$$\frac{RTA}{4Fv\omega P_0}<0.1 \tag{1.20}$$

theory predicts this amplitude to be inversely proportional to P_0; the above condition (eqn.1.20) is equivalent to an amplitude of the AC component less than 4.2mV at 700°C. The reason for this limitation is that the AC component of the EMF deviates from a pure sinusoid as its amplitude becomes higher (eqn.1.19). The measurement of the external oxygen partial pressure (P_1) was then made relative to the known internal reference P_0 using the DC component of the EMF, which is proportional to $\ln(P_1/P_0)$. The pressure P_0 was adjusted by applying a bias current to the pump in order to satisfy eqn.(1.20), and ideally this pressure is best maintained constant in which case the computation of P_1 requires the measurement of the DC component only. In the present work, various modifications were made to the originally suggested circuit diagram to achieve successful practical implementation. These modifications permitted substantial improvement of the signal-to-noise ratio: numerical integration of the theoretical equation (1.19) suggested that by using a PSD (with a square wave reference) for the measurement of the amplitude of the AC component, it should be possible to use AC components with amplitude of up to 17mV without significant loss of the required inverse-proportionality between the output of the PSD and P_0; the maximum error introduced was calculated to be 2%. Tests were made in the oxygen partial pressure range 1-10kPa, and the results obtained showed excellent agreement with the theory. It was not possible to maintain the mean oxygen partial pressure inside the device constant due to the practical limitations of physical and electrochemical leakage through the seal. Therefore the computation of P_1 required simultaneous measurement of the output of the PSD (i.e. for the computation of P_0) and the DC component of the EMF. This disadvantage could be avoided by developing a device with lower leakage: this may be achievable by using a glass rather than a gold seal.

The Tracking Mode was proposed, in the present work, as an improvement of the Potentiometric Mode. This system was primarily designed for minimum interference of leakage. The idea was based on maintaining the ratio (P_1/P_0) close to unity in order to minimise leakage effects. Moreover it was predicted that keeping the ratio (P_1/P_0) close to unity should result in a small DC component of the EMF [i.e. depending mainly on the log of the ratio (P_1/P_0)]. Consequently high amplification of the gauge EMF was possible without the risk of saturation of the electronics, thus improving the performance of the system. This Tracking Mode was implemented in two ways.

The first implementation of this mode was based on applying a bias current to the pump in order to keep the mean value of the gauge EMF equal to zero. Theoretical analysis indicated that such a constraint should result in

P_0 satisfying the equation

$$P_0 = P_1 + \frac{1}{4P_1}\left[\frac{RTA}{4F\nu\omega}\right]^2 \tag{A.23}$$

According to this relationship $\frac{1}{2}<(P_1/P_0)<1$ depending on the amplitude of the gauge EMF. This analysis also indicated that, at steady state, the gauge EMF should be given by

$$E = -\frac{RT}{4F}\ln\left[1 + \frac{R^2T^2A^2}{64F^2\nu^2\omega^2P_1^2} + \frac{RTA}{4F\nu\omega P_1}\cos x\right] \tag{A.21a}$$

Note that this mode of operation should be independent of the amplitude of the EMF (i.e. distortion from a sinusoid) allowing operation with large signal-to-noise ratio. By converting this EMF into DC output, P_1 may easily be determined: three AC-DC converters were suggested and theoretical simulation of their outputs as a function of the degree of distortion (from a sinusoid) of the EMF revealed interesting results. By using a simple RMS converter consisting of a rectifier followed by an averaging low pass filter, its output may be written

$$V_{01} = \frac{1}{\pi}\int_0^{\pi} |E|\, dx \tag{4.3}$$

No analytical solution was found for the above integral; however numerical integration indicated that to a close approximation

$$V_{01} = \left(\frac{R^2T^2A^2}{8\pi F^2\nu\omega}\right)\frac{1}{P_1} \tag{4.4}$$

regardless of the distortion of the gauge EMF. This inverse-proportionality between the output of the RMS converter and P_1 should make the computation of P_1 easy even when using analog electronics.

The second implementation was based on keeping the ratio $(P_1/P_0)=1$. Experimentally this was achieved by converting the gauge EMF into a square wave using a zero-crossing detector and keeping the mark-to-space ratio of the resulting square wave equal to 1 by applying a bias current to the pump in order to maintain $(P_1=P_0)$. The expression of the gauge EMF is then reduced to

$$E = -\frac{RT}{4F}\ln\left[1+\frac{RTA}{4F\nu\omega P_1}\cos x\right] \tag{4.18}$$

and the computation of P_1 may easily be achieved, for example, from a measurement of the amplitude of the positive peak (V_m) of the EMF,

$$P_1 = \frac{RTA}{4F\nu\omega}\frac{1}{1-\exp\left(\frac{-4F}{RT}V_m\right)} \tag{4.20}$$

The two described implementations with the various AC-DC converters were tested in the range 1-10kPa, and the results obtained showed excellent agreement with the theory; fast response (<1.5s) to changes in oxygen partial pressure were obtained. Unlike the Potentiometric Mode, the computation of P_1 was achieved by measuring a single DC output. Moreover, the electronics used were relatively simple and the operation with highly distorted gauge EMFs (i.e. with high amplitude) improved the signal-to-noise ratio and minimised offset problems.

The sensor normally operates in the temperature range 650-800°C. Theory predicted and experimental results confirmed large temperature dependence of the sensor output. Consequently, temperature compensation of the sensor-electronics output was investigated. Temperature compensation of the output of the RMS converter used in the Tracking Mode (eqn.4.4) was suggested and shown to be feasible using simple electronics. It was shown that by using a thermocouple, this compensation may be achieved in two ways: The first method was based on dividing the output of the converter (eqn.4.4) by T^2; where T^2 may be obtained from a linear approximation of the thermocouple EMF (Pt-Pt13Rh) within the operating temperature range of the sensor (650-800°C). The second method did not require a divider and was based on adjusting the ratio (P_1/P_0) in order to compensate for temperature variations. The system was optimised as to have a ratio (P_1/P_0) close to unity in order to minimise leakage effects; this led to $0.42<(P_1/P_0)<1.3$. Experimental results showed good agreement with the theory over the whole range of operating temperature of the sensor: the first method showed a compensation with better than 1.2% error over the temperature range 650-800°C while the compensation using the second method was within 4.2% of ideal within the same range of temperature.

7.1.2 Leaky devices

Leakage is an effect normally observed with supposedly fully-sealed devices. This effect may become a problem as the internal volume of the device is decreased. Consequently, the behaviour of non-hermetically sealed devices in the AC mode has been considered. Theory of operation of leaky devices was developed by considering a device with a diffusion pore subject to a sinusoidal pumping current; in such a system oxygen is electrochemically transferred into and out of the device via the solid electrolyte while the pore allows a certain amount of oxygen to diffuse into and out of the internal volume. By combining the two effects, the theory showed that the expression of the internal oxygen partial pressure may be determined by solving a single first degree differential equation. The expression of the gauge EMF was then developed for a sinusoidal current

$$E = -\frac{RT}{4F}\ln\left[1+\frac{RTA}{4Fv\omega P_1}\cos(\Psi)\cos(x+\Psi)\right] \tag{6.19}$$

where

$$\Psi = \tan^{-1}\left(\frac{DS}{\omega vL}\right) \tag{6.11a}$$

This theory suggested similar behaviour to that of fully-sealed devices, with a difference manifested by the presence of a phase shift and amplitude change in the gauge EMF of leaky devices. Theory predicts that this phase shift (Ψ) and amplitude change (by a factor $\cos\Psi$) should depend on the geometry and dimensions of the leak, the oxygen diffusion coefficient and the operating frequency of the AC current. Interestingly, eqn.(6.19) indicates that the diffusion pore should maintain the ratio $(P_1/P_0)=1$ without the need for a control loop. Theory suggests also that, besides measuring the oxygen partial pressure, a measurement of the phase shift should provide a reading of the absolute pressure since, according to the molecular theory of gases, the oxygen diffusion coefficient should be inversely proportional to the absolute pressure and independent of the oxygen concentration. Experiments under various conditions (i.e. hole size, frequency, oxygen partial pressure, amplitude of the pumping current and temperature) showed general agreement with the predicted theory with a minor deviation concerning the dependence of the phase shift on the oxygen concentration which was not predicted by the theory. Importantly, it has been shown that, when operated in the AC mode, devices with a substantial leak may still be used for oxygen partial pressure measurement, with a concomitant substantial simplification of the electronics compared with the fully-sealed devices since, in the case of leaky devices, no feedback loop is required. Another application of this theory of operation of leaky devices is that the meaaurement of the phase shift may be used to check the integrity of the seal in fully-sealed devices. In fact a continuous measurement of the phase shift may be used to compensate for any amplitude change (of the gauge EMF) caused by leakage that might appear with sensor aging for example. This compensation may be achieved using digital techniques.

7.2 FURTHER WORK

7.2.1 Response of the sensor

The sensor used was based on zirconia electrolyte-platinum electrode combination and was operated at around 700°C. This high temperature was necessary in order to achieve acceptable response characteristics which are related to electrolyte conductivity and electrode kinetics. Substantial advantages may be gained by improving the devices to allow them to operate below 500°C. There would be reduction in the power required for heating the device and more importantly the life of the thick film printed heaters used (and the complete sensor as a consequence) would increase substantially. Moreover, for the same operating temperature, an improvement of the response of the electrodes should enable the operating frequency of the AC current to be raised making the practical implementation of the electronics easier and the response of the whole system to changes in oxygen partial pressure faster.

7.2.2 Leaky devices

The minor deviation from the predicted theory of operation of leaky pump-gauge devices developed in Chapter 6 should be investigated. Suggestions were made in section (6.6.3) and could form a basis for this investigation. The theoretical model used may be improved and could lead to a better understanding of the behaviour of these devices in the AC mode. This study could lead to a system where leaky devices may be used to measure the barometric pressure and oxygen partial pressure simultaneously.

7.2.3 Operation in the substoichiometric region

The fully-sealed pump-gauge device offers the advantage of distinguishing the two sides of stoichiometry (Maskell 1991a). Experiments must be carried out to verify this prediction. The electronic systems for signal processing built throughout the present work are appropriate for this purpose.

REFERENCES

[1] Agrawal Y.K., Short D.W., Gruenke R., Rapp, R.A., (1974), J. Electrochem. Soc. 121, pp. 354-360.

[2] Alcock C.B. and Zador S., (1972), J. Appl. Electrochem. 2, pp. 289-299.

[3] Alesksakov G.N. and Godin Y.G., (1982), Élektrokhimiya, 18 (1), pp.109-113.

[4] Babu T.K.M. and Wong T.W., (1989), Int. J. Electronics, 67 (1), pp. 147-151.

[5] Bach J.H., Street P.J., and Twamley C.S., (1970), J. Phys. E: Sci. Instrum. 3, pp. 281-286.

[6] Badwal S.P.S, Bannister M.J., and Ciacchi F.T, (1988), J. Appl. Electrochem. 18, pp. 608-613.

[7] Bames R.N. and Williams C.C., (1973)," A precision digital phase meter" presented at the IEE Conf. Digital Instrum., Nov. 12-14.

[8] Beekmans N.M. and Heyne L., (1970), Philips Tech. Rev. 31, p112.

[9] Benammar M. and Maskell W.C., (1989), J. Phys. E: Sci. Instrum. 22, pp. 933-936.

[10] Bentley J.P., (1984), J. Phys. E: Sci. Instrum. 17 , pp. 430-439.

[11] Bergman I., (1970), UK Patent 1200595.

[12] Bergman I., (1974), UK Patent 1344616.

[13] Bergman A.P. and Franx C., (1984), International Gas Research Conference, p.805

[14] Bervas A., (1985), Int. J. Electronic 59, pp. 239-243

[15] Blair D.P. and Sydenham P.H., (1975), J. Phys. E: Sci. Instrum. 8, pp.621-627.

[16] Bogue R., (1990), Sixth sense: Information exchange in sensors R&D 8, DTI publication, p.2.

[17] Bonanos N., Slotwinski R.K., Steele B.C.H. and Butler E.P., (1984), J. Mater. Sci. 19, pp 785-793.

[18] Brand L., (1962), Advanced Calculus, 4th edition, p. 297.

[19] Brignell J.E. and Dorey A.P., (1983), J. Phys. E: Sci. Instrum. 16, pp. 952-958.

[20] Butler E.P., Slotwinski R.K., Bonanos N., Drennan J. and Steele B.C.H., (1984), Advances in Ceramics, Vol.12, ed N Claussen et al (Columbus, Ohio, Amer. Soc.) pp. 572-584.

[21] Calvert W.R. (1968), MATLAB 275.

[22] Chapman S. and Cowling T.G., (1952), "The Mathematical Theory of Non-uniform Gases", 2nd edition, Cambridge Univ. Press, London.

[23] Chauprade R., (1977), IEEE Trans. Industrial Applications 13, pp. 281-297.

[24] Clayton G.B., (1971), Operational Amplifiers, Butterworth, p.115.

[25] Clayton, G.B., (1973), Wireless World, July, pp. 355-356.

[26] Cleary J.G. and Elikan L., (1975), US Pat. 3915828.

[27] Cox P.P., (1973), U.S. Patent 3 725 781.

[28] Crank J., (1956), The Mathematics of Diffusion, Oxford University Press, second edition, p.2.

[29] DeJong H.L., (1983), U.S. Pat., 4,384,935.

[30] Deportes C.H., Henault M.P.S., Tasset F. and Vitter G.R.R., (1977), US Pat. 4045319.

[31] Dietz H., (1982), Solid State Ionics 6, pp. 175-183.

[32] Dietz H. Haecker W. and Jahnke H., (1977), Advances in Electrochemistry and Electrochemical Engineering, Vol.10, ed. H. Gerischer and C.W. Tobias (New York, Wiley-Interscience) pp 1-90.

[33] Evans W.A. and Skyes A.M., (1989), IEE Proc. G 136 (5), pp 285-292.

[34] Evans W.A. and Towers M.S., (1980), IEE Proc. G 127 (3), pp. 119-128.

[35] Fairbank L.H., (1977), Heat Treatment Metals 4, p.95.

[36] Fate W.A., Hetrick R.E. and Vassell W.C., (1981), Appl. Phys. Lett. 39 (11), pp. 924-926.

[37] Filanovsky I.M. and Fortier G.J., (1985), Electronics Letters 21 (18), pp. 791-792.

[38] Filanovsky I.M. and Stromsmoe K.A., (1986), IEEE Int. Symp. Cir. Systems, Vol. 2, pp. 574-578, California: May 5-7.

[39] Fouletier J., (1976), PhD Thesis, University of Grenoble.

[40] Fouletier J., (1982/3), Sensors and Actuators 3, pp. 295-314.

[41] Fouletier J., Seineara H. and Kleitz M., (1974), J. Appl. Electrochem. 4 , 305

[42] Fouletier J., Vitter G. and Kleitz M., (1975), J. Appl. Electrochem. 5, pp. 111-120.

[43] Franx C. , (1982), paper presented at 48th Autumn Mtg.Institution of Gas Engrs., Institution of Gas Engineers, London, Communication 1198.

[44] Franx C., (1984), Proc. Sensors and Actuators Symposium, Nov. 1-2, Kluwer, Deventer, The Netherlands.

[45] Franx C., (1985), Sensors and Actuators 7, pp. 263-270.

[46] Froelicher M., Gabrielli C. and Toque J.P., (1980), J. Appl. Electrochem. 10, pp. 71-74.

[47] Fuller E.N. and Giddings J.C., (1965), J. Gas Chromatogr. 3, p.222.

[48] Fuller E.N., Shettler P.D., and Giddings J.C., (1966), Ind. Eng. Chem. 58 (5), p.18.

[49] Galbright J.E., (1982), EDN, April issue p.101.

[50] Gradshteyn I.S. and Ryzhic I.M., (1980), 'Table of Integrals, Series, and Products', Academic Press, p.593.

[51] Graeme J.G., (1973), Applications of Operational Amplifiers, McGraw-Hill, p. 112.

[52] Graeme J.G., Tobey G.E. and Huelsman L.P., (1971), Operational Amplifiers: Design and Applications, McGraw Hill N.Y., p. 228.

[53] Haaland D.M., (1977), Analytical Chemistry 49 (12), pp. 1813-1817.

[54] Haldane J.S. and Graham J.I., (1935), Methods for Air Analysis (London: Griffin).

[55] Hart B.L. and Barker R.W.J., (1975), IEEE J. Solid-State Circuits 10, pp. 501-503.

[56] Haslett J.W. and Rao M.K.N., (1980), IEEE Trans. Instrum. Meas. 29 (3), pp.212-213.

[57] Hetrick R.E., (1981), U.S. Pat. 4,272,331.

[58] Hetrick R.E., Fate W.A. and Vassell W.C., (1981), Appl. Phys. Lett. 38 (5), pp. 390-392.

[59] Hetrick R.E., Fate W.A. and Vassell W.C., (1982), IEEE Trans. on Electron Devices 29 (1), pp. 129-132.

[60] Heyne L., (1976),in "Measurement of Oxygen", (Ed. H. Degn et al (Proc. Int. Symp. Odense Univ. 26-27 Sept. 1974, Elsevier, Amsterdam), pp. 65-88.

[61] Hickam W.M., (1967), US Pat. 3347767.

[62] Huang S.M., Stott A.L., Green R.G. and Beck M.S., (1988), J. Phys. E: Sci. Instrum. 21, pp 242-250.

[63] Huehne K., (1972), EDN Magazine, Aug.1, pp. 38-41.

[64] Huijsing J.H., (1990), IEE Proc. G. 137 (2), pp. 131-136.

[65] Ioannou A.S. and Maskell W.C., (1991), Proc. Symp. Deposition and Charaterisation of Electronic Materials, 17-19 July, Manchester, To be published by Royal Society of Chemistry.

[66] Jeng Y.C., (1988), IEEE Trans. Instrum. Meas. 37 (3), pp. 358-362.

[67] Jones R.V. and Richards J.C.S., (1973), J. Phys. E: Sci. Instrum. 6, pp. 589-600.

[68] Jones T.A., (1989), Measurement and Control 22, July/August isuue, pp. 176-182.

[69] Jou H.L., Chu H.Y., and Huang C.L., (1988), Proceedings of 3rd Symposium of the Technology of Education, Taiwan, pp. 313-323.

[70] Jou H.L., Chu H.Y., and Huang C.L., (1991), Int. J. Electronics 70 (2), pp. 367-375.

[71] Joyce J.W., (1968), HDL-TM 68-30.

[72] Joyce J.W. and Woods R.L., (1975), HDL-TM 75-17.

[73] Jung W.G., (1974), IC Op-Amp Cookbook, H.W. Sams-Macmillan, Indianapolis, Third edition.

[74] Kahler R.L., (1979), IEEE Trans. Instrum. Meas. 28 (2), pp. 162-164.

[75] Kaneko H., Maskell W.C., and Steele, B.C.H., (1987), Solid State Ionics 22, pp. 161-172.

[76] Kaplan A., Jurgens C. and Yu K., (1971), Instrum. Control Systems, February issue, pp. 113-4

[77] Karybakas C.A. and Micholtsis G.A., (1980), Int. J. Electronics 49 (1), pp. 67-72.

[78] Kobayachi N., Akatsuka T., Nakano J., Kamo T., and Matsushita S., (1984), JSAE Review, July, pp. 106-111.

[79] Kocache R., (1986), J. Phys. E: Sci. Instrum. 19, pp. 401-412.

[80] Kocache R.M.A. and Holman D.F., (1978), UK Pat. 1604445.

[81] Kocache R.M.A. and Holman D.F., (1979), UK Pat. 2052751.

[82] Mahmood M.K., Allos J.E., and Abdul-Karim M.A.H., (1985), IEEE Trans. Instrum. Meas. 34 (3), pp. 413-417.

[83] Marzetta L.A., (1971), IEEE Trans. Instrum. Meas. 20 (4), pp. 296-301.

[84] Maskell W.C., (1986), UK Patent 2 187 842 B.

[85] Maskell W.C., (1988), UK Registred Design N. 1053348.

[86] Maskell W.C., (1991a), Chapter 1 in "Techniques and Mechanisms in Gas Sensing", P.T. Moseley et al (Ed), Adam Hilger, Bristol, In Press.

[87] Maskell W.C., (1991b), UK Patent Application 9104223.4.

[88] Maskell W.C. and Steele B.C.H, (1986), J. Appl. Electrochem. 16, pp. 475-489.

[89] Maskell W.C. and Steele B.C.H, (1988), Solid State Ionics 28-30, pp. 1677-1681.

[90] Maskell W.C., Kaneko H., and Steele B.C.H., (1986), 2nd Int. Mtg. on Chemical Sensors, Bordeaux, 7-10 July, pp. 302-305.

[91] Maskell W.C., Kaneko H., and Steele B.C.H., (1987), J. Appl. Electrochem. 17, pp. 489-494.

[92] Meas Y., (1978), PhD Thesis, University of Grenoble.

[93] Meyer-Ebrecht D., (1972), Proc. IEEE Lett. 60, p.736.

[94] Micheletti R., (1991), IEEE Trans. Instrum. Meas. 40 (1), pp. 40-42.

[95] Mikhael W.B. and Tu S., (1984), IEEE Trans. on Circuits and Systems 31, pp. 280-293.

[96] Miramontes G. and Castro M., (1990), Meas. Sci. Technol. 1, pp. 485-490.

[97] Morgan F.D., Madden T.R., and Bennett B.R., (1986), IEEE Trans. Instrum. Meas. 35 (3), pp. 287-292.

[98] Mukhopadhyay P.K. and Raychaudhuri A.K., (1986), J. Phys. E: Sci. Instrum. 19, pp. 792-793.

[99] Oliver B.M. and Cage J.M., (1971), Electronic Measurements and Instrumentation, McGraw-Hill, Chap. 9, p.264.

[100] Pardy D., (1969), J. Sci. Instrum., Series 2, 2, pp. 526-530.

[101] Patranabis D., Ghosh S., Bandyopadhyay S., and Sarkar S., (1988), IEEE Trans. Instrum. Meas. 37 (1), pp. 58-61.

[102] Patranabis D., Sarkar S., Bandyopadhyay S., and Ghosh S., (1986), IEEE. Trans. Instrum. Meas. 35 (4), pp. 644-646.

[103] Patterson M.C. and Dann R.G., (1985), Communication 1270, 51st Autumn Meeting of the Institution of Gas Engineers, London, Nov.

[104] Paull C.J. and Evans W.A., (1974), The Radio and Electronic Engineer 44 (10), pp. 523-532.

[105] Philips N.V., (1971), U.K. Pat. 1 229 610, 28 April.

[106] Pichler H. and Pavuza F., (1988), J. Inst. Electronic & Radio Engineers 58 (5), pp. 244-50.

[107] Regtien P.P.L. and Trimp P.J., (1990), Sensors and Actuators A21-A23, pp. 615-618.

[108] Richman P. and Walker N., (1971), IEEE Trans. Instrum. Meas. 20 (4), pp. 313-319.

[109] Riggs W. and Evans W.A., (1981), IEE Proc. G. 128 (2), pp. 93-99.

[110] Rohr J.T., (1983), U.S. Pat. 4 394 222.

[111] Sayles D.A., (1975), US Pat. 3869370.

[112] Shepherd J.P. and Sandberg C.J., (1984), Rev. Sci. Instrum. 55 (10), pp. 1696-1699.

[113] Shubba V. and Ramesh T.G., (1986), J. Phys. E: Sci. Instrum. 19, pp. 916-918.

[114] Soejima S. and Mase S., (1985), SAE Paper 850378.

[115] Stacey F.D., Rynn J.M.W., Little E.C., and Croskell C., (1969), J. Sci. Instrum., Series 2, 2, pp.945-949.

[116] Stein R.L., (1976), BuMines-RI-8102.

[117] Stroud K.A., (1970), Engineering Mathematics Programmes and Solutions, Third Edition, MACMILLAN EDUCATION Ltd, p.711.

[118] Subbarao E.C., (1981), Advances in Ceramics, Vol. 3, Ed. A.H. Heuer and L.W. Hobbs (Columbus, Ohio, Amer. Soc.) pp. 1-24.

[119] Tay E.W. and Murti V.G.K., (1984), Electronics Lett. 20 (10), pp 431-432.

[120] Tedmon C.S. Jr., Spacil H.S., and Mitoff S.P., (1969), J. Electrochem. Soc. 116, p.1170.

[121] Towers M.S., (1982), IEE Proc. G. 129 (1), pp. 19-25.

[122] Vannerson E. and Smith K.C., (1974), IEEE J. of Solid-State Circuits 9 (4), pp. 176-179.

[123] Vitter G., Foster P., Lahlou M. and Gutierrez M., (1983), Solid State Ionics 9&10, pp. 1273-76.

[124] Wagdy M.F. and Lucas M.S.P., (1987), IEEE Trans. Instrum. Meas. 36 (3), pp. 721-724.

[125] Wang C.L., Ghosh P.K., and Kornreich P., (1989), J. Vac. Sci. Technol. A. 7 (3), pp. 2393-6.

[126] William D.S. and Paul J.R., (1989), Research and Development, Nov. issue, pp. 79-82.

[127] Williams P., (1965), J. Sci. Instrum. 42, pp. 474-476.

[128] Williams D.E. and McGeehin P., (1984), Electrochemistry 9, p. 246.

[129] Winnubst A.J.A., Scharenborg A.H.A. and Burggraaf A.J., (1985), J. Appl. Electrochem. 15, 139.

[130] Wojtyna R., (1989), Int. J. Electronics 67 (4), pp. 577-583.

[131] Young C.T. and Bode J.D., (1979), Society of Automative Engineers, Warrendale, PA, SAE Trans 88, 790143.

[132] Yuan D. and Kroger F.A., (1969), J. Electrochem. Soc. 116, pp. 594.

[133] "Perry's Chemical Engineer's Handbook", Perry R.H. (late editor), Green D.W. (editor), sixth edition, 1984, McGraw-Hill, p.3.285.

APPENDICES

APPENDIX A: DERIVATION OF THE EXPRESSION FOR THE AC COMPONENT IN THE TRACKING MODE

In this section, the expression for the AC component of the gauge EMF is derived for a sealed pump-gauge operated in the Tracking Mode (Chapter 4 and Chapter 5). The expressions of the AC gauge EMF were calculated under the following conditions:

Chapter 4

The gauge EMF is given by eqn.(1.19):

$$E = \frac{RT}{4F}\ln\left[\frac{P_1}{P_0}\right] + \frac{RT}{4F}\ln\left[1 + \frac{RTA}{4Fv\omega P_0}\cos x\right] \tag{1.19}$$

where

$$\frac{RTA}{4Fv\omega P_0} < 1 \tag{1.17}$$

The tracking condition is given by eqn.(4.1):

$$\frac{1}{\pi}\int_0^\pi E\,dx = 0 \tag{4.1}$$

Chapter 5

The gauge EMF is given by eqn.(1.19). The tracking condition is given by:

$$\frac{1}{\pi}\int_0^\pi E\,dx = V_r \tag{5.1}$$

where V_r is a DC reference voltage.

ANALYSIS

In the following, the analysis relates to the general case. The relevant equations used in each chapter are given in the end of this Appendix. Let the general expression of the gauge EMF be:

$$E = K \ln\left[\frac{P_1}{P_0}\right] - K \ln\left[1 + \frac{W}{P_0}\cos(x)\right] \tag{A.1}$$

where

$$K = \frac{RT}{4F} \tag{A.1a}$$

and

$$W = \frac{RTA}{4Fv\omega} \tag{A.1b}$$

The general expression of the mean value of the gauge EMF be:

$$V_r = \frac{1}{\pi}\int_0^\pi E\, dx \tag{5.1}$$

Equation (4.1) is the special case where V_r=0.

Substituting for E from eqn.(A.1) in eqn.(5.1) gives

$$V_r = K\left[\ln\left(\frac{P_1}{P_0}\right) - \frac{1}{\pi}\int_0^\pi \ln\left(1+\frac{W}{P_0}\cos x\right)dx\right] \tag{A.2}$$

The expression of the mean internal oxygen partial pressure P_0 may be determined by developing eqn.(A.2). The solution of the integral in eqn.(A.2) is given by Brand (1962).

$$\int_0^\pi \ln\left(1+\frac{W}{P_0}\cos x\right)dx = \pi \ln\left[\frac{1+\sqrt{1-\left(\frac{W}{P_0}\right)^2}}{2}\right] \tag{A.3}$$

It followa that:

$$V_r = K\left[\ln\left(\frac{P_1}{P_0}\right) - \ln\left(\frac{1+\sqrt{1-\left(\frac{W}{P_0}\right)^2}}{2}\right)\right] \tag{A.4}$$

The expression for the AC component as a function of the mean internal O_2 pressure P_0 may now be derived. From eqn.(A.1) and eqn.(A.4)

$$E-V_r = K\left[\ln\left(\frac{1+\sqrt{1-\left(\frac{W}{P_0}\right)^2}}{2}\right) - \ln\left(1+\frac{W}{P_0}\cos x\right)\right] \tag{A.5}$$

In order to express the AC component in eqn.(A.5) as a function of P_1, a well defined relation between P_1 and P_0 must be found. From eqn.(A.4)

$$V_r = K\ln\left[\frac{2P_1}{P_0+P_0\sqrt{1-\left(\frac{W}{P_0}\right)^2}}\right] \tag{A.6}$$

Rearranging

$$P_1 = \frac{P_0}{2}\left[1+\sqrt{1-\left(\frac{W}{P_0}\right)^2}\right]\exp\left(\frac{V_r}{K}\right) \tag{A.7}$$

It follows

$$\sqrt{1-\left(\frac{W}{P_0}\right)^2} = \frac{2P_1}{P_0\exp\left(\frac{V_r}{K}\right)} - 1 \tag{A.8}$$

Squaring both sides of eqn.(A.8) gives

$$-W^2 = \frac{4P_1^2}{\exp^2\left(\frac{V_r}{K}\right)} - \frac{4P_1 P_0}{\exp\left(\frac{V_r}{K}\right)} \tag{A.9}$$

The expression for P_0 may then be written

$$P_0 = \frac{P_1}{\exp\left(\frac{V_r}{K}\right)} + \frac{W^2}{4P_1}\exp\left(\frac{V_r}{K}\right) \tag{A.10}$$

Equation (A.10) may be written

$$P_0 = \frac{P_1}{Y} + \frac{W^2}{4P_1}Y \tag{A.11}$$

where

$$Y = \exp\left(\frac{V_r}{K}\right) \tag{A.12}$$

From eqn.(A.11) it follows that

$$\frac{W}{P_0} = \frac{W}{\frac{P_1}{Y} + \frac{W^2}{4P_1}Y} \tag{A.13}$$

$$= \frac{4P_1 YW}{4P_1^2 + W^2 Y^2} \tag{A.14}$$

And hence

$$1 + \frac{W}{P_0}\cos x = \frac{4P_1^2 + W^2Y^2 + 4P_1 YW\cos x}{4P_1^2 + W^2Y^2} \tag{A.15}$$

and

$$1+\sqrt{1-\left(\frac{W}{P_0}\right)^2} = \frac{8P_1^2}{4P_1^2+W^2Y^2} \tag{A.16}$$

Equation (A.5) may then be written:

$$\begin{aligned} E-V_r &= K\left[\ln\left(\frac{4P_1^2}{4P_1^2+W^2Y^2}\right) - \ln\left(\frac{4P_1^2+W^2Y^2+4P_1YW\cos x}{4P_1^2+W^2Y^2}\right)\right] \\ &= K\ln\left(\frac{4P_1^2}{4P_1^2+W^2Y^2+4P_1YW\cos x}\right) \\ &= -K\ln\left[1+\left(\frac{WY}{2P_1}\right)^2+2\left(\frac{WY}{2P_1}\right)\cos x\right] \end{aligned} \tag{A.17}$$

Equation (A.17) may be written

$$E-V_r = -K\ln\left(1+u^2+2u\cos x\right) \tag{A.18}$$

where
$$\begin{aligned} u &= \frac{WY}{2P_1} \\ &= \frac{W}{2P_1}\exp\left(\frac{V_r}{K}\right) \end{aligned} \tag{A.19}$$

Equation (A.18) gives the general expression for the AC component of the EMF for $(W/P_0)<1$ [obtained from (1.17) and (A.1b)]. This condition may be expressed as a function of u. Substituting for P_1 (given in eqn.(A.7)) in the expression of u gives:

$$u = \frac{W}{P_0\left(1+\sqrt{1-\left(\frac{W}{P_0}\right)^2}\right)} \tag{A.20}$$

From eqn.(A.20) it can be seen that $(W/P_0)<1$ [from eqn.(1.17) and (A.1b)] is equivalent to u<1. Therefore eqn.(A.18) is the general equation of the EMF and is valid for u<1.

CONCLUSION

In the following the expressions of the gauge EMF and P_0 are given for the various cases described in the beginning of the Appendix.

Chapter 4

The expression of the gauge EMF is given by:

$$E = -\frac{RT}{4F}\ln(1+u^2+2u\cos x) \tag{A.21}$$

where

$$u = \frac{RTA}{8Fv\omega P_1} \tag{A.22}$$

The expression of the mean internal oxygen partial pressure is given by:

$$P_0 = P_1 + \frac{1}{4P_1}\left[\frac{RTA}{4Fv\omega}\right]^2 \tag{A.23}$$

Chapter 5

The expression for the AC component of the gauge EMF is given by eqn.(A.18) where

$$u = \frac{RTA}{8Fv\omega P_1}\exp\left(\frac{4F}{RT}V_r\right) \tag{A.24}$$

The expression of P_0 is given by:

$$P_0 = \frac{P_1}{\exp\left(\frac{4F}{RT}V_r\right)} + \frac{1}{4P_1}\left[\frac{RTA}{4F\nu\omega}\right]^2 \exp\left(\frac{4F}{RT}V_r\right) \qquad \text{(A.25)}$$

From (A.20) and (A.1b), u may also be expressed as a function

of P_0

$$u = \frac{RTA}{4F\nu\omega P_0} \frac{1}{1+\sqrt{1-\left(\frac{RTA}{4F\nu\omega P_0}\right)^2}} \qquad \text{(A.26)}$$

APPENDIX B: NUMERICAL INTEGRATION

In this section, a simple Pascal program has been written to evaluate the following integral.

$$V_{01} = \frac{1}{\pi}\int_0^{\pi} \left| -\frac{RT}{4F}\ln(1+u^2+2u\cos x)\right| dx \tag{B.1}$$

where u is given in Appendix A by eqn.(A.24)

$$u = \left[\frac{RTA}{8Fv\omega}\exp\left(\frac{4F}{RT}V_r\right)\right]\frac{1}{P_1} \tag{A.24}$$

The term (u) may also be expressed as a function of the mean internal pressure (P_0). It is given in Appendix (A) by eqn.(A.26).

$$u = \frac{RTA}{4Fv\omega P_0}\,\frac{1}{1+\sqrt{1-\left(\dfrac{RTA}{4Fv\omega P_0}\right)^2}} \tag{A.26}$$

The term (u) represents the level of distortion of the AC component (i.e. deviation from a sinusoid). It has been shown in Appendix (A) that $u<1$.

V_{01} represents a DC output of an RMS converter. This converter has been used to convert the AC component of the EMF into a reading of oxygen partial pressure (P_1) in the sample gas. The purpose of this numerical integration was to investigate the expression of V_{01} for highly distorted signals (i.e high values of u) which should enable operation with high amplitudes of the gauge EMF.

Note that in Chapter (4), the reference voltage (V_r) was equal to zero. However in Chapter (5), V_r was non zero for the purpose of temperature compensation. Therefore analysis in this section was done for the general case (i.e. arbitrary V_r).

The computer program was written for the calculation of

$$H = \frac{1}{4u}\int_0^{\pi} |\ln(1+u^2+2u\cos x)|\, dx \tag{B.2}$$

using Simpson's approximation. The number of intervals used was (400).

The results shown in Table (B.1) suggest that the term (H) may be assumed constant and equal to (1) within a wide range of u ($0<u<0.87$). The maximum deviation from unity for values of u up to 0.98 is 1% (figure B.1). The practical implications for this finding are very significant.

First the uniformity of the term (H) over a wide range of (u) predicts that the output of the RMS converter (V_{01}) should be proportional to (u). This means that V_{01} should be inversely proportional to the external partial pressure (P_1) over a very wide range of oxygen partial pressure. Since H=1, from eqn.(A.24) and eqn.(B.2),

$$V_{01} = \left[\frac{R^2T^2A}{8\pi F^2 \nu\omega} \exp\left(\frac{4F}{RT}V_r\right)\right] \frac{1}{P_1} \tag{B.3}$$

This inverse proportionality makes the computation of P_1 easy even when using analogue techniques. The expression for P_1 may be written:

$$P_1 = \left[\frac{R^2T^2A}{8\pi F^2 \nu\omega} \exp\left(\frac{4F}{RT}V_r\right) \right] \frac{1}{V_{01}} \tag{B.4}$$

Secondly the possibility of using high values for the term (u) offers the advantage of using high amplitudes of the gauge EMF. It can be shown that the amplitude peak-to-peak (E_{pp}) of the gauge EMF is given by:

$$E_{pp} = -\frac{RT}{2F} \ln\left[\frac{1-u}{1+u}\right] \tag{B.5}$$

Table (B.1) shows the calculated E_{pp} at 700°C for the values of u ranging from 0.05 to 0.87. It is clear that E_{pp} increases dramatically (figure B.2a) for high values of u. For example E_{pp}=111mV at 700°C when u=0.87. In practical terms, using high amplitudes for the gauge EMF should improve the signal to noise ratio and minimise the effects of offset.

The ratio between the external and mean internal pressures may be determined from eqn.(A.7) in Appendix (A)

$$\frac{P_1}{P_0} = \exp\left(\frac{4F}{RT}V_r\right) \frac{1+\sqrt{1-\left(\frac{RTA}{4F\nu\omega P_0}\right)^2}}{2} \tag{B.6}$$

For V_r=0, this ratio is

$$\frac{P_1}{P_0} = \frac{1+\sqrt{1-\left(\frac{RTA}{4F\nu\omega P_0}\right)^2}}{2} \tag{B.6a}$$

As shown in figure (B.2b) for V_r=0, the ratio (P_1/P_0) varied by a factor of two within the wide range of (u). From eqn.(B.6a), $0<(RTA/4F\nu\omega P_0)<1$ is equivalent to $1<(P_1/P_0)<0.5$. This is not expected to cause any significant electrochemical leak at the normal operating frequency (4Hz). Chapter (6) gives further details about leakage mechanisms.

$\frac{RTA}{4Fv\omega P_0}$	u	P_1/P_0 (V_r=0)	E_{pp} / mV (at 700°C)	H
0.1	0.0501	0.997	4.20	1.00003
0.2	0.101	0.990	8.50	1.00015
0.3	0.153	0.977	12.98	1.00033
0.4	0.208	0.958	17.76	1.00061
0.5	0.268	0.933	23.03	1.00100
0.6	0.333	0.900	29.06	1.00155
0.7	0.408	0.857	36.37	1.00235
0.8	0.500	0.800	46.07	1.00354
0.9	0.627	0.718	61.74	1.00561
0.91	0.643	0.707	64.06	1.00592
0.92	0.660	0.696	66.64	1.00625
0.93	0.680	0.683	69.55	1.00664
0.94	0.700	0.670	72.89	1.00707
0.95	0.724	0.656	76.82	1.00755
0.96	0.750	0.640	81.60	1.00812
0.97	0.780	0.621	87.74	1.00882
0.98	0.817	0.599	96.35	1.00973
0.99	0.867	0.570	111.00	1.01103

Table (B.1): *Tracking Mode: calculated values for (P_1/P_0) and E_{pp} and investigation of the linearity of the RMS converter output when using EMFs with increasingly high distortion.*

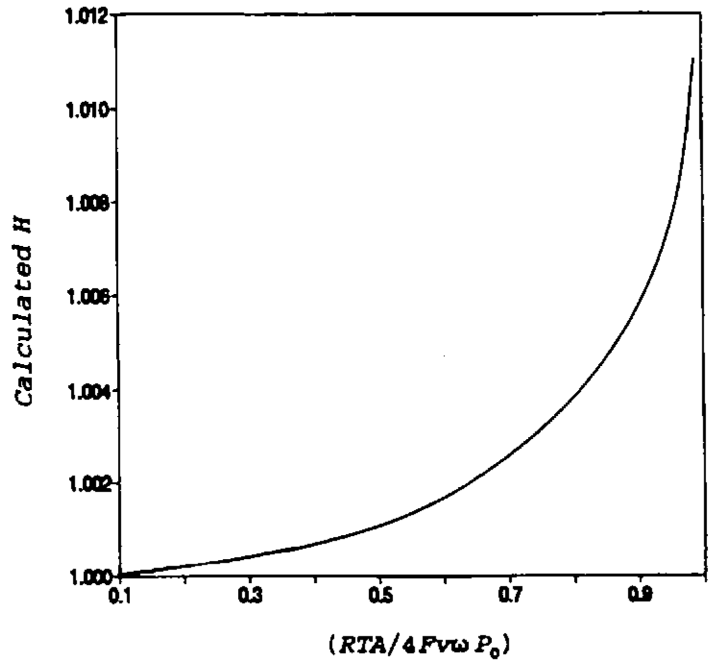

Figure (B.1): Dependence of the calculated integral (H) on the level of distortion of the gauge EMF.

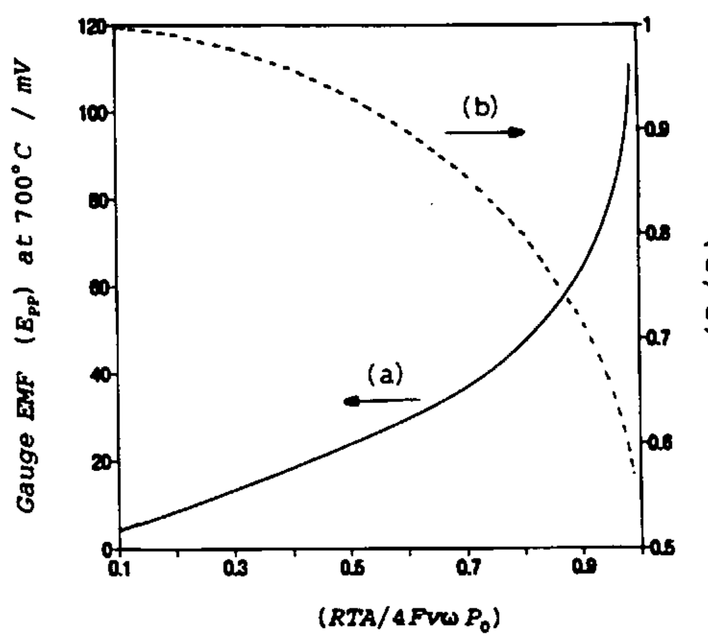

Figure (B.2): Variation of the amplitude of the gauge EMF, E, and (P_1/P_0) as a function of the level of distortion of E.

APPENDIX C: CALCULATION OF THE EXPRESSION OF THE INTERNAL PARTIAL PRESSURE FOR A LEAKY PUMP-GAUGE

In the following the differential equation (eqn.6.10) is solved and a simple expression for P_2 is derived. Equation (6.10) may be written

$$\frac{dP}{dt} + MP = N \tag{C.1}$$

where

$$P = P_2 - P_1 \tag{C.1a}$$

$$M = \frac{DS}{\nu L} \tag{C.1b}$$

$$N = K(A \sin \omega t + I_0) \tag{C.1c}$$

$$K = -\frac{RT}{4F\nu} \tag{C.1d}$$

Equation (C.1) may be solved using the Integration Factor method (Stroud 1970). The Integration Factor (IF) is given by:

$$IF = e^{\int M dt} = e^{Mt} \tag{C.2}$$

The following equation may also be written:

$$P.IF = \int N.IF \; dt \tag{C.3}$$

Substituting for IF in eqn.(C.3) gives

$$\begin{aligned} P.e^{Mt} &= K\int (A\ \sin\omega t + I_o) e^{Mt} dt \\ &= \frac{KI_o}{M} e^{Mt} + KA \int \sin\omega t\ e^{Mt} dt \end{aligned} \tag{C.4}$$

The integral in eqn.(C.4) may be solved by integration by parts. Equation (C.4) may then be written:

$$P.e^{Mt} = \frac{KAe^{Mt}}{M^2+\omega^2}\,[M\ \sin\omega t\ -\ \omega\ \cos\omega t]\ +\ \frac{KI_o e^{Mt}}{M}\ +\ C \tag{C.5}$$

where C is a constant. It follows that

$$P = \frac{KA}{M^2+\omega^2}[M\ \sin\omega t\ -\ \omega\ \cos\omega t]\ +\ \frac{KI_o}{M}\ +\ Ce^{-Mt} \tag{C.6}$$

Because M>0 (see eqn.(C.1b), the exponential in eqn.(C.6) is a rapidly decaying term and therefore may be ignored at steady oscillatory state. Equation (C.6) may then be written:

$$P = \frac{KA}{M^2+\omega^2}[M\ \sin\omega t\ -\ \omega\ \cos\omega t]\ +\ \frac{KI_o}{M} \tag{C.7}$$

Equation (C.7) may be simplified by writing

$$\frac{KA}{M^2+\omega^2}[M\ \sin\omega t\ -\ \omega\ \cos\omega t] = \Delta\ \cos(\omega t\ +\ \Psi) \tag{C.8}$$

By developing the second term of eqn.(C.8), the following equations may be written:

$$\frac{KAM}{M^2+\omega^2} = -\Delta\ \sin\Psi \tag{C.9}$$

$$\frac{-KA\omega}{M^2+\omega^2} = \Delta\ \cos\Psi \tag{C.10}$$

From eqn.(C.9) and eqn.(C.10) the expressions of Ψ and Δ may be deduced. The ratio of eqn.(C.9) and eqn.(C.10) gives,

$$\Psi = Arctan(\frac{M}{\omega}) \tag{C.11}$$

Squaring and adding eqn.(C.9) and eqn.(C.10) gives

$$\Delta = \frac{-KA}{\omega} \cos\Psi \tag{C.12}$$

Equation (C.7) may then be written

$$P = \Delta \cos(\omega t + \Psi) + \frac{KI_o}{M} \tag{C.13}$$

The expression for the internal oxygen partial pressure may then be written using eqn.(C.1a) and eqn.(C.13).

$$P_2 = \Delta \cos(\omega t + \Psi) + \frac{KI_o}{M} + P_1 \tag{C.14}$$

Thus

$$P_2 = \frac{RTA}{4Fv\omega}\cos\Psi \cos(\omega t + \Psi) - \frac{RTLI_0}{4FDS} + P_1 \tag{C.15}$$

APPENDIX D: MODEL OF FULLY SEALED AND LEAKY PUMP-GAUGES

D.1 Perfectly sealed device

It has been shown in Chapter (1) that if a current is applied to the pump of a fully sealed device, oxygen can be transferred into or out of the internal volume. This causes a variation of the internal oxygen partial pressure. This process is governed by the following equation

$$\frac{dP_2}{dt} = -\frac{RT}{4Fv} I \qquad (1.12)$$

where P_2 : internal oxygen partial pressure

T : operating temperature

v : internal volume

I : applied current

R,F: usual significance

Assuming the external partial pressure (P_1) is constant then eqn.(1.12) may be written

$$\frac{dP}{dt} = -\frac{RT}{4Fv} I \qquad (D.1)$$

where $P=P_2-P_1$: oxygen partial pressure difference across the gauge of the sensor. The described fully sealed device behaves like an ideal capacitor. When a charging current is applied to an ideal capacitor, the potential difference (V_c) across it is given by the following equation

$$\frac{dV_c}{dt} = \frac{I}{C} \tag{D.2}$$

When comparing eqn.(D.1) and eqn.(D.2), it can be seen that the internal volume of the device acts as a "capacitor" which is charged or discharged by an oxygen flux resulting from the applied current. The oxygen partial pressure difference across the gauge is then equivalent to the voltage difference across the capacitor.

It has been shown in Chapter (1) that with an imposed sinusoidal pumping current, the pressure difference across the gauge oscillates at the same frequency with a 90° phase shift. An ideal capacitor subject to the same current develops a sinusoidal voltage with a 90°phase shift.

D.2 Leaky device

It has been demonstrated in Appendix (C) that (eqn.C.1) for a device with diffusion hole the following equation may be written

$$\frac{dP}{dt} + \frac{DS}{vL}P = -\frac{RT}{4Fv}I \tag{D.3}$$

where D: gas diffusion constant

L: hole length (i.e. thickness of the electrolyte)

S: cross-sectional area of the hole

On the other hand a leaky capacitor may be represented by an ideal capacitor (C) with a leakage resistor (R_L) across it.

Under a charging current, such a capacitor develops a voltage given by the following differential equation

$$\frac{dV_c}{dt} + \frac{V_c}{R_L C} = \frac{I}{C} \tag{D.4}$$

Comparing eqn.(D.3) and eqn.(D.4) it can be seen that the conductance ($1/R_L$) is equivalent to (DS/L). These two terms are responsible for the leakage mechanism in the leaky capacitor and leaky sensor respectively. The leakage current in the resistor is proportional to the voltage across the capacitor; similarly the flux of oxygen leaking through the pore is proportional to the pressure difference ($P=P_2-P_1$) across the gauge. In both cases the aystem ia more affected by leakage for lower values of the "charging" capacitor (C or v) and higher values for the terms responsible for leakage ($1/R_L$ or DS/L).

CAPACITOR	PUMP-GAUGE DEVICE
capacitance (C)	internal volume (v)
voltage across C (V_C)	O_2 pressure ($P=P_2-P_1$)
leakage resistor (R_L)	(L/DS)

***Table (D.1)**: Equivalence between capacitors and pump-gauge devices.*

It has been ahown in Chapter (6) that for a sinusoidal pumping current, leaky devicea exhibit a phaae shift and amplitude change of the oxygen partial pressure difference across the gauge of the device. This phase shift and amplitude change depend on the rate of gas leakage and operating frequency. It can be shown that a leaky capacitor would behave in the same way under an imposed sinusoidal charging current. From the behaviour of leaky devices with sinusoidal current a direct method was presented (Chapter 6) for leakage testing of fully sealed devices. This method can also be used for testing leakage of capacitors. The similarity between pump-gauge devices and capacitors can be further extended: perfectly sealed devices (i.e. free from all formes of leakage) just like ideal capacitors (i.e. free from leakage) are impossible to make.

APPENDIX E: DIFFUSION ALONG A TAPERED HOLE

It has been suggested in chapter (6) that the laser-drilled holes used for testing physical leakage were of a conical shape. In the following an equivalent hole with constant cross-sectional radius will be determined. The analysis is based on diffusion law.

The laser drilled pore is assumed perfectly conical as shown in figure (E.1). Let the radii of the two ends of the hole be r_1 and r_2. Let the pore separate two gas concentrations c_1 and c_2. Let the radius of the circular element AB be r. Let this element separate concentrations c and c+δc. If dx is an elementary distance within the pore, the gas flux J is given by Fick's first law

$$J = -\pi D r^2 \frac{dc}{dx} \tag{E.1}$$

If L is the total length of the pore, then

at $\quad x=0\ ,\ r=r_1$

$\quad\quad x=L\ ,\ r=r_2.$

The radius r of the element AB may be expressed as a function of x, r_1 and r_2. It can be shown that

$$r = r_1 - \left(\frac{r_1 - r_2}{L}\right)x \tag{E.2}$$

Differentiating eqn.(E.2) we have

$$dr = \left(\frac{r_2 - r_1}{L}\right)dx \tag{E.3}$$

Substituting into eqn.(E.1) from eqn.(E.3)

$$J = \pi D r^2 \left(\frac{r_1 - r_2}{L} \right) \frac{dc}{dr} \tag{E.4}$$

At equilibrium the flux J is constant. Equation (E.4) may be written

$$dc = \frac{J L}{\pi D (r_1 - r_2)} \frac{dr}{r^2} \tag{E.5}$$

Integrating the two terms of eqn.(E.5)

$$\int_{c_1}^{c_2} dc = \frac{J L}{\pi D (r_1 - r_2)} \int_{r_1}^{r_2} \frac{dr}{r^2} \tag{E.6}$$

This gives

$$c_2 - c_1 = \frac{J L}{\pi D (r_1 - r_2)} \left[\frac{1}{r_1} - \frac{1}{r_2} \right] \tag{E.7}$$

The following equation may then be written:

$$J = \pi D (r_1 r_2) \frac{c_1 - c_2}{L} \tag{E.8}$$

Equation (E.8) gives the expression for the flux through a hole of conical shape. The flux in a cylindrical hole is given by eqn.(E.9).

$$J = \pi D r^2 \frac{c_1 - c_2}{L} \tag{E.9}$$

When comparing eqn.(E.8) and eqn.(E.9), it can be seen that the tapered hole behaves like a straight hole with constant cross-sectional radius (r) given by the geometric mean of r_1 and r_2.

If ϕ_{min} and ϕ_{max} are the minimum and maximum hole diameters of the tapered hole, then the hole behaves like a straight hole with a diameter given by:

$$\Phi = \sqrt{\Phi_{min}\Phi_{max}} \tag{E.10}$$

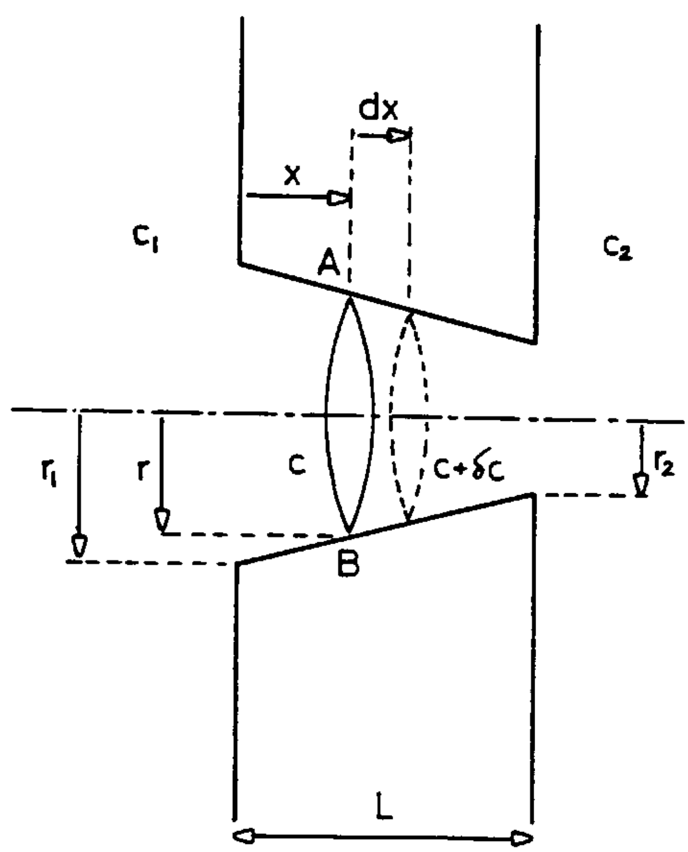

Figure (E.1): *Diffusion along a tapered hole*

APPENDIX F: PHASE SHIFT MEASUREMENT

In chapter (6), the operation of leaky pump-gauge devices in the AC mode has been investigated. The leak in these devices caused a phase shift between the pumping current and gauge EMF. In the following the method adopted for the measurement of the phase shift (Ψ) is described.

Let the general expression for the pumping current be

$$I = A \sin x + I_0 \tag{6.9}$$

where I_0 represents a DC component in the pumping current. The resulting gauge EMF is given by equation (6.14)

$$E = -\frac{RT}{4F}\ln\left[1-\frac{RTLI_0}{4FDSP_1}+\frac{RTA}{4F\nu\omega P_1}\cos\Psi\cos(x+\Psi)\right] \tag{6.14}$$

Assuming that the instrumentation amplifier has a DC offset e_0, the general equation of the gauge EMF would then be

$$E_g = -\frac{RT}{4F}\ln\left[1-\frac{RTLI_0}{4FDSP_1}+\frac{RTA}{4F\nu\omega P_1}\cos\Psi\cos(x+\Psi)\right]+e_0 \tag{F.1}$$

The method for the phase shift measurement was based on converting the pumping current and gauge EMF into square waves using zero-crossing comparators. As shown in figure (F.1), in each cycle of these periodic signals, I and E_g (or E) intersect zero twice. Let the zero crossing angles be (x_1 and x_2) for I; and (y_1 and y_2) for E_g. The zero-crossing angles of the current are given by

$$x_1 = \sin^{-1}\left(-\frac{I_0}{A}\right) \tag{F.2}$$

and $\quad x_2=\pi-x_1$ (F.3)

On the other hand, the periodic zero-crossing of the EMF occurs when $E_g=0$. Applying this condition to equation (F.1)

$$\exp\left(\frac{4F}{RT}e_0\right) = 1-\frac{RTLI_0}{4FDSP_1}+\frac{RTA}{4Fv\omega P_1}\cos\Psi\ \cos(x+\Psi) \tag{F.4}$$

Equation (F.4) is true for $x=y_1$ and $x=y_2$ where

$$y_1 = -\Psi+\cos^{-1}\left[\frac{4Fv\omega P_1}{RTA\cos\Psi}\left(-1+\exp\left(\frac{4F}{RT}e_0\right)+\frac{RTLI_0}{4FDSP_1}\right)\right] \tag{F.5}$$

and

$$y_2 = 2\pi-2\Psi-y_1 \tag{F.6}$$

By referring to figure (F.1) it may be seen that, for the falling edges of the square waves, E_g (or E) lags I by an angle given by

$$\Psi_F = y_2-x_2 \tag{F.7}$$

For the rising edges of the square waves, E_g (or E) lags I by an angle given by

$$\Psi_R = y_1-x_1 \tag{F.8}$$

From equation (F.3), (F.6) and (F.7)

$$\Psi_F = \pi-2\Psi-(y_1-x_1) \tag{F.9}$$

It follows

$$\Psi = \frac{\pi}{2}-\frac{\Psi_F+\Psi_R}{2} \tag{F.10}$$

The measurement of the two angles can be easily made by using a Timer/Counter as described in chapter (6). The falling and rising edges of the square waves may be used to start and stop the counter in order to measure the duration of the pulses x_1y_1 and x_2y_2. This measurement may then be converted into a measure of the two angles Ψ_F and Ψ_R. Thus by applying this method, the errors caused by the offsets in the various parts of the electronics may be minimised.

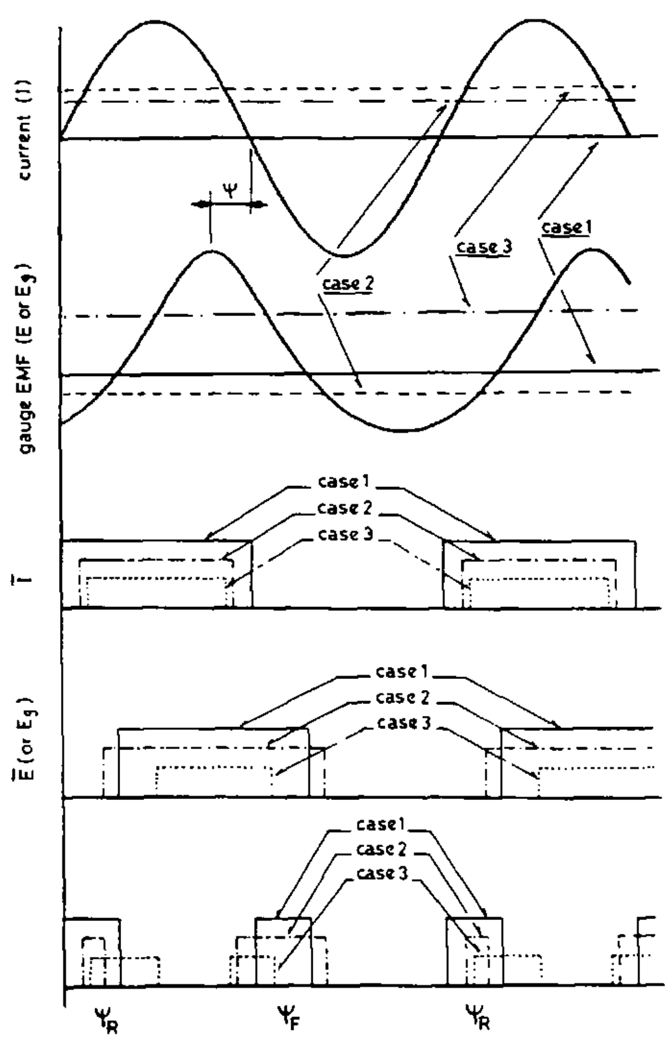

Figure (F.1): Measurement of the phase shift between two signals containing DC offset. (Adopted from Wagdy and Lucas 1987)

APPENDIX G: ELECTRONIC CIRCUIT DIAGRAMS

G.1 INTRODUCTION

In this section, the detailed electronic circuits built and used throughout this work are given. In the first part of this appendix, circuits used for particular functions are described. In the second part, complete circuit diagrams are given for the various electronic circuits built for operation of the oxygen pump-gauge devices.

G.2 GENERAL

DC power supplies

The electronics used in the present work required the use of a ±15V and +5V DC power supplies. Figure (G.1) gives the circuit diagram of the ±15V supply. The RC4195NB voltage regulator has a maximum output current of ±100mA, and is internally protected against overload. Figure (G.2) gives the circuit diagram of the +5v supply used. It is a classic circuit based on a 7805 voltage regulator with a maximum output current of 1A.

Sinewave generators

Two types of sinewave generators were used in the present work. Figure (G.3) shows the circuit diagram of the first generator which was an analogue sinusoidal oscillator adopted from Jung (1974) and may be used to produce two sinusoidal signals in quadrature. In the present application the advantage of having two signals in quadrature obviated the need for 90°

phase shifters. The circuit of figure (G.3) was based on two amplifiers, A_1 acted as a non-inverting integrator while A_2 was an inverting integrator. The two amplifiers were connected in cascade to form a feedback loop. The feedback loop was represented by two differential equations

$$RC\frac{de_s}{dt} = e_c \tag{G.1}$$

$$RC\frac{de_c}{dt} = -e_s \tag{G.2}$$

The solution of these differential equations is represented by a sinusoidal oscillation of frequency

$$f = \frac{1}{2\pi RC} \tag{G.3}$$

The signals e_c and e_s are in quadrature.

In theory all capacitors and all resistors (except R_2) are equal. However, in practice R_1 was made slightly larger than the other resistors to ensure sufficient positive feedback for oscillations. The zener diodes were used to stabilise the amplitude of the oscillations. The trimmer R_2 was used to set the amplitude of the signals to any value above the zener voltage of the diodes. The distortion of the signals obtained depended strongly on the choice of the components; with highly matching components, a total distortion of less than 1% could be obtained (Jung 1974). Note that this oscillator is ideal only for applications where constant frequency is required. This is because the frequency can not be varied by adjusting the value for one component only.

Digital storage of waveform samples provides a means whereby waveshapes can be programmed to suit the application. Simple digital-to-analogue conversion of a sequence of samples results in a zero-order reconstruction of the stored signal. The circuit of figure (G.4) was used to generate a sinusoidal signal with variable frequency. The circuit consisted of an EPROM (2764) in which samples of the sinewave were stored, a binary counter (4040B) used as pointer to sequentially select the addresses of the stored samples and a digital-to-analogue (DAC) converter (ZN435) to convert the stored samples into staircase approximation of the sinewave. The TTL clock at the input of the counter sets the frequency of read-out of the samples and therefore of the frequency of the sinewave.

The circuit of figure (G.4) was based on the use of 8 bit chips. Therefore in order to have reasonable approximation of the sinewave, all bits were used to represent the amplitude of the signal; 256 samples were stored and represent the positive half of the sinewave. Hence, the output of the DAC was a rectified sinewave. The full sinewave was obtained using a +1/-1 multiplier built around A_2 and the transistor Q. The multiplier was controlled by the counter which synchronised the waveform generation (Huehne 1972).

The frequency of the clock was 512 times higher than that of the sinewave. Since the maximum frequency used in the present work was less than 10Hz, the maximum frequency of the clock required was less than 5kHz which could easily be obtained from any function generator or simply from a multivibrator. However if signals with much higher frequency are required, other techniques may be used to minimise the number of stored samples without affecting the quality of generated signal. With added complexity, the principle of ROM read-out may be improved by using interpolation technique (Evans and Towers, 1980). This technique may be practically implemented (Towers, 1982) by using multiplying digital-to-analogue converters (MDAC).

Voltage to current converter

In the present work two bipolar voltage-to-current converter with grounded load were used. Figure (G.5) gives the circuit diagram of the first converter; this was adopted from Froelicher et al (1980) and was based on the use of a single amplifier. By referring to figure (G.5), the following equations may be written

$$I_{in} = \frac{V_{in} - V_L}{R_1} \tag{G.4}$$

$$V_0 - V_L = -R_2 I_{in} \tag{G.5}$$

$$V_L = V_0 - R_2\left(I_L + \frac{V_L}{R_1}\right) \tag{G.6}$$

From eqn.(G.4) and eqn.(G.5)

$$V_0 = -\frac{R_2}{R_1}(V_{in} - V_L) + V_L \tag{G.7}$$

Substituting for V_0 in eqn.(G.6) gives

$$I_0 = -\frac{V_{in}}{R_1} \tag{G.8}$$

For a given input voltage, the current through the load is given by eqn.(G.8). In practice, care must be taken to ensure that the output (V_0) of the amplifier does not saturate for the maximum current (I_L) through the load, the choice of R_2 must be made to ensure this.

Figure (G.6) gives the circuit diagram of the second converter. This converter was adopted from Morgan et al (1986) and was built around three amplifiers. The circuit operated in such a way that the voltage across the resistor R_0 was maintained equal to the input voltage (V_i). The following equations may be written

$$V_{in} = V_0 - V_L \tag{G.9}$$

$$V_0 - V_L = R_0 I_L \tag{G.10}$$

From eqn.(G.9) and eqn.(G.10)

$$I_L = \frac{V_{in}}{R_0} \tag{G.11}$$

Equation (G.11) indicates that the current through the load should be proportional to the input voltage.

Instrumentation amplifier

Three types different instrumentation amplifiers were used. The first two were dedicated single chip amplifiers: INA110 and INA102. The gain in these amplifiers may be set to various values by shorting appropriate pins, other gain values may be obtained by adding a single resistor. The third instrumentation amplifier was a classic three operational amplifiers configuration as shown in figure (G.16).

Analogue multiplier

The multiplier used was of the type SG1495. The connection diagram of this multiplier is shown in figure (G.7). the various trimmers were used for offset and gain adjustment.

Analogue divider

The analogue divider (Clayton 1971) used was built around an analogue multiplier and an amplifier as shown in figure (G.8). The current through the two resistors is given by

$$i = \frac{V_1}{R} = -\frac{V_0 V_2}{R} \tag{G.12}$$

This led to

$$V_0 = -\frac{V_1}{V_2} \tag{G.13}$$

Hence the output of the amplifier should be equal to the ratio of the two input voltages V_1 and V_2.

Squarer

The squarer used (figure G.9) was adopted from Shubba and Ramesh (1986), and was based on logarithmic converters. All log converters are normally built around pn junctions and employ the V_{BE} characteristic of silicon planar transistor for V_{CB} of 0V. Jung (1974) gives an excellent tutorial on log converters and their use to produce exponential, logarithmic, square, multiplication, square-root and raising to the power functions.

G.3 DETAILED CIRCUITS USED WITH THE SENSORS

This section is divided into sub-sections. In each sub-section the electronic circuits used in a particular chapter of the present thesis are discussed. In the following, these sub-sections are referred to by the chapter they represent.

G.3.1 Chapter 3

Figure (G.10) gives the detailed electronic circuit used for implementing the Potentiometric Mode of operation [i.e. described by the schematic diagram given in figure (3.7)]. The sine/cosine generator, of the type shown in figure (G.3), was built around A_1 and A_2. The voltsge-to-current converter, of the type shown in figure (G.5), was built around A_4. The amplitude of the pumping current may be set by adjusting the amplitude of the pumping sinewave using the trimmer R_{48}. The gauge EMF was amplified (x200) using an instrumentation amplifier (IC_1). The phase sensitive detector (PSD) was of the type +1/-1 multiplier followed by a low pass filter and was built around A_6, A_8 and the FET transistor (Q). The square wave reference for this PSD was obtained from a zero-crossing comparator built around A_9. The component E_0 of the gauge EMF was measured using the sample and hold (IC_2) triggered with positive pulses obtained from the zero-crossing comparator (A_8) and the differentiator built around R_{31}, R_{32} and C_6. The window comparator (Graeme 1973) was built around A_{11}, its input was equal to E_0. The reference voltage was obtained from A_{10} by appropriate adjustment of the trimmer R_{37}. The low pass filter built around R_{33} and C_7 was used to allow soft start of the loop (refer to chapter 3 for further details). The bias signal used to adjust the mean internal oxygen partial pressure was obtained from the summer A_7 and the amplifier/limiter built around A_8.

G.3.2 Chapter 4

Two implementations were described for the Tracking Mode of operation.

G.3.2.1 Method 1: Constant mean value of the gauge EMF

Figure (G.11) gives the detailed electronic circuit used for implementing this mode described by the schematic diagram of figure (4.1). The sine/cosine generator of the type shown in figure (G.3) was built around A_2 and A_3. The voltage-to-current converter was built around A_5. The instrumentation amplifier (IC_2) was of the type INA110 with an amplification of (x500). The low pass filter and amplifier/limiter used to produce the bias signal for controlling P_0 were built around A_6. The RMS converter (producing the DC output V_{01}) was built around a full-wave rectifier (A_8 and A_9) and a low pass filter (A_{10}). The PSD (producing the output V_{02}) was built around an analogue multiplier (IC_1 and A_1) and a low pass filter (A_{11}). The sample and hold circuit (IC_3) used to produce the output V_{03} was triggered with positive pulses obtained from a zero-crossing comparator (A_7) and a differentiator (built around R_{35}, R_{36} and C_5).

G.3.2.2 Method 2: Constant mark-to-space ratio

Figure (G.12) gives the detailed circuit diagram for implementing this mode of operation [described by the schematic diagram of figure (4.2)]. The sine/cosine generator used was of the type given in figure (G.3) and was built around A_1 and A_2. The voltage-to-current converter was built around A_4. The instrumentation amplifier (IC_1) used was of the type INA110 and was wired to provide an amplification of (x500). The amplified gauge EMF was converted into square wave using the zero-crossing comparator built around A_5. The bias signal for controlling the mark-to-space ratio (MSR) was then obtained from the low pass filter/amplifier/limiter built around A_6. The output of the circuit, from which external oxygen partial pressure was computed, was produced by the sample and hold (IC_2). The triggering of the sample and hold was obtained using a combination of zero-crossing comparator (A_7) and differentiator (R_{20}, R_{21} and C_5).

G.3.3 Chapter 5

Two modes of temperature compensation were described in chapter 5.

G.3.3.1 Reference voltage equal to zero

This mode of operation is represented by the schematic diagram of figure (5.4). Temperature compensation was shown to be possible by dividing the output of the RMS converter by T^2. The operating temperature was measured with a type R thermocouple. Within the range of operating temperature, it has been shown that the thermocouple EMF (e) may be converted into T^2 using two methods. The first method consisted of expressing (T) as a linear function of (e); then T^2 was obtained using a squarer. The second method was based on expressing T^2 as a linear function of (e).

The detailed electronic circuit for this mode of temperature compensation is shown in figure (G.13). The thermocouple EMF (e) was amplified (x1000) using an instrumentation amplifier (IC_1). The amplified thermocouple EMF was then converted into T^2 using the two methods described. For the first method, the amplified e was converted into T using A_1. T^2 was then obtained using the squarer of figure (G.9) built around A_4 and A_5. The two amplifiers A_2 and A_6 were used for calibration purpose. The second method was implemented using the circuit built around A_3. The analogue divider [figure (G.8)] was built around A_8 and the multiplier (built around IC_2 and A_7). A switch (SW) was used to select T^2 from the first or second approximation. The input (V_{01}) of the divider was obtained from the RMS converter of figure (G.11).

G.3.3.2 Variable reference voltage

In this mode of operation the sensor was operated in a similar way to the Tracking Mode described in chapter (4). The difference, however, is that the DC component of the gauge EMF was expressed as a function of temperature. This was achieved by keeping the measured DC component of the gauge EMF to a reference voltage (expressed as a function of T) using a bias signal as shown in the schematic diagram of figure (5.5).

The detailed electronic circuit used for testing this mode of temperature compensation is shown in figure (G.14). The sinusoidal oscillator was built around A_1 and A_2. The voltage-to-current converter, of the type shown in figure (G.6), was built around A_5, A_6 and A_7. The gauge EMF was amplified (x1000) using an instrumentation amplifier (IC_1). The DC component of the gauge EMF, as indicated in figure (G.14) was obtained from the low pass filter built around A_8. The required reference voltage was obtained from the thermocouple EMF using an instrumentation amplifier (IC_2) and the amplifiers A_9 and A_{10}. The bias signal, representing the difference between the DC component and reference voltage, was obtained from A_{11}. The AC component of the gauge EMF was obtained from the amplified gauge EMF and its DC component using A_{12}. This AC component was then converted into temperature-compensated DC output using the RMS converter built around the full wave rectifier (A_{13} and A_{14}) and the low pass filter (A_{15}).

G.3.4 Chapter 6

In this section two circuits are described. The first was used for testing the theory of AC operation of leaky devices; while the second was a simple circuit for oxygen partial pressure measurement.

G.3.4.1 Circuit 1

Figure (6.1) represents the schematic diagram of the electronics used for testing the theory of AC operation of leaky and "fully-sealed" devices. Figure (G.15) shows the full electronic circuit used. The testing of the devices was made in three modes. These modes required the generation of a pure sinusoidal current, a DC current and a sinusoidal current with DC offset. The sinewave generator used was of the type shown in figure (G.4), this required the use of a function generator to produce the TTL clock. The DC voltage was obtained from a stable power source. The voltage-to-current converter was built around A_6. The gauge EMF was amplified (x500) using an instrumentation amplifier (IC_2). The tests made consisted of measuring the amplitude and phase of the gauge EMF under various conditions. The measurement of the phase shift was achieved using a Timer/Counter (chapter 2). The measurement of the amplitude of the gauge EMF was made using a sample and hold circuit (IC_1). The trigger input of the sample and hold was obtained from the sinewave using a combination of zero-crossing comparator (A_1) and differentiator.

G.3.4.2 Circuit 2

This circuit was designed for the measurement of oxygen partial pressure using devices with diffusion pore(s) operated in the AC mode. The principle of operation consisted of applying a sinusoidal current to the pump of the device and simply measuring the amplitude of the gauge EMF. Oxygen partial pressure in the sample gas may then be determined from the measured amplitude.

As shown in figure (G.16), the proposed circuit may be built around ordinary components. Thus the cost may be kept to a minimum. The sinusoidal oscillator was built around A_1 and A_2. The voltage-to-current converter was built around A_3. The instrumentation amplifier used to amplify the gauge EMF, was built around A_4, A_5 and A_6. The measurement of the amplitude of the gauge EMF may be achieved by using a sample and hold circuit (IC_1).

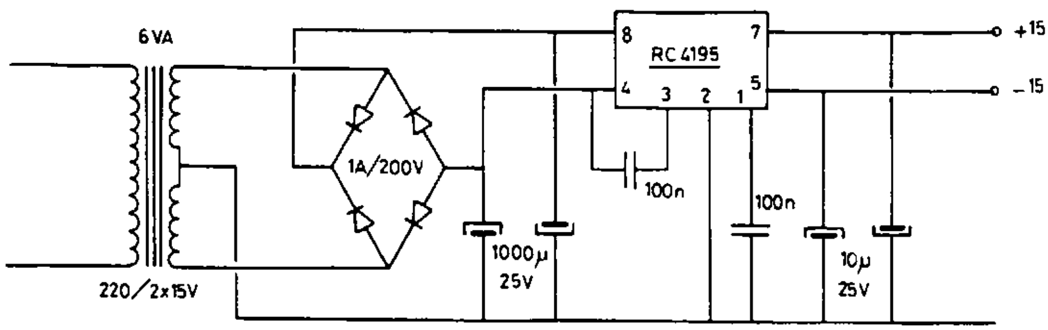

Figure (G.1): ±15V / ±100mA power supplly. (Source: RS components catalogue)

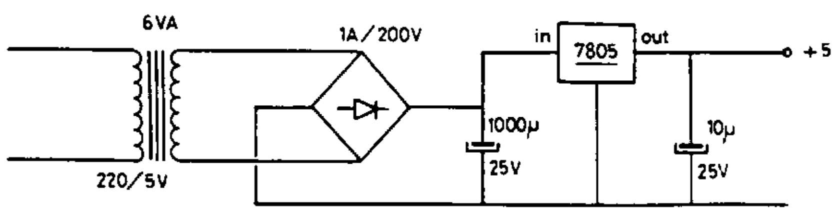

Figure (G.2): +5V / 1A power supply.

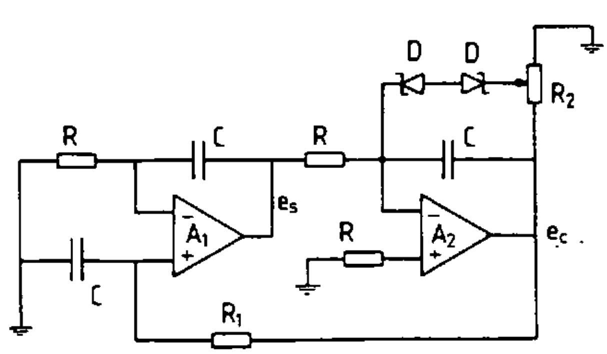

Figure (G.3): Sinusoidal oscillator generating two signals (e_s and e_c) in quadrature. (Source: Jung 1974)

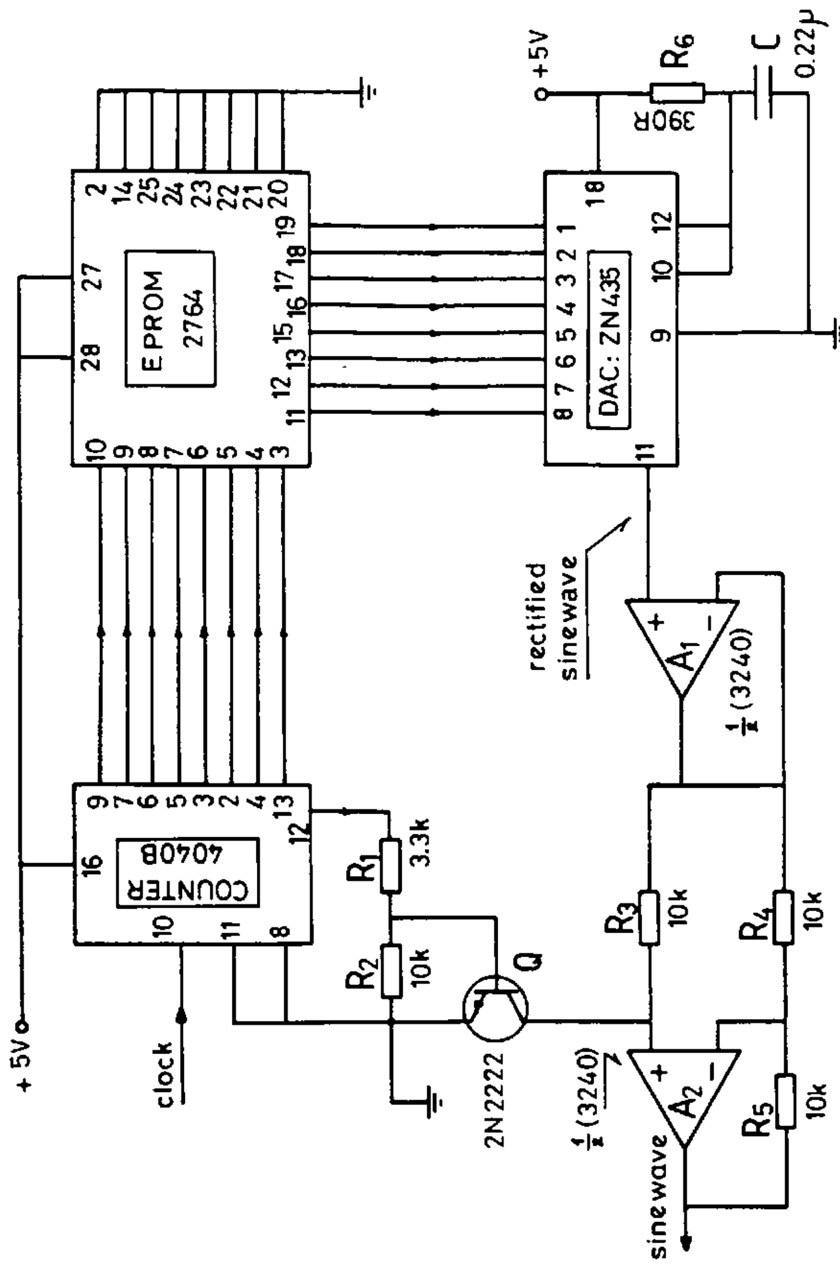

Figure (G.4): ROM read-out type digital sinewave generator. The two amplifiers were powered from ±15V; the offset adjustment is not shown.

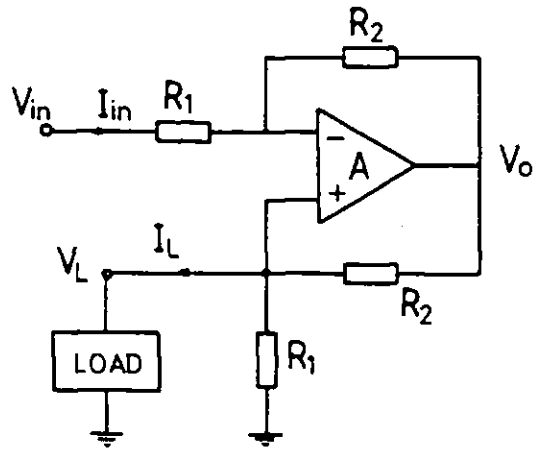

Figure (G.5): Voltage-to-current converter. $I_L=-(V_{in}/R_1)$.
(Source: Froelicher et al 1980)

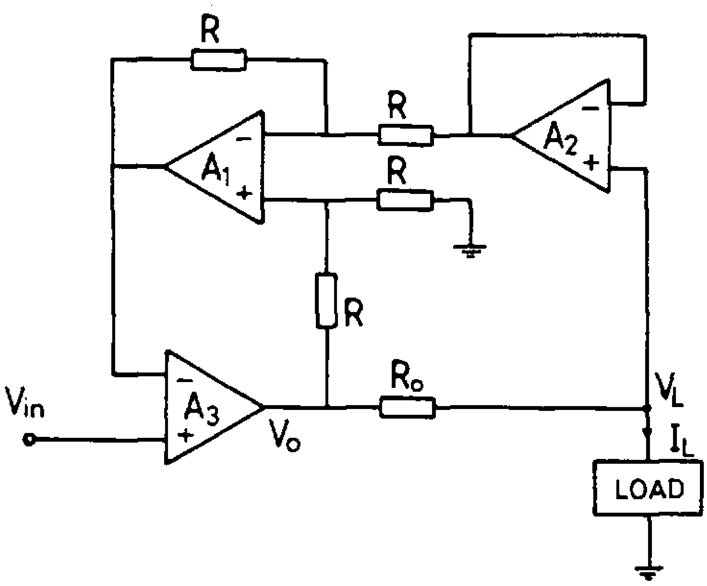

Figure (G.6): Voltage-to-current converter with high input impedance.
$I_L=(V_{in}/R_0)$. (Source: Morgan et al 1986)

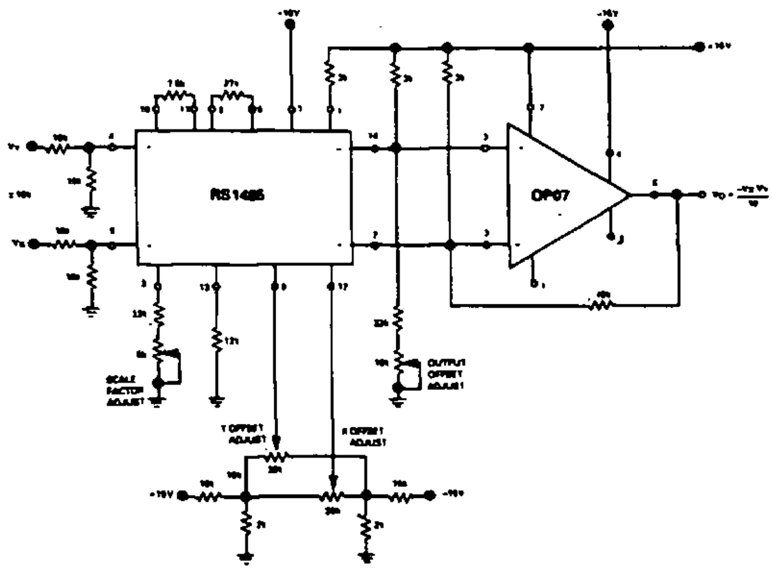

Figure (G.7): Four quadrant analogue multiplier.
(Source: RScomponents, data sheet N.5207)

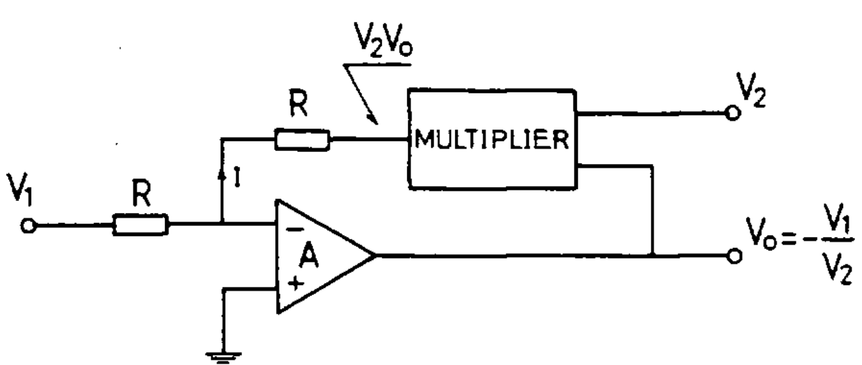

Figure (G.8): Basic analogue divider based on the use of an analogue multiplier. (Source: Clayton 1971)

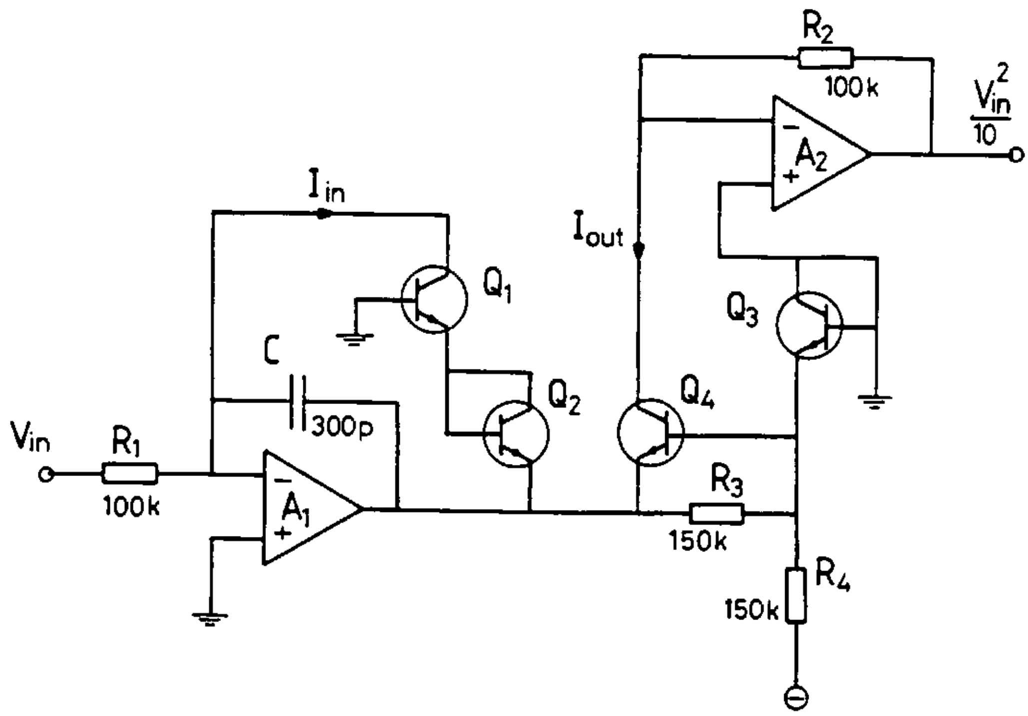

Figure (G.9): Analogue squarer for positive input voltage.
(Source: Shubba and Ramesh 1986)

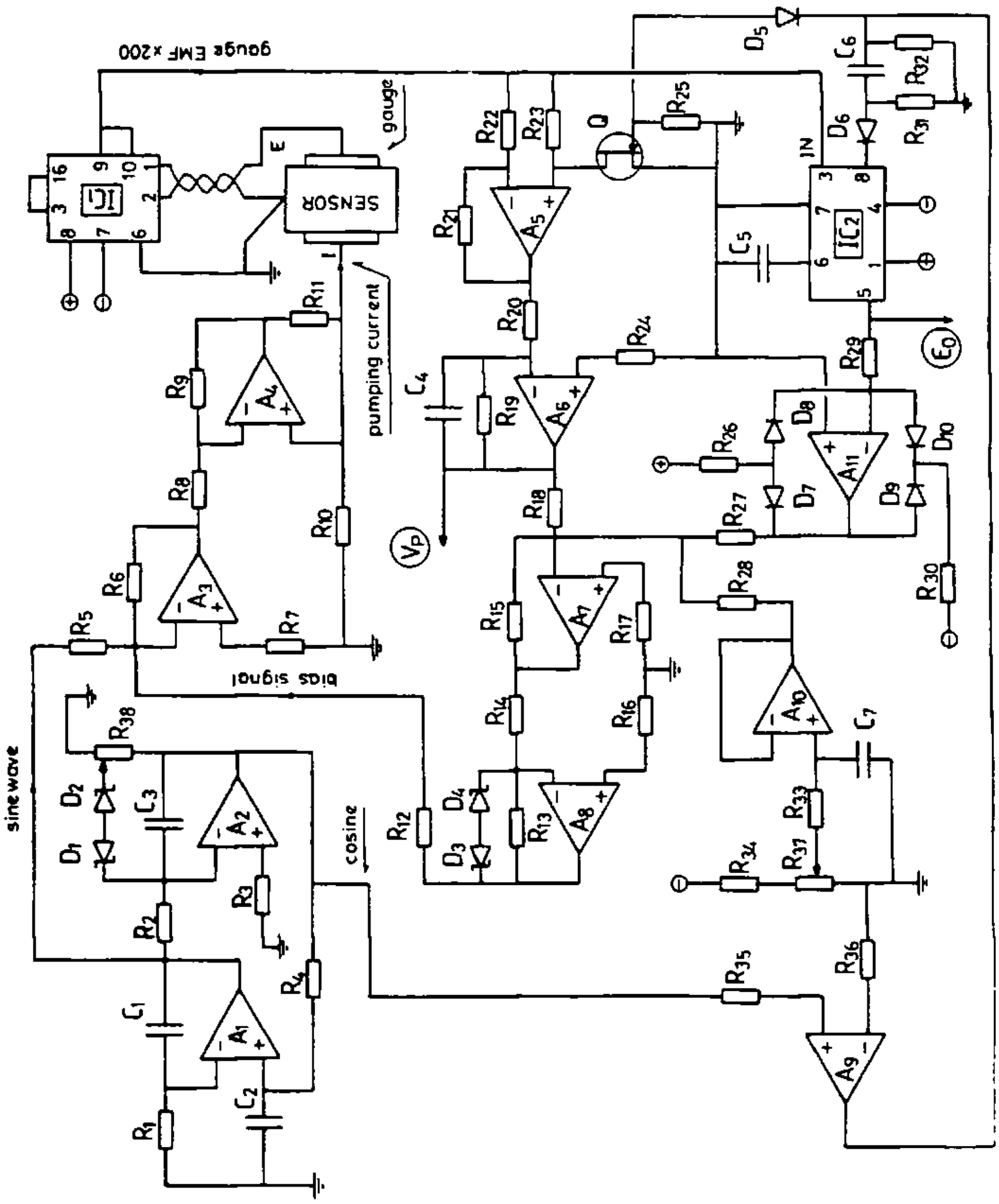

Figure (G.10): Electronic circuit used for the measurement of oxygen partial pressure (P_1) using sealed pump-gauge device operated in the Potentiometric Mode (chapter 3). P_1 was computed from V_P and E_0.

List of components in figure (G.10)

IC_1: INA110 (Ampl. x200).
IC_2: LF398 (Sample/hold).
A_1, A_2: ½ 3240 (OPAMP)
A_3 : ¼ TLO74 (Quad OPAMP)
A_4 : 3140 (OPAMP)
A_5-A_{11}: ¼ TLO74
Q : 2N4092 (FET)
D_1 - D_4 : 4.3V / ¼W Zeners
D_5 - D_6 : 1N4148 Signal diodes
C_1 - C_3 : 0.1 µF
C_4 : 2 µF
C_5 : 0.1 µF
C_6 : 4700pF
C_7 : 2 µF
R_1 : 363k
R_2 : 390k
R_3 : 363k
R_4 : 390k
R_5, R_6 : 10k
R_7 : 3.3k
R_8 - R_{11}: 6.8k
R_{12} - R_{15} : 10k
R_{16}, R_{17} : 3.3k
R_{18} : 10k
R_{19}, R_{20} : 1.8M
R_{21} - R_{23} : 10k
R_{24} : 180k
R_{25} : 10k
R_{26} : 18k
R_{27}, R_{28} : 10k
R_{29} : 4.7k
R_{30} : 18k
R_{31}, R_{32} : 22k
R_{33} : 1M
R_{34} : 6.8k
R_{35}, R_{36} : 22k
R_{37} : 1k
R_{38} : 10k

The trimmers R_{37}, R_{38} were of the 10 turn type.
The circuit was powered from ±15V supply; bypass capacitors were used for each IC.

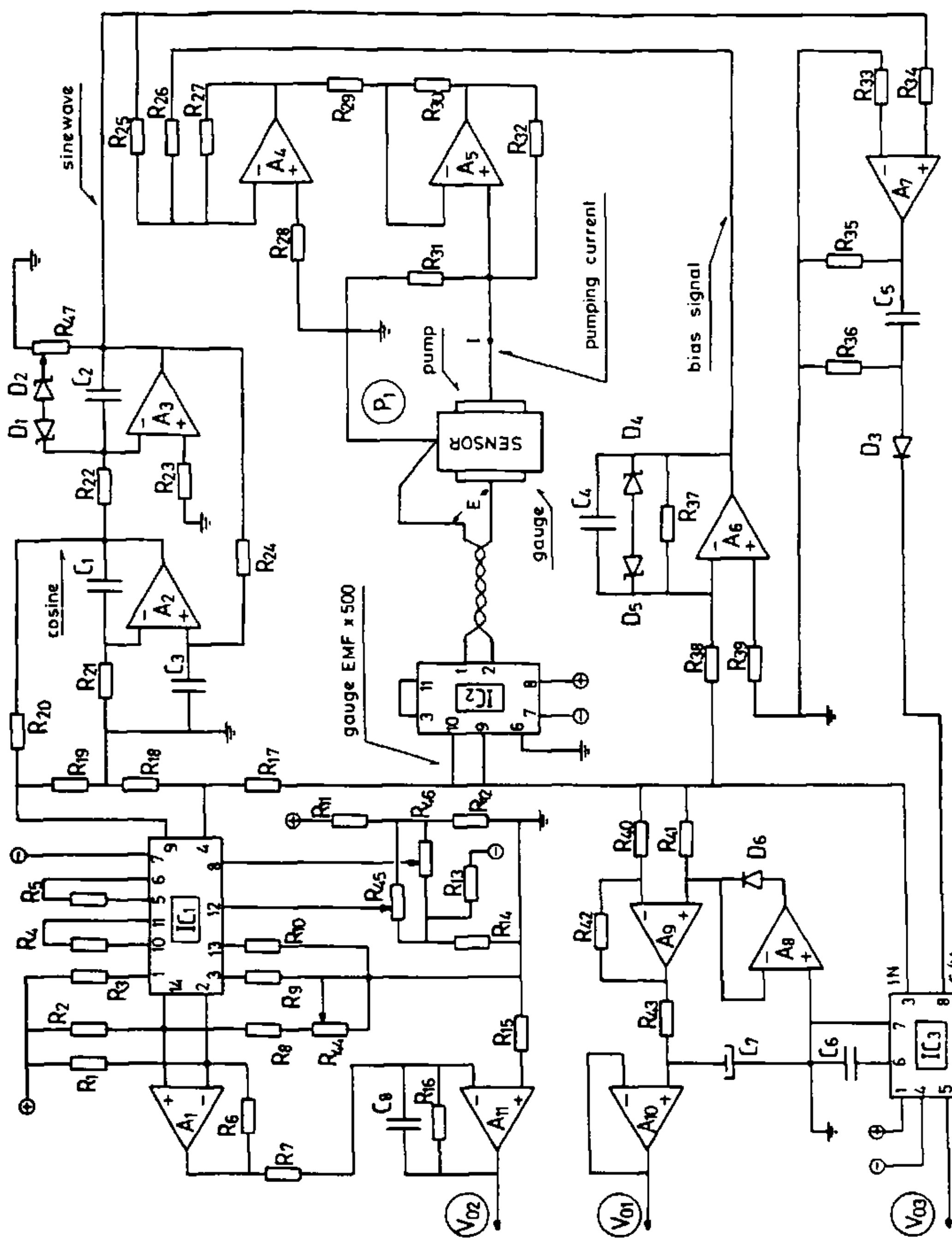

Figure (G.11): *Electronic circuit used for the measurement of oxygen partial pressure (P_1) using sealed pump-gauge device operated in the Tracking Mode (Method 1 in chapter 4). P_1 may be computed from V_{01}, V_{02} or V_{03}.*

List of components in figure (G.11)

IC_1 : SG1495 (Analogue multiplier)
IC_2 : INA110 (Instrum. Ampl. x500)
IC_3 : LF398 (Sample and hold)
A_1 - A_{11} : ¼ TLO74 (Quad OPAMP)
C_1 - C_3 : 0.1μF
C_4 : 2.2μF
C_5 : 4700pF
C_6 : 0.1μF
C_7 : 10μF/25V
C_8 : 2.2μF
D_1, D_2 : 4.3V/ ¼W Zeners
D_3 : 1N4148
D_4, D_5 : 4.3V/ ¼ Zeners
D_6 : 1N4148
R_1 - R_3 : 3.3k
R_4 : 8.2k
R_5 : 27k
R_6 : 39k
R_7 : 1M
R_8 : 33k
R_9 : 15k
R_{10} : 12k
R_{11} : 15k
R_{12} : 2.7k
R_{13} : 15k
R_{14} : 2.7k
R_{15} : 390k
R_{16} : 1.8M
R_{17} - R_{20} : 10k
R_{21} : 363k
R_{22} : 390k
R_{23} : 363k
R_{24} : 390k
R_{25} : 10k
R_{26} : 12k
R_{27} : 10k
R_{28} : 3.3k
R_{29} - R_{32} : 6.8k
R_{33} - R_{36} : 22k
R_{37} : 1.8M
R_{38} : 330k
R_{39} - R_{42} : 10k
R_{43} : 220k
R_{44} : 10k
R_{45}, R_{46} : 22k
R_{47} : 10k

The trimmers R_{44} - R_{47} are of 10 turn type.
The circuit was powered from ±15V supply; bypass capacitors were used for each IC.

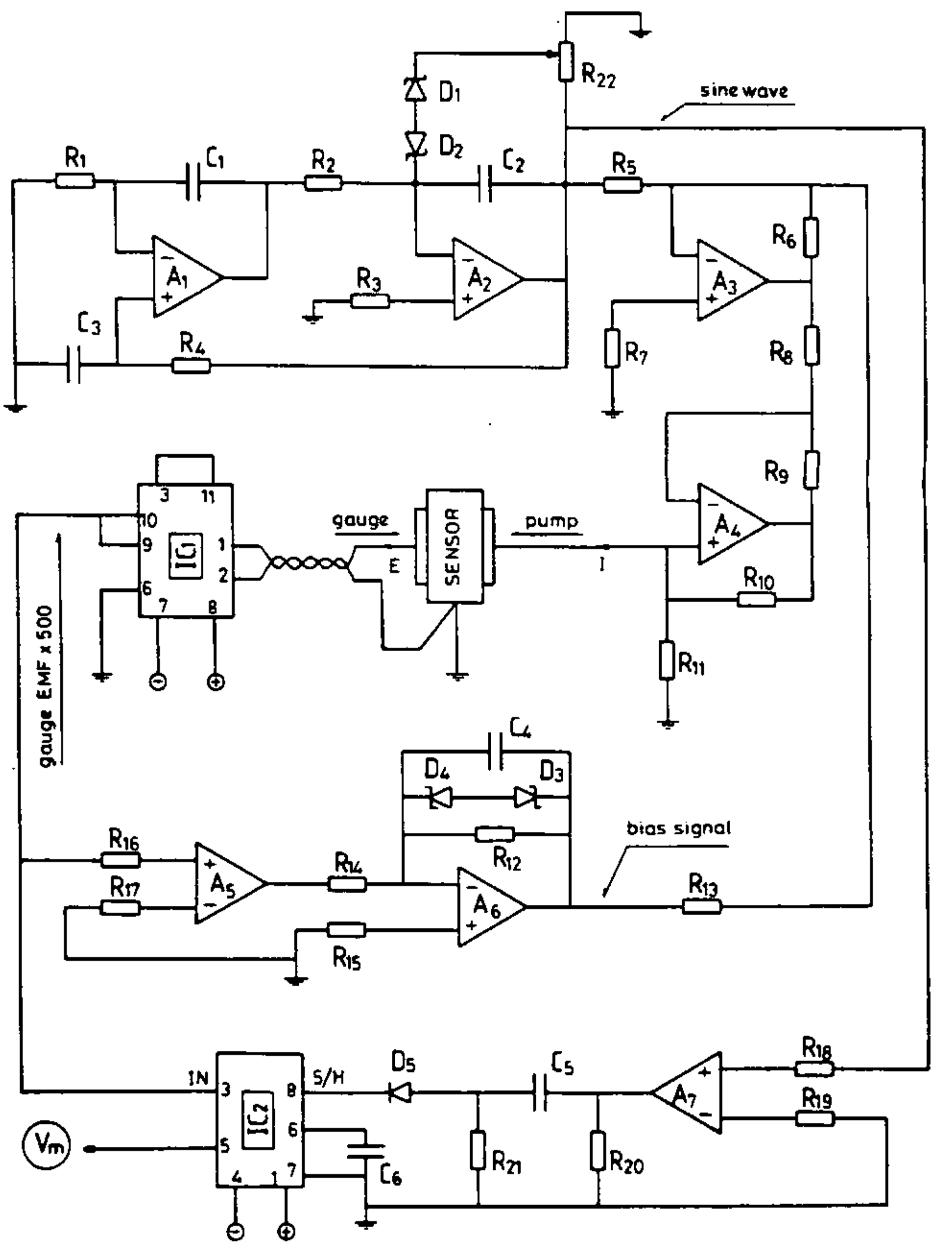

Figure (G.12): *Electronic circuit used for the measurement of oxygen partial pressure (P_1) using sealed pump-gauge device operated in the Tracking Mode (Method 2 in chapter 4). P_1 was computed from V_m.*

List of components in figure (G.12)

IC_1 : INA110 (Instrum. ampl. x500)
IC_2 : LF398 (Sample and Hold)
A_1 - A_7 : ¼ TLO74 (Quad Opamp)
C_1 - C_3 : 0.1μF
C_4 : 2.2μF
C_5 : 4700pF
C_6 : 0.1μF
R_1 : 363k
R_2 : 390k
R_3 : 363k
R_4 : 390k
R_5, R_6: 10k
R_7 : 3.3k
R_8 -R_{11} : 6.8k
R_{12} : 1.8M
R_{13} : 12k
R_{14} : 330k
R_{15} : 220k
R_{16} - R_{21} : 22k
R_{22} : 10k

The trimmer R_{22} is of the 10 turn type.
The circuit was powered from ±15V supply; bypass capacitors were used for each IC.

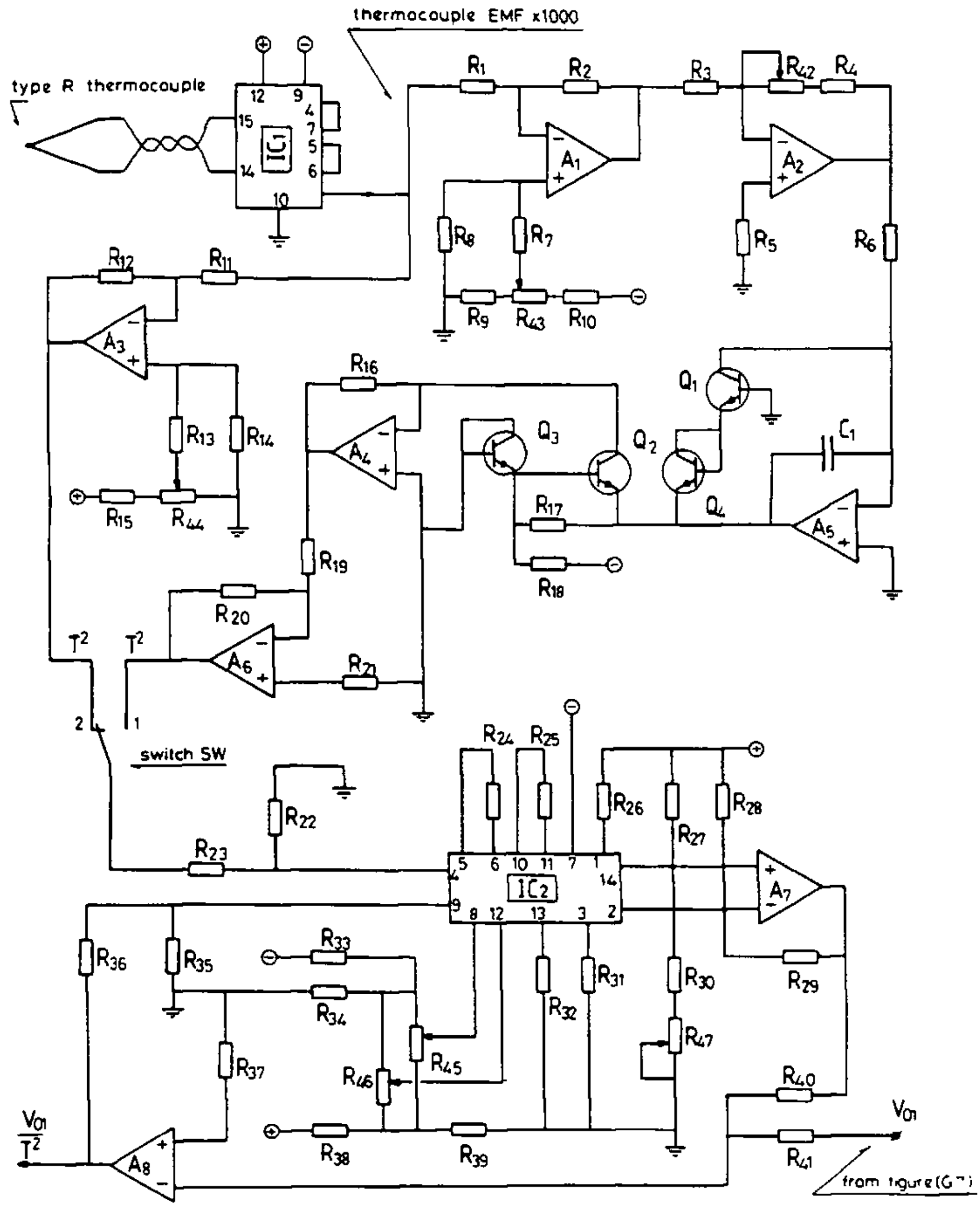

Figure (G.13): Electronic circuit used for temperature compensation of the output V_{01} in Fig.(G.11). The thermocouple was used for the measurement of the temperature of the sensor.

List of components in figure (G.13)

IC_1 : INA102 (Instrum. Amplifier x1000)
IC_2 : SG1495 (Analogue multiplier)
A_1 - A_6 : ¼ TLO74 (Quad opamp)
C_1 : 300pF
Q_1 - Q_4 : $_{1/6}$ CA3086 (Transistor array)
R_1, R_2 : 12k
R_3 : 47k
R_4 : 27k
R_5 : 22k
R_6 : 100k
R_7 : 47k
R_8 : 120k
R_9 : 3.3k
R_{10} : 12k
R_{11}, R_{12} : 15k
R_{13} : 47k
R_{14} : 120k
R_{15} : 22k
R_{16} : 22k
R_{16} : 100k
R_{17}, R_{18} : 150k
R_{19}, R_{20} : 12k
R_{21} : 47k
R_{22}, R_{23} : 10k
R_{24} : 27k
R_{25} : 8.2k
R_{26} - R_{28} : 3.3k
R_{29} : 39k
R_{30} : 33k
R_{31} : 15k
R_{32} : 12k
R_{33} : 15k
R_{34} : 2.7k
R_{35}, R_{36} : 10k
R_{37} : 3.3k
R_{38} : 15k
R_{39} : 2.7k
R_{40}, R_{41} : 12k
R_{42} : 10k
R_{43} : 1k
R_{44} : 1k
R_{45}, R_{46} : 22k

The trimmers R_{42} - R_{46} were 10 turn type.
The circuit was powered from ±15V supply.

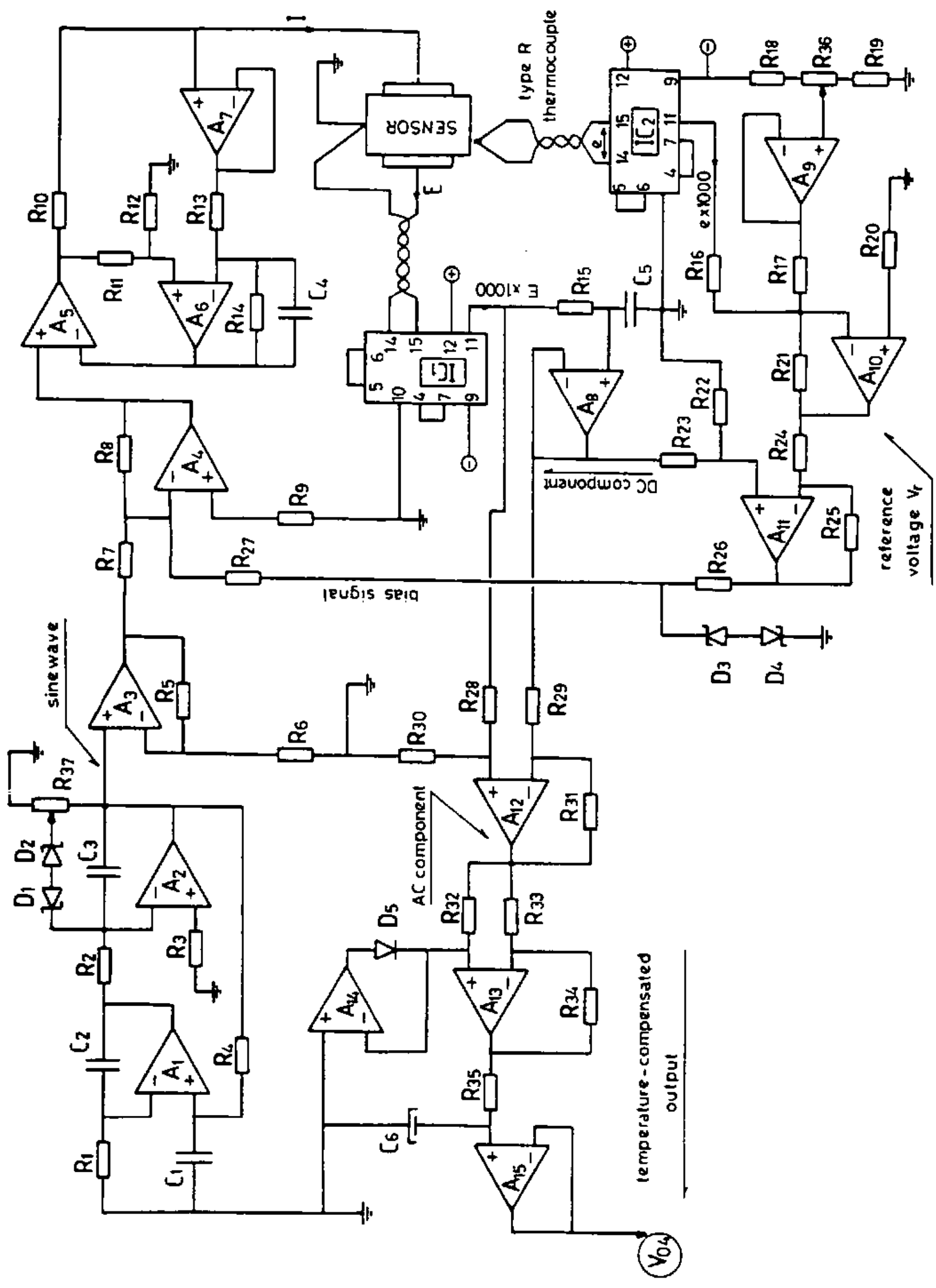

Figure (G.14): Detailed diagram of the circuit used for the measurement of oxygen partial pressure, un-influenced by temperature variations.

List of components in figure (G.14)

IC_1, IC_2 : INA102 (Instrum. Amplifier x1000)
A_1 - A_{15} : ¼ TLO74 (Quad opamp)
C_1 - C_3 : 0.1μF
C_4 : 0.001μF
C_5 : 2μF
C_6 : 30μF
D_1 - D_4 : 4.3V/ 0.25W
D_5 : 1N4148
R_1 : 363k
R_2 : 390k
R_3 : 363k
R_4 : 390k
R_5 : 12k
R_6 - R_8 : 22k
R_9 : 4.7k
R_{10} - R_{12} : 10k
R_{13} : 4.7k
R_{14} : 10k
R_{15} : 1.8M
R_{16}, R_{17} : 13.3k
R_{18} : 10k
R_{19} : 8.2k
R_{20} : 3.3k
R_{21}, R_{22} : 47k
R_{23}, R_{24} : 10k
R_{25} : 47k
R_{26} : 5.6k
R_{27} : 18k
R_{28} - R_{31} : 27k
R_{32} - R_{34} : 10k
R_{35} : 180k
R_{36} : 2k
R_{37} : 10k

The trimmers R_{35}, R_{37} were 10 turn.
The circuit was powered from ±15V supply.
All ICs had bypass capacitors (not shown).

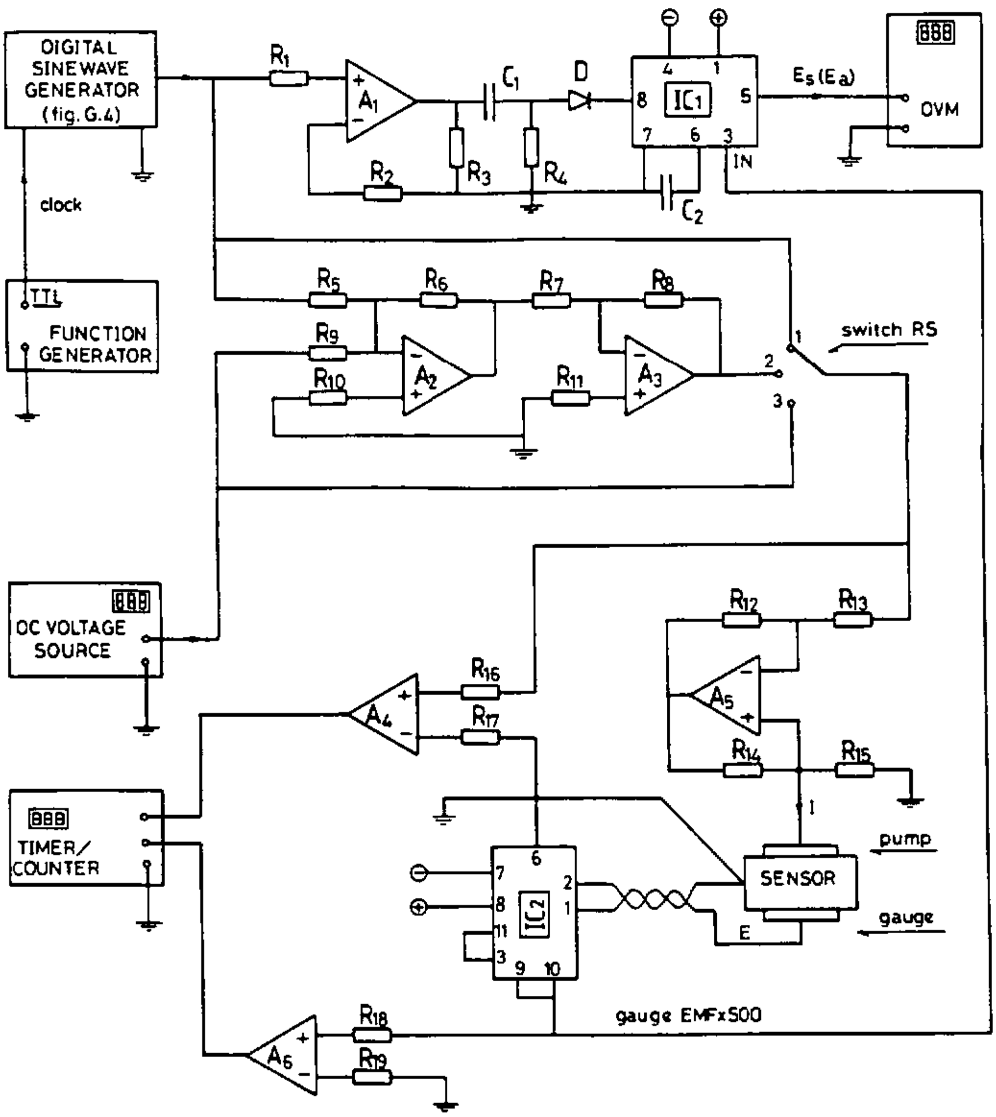

Figure (G.15): Diagram of the circuit used for testing the theory of operation of leaky devices in the AC and DC modes. The switch RS enabled the selection of the mode of operation:

AC mode: switch in position 1,

AC+DC mode:........................... 2,

DC mode: .... 3.

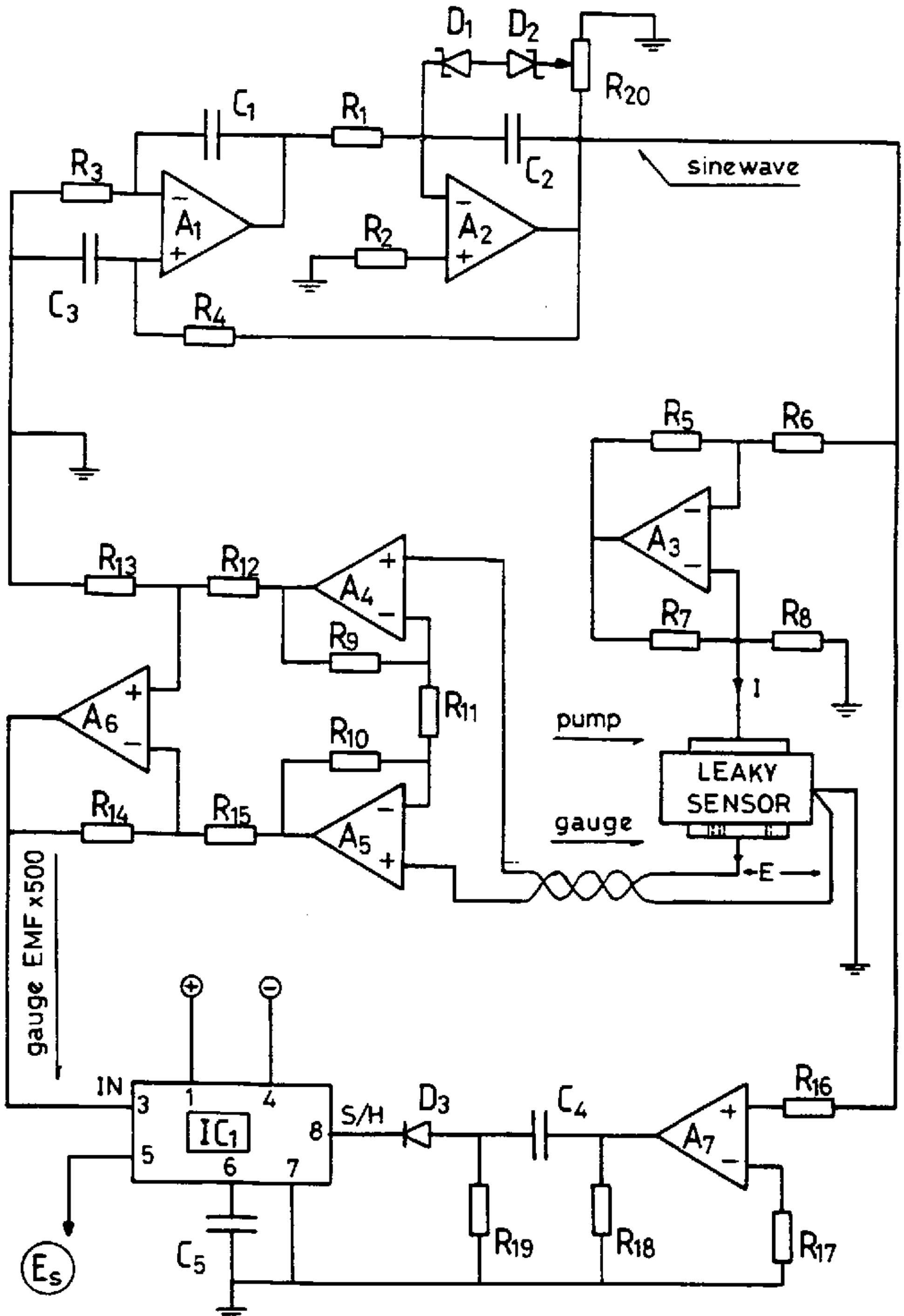

Figure (G.16): Simple circuit for the measurement of oxygen partial pressure using leaky devices.

List of components in figure (G.15)

IC_1 : LF398 (Sample and Hold)
IC_2 : INA110 (Instrum. Amplifier)
A_1 : ¼ TLO74
A_2, A_3 : ½ 3240
A_4 : ¼ TLO74
A_5 : 3140
A_6 : ¼ TLO74
C : 4700pF
D : 1N4148
R_1 - R_4 : 22k
R_5 - R_9 : 10k
R_{10} : 3.3k
R_{11} : 4.7k
R_{12} - R_{15} : 6.8k
R_{16} - R_{19} : 22k

All ICs had 0.01µF bypass capacitors (not shown).
The digital sinewave generator was powered from +5V and ±15V.

List of Components in figure (G.16)

IC_1 : LF398 (Sample and Hold)
C_1 - C_3 : 0.1µF
C_4 : 4700pF
C_5 : 0.1µF
D_1, D_2 : 4.3V/ 0.25W
D_3 : 1N4148
R_1 : 390k
R_2, R_3 : 363k
R_4 : 390k
R_5 - R_8 : 6.8k
R_9, R_{10} : 22k
R_{11} : 56R
R_{12} - R_{15} : 10k
R_{16} - R_{18} : 22k

The circuit was powered from ±15V.
0.01µF bypass capacitors were used for each IC.